

FACILITY FORM 602	<u>N70-29537</u>	
	(ACCESSION NUMBER)	(THRU)
	<u>159</u>	<u>1</u>
	(PAGES)	(CODE)
	<u>CR-110246</u>	<u>14</u>
	(NASA-CR OR TMX OR AD NUMBER)	(CATEGORY)

JET PROPULSION LABORATORY
CALIFORNIA INSTITUTE OF TECHNOLOGY
PASADENA, CALIFORNIA



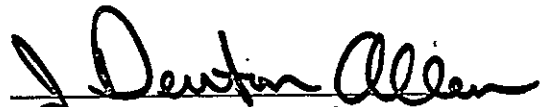
750-7

PHOTOHELIOGRAPH .
PRIMARY MIRROR DEVELOPMENT

August 12, 1968

R. F. Freeman
C. D. Porter
H. H. Mu

Approved by:

A handwritten signature in black ink, reading "J. Denton Allen". The signature is written in a cursive style with a large, prominent "J" and "A".

J. Denton Allen, Task Leader,
Photoheliograph Task

JET PROPULSION LABORATORY
CALIFORNIA INSTITUTE OF TECHNOLOGY
PASADENA, CALIFORNIA

Copyright ©1968
Jet Propulsion Laboratory
California Institute of Technology

Prepared Under Contract No. NAS7-100
National Aeronautics & Space Administration

FOREWORD

This report covers work on one phase of the photoheliograph development task, NASA Code 945-84-00-01-00, for the period November 1967 through June 1968. The photoheliograph has been proposed to NASA for the Apollo telescope mount (ATM) by Caltech, with Professor Harold Zirin as the principal investigator and Dr. Robert Howard of Mt. Wilson and Palomar Observatories the co-investigator (see TM 33-369, November 1967). The objective of the investigation is to obtain high resolution cinematographs in white light near ultraviolet and narrow band hydrogen alpha. Because of the ATM program uncertainties, emphasis has been placed on areas of technology that are somewhat mission-independent, but the ATM spacecraft has been used to establish design constraints.

CONTENTS

Primary Mirror Development	1
Appendix A - Structural Analysis of the Photoheliograph Primary Mirror	18
Appendix B - Explanation of One-Half Optical Path Difference Calculation	49
Appendix C - Thermal Analysis of the Photoheliograph Primary Mirror	50

PHOTOHELIOGRAPH PRIMARY MIRROR DEVELOPMENT

In a near-diffraction limited system, the ultimate success of the system depends on the proper choice and fabrication of materials for the optical elements. The primary mirror functional requirements are listed in Table 1. These requirements necessitate use of a primary mirror material of extremely high optical quality and mechanical dimensional stability and low thermal distortion under solar heating conditions during service in orbit.

In order to select an optimum material to meet these requirements, an index, called the Thermal Distortion Index (TDI) was used for evaluating the thermal-physical merits of various candidate optical primary mirror materials. This index is independent of geometric configuration and is a function only of the physical properties of the materials. The TDI is a qualitative measure of the ability of a material to resist a change in its dimensions with a temperature gradient applied across the material. The TDI is the ratio of the coefficient of thermal expansion to the thermal diffusivity or

$$\text{TDI} = \alpha / \frac{K}{\rho C_p}$$

where

α = coefficient of linear thermal expansion

K = thermal conductivity

C_p = specific heat

ρ = density

A low numerical number is desired for the TDI because materials having a low TDI have a lesser tendency to support temperature gradients and will stabilize quicker with less optical distortion. Also a high elastic modulus to density ratio (E/ρ) makes possible a stiffer structure for a given weight. A low TDI ratio coupled with a low elastic limit and a low damping capacity would point toward problems during launch. Pertinent physical properties and TDI's of a number of candidate materials are given in order of decreasing index in Table 2.

Table 1. Photoheliograph, Primary Mirror Functional Requirements

The Photoheliograph primary mirror design and fabrication shall assure the following:

1. Systematic wavefront accuracy of the total optical system is $1/8$ th wave or better over a two-arc-minute half-field, and random, small-scale errors are $1/50$ th wave or less during operation of the telescope.
2. Thermal distortion does not degrade the systematic error by more than $1/20$ th wave during operation of the telescope.
3. Vibration, shock, acoustic, and thermal cycling environments do not permanently degrade the systematic error to more than that specified in Requirement 1.
4. During telescope operation, the primary mirror can be rigidly supported within ± 0.004 in. of a predetermined "aligned" position with the optical axis tilted no more than 0.5 arc-minutes from the predetermined "aligned" condition.
5. Operation in a 1-g gravity field will distort the mirror surface no more than $1/40$ wave from the surface figure expected in a 0-g field.

Table 2. Comparison of Thermal Performance for Various Candidate Primary Mirror Materials

Material	α ($10^{-6}/^{\circ}\text{F}$)	ρ ($\text{Lb}/\text{in.}^3$)	C_p ($\text{Btu}/\text{lb}-^{\circ}\text{F}$)	K ($\text{Btu}/\text{Hr}-\text{Ft}-^{\circ}\text{F}$)	TDI ($10^{-10} \text{ Hr}-\text{Ft}/^{\circ}\text{F}-\text{in.}^3$)	E ($10^6 \text{ lb}/\text{in.}^2$)	E/ ρ (10^6 in.)
300 Series Stainless Steel	9.2	0.29	0.12	9.4	340	28	97
Titanium (Com'l. pure)	5.0	0.16	0.13	9.8	106	16.5	103
Nickel (Com'l. pure)	7.4	0.32	0.11	45.0	58	30	94
Fused Silica (7940) ⁽¹⁾	0.28	0.079	0.17	0.77	49	10.6	134
Brass (70 Cu, 30 Zn)	11.1	0.31	0.09	70.0	44	16	52
Aluminum (5052)	13.2	0.097	0.23	80.0	37	10.2	105
Magnesium (ZK60)	14.5	0.066	0.24	69.0	33	6.5	98
Tantalum (Com'l. pure)	3.6	0.60	0.036	31.0	25	27	45
Invar	0.5	0.29	0.12	7.8	22	21	72
Beryllium	6.4	0.066	0.45	104.0	18	42	635
CER-VIT C-101 ⁽³⁾	0.08	0.090	0.22	0.97	16	13.4	149
Copper (Com'l. pure)	9.3	0.32	0.092	225.0	12	16	50
Silver (Com'l. pure)	10.6	0.38	0.056	242.0	9.3	10.5	28
U. L. E. Fused Silica (7971) ⁽²⁾	0.03	0.079	0.18	0.75	5.7	9.8	124
Tungsten (Com'l. pure)	2.4	0.70	0.034	116.0	4.9	50	71
Super Invar	0.1	0.29	0.12	8.0	4.4	21	72
Graphite (Molded)	1.4	0.064	0.20	70.0	2.5	0.7	11
⁽¹⁾ Corning Glass Works amorphous fused silica glass. ⁽²⁾ Corning Glass Works amorphous ultra low expansion (U. L. E.) fused silica glass. ⁽³⁾ Owens Illinois crystallized glass. NOTE: Table compiled by R. A. Happe							

A number of materials can be eliminated on the basis of the following rationale. Stainless steel (300 series) and titanium have very high TDI. Nickel and brass have moderately high TDI and are not competitive with copper. Magnesium does have a low TDI, but is not competitive with aluminum with regard to figuring coatings, corrosion resistance and fabricability such as brazing. Tantalum is expensive and has a low E/ρ ratio. Copper has a low E/ρ ratio, is too soft to figure, and compatible hard figuring coatings are not available. Silver has a very low E/ρ and appears to have no particular advantages over copper. Tungsten has a low TDI but is expensive, very difficult to machine, and material availability for the size of the primary mirror is questionable. Graphite has a very low E/ρ ratio and would be almost impossible to figure to the near diffraction limited tolerances required.

The surviving candidates are listed below.

Fused Silica (7940)
 Aluminum (5052)
 Invar
 Beryllium
 CER-VIT C-101
 U. L. E. Fused Silica (7971)
 Super Invar

A static (equilibrium) thermal distortion computation was made for each of the candidate materials in a flat mirror blank configuration. The configuration was a one-in. -thick, 31.5-in. -dia. blank, simply supported around the entire periphery. The back face was held at 70°F; the front face with a solar absorptance (α_s) of 0.14 was sun illuminated. The maximum equilibrium displacement of the front surface was computed for each material. The materials with the minimum steady-state deflections were Super Invar, U. L. E. fused silica (7971), and CER-VIT C-101.

Concurrently with the above analysis, a study was made to determine the effect of primary mirror configuration on the maximum steady-state deflection. Figure 1 compares the displacement of a fused silica flat mirror with configurations thicker at the outside, thinner at the center, and vice versa. The configuration corresponding to the bottom curve of Figure 1 was chosen for further analysis.

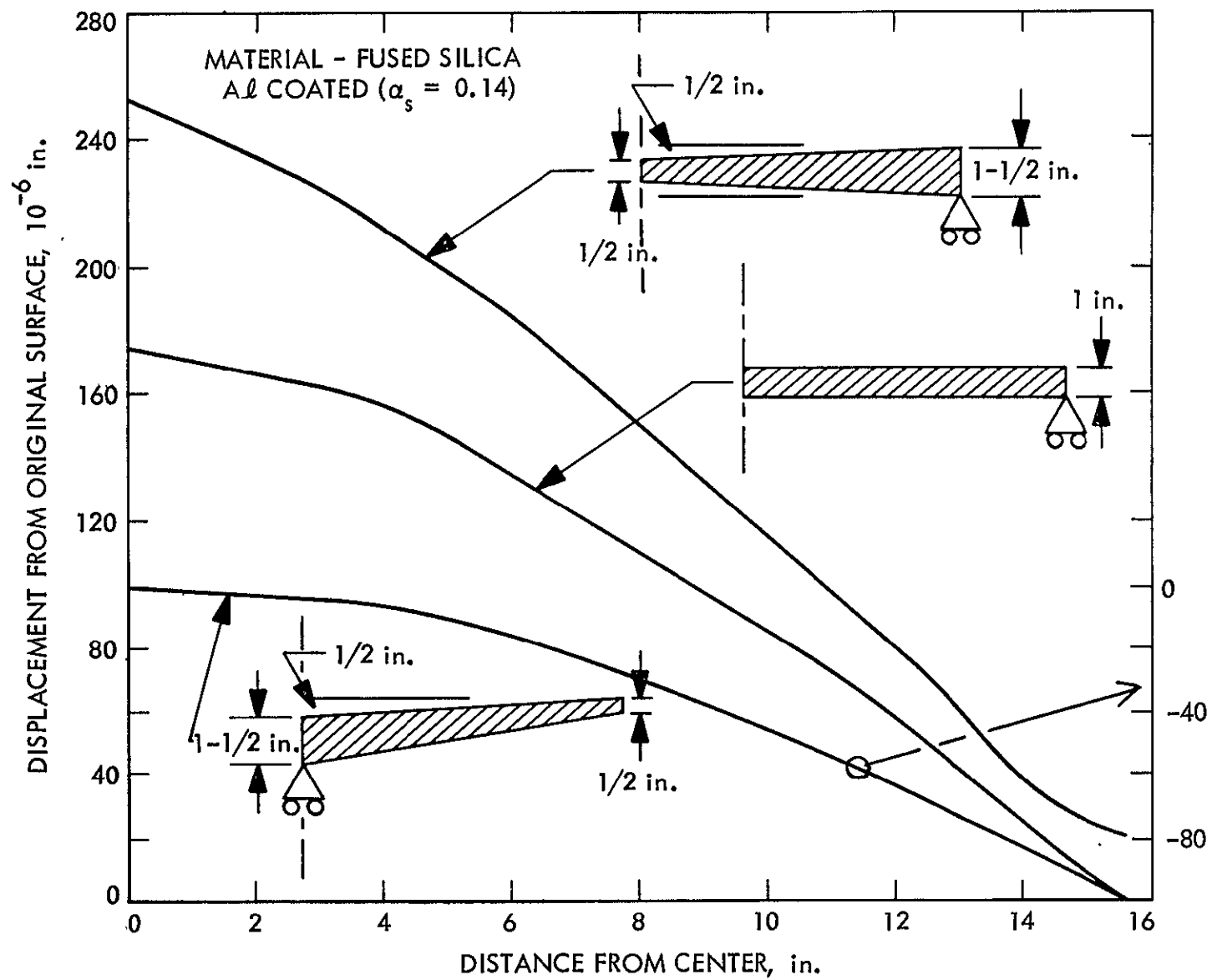


Figure 1. Effect of Primary Mirror Design on Thermal Distortion, F/49 Gregorian Telescope

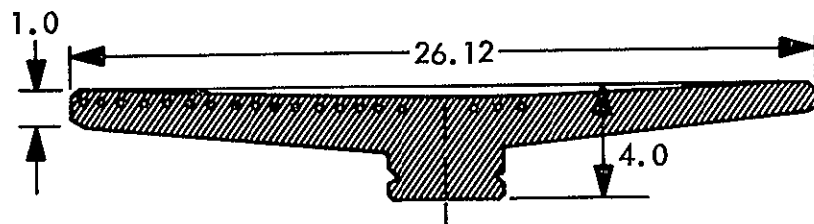
Further investigation revealed that although Super Invar was developed in the early 1930's, little was known about its metallurgical and fabrication characteristics. It was felt that a development program would have to be accomplished before Super Invar could be considered as a candidate for the primary mirror. This development program would have to include as a minimum, the following:

1. Investigate the effects of impurities on the coefficient of linear thermal expansion (α) and the inclusion count of annealed, wrought material.
2. Develop optimum heat treatment for minimum α and optimum dimensional stability.
3. Develop figuring techniques to the stringent optical tolerances required for the primary mirror.

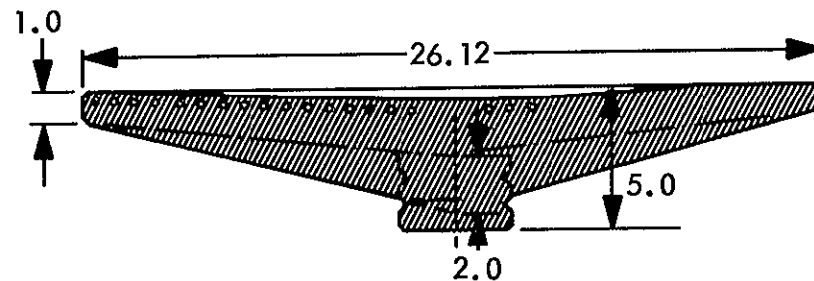
The cost of this program was estimated to be in the neighborhood of \$225K which could not be justified within the constraints of the program.

The two materials left for consideration as candidates for the primary mirror were U.L.E. fused silica and CER-VIT C-101. Throughout the preliminary development phase of the primary mirror, serious consideration had been given to an active internal cooling system to minimize the mirror optical distortions and to reduce the heat flux from the primary mirror system such that the overall telescope heat transfer to the ATM spar was less than 0.6 Btu/hr. Since 50 watts are calculated to be absorbed by the primary mirror, the need arose for active internal cooling to maintain its equilibrium temperature at approximately the same temperature as the ATM spar. Installing coils on the back surface of the mirror necessitated use of a very low expansion material such as Super Invar or possibly U.L.E. fused silica itself. The problem of the attachment of the coils had no clear solution and the resultant thermal and mechanical distortions were much higher than required for internal cooling the mirror on its neutral axis. Radiative cooling required that the back surface of the mirror viewed a refrigerated surface (heat sink) with an emissivity of 0.9 held at -40°F . The heat sink surface would require advanced development work to attain a refrigeration cycle capable of operating reliably for a long time in a zero g field.

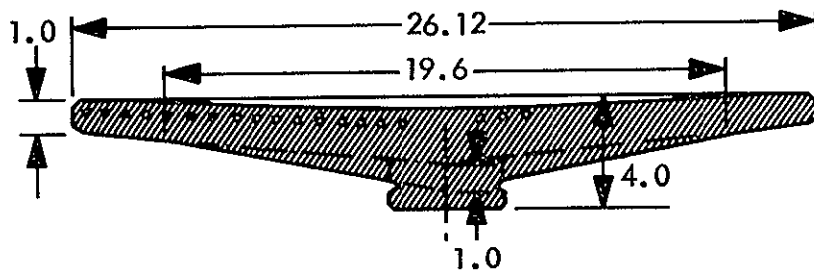
A design evolved for locating the cooling coils on the neutral axis of a 65-cm primary mirror corresponding to configuration No. 1 of Figure 2. The



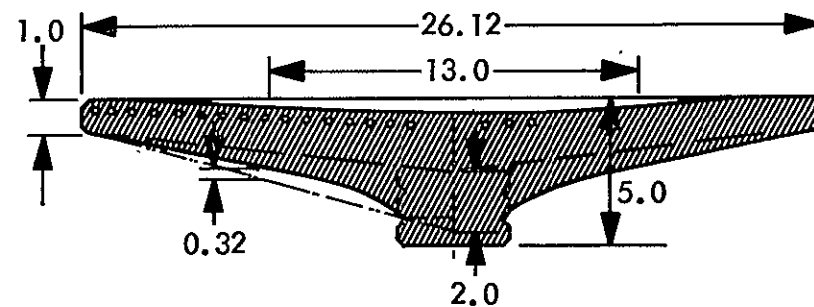
CONFIGURATION No. 1



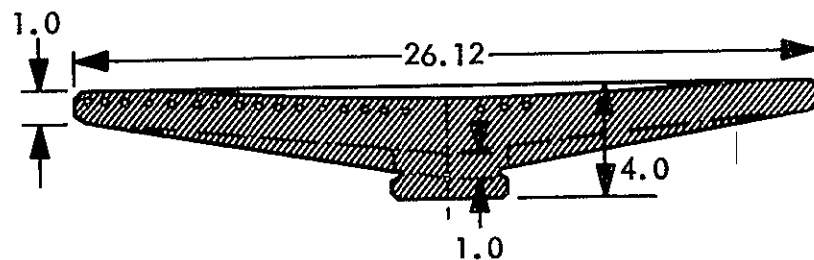
CONFIGURATION No. 4



CONFIGURATION No. 2



CONFIGURATION No. 5



CONFIGURATION No. 3

Figure 2. Primary Mirror Configuration Identifications

fabrication concept involved using amorphous U.L.E. fused silica, installing the cooling channel grooves in the top piece, and then fusing the top and bottom plates together.

CER-VIT C-101 is a crystalline glass and cannot be fused to itself and still maintain its desired physical properties after fusing. Lengthy discussions were held with the Owens-Illinois technical personnel for practical solutions to an active internally cooled CER-VIT C-101 mirror. A telecon with Dr. Simmons on 21 March, 1968 revealed that Owens-Illinois chose not to bid on manufacturing a primary mirror blank from CER-VIT C-101 with internal cooling coils. Because of limited time and manpower other techniques for active cooling a CER-VIT C-101 primary mirror blank other than internally could not be pursued.

The effects of gravity sag on configuration No. 1 for U.L.E. fused silica were checked and it was found that the $1/2$ optical path difference ($1/2$ O.P.D.) was a nineteenth of a wave (see Table 3). The structural analysis is described in Appendix A. The O.P.D. is actually twice this or $\lambda/9.5$, which is clearly unacceptable (see Item 5, Table 1, which requires a minimum O.P.D. of $\lambda/40$ due to gravity g sag). The $1/2$ O.P.D. is illustrated schematically in Figure 3 and is self-explanatory. The $1/2$ O.P.D. calculation is described in Appendix B. A sample $1/2$ O.P.D. calculation is given in Table 4.

The effect of g sag on four other configurations (see Figure 2) was calculated for U.L.E. fused silica and the results tabulated in Table 3. Two satisfactory shapes were configurations 2 and 5. Although configuration 5 gave a slightly better $1/2$ O.P.D., its parabolic back face would be more difficult to fabricate than the double tapered back of configuration 2. Therefore configuration 2 was considered for further analysis with U.L.E. fused silica.

Recent work on beryllium dimensional stability from Battelle Memorial Institute indicated that grades with high BeO contents (4-5%) vs 2% for the former S200D grade and a smaller grain size, 10 microns average with no single grain exceeding 15 microns, increased the precision elastic limit, P.E.L. (the stress required to induce a permanent strain of $1\mu\text{in./in.}$) from 8000 psi to as high as 40,000 psi. This increased dimensional stability led to speculation of its candidacy again as a primary mirror blank material. Gravity sag calculations for configurations 2 and 5 revealed that the effect of g sag was insignificant (see Table 3).

Table 3. Distortion Analysis - Gravity Sag

Material	Primary Mirror Configuration	1/2 Optical Path Difference (1/2 OPD)	Focus Change (Inches)
U.L.E. Fused Silica	1	$\frac{\lambda}{19}$	0.0051
U.L.E. Fused Silica	2	$\frac{\lambda}{185}$	0.0030
U.L.E. Fused Silica	3	$\frac{\lambda}{48}$	0.0031
U.L.E. Fused Silica	4	$\frac{\lambda}{44}$	0.0023
U.L.E. Fused Silica	5	$\frac{\lambda}{250}$	0.0021
Beryllium	5	$\frac{\lambda}{1000}$	0.0005
Beryllium	2	$\frac{\lambda}{909}$	0.0006

Table 4. Calculation of 1/2 O.P.D. for ULE Fused Silica, Configuration No. 1, 1 G Load in -Y Direction

X	X ²	= (X ² y/4f)	$\frac{\Delta y}{10^{-6} \text{ in.}}$	$\frac{\Delta y - \Delta y_0}{\Delta y=0 @ X=0}$ (10 ⁻⁶ in.)	y'' = y + (Δy-Δy ₀)	y'	= (y' - y'', 10 ⁻⁶ in.)
0	0	0	+0.088	0	0	0	0
2	4	0.010160000	-0.286	-0.374	0.010159626	0.010159469	-0.157
4.32	18.66240	0.047402496	-2.509	-2.597	0.047399899	0.047400018	+0.119
6.04	36.48160	0.092663265	-5.238	-5.326	0.092657939	0.092658421	+0.482
8.07	65.12490	0.165417247	-9.381	-9.469	0.165407778	0.165408600	+0.822
9.79	95.84410	0.243444016	-13.532	-13.620	0.243430396	0.243431289	+0.893
11.82	139.71240	0.354869499	-18.953	-19.041	0.354850458	0.354850947	+0.489
12.79	163.58410	0.415503618	-21.634	-21.722	0.415481896	0.415481896	0

$$f' (@X=12.79 \text{ in.}) = \frac{X^2}{4y''} = \frac{163.58410}{4y''} = \frac{40.896025}{0.415481896} = 98.43034171$$

$$y' = \frac{X^2}{4f'} = \frac{X^2}{4(98.43034171)} = 0.002539867236X^2$$

$$\Delta f = f' - f = 0.0051 \text{ in.}$$

$$AT\lambda = 5000 \text{ \AA}, \quad \lambda = 20 \times 10^{-6} \text{ in. (20 micro inches), or 1 microinch (1 } \mu \text{ in.)} = \lambda/20$$

Maximum deviation above (y'-y'') is 1.05 μ in.

$$\frac{1 \mu \text{ in.}}{\frac{\lambda}{20}} : \frac{1.05 \mu \text{ in.}}{\frac{\lambda}{X}}, \therefore X = 19.05, \text{ the } 1/2 \text{ O.P.D. is } \therefore \frac{\lambda}{19}$$

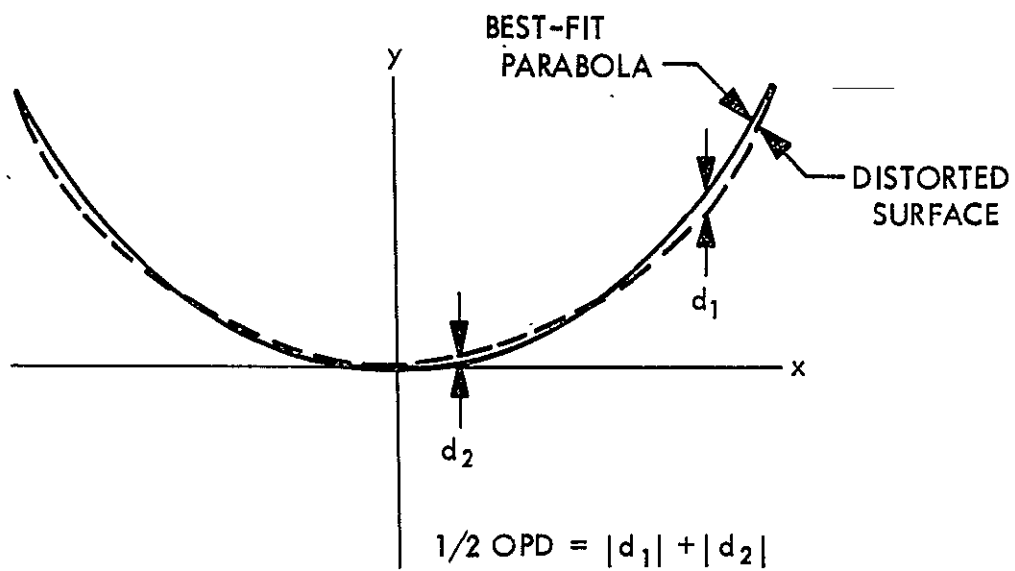
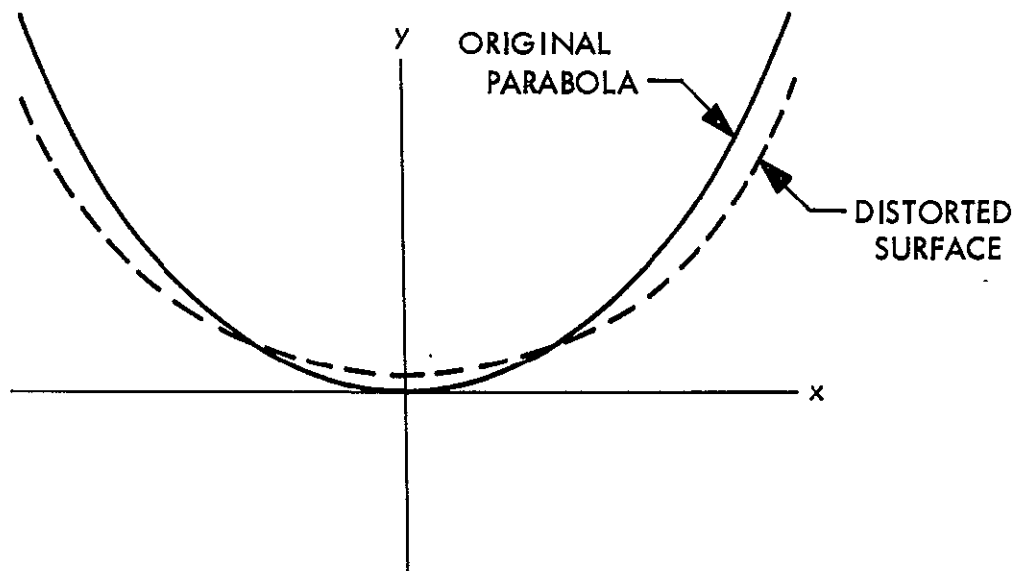


Figure 3. Definition of 1/2 OPD

A detailed thermal analysis was made of configuration 1 in U.L.E. fused silica before the computer results of the g -sag distortions of the other configurations were made available. These results are tabulated in Table 5. The thermal analysis is described in Appendix C. The coolant used was 80% methanol, 20% water which entered the mirror at 70°F at 16 psia. It can be seen that turbulent flow gives slightly better results than laminar flow and that the coolant fluid flow direction is better from the mirror inside to the mirror outside. Because of the unknown possible problems of vibration induced by turbulent flow it was decided to choose the conservative (lower flow rate) laminar flow, with the flow from inside to outside. It was recognized that turbulent flow gave a 1°F radial temperature rise from the mirror inside to outside where laminar flow gave a 3°F temperature rise. The 1/2 O.P.D. for U.L.E. fused silica corresponding to the thermal condition chosen above for configuration 2 was a satisfactory $\lambda/55$. The local deflection of the U.L.E. fused silica mirror reflecting surface due to cooling fluid pressure (16 psi) corresponded to a 1/2 O.P.D. of $\lambda/500$, and the deflection of the reflecting surface from the 70°F laminar flow temperature distribution (thermal ripple) corresponded to a 1/2 O.P.D. $\lambda/2000$, both insignificant.

Because of the known fabrication difficulties of installing cooling channels internally in a beryllium mirror blank, and because of the limited time available, it was decided to compare a back face radiatively cooled beryllium mirror blank with a U.L.E. fused silica mirror blank both of configuration 2, the back face double taper. The results (Table 5) show that for a temperature gradient on the mirror back, 3°F rise from inside to outside, the 1/2 O.P.D. for U.L.E. fused silica was $\lambda/20$ and the 1/2 O.P.D. for beryllium $\lambda/4$. Moving the coolant to the back of the mirror not only loses the advantages of close proximity to the heated surface, but does not avoid problems. The beryllium could not be considered for further analysis because of the poor optical performance (even $\lambda/20$ is marginal). Another problem with beryllium is that a nickel-phosphorous Kanigen coating would be required for figuring. This coating presents a poorer optical surface than glass and is insufficient for use in the near ultraviolet as UV-scattering results.

Table 6 lists the results of the transient thermal distortion analysis for U.L.E. fused silica, configuration 2, with laminar flow from mirror inside to

Table 5. Distortive

Material	Primary Mirror Configuration	Thermal Condition	1/2 Optical Path Difference (1/2 OPD)	Focus Change (Inches)
U. L. E. Fused Silica	1	Laminar flow, uniform 70°F coolant temperature	$\frac{\lambda}{57}$	0.0008
U. L. E. Fused Silica	1	Turbulent flow, uniform 70°F coolant temperature	$\frac{\lambda}{78}$	0.0006
U. L. E. Fused Silica	1	Turbulent flow from outside to inside	$\frac{\lambda}{72}$	0.0006
U. L. E. Fused Silica	1	Turbulent flow from inside to outside	$\frac{\lambda}{83}$	0.0007
U. L. E. Fused Silica	1	Laminar flow from outside to inside	$\frac{\lambda}{49}$	0.0007
U. L. E. Fused Silica	1	Laminar flow from inside to outside	$\frac{\lambda}{67}$	0.0010
U. L. E. Fused Silica	2	Temperature gradient on mirror back, 3°F rise from inside to outside	$\frac{\lambda}{20}$	0.0025
Beryllium	2	Temperature gradient on mirror back, 3°F rise from inside to outside	$\frac{\lambda}{4}$	0.0417
U. L. E. Fused Silica	2	Laminar flow from inside to outside	$\frac{\lambda}{55}$	0.0007

Table 6. Distortion Analysis - Transient Thermal

Material	Primary Mirror Configuration	Thermal Condition	Minutes of Direct Solar Illumination	1/2 Optical Path Difference (1/2 OPD)	Focus Change (Inches)
U.L.E. Fused Silica	2	Laminar flow from inside to outside	12	$\frac{\lambda}{49}$	0.0011
U.L.E. Fused Silica	2	Laminar flow from inside to outside	24	$\frac{\lambda}{59}$	0.0010
U.L.E. Fused Silica	2	Laminar flow from inside to outside	36	$\frac{\lambda}{61}$	0.0009

outside. It can be seen that the optical performance is increasing from 12 to 36 minutes solar illumination-time from passing from earth shade to direct solar illumination; the optical performance for each time-period is acceptable. The mirror starts the sun portion of the orbit at 70°F. The coolant fluid starts at this temperature by means of a fluid temperature controlled loop as shown in the schematic in Figure 4. The schematic is correct except for the fact that the fluid should enter at the innermost channel at 70°F.

The U.L.E. fused silica mirror blank containing the integral cooling channels is fabricated in the following way. An approximate spiral channel would be sandblasted into the forward face of the bottom plate of the mirror, the channels fire polished, and the top (approximately one-half inch thick) and bottom plates fused together. The procedure would be to heat slowly to 1000°C, then quickly to 1600°C for fusing, and then sag over a refractory mold to general shape at just under 1600°C. The sagging process might introduce sufficient change of the front face contour from that desired such that subsequent optical grinding of the front face could decrease the 0.5-in. nominal thickness of the mirror front plate by as much as 0.15 in. This will result in a negligible change of 1/2 O.P.D. ($\lambda/56$ vs $\lambda/55$ 1/2 O.P.D. for a uniform 0.50 inch front plate thickness). The mirror blank would then be rough ground, and annealed at 1000°C. The U.L.E. fused silica mirror blank fabricator, Corning Glass Works, will guarantee 90% fusion with 100% fusion around the outside periphery. It is planned to let the purchase obligation for one primary mirror blank flight verification unit with integral cooling channels.

One disadvantage of U.L.E. fused silica is that high internal stress causes some concern optically and mechanically. The internal stress arises from inability to completely anneal U.L.E. fused silica. These stresses cause optical birefringence. The magnitude of the measured birefringence, therefore, is a measure of the internal stresses. Corning Glass Works will only guarantee a value of 50 millimicrons per centimeter of transmitted light path. One other disadvantage is that it is a fairly new material and the fabrication, testing, and figuring techniques probably have not been optimized yet.

CER-VIT C-101, the Owens-Illinois non-fusible crystallized glass has a minimum guaranteed value about 1/5 the birefringence that the Corning product has. It has been on the market about two years longer than U.L.E. fused silica and the optical figuring people have gained much more experience in

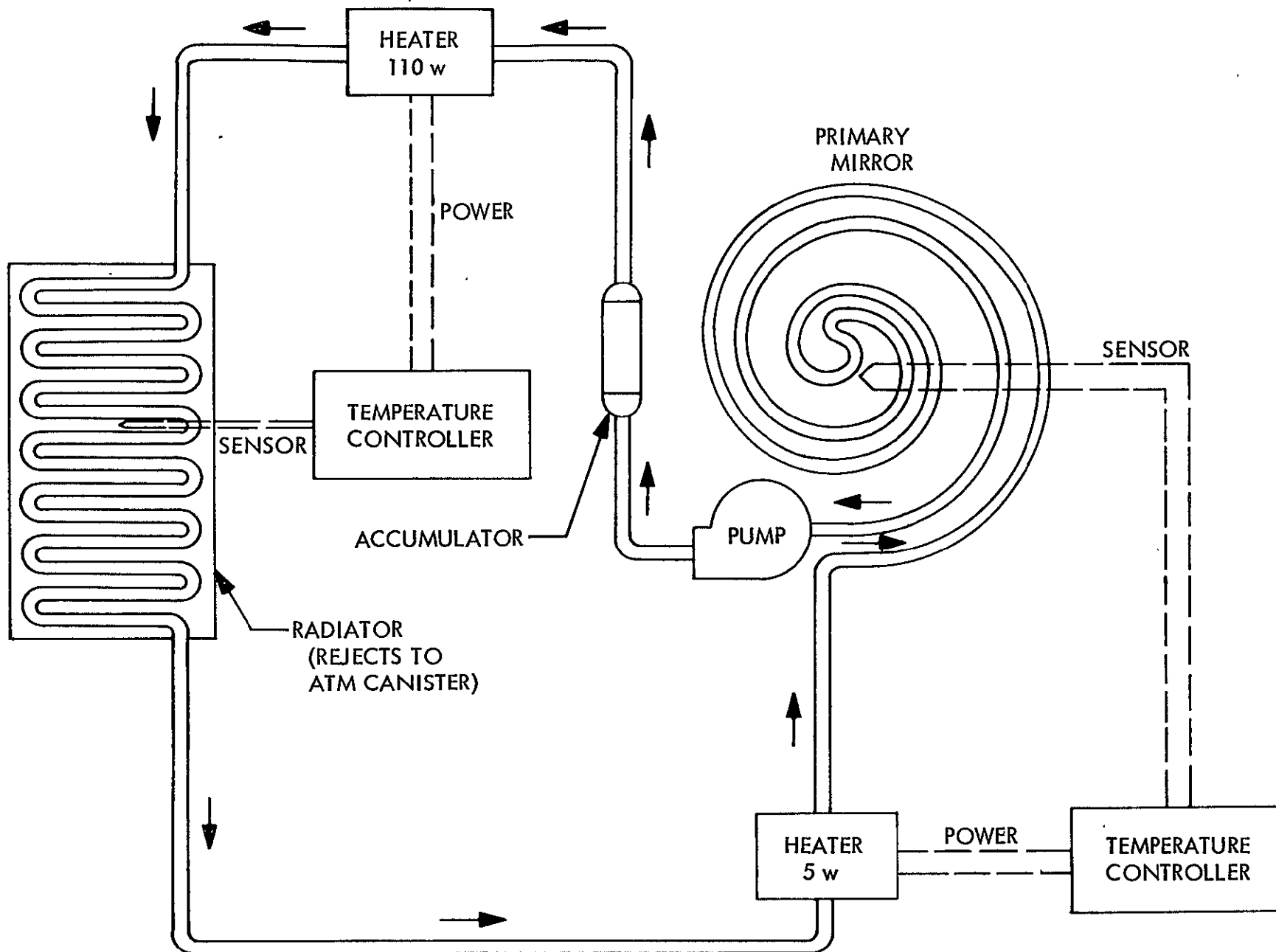


Figure 4. Fluid Temperature Controlled Primary Mirror Schematic

working with this material. With a premium select grade of CER-VIT C-101, a coefficient of thermal expansion can be obtained virtually identical to that of U.L.E. fused silica, i.e., $0.03 \times 10^{-6}/^{\circ}\text{F}$. Because of these desirable qualities, engineering discussions shall be reopened with Owens-Illinois concerning the problem of thermal coupling to the premium select CER-VIT C-101 mirror blank, if it appears Corning is unable to fabricate a U.L.E. fused silica primary mirror blank. The design shall be specifically developed for a mirror blank without internal cooling.

APPENDIX A
STRUCTURAL ANALYSIS OF THE PHOTOHELIOGRAPH
PRIMARY MIRROR

INTRODUCTION

The objective of the report is to summarize the analytical effort to date on the structural analyses of the primary mirror. The analyses consist of the thermal and gravitational distortion of various mirror configurations and materials.

First, a brief discussion of the theory and assumptions are presented; second, the effort to verify the analysis method by solution of example problems is presented; and third, the results of all analysis to date are summarized in Table 7.

THEORETICAL DEVELOPMENT

The analyses were performed by use of a digital computer program titled "ELAS"⁽¹⁾. The theoretical description to follow includes only that pertinent to the mirror.

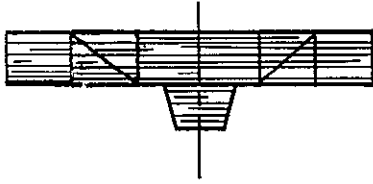
A finite element approach is used to characterize the structure of the mirror. The mirror is discretized into small finite structural elements; within each element the material properties, loading conditions and displacement characterization are assumed constant. A good approximation to the true answer is obtained by an increase of the number of elements in the mirror where the displacement gradients are high.

The geometric and load axisymmetry of the mirror reduced the analysis to a two-dimensional problem. A triangular torus and quadrilateral torus finite elements are used to represent the mirror.

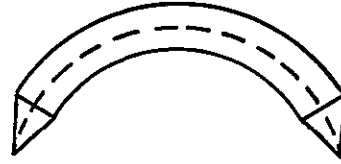
⁽¹⁾ Utku, S., and Akyz, F.A., "ELAS - A General-Purpose Computer Program for the Equilibrium Problems of Linear Structures", JPL TR 32-1240, Vol. 1, Feb. 1, 1968.

Table 7. Summary of the Computer Analyses on the Photoheliograph Primary Mirror

Run No.	Conf.	Material	Conditions	Maximum Effective Stress (P. S. I.)	Maximum Stress Node Location	Maximum Defl. in Y Direction, Inches $\times 10^{-6}$	Maximum Defl. in X Direction, Inches $\times 10^{-6}$
1	1	ULE Fused Silica	Laminar flow, uniform 70°F coolant temperature	0.55	54	-3.489	1.867
2	1	ULE Fused Silica	1 G load, mirror support down	4.62	30	-22.372	2.478
3	1	ULE Fused Silica	1 G load, mirror support up	3.84	21	22.372	-2.478
4	1	ULE Fused Silica	Turbulent flow, uniform 70° coolant temperature	0.41	100	-2.768	0.929
5	1	ULE Fused Silica	Turbulent flow from outside to inside	0.52	65	-2.422	1.094
6	1	ULE Fused Silica	Laminar flow from outside to inside	0.78	52	-2.499	2.366
7	1	ULE Fused Silica	Laminar flow from inside to outside	0.50	86	-4.294	2.454
8	1	ULE Fused Silica	Turbulent flow from inside to outside	0.35	86	-3.051	1.126
9	2	ULE Fused Silica	1 G load	18.05	47	-12.938	1.782
10	3	ULE Fused Silica	1 G load	10.45	47	-13.485	1.897
11	4	ULE Fused Silica	1 G load	29.05	47	-10.220	1.723
12	5	ULE Fused Silica	1 G load	21.52	47	-9.640	1.534
13	5	Beryllium	1 G load	17.78	47	-2.046	0.323
14	2	Beryllium	1 G load	14.91	47	-2.715	0.375
15	2	ULE Fused Silica	1 G load, the mirror was supported at the outside edge	8.44	261	-4.233	-0.671
16	2	ULE Fused Silica	1 G load, the mirror cooling channels were removed	18.51	47	-13.123	1.786
17	2	Beryllium	1 G load, the mirror cooling channels were removed	15.30	47	-2.757	0.376
18	2	ULE Fused Silica	Temperature gradient on mirror back, 3°F rise from inside to outside	1.50	72	-10.827	4.293
19	2		Void, incorrect temperature instruction chosen				
20	2	Beryllium	Same conditions as Run No. 18	393.50	241	-190.969	143.129
21	2	ULE Fused Silica	Laminar flow from inside to outside	0.53	212	-3.011	2.341
22	2	ULE Fused Silica	Laminar flow from inside to outside 12 min. sun illumination	0.55	54	-4.824	1.938
23	2	ULE Fused Silica	Laminar flow from inside to outside 24 min. sun illumination	0.53	191	-4.493	2.213
24	2	ULE Fused Silica	Laminar flow from inside to outside 36 min. sun illumination	0.56	212	-4.113	2.289
25	2	CER-VIT	Same conditions as Run No. 18	1.92	71	-9.777	3.850
26	2	ULE Fused Silica	Mirror 15 min. thinner at center line due to fabrication	0.55	212	-2.784	2.292
27*							
28*							
29*							
30*							
31	2	ULE Fused Silica	Local deflection of mirror reflecting surface due to cooling channel pressure (16 psi)	32.85	77	0.282	-0.171
32	2	ULE Fused Silica	Local deflection of mirror reflecting surface from temperature distribution of 70°F laminar flow (thermal ripple)	1.93	34	-0.0955	0.136
*Still in progress							



Cross Section of a Mirror



Half of a Triangular Torus

Each node is represented by two translational degrees of freedom and the relationship between nodal displacements and forces for each element is derived. The relationships for all elements of the mirror are assembled, the boundary conditions are imposed, the loads are applied, and the equations are solved for the deflections and stresses.

The stiffness finite element approach is used where a displacement function for each element is defined to match the nodal displacements and to insure displacement continuity between elements. From the displacement function and material characteristics the following relation between the nodal displacements and forces are obtained for each finite element. For the i^{th} element,

$$[K]_i \{\delta\}_i = \{f^p\}_i$$

where

$$[K]_i = \text{stiffness matrix for } i^{\text{th}} \text{ element}$$

$$\{\delta\}_i = \text{nodal displacement for } i^{\text{th}} \text{ element}$$

$$\{f^p\}_i = \text{nodal forces for } i^{\text{th}} \text{ element}$$

The equations of equilibrium for the entire mirror are obtained by generation of the total stiffness matrix by the addition of all elemental stiffness matrices, elimination of rows and columns of stiffness matrices corresponding to restraints, and the application of either thermal or gravitation forces. The equation is

$$[K] \{\delta\} = \{F\}$$

where

$$\begin{aligned} [K] &= \text{stiffness matrix of total structure} \\ \{\delta\} &= \text{unknown nodal displacements} \\ \{F\} &= \text{applied force} \end{aligned}$$

The equation is solved for the nodal displacements by

$$\{\delta\} = [K]^{-1} \{F\}$$

The stresses are evaluated assuming infinitesimal deflections and by use of the material characteristics of the finite elements.

The stiffness finite element approach or approximation to the true structure provides displacements which are a lower bound on the average. Lower bound on the average means that the true average deflection of the mirror is never less than the computed average deflection. The true solution is converged upon as the finite elements are reduced in size.

In addition to the verification of the accuracy of ELAS, a verification of the adequacy of the finite element size is necessary since the results provide a nonconservative lower bound. In many situations the mirror was subdivided and the significant subdivisions were analyzed separately. This allowed more detail evaluation because of the ELAS limitation in the maximum allowable nodes or degrees of freedom.

Check Problems

As indicated in the previous paragraph, the adequacy of ELAS and mesh size was verified.

First, an infinitely long thick cylinder with a thermal gradient through the thickness (see Figure 5) was solved with ELAS. The problem was chosen because an exact solution is available from the literature (Theory of Elasticity by Timoshenko and Goodier). As shown in Figure 6, the correlation between ELAS and Timoshenko was within accuracy of the graph.

The second problem was a rocket nozzle in which an exact solution does not exist. A cross-section of the nozzle showing the computer elements and nodes (mesh) can be seen in Figure 7. However, an approximate solution to this complex geometric shape with thermal loading had been solved by use of a well established computer program referred to as "Rohm-Hass". As shown in Figures 8 to 15, a good correlation was obtained.

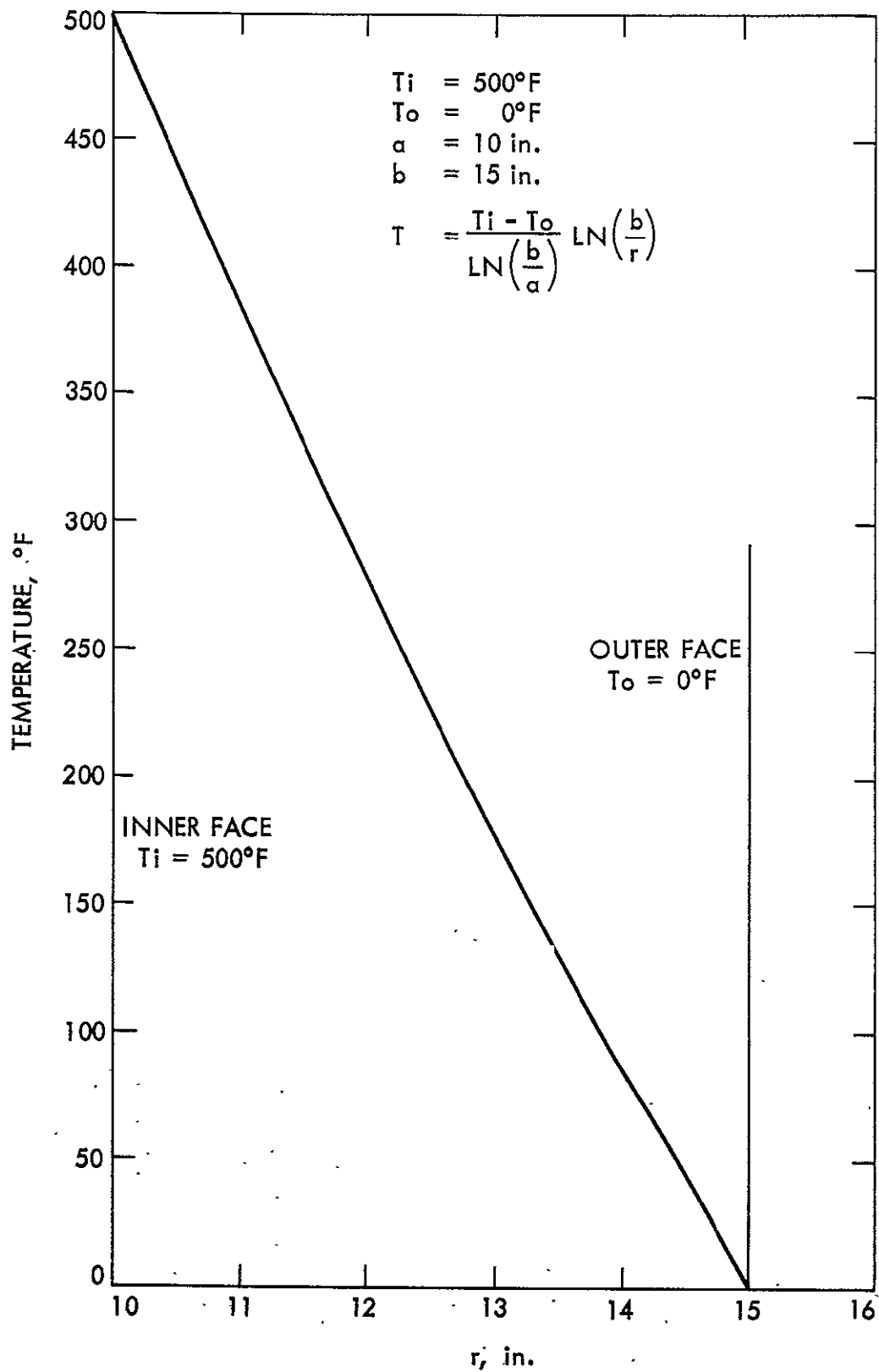
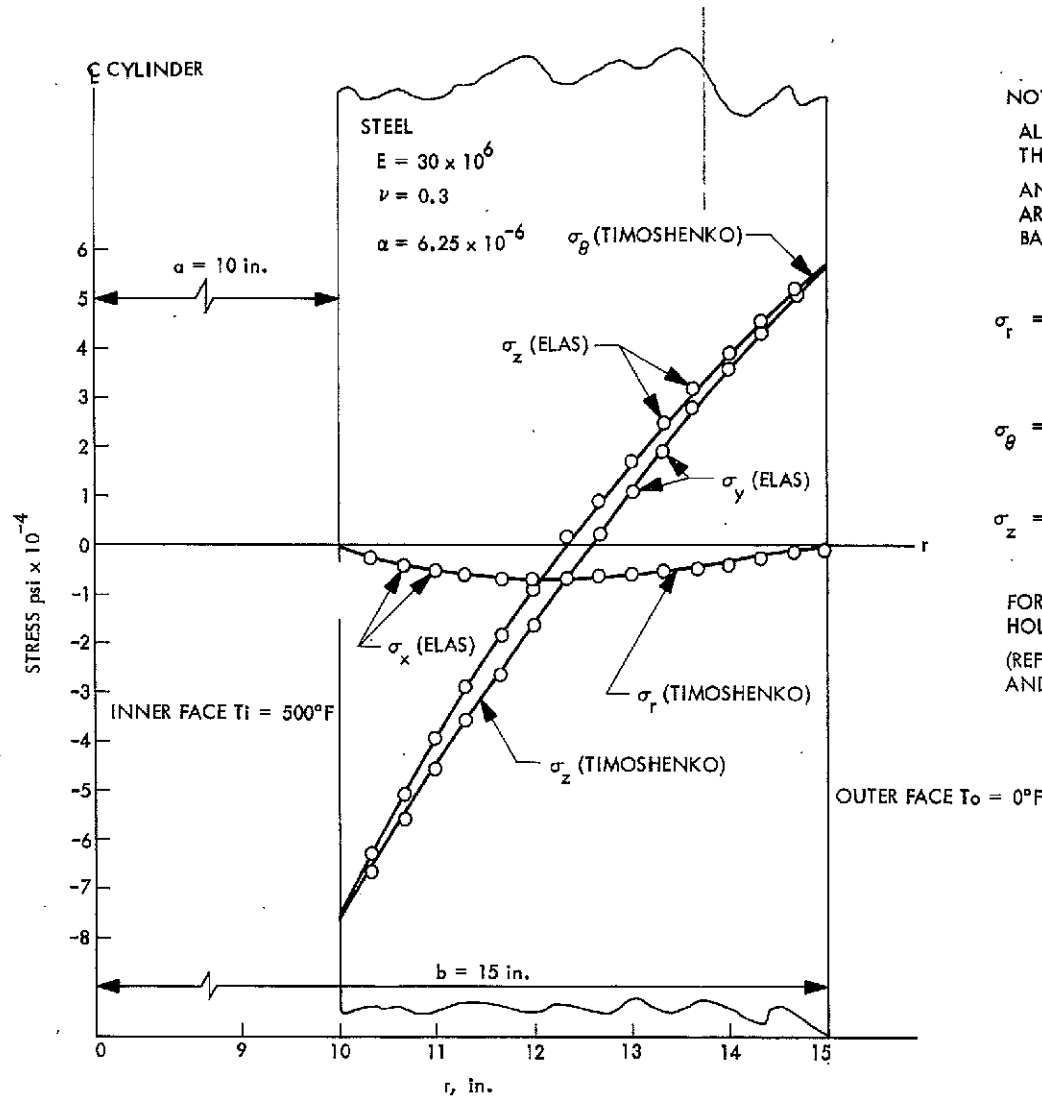


Figure 5. Infinitely Long Cylinder with a Thermal Gradient through the Thickness



SAMPLE PROBLEM

NOTE:

ALL THE CIRCLES ARE THE RESULTS OF THE OUTPUT OF "ELAS" PROGRAM AND THE CURVE LINES SHOWN ON THE LEFT ARE PLOTTED FROM THE CALCULATIONS BASED UPON THE FOLLOWING FORMULAS:

$$\sigma_r = \frac{\alpha E T_i}{2(1-\nu) \ln(b/a)} \left[-\ln \frac{b}{r} - \frac{a^2}{(b^2 - a^2)} \left(1 - \frac{b^2}{r^2} \right) \ln \frac{b}{a} \right]$$

$$\sigma_\theta = \frac{\alpha E T_i}{2(1-\nu) \ln(b/a)} \left[1 - \ln \frac{b}{r} - \frac{a^2}{(b^2 - a^2)} \left(1 + \frac{b^2}{r^2} \right) \ln \frac{b}{a} \right]$$

$$\sigma_z = \frac{\alpha E T_i}{2(1-\nu) \ln(b/a)} \left[1 - 2 \ln \frac{b}{r} - \frac{2a^2}{(b^2 - a^2)} \ln \frac{b}{a} \right]$$

FOR LONG CYLINDER WITH A CONCENTRIC CIRCULAR HOLE, UNDER THE CONDITION OF STEADY HEAT FLOW (REF TO Pg 413, THEORY OF ELASTICITY BY TIMOSHENKO AND GOODIER)

Figure 6. Curve Showing Correlation of "Elas" Program

FOLDOUT FRAME 1

FOLDOUT FRAME 2

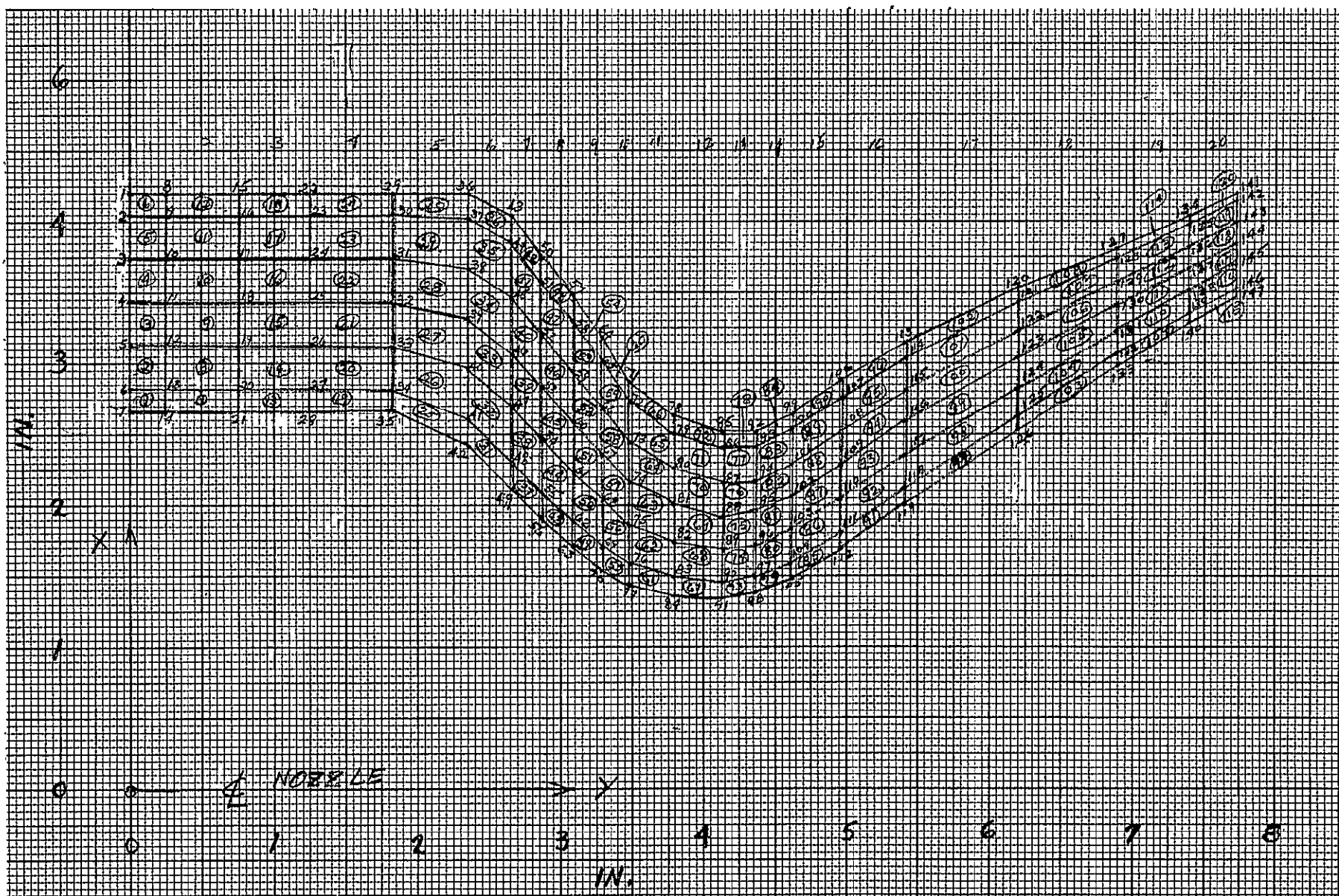


Figure 7. A Section of Rocketdyne Engine Nozzle

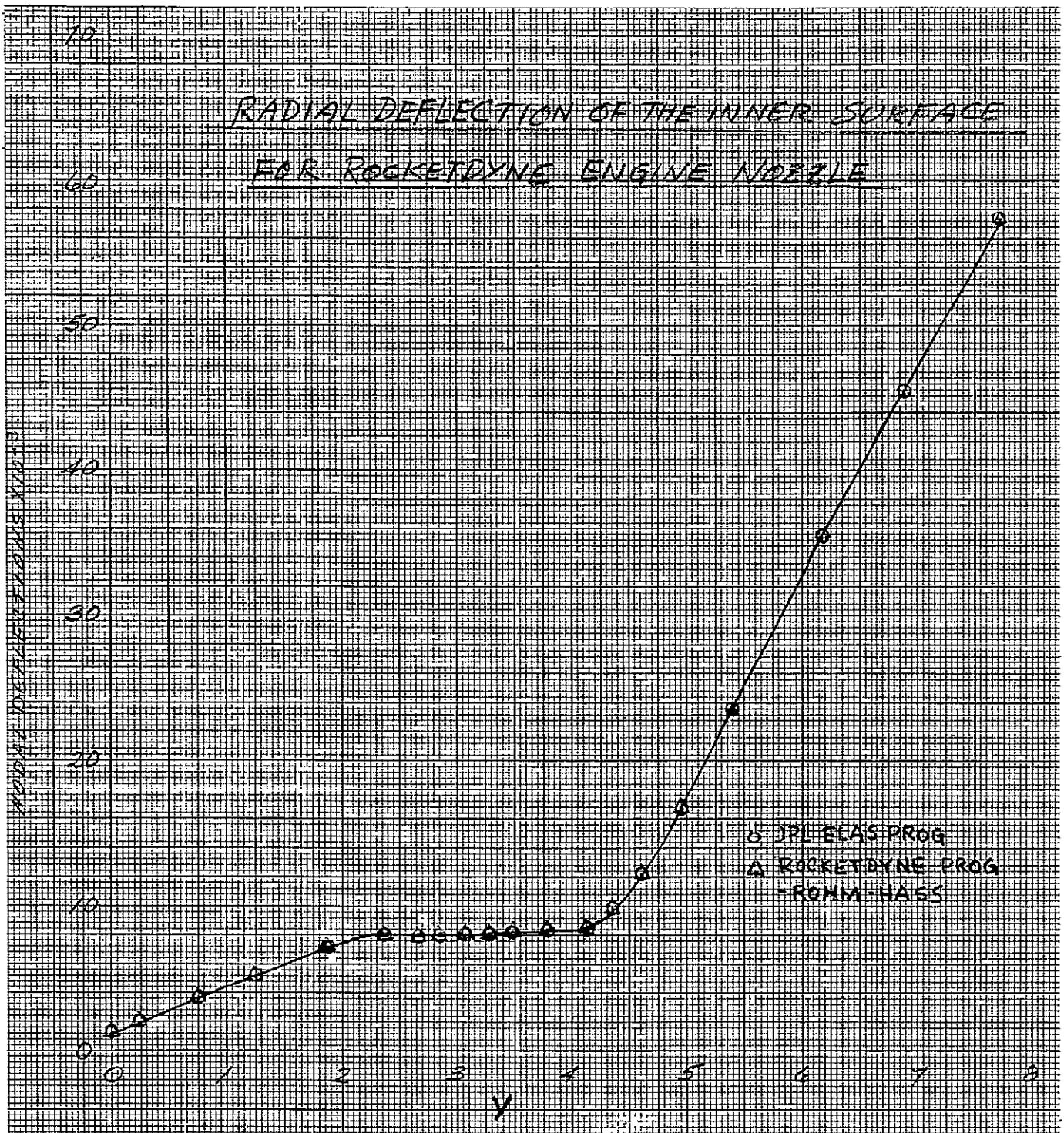


Figure 8. Radial Deflection of the inner Surface for Rocketdyne Engine Nozzle

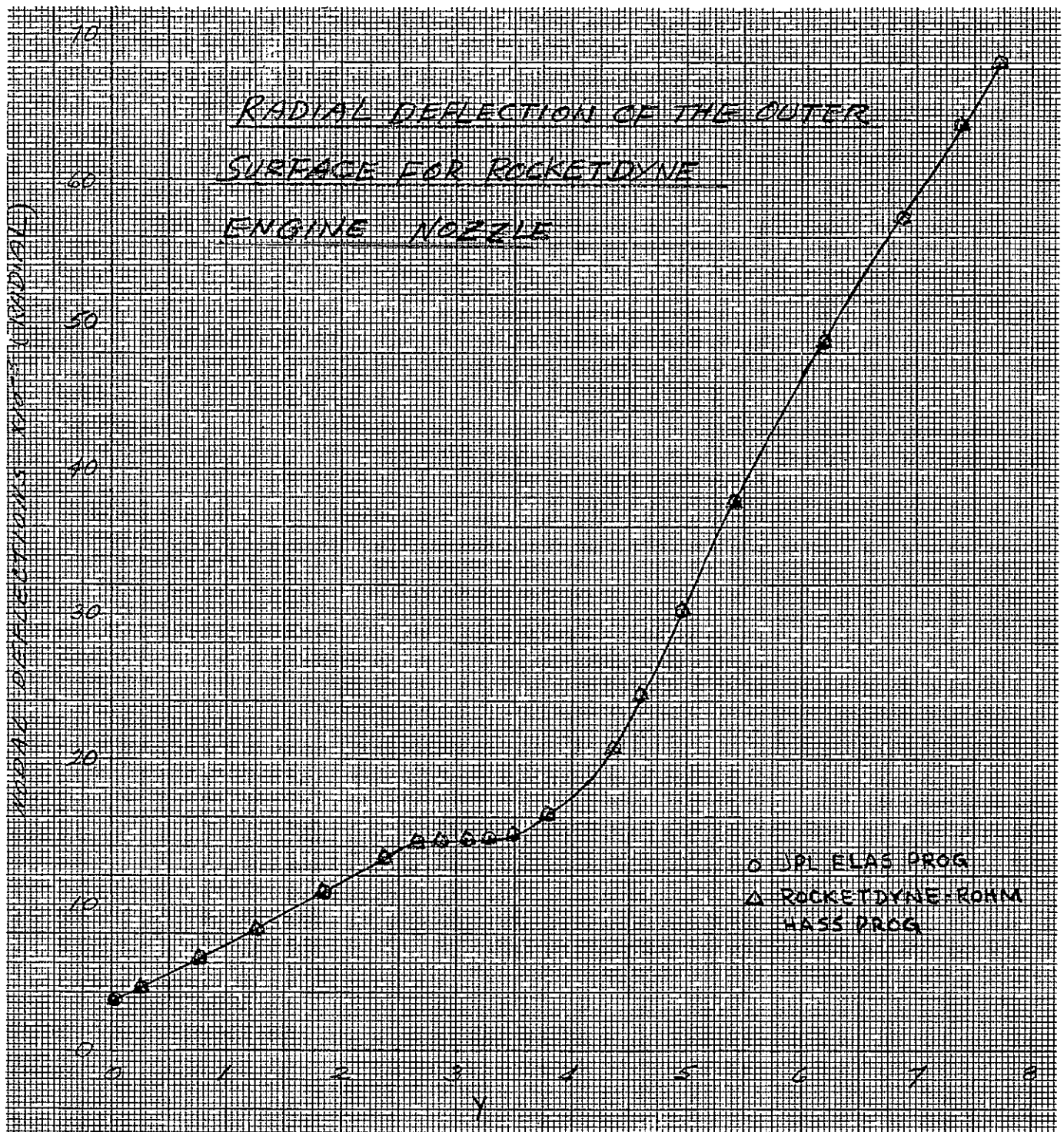


Figure 9. Radial Deflection of the Outer Surface for Rocketdyne Engine Nozzle

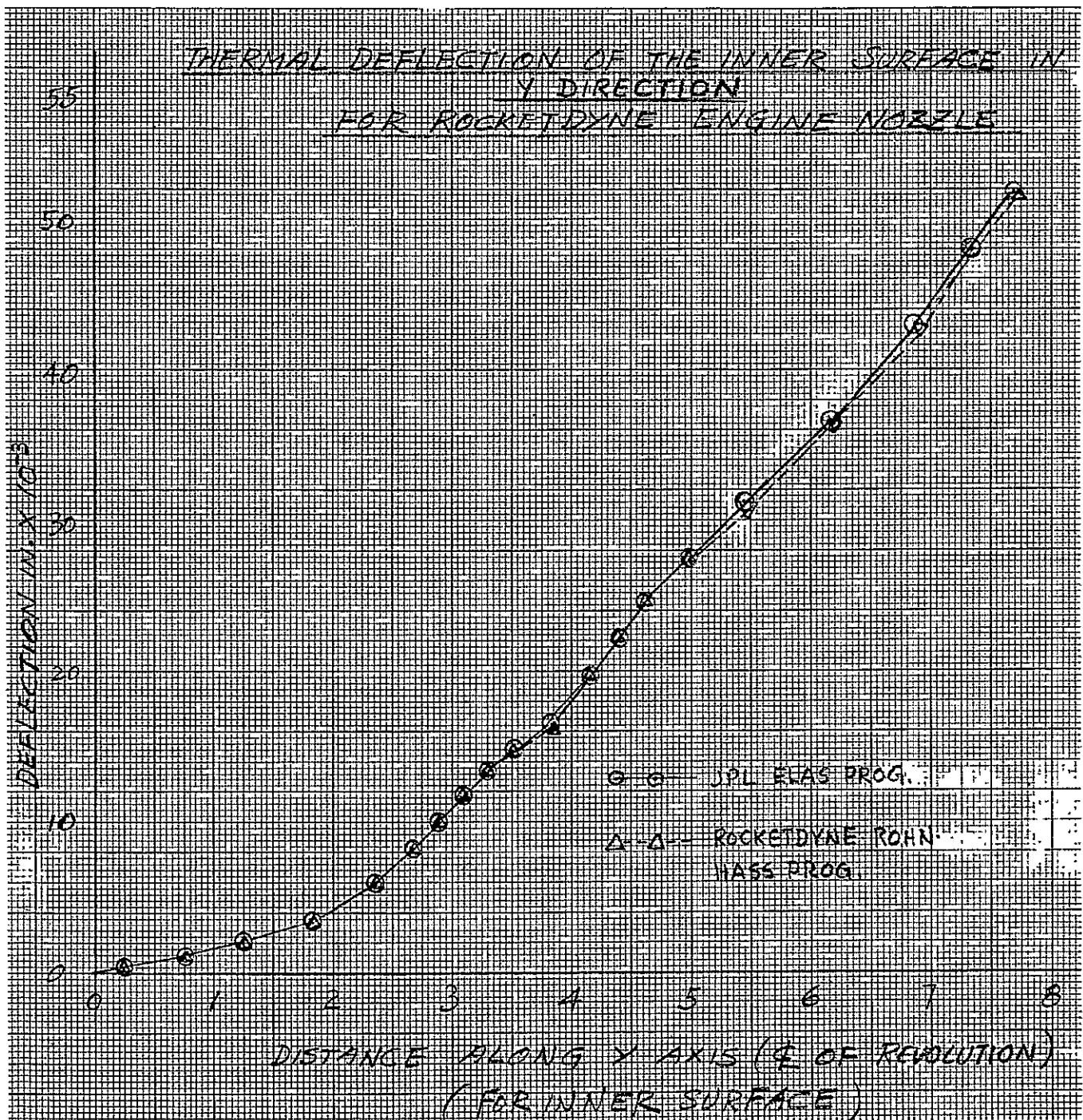


Figure 10. Thermal Deflection of the Inner Surface in Y Direction
for Rocketdyne Engine Nozzle

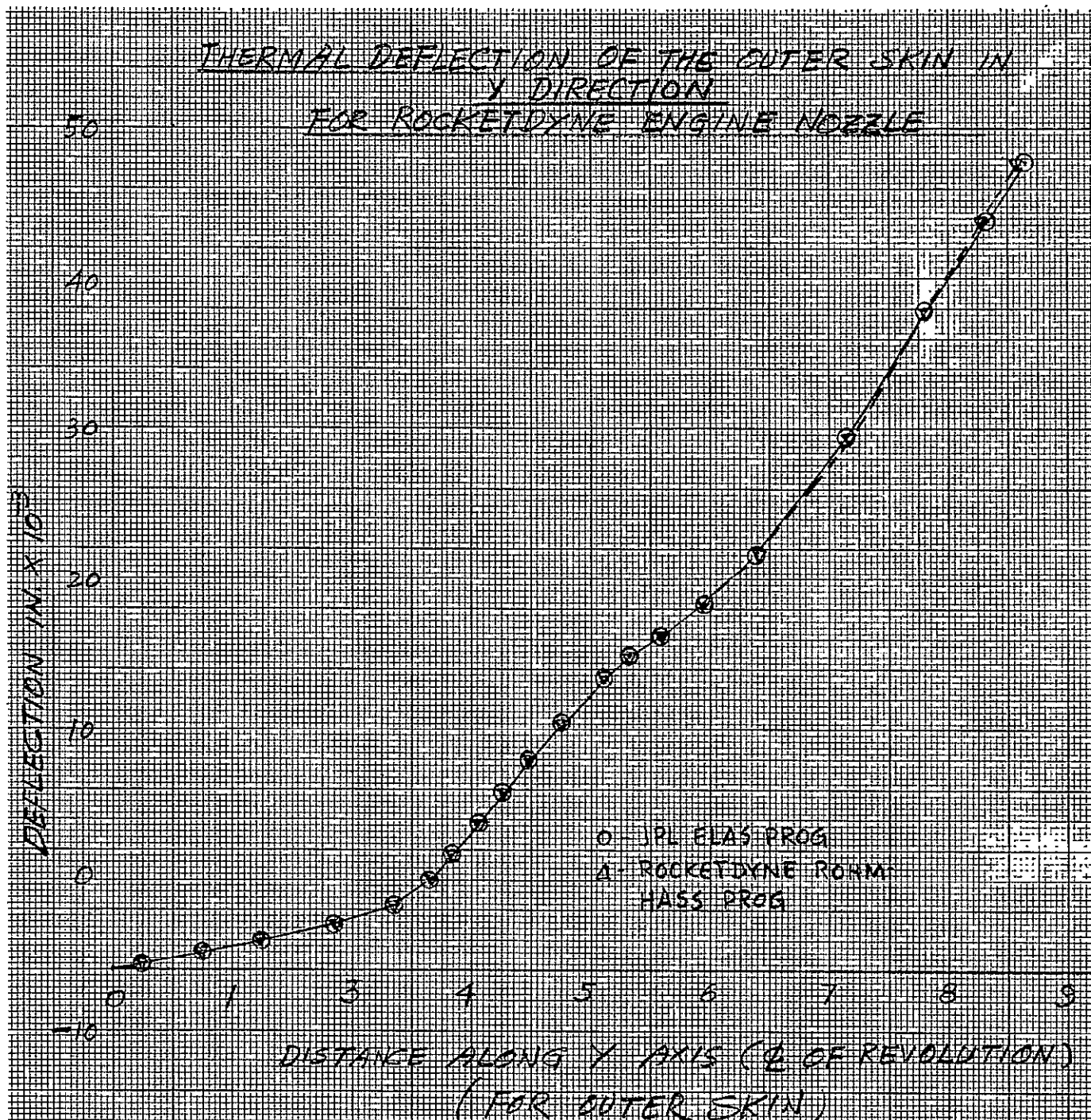


Figure 11. Thermal Deflection of the Outer Skin in Y Direction for Rocketdyne Engine Nozzle

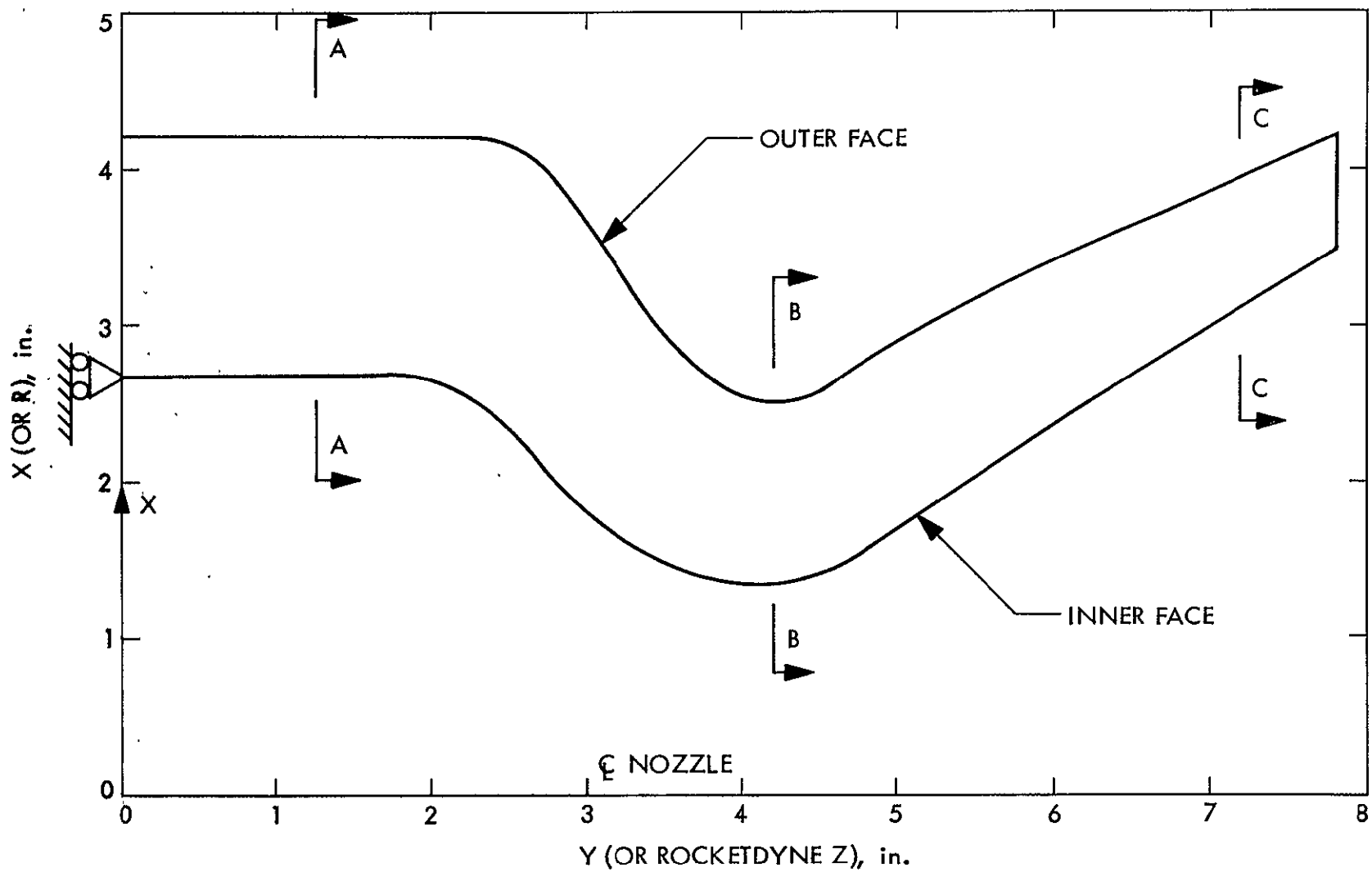
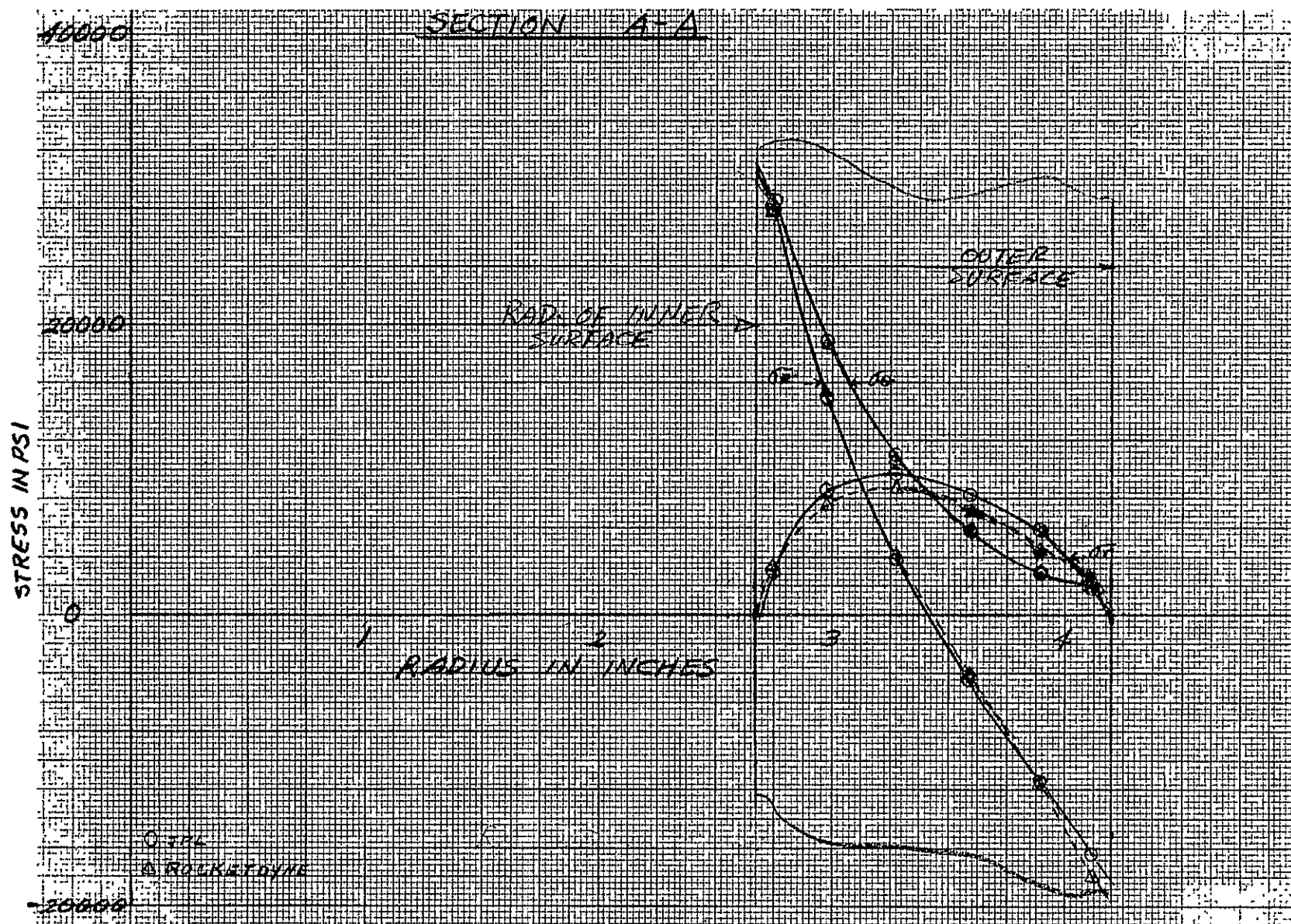


Figure 12. Longitudinal Section of Rocketdyne Engine Nozzle



NOTE: Rocketdyne Program Computed the Stress on each Element; while JPL Program Computed Stress at Node Points. The JPL Plotting Point is the Average of Four Corners of each Element.

Figure 13. Rocketdyne Engine Nozzle, Section A-A

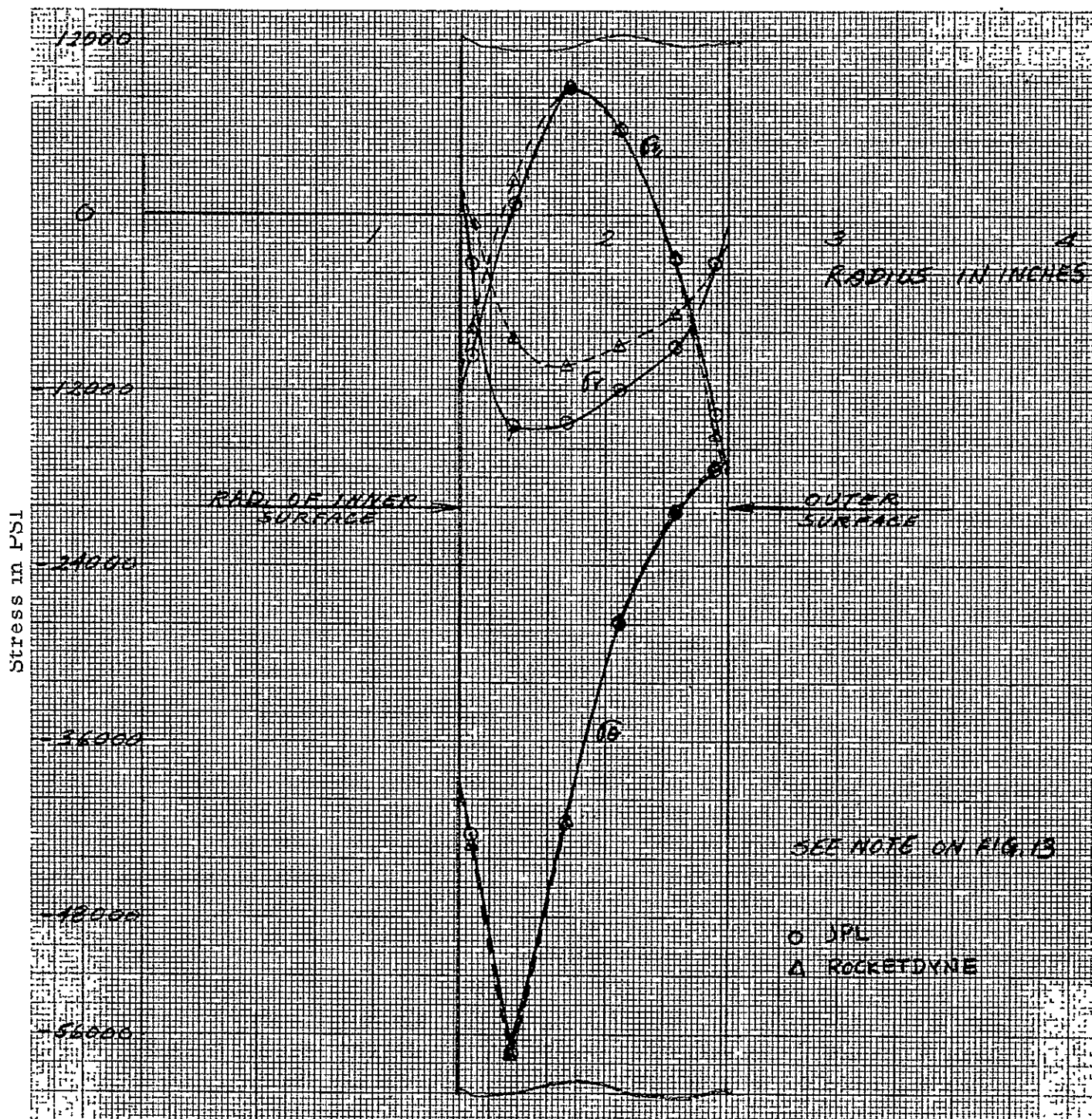


Figure 14. Rocket Engine Nozzle, Section B-B

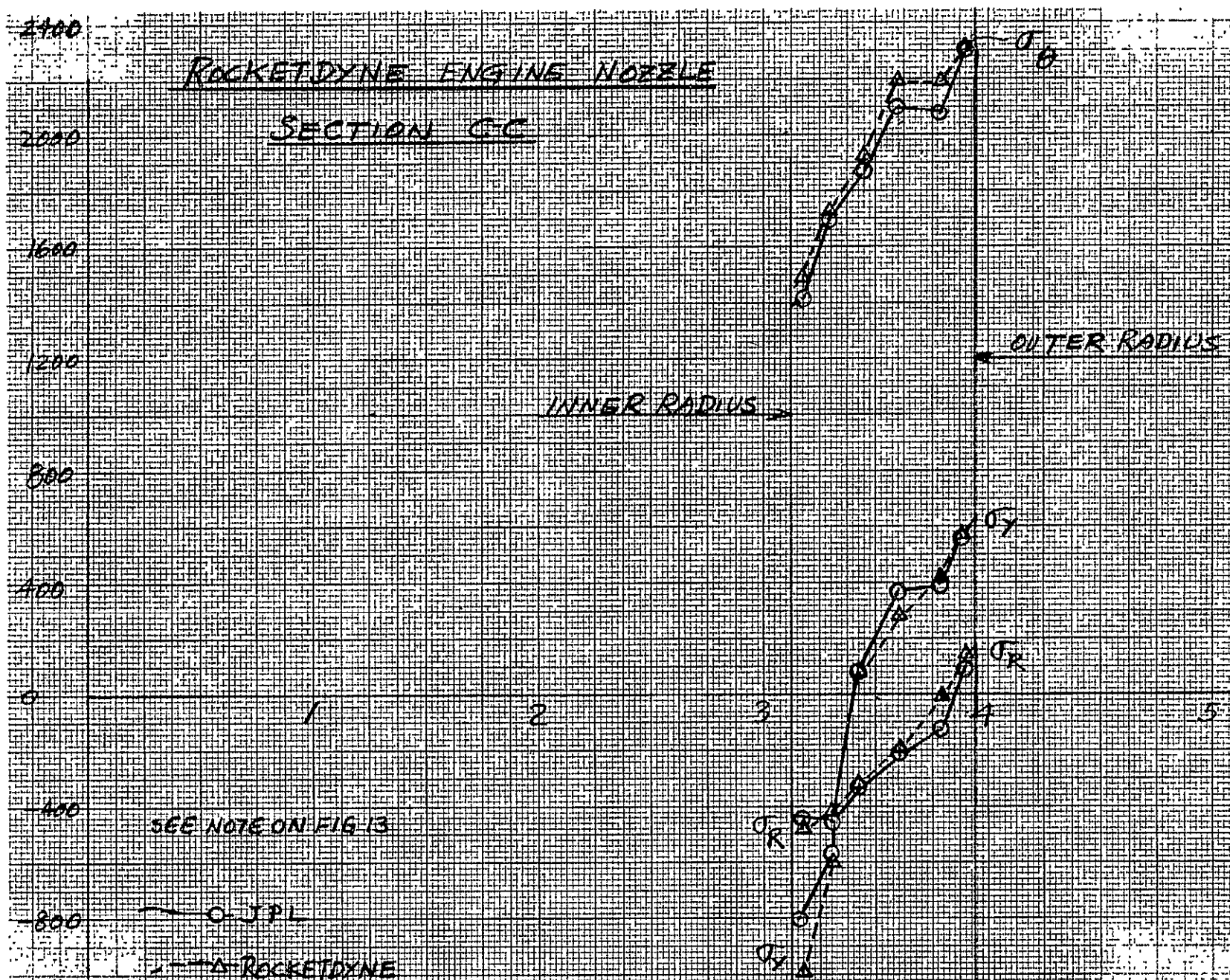


Figure 15. Rocketdyne Engine Nozzle, Section C-C

The solutions of samples provided confidence in ELAS.

EXAMPLE PROBLEM

A typical example is the evaluation of the thermal distortion of a mirror subjected to a 3°F rise from inside to outside in the fluid used to cool the mirror. As shown on Figure 16, the fluid passed through the cooling holes in the center of the mirror. Because of geometric and loading axisymmetry, only one-half of any mirror cross-section adequately defines its structural behavior.

As shown in Figure 16, the mirror is idealized by 247 nodes and 190 finite elements. The temperatures for each element were obtained from the temperature control computer program defined in Appendix C.

A sample computer output describes in detail the necessary input and the available output. The explanation of significant values are:

- (1) Table 8 with the title of the analysis GREGORIAN PRIMARY MIRROR summarizes the control parameters.
- (2) Table 9 titled MATERIAL PROPERTIES, defines the material properties of the U.L.E. fused silica used for the analysis. Note that the properties are assumed constant over the temperature range for this particular problem. Also in Table 9, TEMPERATURE INCREASE TYPES defines the total different temperature increases in the finite elements used for the analysis.
- (3) Table 10 defines NODAL COORDINATES as the X and Y locations of each node.
- (4) Table 11 defines the MESH TOPOLOGY as the definition of each finite element. Each finite element is completely defined by the node points which define the element as well as the material characteristics and temperature changes.
- (5) Table 12 gives the NODAL DEFLECTION output. For each node the displacement along the X and Y axes are given.

Table 8. Linear Elasticity Problem

GREGORIAN PRIMARY MIRROR			
TOTAL NUMBER OF NODES	247		
TOTAL NUMBER OF FINITE ELEMENTS	190		
DEGREES OF FREEDOM AT A NODE	2		
ITYPE VALUE	0	0 FOR ISOTROPIC, 1 FOR ORTHOTROPIC, 2 FOR GENERAL MATERIAL	
IGEM VALUE	0	0 FOR 2-, 1 FOR 3-DIMENSIONAL STRUCTURES	
ISTR VALUE	0	1 FOR PLANE STRAIN CASE, 0 OTHERWISE	
MAXIMUM NUMBER OF CONTACTS IN AN ELEMENT	4		
CONTACT NUMBER INCLUDING DUMMIES	7		
IBN VALUE	10	NUMBER OF SUPRESSED DEGREES OF FREEDOM IF NO MULTIPLE CONNECTIONS	
TOTAL NUMBER OF CONCENTRATED LOADS	0		
PRESSURE TYPES	0		
MATERIAL TYPES	1		
THICKNESS TYPES	0		
TEMPERATURE CHANGE TYPES	.99		
TEMPERATURE GRADIENT TYPES ALONG Y	-0		
TEMPERATURE GRADIENT TYPES ALONG Z	-0		
AREA TYPES	-0		
TORSION CONSTANT TYPES	-0		
Y MOMENT OF INERTIA TYPES	-0		
Z MOMENT OF INERTIA TYPES	-0		
NUMBER OF ANGLES FIXING PRINCIPAL AXES	-0		
INX VALUE	4	NUMBER OF THE LINK FROM WHICH RETURN-TO-BEGINNING IS MADE	
INP VALUE	1	0 MINIMUM PRINT, 1 PARTIAL PRINT, 2 COMPLETE PRINT	
ISHUF VALUE	1	0 NO RELABELLING, 1 RELABEL, 2 OR 3 READ CARDS FOR RELABELLING	
ICOR VALUE	-0	0 READ CARDS, 1 CALL SUBROUTINE CORG FOR COORDINATES	
IBON VALUE	-0	0 READ CARDS, 1 CALL SUBROUTINE BUNG FOR BOUNDARY CONDITIONS	
IMES VALUE	-0	0 READ CARDS, 1 CALL SUBROUTINE MESG FOR MESH TOPOLOGY	
IPIR VALUE FOR SHELL LOCAL NODAL AXES	-0	0 ASSUME ZERO, 1 COMPUTE AS PRINCIPAL, 2 READ AS INPUT	
CHAIN PROGRAM TAPE NUMBER	2		
SCRATCH TAPE NUMBER	3	0 OR - DO NOT COMPUTE RESIDUALS, OTHERWISE COMPUTE	
ACCELERATION*UNIT MASS	-0.		
DIRECTION COSINES OF ACCELERATION	-0.	-0.	-0.

Table 9. Material Properties

MATERIAL PROPERTIES									
TP	E	G	ALPHA	TP	E	G	ALPHA		
1	0.98000E 07	0.42000E 07	0.28000E-07						
TEMPERATURE INCREASE TYPES									
1	0.29800E 01	2	0.30200E 01	3	0.30900E 01	4	0.32200E 01	5	0.32500E 01
6	0.32800E 01	7	0.33000E 01	8	0.33400E 01	9	0.34000E 01	10	0.34300E 01
11	0.34600E 01	12	0.35200E 01	13	0.35600E 01	14	0.36100E 01	15	0.36500E 01
16	0.37100E 01	17	0.37400E 01	18	0.37700E 01	19	0.38100E 01	20	0.38500E 01
21	0.39000E 01	22	0.39300E 01	23	0.39500E 01	24	0.39800E 01	25	0.40100E 01
26	0.41100E 01	27	0.41400E 01	28	0.41600E 01	29	0.41900E 01	30	0.42100E 01
31	0.42400E 01	32	0.43100E 01	33	0.43300E 01	34	0.43700E 01	35	0.44300E 01
36	0.44600E 01	37	0.45100E 01	38	0.45300E 01	39	0.45800E 01	40	0.46400E 01
41	0.46700E 01	42	0.47100E 01	43	0.47600E 01	44	0.47800E 01	45	0.48200E 01
46	0.48600E 01	47	0.49000E 01	48	0.49300E 01	49	0.49600E 01	50	0.50200E 01
51	0.50800E 01	52	0.51400E 01	53	0.51700E 01	54	0.52100E 01	55	0.53300E 01
56	0.53700E 01	57	0.54000E 01	58	0.54500E 01	59	0.55600E 01	60	0.56000E 01
61	0.56300E 01	62	0.56600E 01	63	0.57000E 01	64	0.57700E 01	65	0.57900E 01
66	0.59100E 01	67	0.59500E 01	68	0.59900E 01	69	0.60400E 01	70	0.61400E 01
71	0.62200E 01	72	0.62600E 01	73	0.63300E 01	74	0.63800E 01	75	0.64100E 01
76	0.64600E 01	77	0.64900E 01	78	0.65600E 01	79	0.66000E 01	80	0.66500E 01
81	0.67400E 01	82	0.67800E 01	83	0.68400E 01	84	0.68900E 01	85	0.69200E 01
86	0.70300E 01	87	0.70700E 01	88	0.72400E 01	89	0.72800E 01	90	0.73000E 01
91	0.73300E 01	92	0.73800E 01	93	0.74800E 01	94	0.76600E 01	95	0.77100E 01
96	0.79400E 01	97	0.81700E 01	98	0.82200E 01	99	0.83400E 01		

Table 10. Nodal Coordinates

NODE	X	Y	Z	NODE	X	Y	Z
1	0.	0.20000E 01	0.	2	0.	0.23800E 01	0.
3	0.	0.26100E 01	0.	4	0.	0.27600E 01	0.
5	0.	0.28800E 01	0.	6	0.	0.30000E 01	0.
7	0.14000E 01	0.20000E 01	0.	8	0.14000E 01	0.24300E 01	0.
9	0.14000E 01	0.26600E 01	0.	10	0.14000E 01	0.28000E 01	0.
11	0.14000E 01	0.29300E 01	0.	12	0.14000E 01	0.30500E 01	0.
13	0.18000E 01	0.20000E 01	0.	14	0.18000E 01	0.24400E 01	0.
15	0.18000E 01	0.26750E 01	0.	16	0.18000E 01	0.28100E 01	0.
17	0.18000E 01	0.29400E 01	0.	18	0.18000E 01	0.30600E 01	0.
19	0.	-0.58400E 00	0.	20	0.	0.22600E-00	0.
21	0.20000E 01	0.12200E 01	0.	22	0.20000E 01	0.20000E 01	0.
23	0.20000E 01	0.24500E 01	0.	24	0.20000E 01	0.26800E 01	0.
25	0.20000E 01	0.28200E 01	0.	26	0.20000E 01	0.29500E 01	0.
27	0.20000E 01	0.30700E 01	0.	28	0.	0.12200E 01	0.
29	0.14000E 01	-0.58400E 00	0.	30	0.24000E 01	0.12550E 01	0.
31	0.24000E 01	0.20000E 01	0.	32	0.24000E 01	0.24650E 01	0.
33	0.24000E 01	0.27000E 01	0.	34	0.24000E 01	0.28350E 01	0.
35	0.24000E 01	0.29650E 01	0.	36	0.24000E 01	0.30800E 01	0.
37	0.14000E 01	0.22600E-00	0.	38	0.14000E 01	0.12200E 01	0.
39	0.28200E 01	0.13050E 01	0.	40	0.28200E 01	0.20000E 01	0.
41	0.28200E 01	0.24800E 01	0.	42	0.28200E 01	0.27100E 01	0.
43	0.28200E 01	0.28500E 01	0.	44	0.28200E 01	0.29800E 01	0.
45	0.28200E 01	0.30500E 01	0.	46	0.18000E 01	-0.58400E 00	0.
47	0.18000E 01	0.22600E-00	0.	48	0.30400E 01	0.13700E 01	0.
49	0.30400E 01	0.20000E 01	0.	50	0.30400E 01	0.24900E 01	0.
51	0.30400E 01	0.27250E 01	0.	52	0.30400E 01	0.28550E 01	0.
53	0.30400E 01	0.29850E 01	0.	54	0.30400E 01	0.31000E 01	0.
55	0.18000E 01	0.12200E 01	0.	56	0.20000E 01	-0.58400E 00	0.
57	0.20000E 01	0.10000E-00	0.	58	0.20000E 01	0.36000E-00	0.
59	0.35700E 01	0.13900E 01	0.	60	0.35700E 01	0.20000E 01	0.
61	0.35700E 01	0.25100E 01	0.	62	0.35700E 01	0.27350E 01	0.
63	0.35700E 01	0.28700E 01	0.	64	0.35700E 01	0.30000E 01	0.
65	0.35700E 01	0.31200E 01	0.	66	0.37900E 01	0.14200E 01	0.
67	0.37900E 01	0.20000E 01	0.	68	0.37900E 01	0.25200E 01	0.
69	0.37900E 01	0.27400E 01	0.	70	0.37900E 01	0.28800E 01	0.
71	0.37900E 01	0.30100E 01	0.	72	0.37900E 01	0.31250E 01	0.
73	0.43200E 01	0.14750E 01	0.	74	0.43200E 01	0.20000E 01	0.
75	0.43200E 01	0.25300E 01	0.	76	0.43200E 01	0.27600E 01	0.
77	0.43200E 01	0.29000E 01	0.	78	0.43200E 01	0.30300E 01	0.
79	0.43200E 01	0.31450E 01	0.	80	0.45400E 01	0.15000E 01	0.
81	0.45400E 01	0.20200E 01	0.	82	0.45400E 01	0.25400E 01	0.
83	0.45400E 01	0.27650E 01	0.	84	0.45400E 01	0.29000E 01	0.
85	0.45400E 01	0.30300E 01	0.	86	0.45400E 01	0.31500E 01	0.
87	0.50700E 01	0.15600E 01	0.	88	0.50700E 01	0.20500E 01	0.
89	0.50700E 01	0.25550E 01	0.	90	0.50700E 01	0.27800E 01	0.
91	0.50700E 01	0.29200E 01	0.	92	0.50700E 01	0.30500E 01	0.
93	0.50700E 01	0.31700E 01	0.	94	0.52900E 01	0.15800E 01	0.
95	0.52900E 01	0.20700E 01	0.	96	0.52900E 01	0.25600E 01	0.
97	0.52900E 01	0.27950E 01	0.	98	0.52900E 01	0.29200E 01	0.
99	0.52900E 01	0.30600E 01	0.	100	0.52900E 01	0.31800E 01	0.
101	0.58200E 01	0.16400E 01	0.	102	0.58200E 01	0.21050E 01	0.

Table 10. Nodal Coordinates (Contd)

103	0.58200E 01	0.25750E 01	0.	104	0.58200E 01	0.28150E 01	0.
105	0.58200E 01	0.29400E 01	0.	106	0.58200E 01	0.30750E 01	0.
107	0.58200E 01	0.31900E 01	0.	108	0.60400E 01	0.16600E 01	0.
109	0.60400E 01	0.21200E 01	0.	110	0.60400E 01	0.25800E 01	0.
111	0.60400E 01	0.28200E 01	0.	112	0.60400E 01	0.29450E 01	0.
113	0.60400E 01	0.30800E 01	0.	114	0.60400E 01	0.32000E 01	0.
115	0.65700E 01	0.17200E 01	0.	116	0.65700E 01	0.21600E 01	0.
117	0.65700E 01	0.26000E 01	0.	118	0.65700E 01	0.28350E 01	0.
119	0.65700E 01	0.29600E 01	0.	120	0.65700E 01	0.31000E 01	0.
121	0.65700E 01	0.32160E 01	0.	122	0.67900E 01	0.17400E 01	0.
123	0.67900E 01	0.21790E 01	0.	124	0.67900E 01	0.26100E 01	0.
125	0.67900E 01	0.28450E 01	0.	126	0.67900E 01	0.29700E 01	0.
127	0.67900E 01	0.31050E 01	0.	128	0.67900E 01	0.32200E 01	0.
129	0.73200E 01	0.18000E 01	0.	130	0.73200E 01	0.22150E 01	0.
131	0.73200E 01	0.26300E 01	0.	132	0.73200E 01	0.28600E 01	0.
133	0.73200E 01	0.29800E 01	0.	134	0.73200E 01	0.31200E 01	0.
135	0.73200E 01	0.32400E 01	0.	136	0.75400E 01	0.18200E 01	0.
137	0.75400E 01	0.22300E 01	0.	138	0.75400E 01	0.26400E 01	0.
139	0.75400E 01	0.28620E 01	0.	140	0.75400E 01	0.29900E 01	0.
141	0.75400E 01	0.31250E 01	0.	142	0.75400E 01	0.32450E 01	0.
143	0.80700E 01	0.18800E 01	0.	144	0.80700E 01	0.22650E 01	0.
145	0.80700E 01	0.26550E 01	0.	146	0.80700E 01	0.28800E 01	0.
147	0.80700E 01	0.30050E 01	0.	148	0.80700E 01	0.31400E 01	0.
149	0.80700E 01	0.32600E 01	0.	150	0.82900E 01	0.19000E 01	0.
151	0.82900E 01	0.22800E 01	0.	152	0.82900E 01	0.26600E 01	0.
153	0.82900E 01	0.28850E 01	0.	154	0.82900E 01	0.30150E 01	0.
155	0.82900E 01	0.31450E 01	0.	156	0.82900E 01	0.32700E 01	0.
157	0.88200E 01	0.19600E 01	0.	158	0.88200E 01	0.23150E 01	0.
159	0.88200E 01	0.26750E 01	0.	160	0.88200E 01	0.29000E 01	0.
161	0.88200E 01	0.30250E 01	0.	162	0.88200E 01	0.31600E 01	0.
163	0.88200E 01	0.32850E 01	0.	164	0.90400E 01	0.19850E 01	0.
165	0.90400E 01	0.23300E 01	0.	166	0.90400E 01	0.26800E 01	0.
167	0.90400E 01	0.29100E 01	0.	168	0.90400E 01	0.30350E 01	0.
169	0.90400E 01	0.31700E 01	0.	170	0.90400E 01	0.32950E 01	0.
171	0.95700E 01	0.20400E 01	0.	172	0.95700E 01	0.23700E 01	0.
173	0.95700E 01	0.26950E 01	0.	174	0.95700E 01	0.29200E 01	0.
175	0.95700E 01	0.30500E 01	0.	176	0.95700E 01	0.31800E 01	0.
177	0.95700E 01	0.33100E 01	0.	178	0.97900E 01	0.20600E 01	0.
179	0.97900E 01	0.23800E 01	0.	180	0.97900E 01	0.27000E 01	0.
181	0.97900E 01	0.29300E 01	0.	182	0.97900E 01	0.30600E 01	0.
183	0.97900E 01	0.31900E 01	0.	184	0.97900E 01	0.33200E 01	0.
185	0.10320E 02	0.21200E 01	0.	186	0.10320E 02	0.24200E 01	0.
187	0.10320E 02	0.27150E 01	0.	188	0.10320E 02	0.29400E 01	0.
189	0.10320E 02	0.30750E 01	0.	190	0.10320E 02	0.32050E 01	0.
191	0.10320E 02	0.33350E 01	0.	192	0.10540E 02	0.21400E 01	0.
193	0.10540E 02	0.24350E 01	0.	194	0.10540E 02	0.27200E 01	0.
195	0.10540E 02	0.29500E 01	0.	196	0.10540E 02	0.30800E 01	0.
197	0.10540E 02	0.32150E 01	0.	198	0.10540E 02	0.33400E 01	0.
199	0.11070E 02	0.22000E 01	0.	200	0.11070E 02	0.24700E 01	0.
201	0.11070E 02	0.27400E 01	0.	202	0.11070E 02	0.29650E 01	0.

Table 10. Nodal Coordinates (Contd)

203	0.11070E 02	0.30950E 01	0.	204	0.11070E 02	0.32300E 01	0.
205	0.11070E 02	0.33500E 01	0.	206	0.11290E 02	0.22250E 01	0.
207	0.11290E 02	0.24800E 01	0.	208	0.11290E 02	0.27450E 01	0.
209	0.11290E 02	0.29700E 01	0.	210	0.11290E 02	0.31000E 01	0.
211	0.11290E 02	0.32350E 01	0.	212	0.11290E 02	0.33600E 01	0.
213	0.11820E 02	0.22800E 01	0.	214	0.11820E 02	0.25200E 01	0.
215	0.11820E 02	0.27600E 01	0.	216	0.11820E 02	0.29900E 01	0.
217	0.11820E 02	0.31150E 01	0.	218	0.11820E 02	0.32500E 01	0.
219	0.11820E 02	0.33800E 01	0.	220	0.12040E 02	0.23050E 01	0.
221	0.12040E 02	0.25350E 01	0.	222	0.12040E 02	0.27650E 01	0.
223	0.12040E 02	0.30000E 01	0.	224	0.12040E 02	0.31200E 01	0.
225	0.12040E 02	0.32600E 01	0.	226	0.12040E 02	0.33850E 01	0.
227	0.12570E 02	0.23600E 01	0.	228	0.12570E 02	0.25750E 01	0.
229	0.12570E 02	0.27800E 01	0.	230	0.12570E 02	0.30150E 01	0.
231	0.12570E 02	0.31400E 01	0.	232	0.12570E 02	0.32700E 01	0.
233	0.12570E 02	0.34000E 01	0.	234	0.12790E 02	0.23850E 01	0.
235	0.12790E 02	0.25900E 01	0.	236	0.12790E 02	0.27950E 01	0.
237	0.12790E 02	0.30200E 01	0.	238	0.12790E 02	0.31420E 01	0.
239	0.12790E 02	0.32750E 01	0.	240	0.12790E 02	0.34100E 01	0.
241	0.12920E 02	0.24000E 01	0.	242	0.13060E 02	0.26000E 01	0.
243	0.13060E 02	0.28000E 01	0.	244	0.13060E 02	0.30250E 01	0.
245	0.13060E 02	0.31500E 01	0.	246	0.13060E 02	0.32800E 01	0.
247	0.12920E 02	0.34150E 01	0.				

Table 11. Mesh Topology and Element Property Types

MESH TOPOLOGY									ELEMENT PROPERTY TYPES											
EL NO	ND-1	ND-2	ND-3	ND-4	ND-5	ND-6	ND-7	ND-8	ELMT	PRES	MTRL	THCK	DTMP	TGDY	TGOZ	AREA	I-XX	I-YY	I-ZZ	FI-Y
1	1	7	8	2	0	0	0	0	16	0	1	0	21	0	-0	0	0	0.	0	0
2	2	8	9	3	0	0	0	0	16	0	1	0	22	0	-0	0	0	0	0	0
3	3	9	10	4	0	0	0	0	16	0	1	0	23	0	-0	0	0	0	0	0
4	4	10	11	5	0	0	0	0	16	0	1	0	23	0	-0	0	0	0	0	0
5	5	11	12	6	0	0	0	0	16	0	1	0	23	0	-0	0	0	0	0	0
6	7	13	14	8	0	0	0	0	16	0	1	0	23	0	-0	0	0	0	0	0
7	8	14	15	9	0	0	0	0	16	0	1	0	26	0	-0	0	0	0	0	0
8	9	15	16	10	0	0	0	0	16	0	1	0	29	0	-0	0	0	0	0	0
9	10	16	17	11	0	0	0	0	16	0	1	0	30	0	-0	0	0	0	0	0
10	11	17	18	12	0	0	0	0	16	0	1	0	31	0	-0	0	0	0	0	0
11	13	22	23	14	0	0	0	0	16	0	1	0	22	0	-0	0	0	0	0	0
12	14	23	24	15	0	0	0	0	16	0	1	0	28	0	-0	0	0	0	0	0
13	15	24	25	16	0	0	0	0	16	0	1	0	32	0	-0	0	0	0	0	0
14	16	25	26	17	0	0	0	0	16	0	1	0	34	0	-0	0	0	0	0	0
15	17	26	27	18	0	0	0	0	16	0	1	0	35	0	-0	0	0	0	0	0
16	19	29	37	20	0	0	0	0	16	0	1	0	19	0	-0	0	0	0	0	0
17	20	37	38	28	0	0	0	0	16	0	1	0	19	0	-0	0	0	0	0	0
18	21	30	31	22	0	0	0	0	16	0	1	0	15	0	-0	0	0	0	0	0
19	22	31	32	23	0	0	0	0	16	0	1	0	20	0	-0	0	0	0	0	0
20	23	32	33	24	0	0	0	0	16	0	1	0	30	0	-0	0	0	0	0	0
21	24	33	34	25	0	0	0	0	16	0	1	0	36	0	-0	0	0	0	0	0
22	25	34	35	26	0	0	0	0	16	0	1	0	40	0	-0	0	0	0	0	0
23	26	35	36	27	0	0	0	0	16	0	1	0	43	0	-0	0	0	0	0	0
24	28	38	7	1	0	0	0	0	16	0	1	0	20	0	-0	0	0	0	0	0
25	29	46	47	37	0	0	0	0	16	0	1	0	18	0	-0	0	0	0	0	0
26	30	39	40	31	0	0	0	0	16	0	1	0	12	0	-0	0	0	0	0	0
27	31	40	41	32	0	0	0	0	16	0	1	0	13	0	-0	0	0	0	0	0
28	32	41	42	33	0	0	0	0	16	0	1	0	24	0	-0	0	0	0	0	0
29	33	42	43	34	0	0	0	0	16	0	1	0	43	0	-0	0	0	0	0	0
30	34	43	44	35	0	0	0	0	16	0	1	0	58	0	-0	0	0	0	0	0
31	35	44	45	36	0	0	0	0	16	0	1	0	71	0	-0	0	0	0	0	0
32	37	47	55	38	0	0	0	0	16	0	1	0	18	0	-0	0	0	0	0	0
33	38	55	13	7	0	0	0	0	16	0	1	0	18	0	-0	0	0	0	0	0
34	39	48	49	40	0	0	0	0	16	0	1	0	9	0	-0	0	0	0	0	0
35	40	49	50	41	0	0	0	0	16	0	1	0	3	0	-0	0	0	0	0	0
36	42	51	52	43	0	0	0	0	16	0	1	0	33	0	-0	0	0	0	0	0
37	43	52	53	44	0	0	0	0	16	0	1	0	55	0	-0	0	0	0	0	0
38	44	53	54	45	0	0	0	0	16	0	1	0	72	0	-0	0	0	0	0	0
39	46	56	57	47	0	0	0	0	16	0	1	0	18	0	-0	0	0	0	0	0
40	47	58	21	55	0	0	0	0	16	0	1	0	18	0	-0	0	0	0	0	0
41	55	21	22	13	0	0	0	0	16	0	1	0	16	0	-0	0	0	0	0	0
42	48	59	60	49	0	0	0	0	16	0	1	0	7	0	-0	0	0	0	0	0
43	49	60	61	50	0	0	0	0	16	0	1	0	6	0	-0	0	0	0	0	0
44	50	61	62	51	0	0	0	0	16	0	1	0	16	0	-0	0	0	0	0	0
45	51	62	63	52	0	0	0	0	16	0	1	0	43	0	-0	0	0	0	0	0
46	52	63	64	53	0	0	0	0	16	0	1	0	60	0	-0	0	0	0	0	0
47	53	64	65	54	0	0	0	0	16	0	1	0	76	0	-0	0	0	0	0	0
48	59	66	67	60	0	0	0	0	16	0	1	0	5	0	-0	0	0	0	0	0
49	60	67	68	51	0	0	0	0	16	0	1	0	1	0	-0	0	0	0	0	0
50	62	69	70	63	0	0	0	0	16	0	1	0	36	0	-0	0	0	0	0	0
51	63	70	71	64	0	0	0	0	16	0	1	0	58	0	-0	0	0	0	0	0
52	64	71	72	65	0	0	0	0	16	0	1	0	75	0	-0	0	0	0	0	0

Table 11. Mesh Topology and Element Property Types (Contd).

53	66	73	74	67	0	0	0	C	16	0	1	0	5	0	-0	0	0	0	0	0
54	67	74	75	68	0	0	0	C	16	0	1	0	6	0	-0	0	0	0	0	0
55	68	75	76	69	0	0	0	C	16	0	1	0	19	0	-0	0	0	0	0	0
56	69	76	77	70	0	0	0	C	16	0	1	0	46	0	-0	0	0	0	0	0
57	70	77	78	71	0	0	0	C	16	0	1	0	63	0	-0	0	0	0	0	0
58	71	78	79	72	0	0	0	C	16	0	1	0	78	0	-0	0	0	0	0	0
59	73	80	81	74	0	0	0	C	16	0	1	0	5	0	-0	0	0	0	0	0
60	74	81	82	75	0	0	0	C	16	0	1	0	2	0	-0	0	0	0	0	0
61	76	83	84	77	0	0	0	C	16	0	1	0	38	0	-0	0	0	0	0	0
62	77	84	85	78	0	0	0	C	16	0	1	0	59	0	-0	0	0	0	0	0
63	78	85	86	79	0	0	0	C	16	0	1	0	77	0	-0	0	0	0	0	0
64	80	87	88	81	0	0	0	C	16	0	1	0	6	0	-0	0	0	0	0	0
65	81	88	89	82	0	0	0	C	16	0	1	0	8	0	-0	0	0	0	0	0
66	82	89	90	83	0	0	0	C	16	0	1	0	21	0	-0	0	0	0	0	0
67	83	90	91	84	0	0	0	C	16	0	1	0	49	0	-0	0	0	0	0	0
68	84	91	92	85	0	0	0	C	16	0	1	0	65	0	-0	0	0	0	0	0
69	85	92	93	86	0	0	0	C	16	0	1	0	80	0	-0	0	0	0	0	0
70	87	94	95	88	0	0	0	C	16	0	1	0	7	0	-0	0	0	0	0	0
71	88	95	96	89	0	0	0	C	16	0	1	0	3	0	-0	0	0	0	0	0
72	90	97	98	91	0	0	0	C	16	0	1	0	40	0	-0	0	0	0	0	0
73	91	98	99	92	0	0	0	C	16	0	1	0	62	0	-0	0	0	0	0	0
74	92	99	100	93	0	0	0	C	16	0	1	0	79	0	-0	0	0	0	0	0
75	94	101	102	95	0	0	0	C	16	0	1	0	9	0	-0	0	0	0	0	0
76	95	102	103	96	0	0	0	C	16	0	1	0	11	0	-0	0	0	0	0	0
77	96	103	104	97	0	0	0	C	16	0	1	0	25	0	-0	0	0	0	0	0
78	97	104	105	98	0	0	0	C	16	0	1	0	51	0	-0	0	0	0	0	0
79	98	105	106	99	0	0	0	C	16	0	1	0	66	0	-0	0	0	0	0	0
80	99	106	107	100	0	0	0	C	16	0	1	0	82	0	-0	0	0	0	0	0
81	101	108	109	102	0	0	0	C	16	0	1	0	10	0	-0	0	0	0	0	0
82	102	109	110	103	0	0	0	C	16	0	1	0	4	0	-0	0	0	0	0	0
83	104	111	112	105	0	0	0	C	16	0	1	0	44	0	-0	0	0	0	0	0
84	105	112	113	106	0	0	0	C	16	0	1	0	65	0	-0	0	0	0	0	0
85	106	113	114	107	0	0	0	C	16	0	1	0	81	0	-0	0	0	0	0	0
86	108	115	116	109	0	0	0	C	16	0	1	0	12	0	-0	0	0	0	0	0
87	109	116	117	110	0	0	0	C	16	0	1	0	14	0	-0	0	0	0	0	0
88	110	117	118	111	0	0	0	C	16	0	1	0	28	0	-0	0	0	0	0	0
89	111	118	119	112	0	0	0	C	16	0	1	0	54	0	-0	0	0	0	0	0
90	112	119	120	113	0	0	0	C	16	0	1	0	69	0	-0	0	0	0	0	0
91	113	120	121	114	0	0	0	C	16	0	1	0	85	0	-0	0	0	0	0	0
92	115	122	123	116	0	0	0	C	16	0	1	0	13	0	-0	0	0	0	0	0
93	116	123	124	117	0	0	0	C	16	0	1	0	8	0	-0	0	0	0	0	0
94	118	125	126	119	0	0	0	C	16	0	1	0	49	0	-0	0	0	0	0	0
95	119	126	127	120	0	0	0	C	16	0	1	0	67	0	-0	0	0	0	0	0
96	120	127	128	121	0	0	0	C	16	0	1	0	84	0	-0	0	0	0	0	0
97	122	129	130	123	0	0	0	C	16	0	1	0	16	0	-0	0	0	0	0	0
98	123	130	131	124	0	0	0	C	16	0	1	0	18	0	-0	0	0	0	0	0
99	124	131	132	125	0	0	0	C	16	0	1	0	32	0	-0	0	0	0	0	0
100	125	132	133	126	0	0	0	C	16	0	1	0	56	0	-0	0	0	0	0	0
101	126	133	134	127	0	0	0	C	16	0	1	0	71	0	-0	0	0	0	0	0
102	127	134	135	128	0	0	0	C	16	0	1	0	87	0	-0	0	0	0	0	0
103	129	136	137	130	0	0	0	C	16	0	1	0	17	0	-0	0	0	0	0	0
104	130	137	138	131	0	0	0	C	16	0	1	0	12	0	-0	0	0	0	0	0
105	132	139	140	133	0	0	0	C	16	0	1	0	52	0	-0	0	0	0	0	0
106	133	140	141	134	0	0	0	C	16	0	1	0	70	0	-0	0	0	0	0	0

Table 11. Mesh Topology and Element Property Types (Contd)

107	134	141	142	135	0	0	0	0	16	0	1	0	87	0	-0	0	0	0	0	0
108	136	143	144	137	0	0	0	0	16	0	1	0	21	0	-0	0	0	0	0	0
109	137	144	145	138	0	0	0	0	16	0	1	0	24	0	-0	0	0	0	0	0
110	138	145	146	139	0	0	0	0	16	0	1	0	37	0	-0	0	0	0	0	0
111	139	146	147	140	0	0	0	0	16	0	1	0	59	0	-0	0	0	0	0	0
112	140	147	148	141	0	0	0	0	16	0	1	0	75	0	-0	0	0	0	0	0
113	141	148	149	142	0	0	0	0	16	0	1	0	89	0	-0	0	0	0	0	0
114	143	150	151	144	0	0	0	0	16	0	1	0	22	0	-0	0	0	0	0	0
115	144	151	152	145	0	0	0	0	16	0	1	0	16	0	-0	0	0	0	0	0
116	146	153	154	147	0	0	0	0	16	0	1	0	55	0	-0	0	0	0	0	0
117	147	154	155	148	0	0	0	0	16	0	1	0	73	0	-0	0	0	0	0	0
118	148	155	156	149	0	0	0	0	16	0	1	0	89	0	-0	0	0	0	0	0
119	150	157	158	151	0	0	0	0	16	0	1	0	26	0	-0	0	0	0	0	0
120	151	158	159	152	0	0	0	0	16	0	1	0	29	0	-0	0	0	0	0	0
121	152	159	160	153	0	0	0	0	16	0	1	0	42	0	-0	0	0	0	0	0
122	153	160	161	154	0	0	0	0	16	0	1	0	64	0	-0	0	0	0	0	0
123	154	161	162	155	0	0	0	0	16	0	1	0	79	0	-0	0	0	0	0	0
124	155	162	163	156	0	0	0	0	16	0	1	0	93	0	-0	0	0	0	0	0
125	157	164	165	158	0	0	0	0	16	0	1	0	27	0	-0	0	0	0	0	0
126	158	165	166	159	0	0	0	0	16	0	1	0	21	0	-0	0	0	0	0	0
127	159	167	168	161	0	0	0	0	16	0	1	0	59	0	-0	0	0	0	0	0
128	161	168	169	162	0	0	0	0	16	0	1	0	78	0	-0	0	0	0	0	0
129	162	169	170	163	0	0	0	0	16	0	1	0	93	0	-0	0	0	0	0	0
130	164	171	172	165	0	0	0	0	16	0	1	0	33	0	-0	0	0	0	0	0
131	165	172	173	166	0	0	0	0	16	0	1	0	35	0	-0	0	0	0	0	0
132	166	173	174	167	0	0	0	0	16	0	1	0	48	0	-0	0	0	0	0	0
133	167	174	175	168	0	0	0	0	16	0	1	0	68	0	-0	0	0	0	0	0
134	168	175	176	169	0	0	0	0	16	0	1	0	83	0	-0	0	0	0	0	0
135	169	176	177	170	0	0	0	0	16	0	1	0	95	0	-0	0	0	0	0	0
136	171	178	179	172	0	0	0	0	16	0	1	0	34	0	-0	0	0	0	0	0
137	172	179	180	173	0	0	0	0	16	0	1	0	26	0	-0	0	0	0	0	0
138	174	181	182	175	0	0	0	0	16	0	1	0	65	0	-0	0	0	0	0	0
139	175	182	183	176	0	0	0	0	16	0	1	0	82	0	-0	0	0	0	0	0
140	176	183	184	177	0	0	0	0	16	0	1	0	95	0	-0	0	0	0	0	0
141	178	185	186	179	0	0	0	0	16	0	1	0	39	0	-0	0	0	0	0	0
142	179	186	187	180	0	0	0	0	16	0	1	0	41	0	-0	0	0	0	0	0
143	180	187	188	181	0	0	0	0	16	0	1	0	53	0	-0	0	0	0	0	0
144	181	188	189	182	0	0	0	0	16	0	1	0	71	0	-0	0	0	0	0	0
145	182	189	190	183	0	0	0	0	16	0	1	0	87	0	-0	0	0	0	0	0
146	183	190	191	184	0	0	0	0	16	0	1	0	96	0	-0	0	0	0	0	0
147	185	192	193	186	0	0	0	0	16	0	1	0	39	0	-0	0	0	0	0	0
148	186	193	194	187	0	0	0	0	16	0	1	0	33	0	-0	0	0	0	0	0
149	188	195	196	189	0	0	0	0	16	0	1	0	69	0	-0	0	0	0	0	0
150	189	196	197	190	0	0	0	0	16	0	1	0	86	0	-0	0	0	0	0	0
151	190	197	198	191	0	0	0	0	16	0	1	0	96	0	-0	0	0	0	0	0
152	192	199	200	193	0	0	0	0	16	0	1	0	45	0	-0	0	0	0	0	0
153	193	200	201	194	0	0	0	0	16	0	1	0	48	0	-0	0	0	0	0	0
154	194	201	202	195	0	0	0	0	16	0	1	0	57	0	-0	0	0	0	0	0
155	195	202	203	196	0	0	0	0	16	0	1	0	76	0	-0	0	0	0	0	0
156	196	203	204	197	0	0	0	0	16	0	1	0	90	0	-0	0	0	0	0	0
157	197	204	205	198	0	0	0	0	16	0	1	0	97	0	-0	0	0	0	0	0
158	199	206	207	200	0	0	0	0	16	0	1	0	44	0	-0	0	0	0	0	0

Table 11. Mesh Topology and Element Property Types (Contd)

159	200	207	208	201	0	0	0	0	16	0	1	0	38	0	-0	0	0	0	0
160	202	209	210	203	0	0	0	0	16	0	1	0	72	0	-0	0	0	0	0
161	203	210	211	204	0	0	0	0	16	0	1	0	88	0	-0	0	0	0	0
162	204	211	212	205	0	0	0	0	16	0	1	0	97	0	-0	0	0	0	0
163	206	213	214	207	0	0	0	0	16	0	1	0	50	0	-0	0	0	0	0
164	207	214	215	208	0	0	0	0	16	0	1	0	52	0	-0	0	0	0	0
165	208	215	216	209	0	0	0	0	16	0	1	0	60	0	-0	0	0	0	0
166	209	216	217	210	0	0	0	0	16	0	1	0	80	0	-0	0	0	0	0
167	210	217	218	211	0	0	0	0	16	0	1	0	93	0	-0	0	0	0	0
168	211	218	219	212	0	0	0	0	16	0	1	0	99	0	-0	0	0	0	0
169	213	220	221	214	0	0	0	0	16	0	1	0	47	0	-0	0	0	0	0
170	214	221	222	215	0	0	0	0	16	0	1	0	41	0	-0	0	0	0	0
171	216	223	224	217	0	0	0	0	16	0	1	0	74	0	-0	0	0	0	0
172	217	224	225	218	0	0	0	0	16	0	1	0	91	0	-0	0	0	0	0
173	218	225	226	219	0	0	0	0	16	0	1	0	98	0	-0	0	0	0	0
174	220	227	228	221	0	0	0	0	16	0	1	0	51	0	-0	0	0	0	0
175	221	228	229	222	0	0	0	0	16	0	1	0	54	0	-0	0	0	0	0
176	222	229	230	223	0	0	0	0	16	0	1	0	61	0	-0	0	0	0	0
177	223	230	231	224	0	0	0	0	16	0	1	0	79	0	-0	0	0	0	0
178	224	231	232	225	0	0	0	0	16	0	1	0	92	0	-0	0	0	0	0
179	225	232	233	226	0	0	0	0	16	0	1	0	98	0	-0	0	0	0	0
180	227	234	235	228	0	0	0	0	16	0	1	0	45	0	-0	0	0	0	0
181	228	235	236	229	0	0	0	0	16	0	1	0	41	0	-0	0	0	0	0
182	230	237	238	231	0	0	0	0	16	0	1	0	69	0	-0	0	0	0	0
183	231	238	239	232	0	0	0	0	16	0	1	0	83	0	-0	0	0	0	0
184	232	239	240	233	0	0	0	0	16	0	1	0	94	0	-0	0	0	0	0
185	234	241	242	235	0	0	0	0	16	0	1	0	49	0	-0	0	0	0	0
186	235	242	243	236	0	0	0	0	16	0	1	0	49	0	-0	0	0	0	0
187	236	243	244	237	0	0	0	0	16	0	1	0	53	0	-0	0	0	0	0
188	237	244	245	238	0	0	0	0	16	0	1	0	67	0	-0	0	0	0	0
189	238	245	246	239	0	0	0	0	16	0	1	0	77	0	-0	0	0	0	0
190	239	246	247	240	0	0	0	0	16	0	1	0	86	0	-0	0	0	0	0
AT 0. SEC. OF RELABELLING					-0 SWEEPS PERFORMED. UPPER OFF-BAND ELEMENT COUNT OF MESH TOPOLOGY MATRIX IS 27390.														
AT 8.95 SEC. OF RELABELLING					370 SWEEPS PERFORMED. UPPER OFF-BAND ELEMENT COUNT OF MESH TOPOLOGY MATRIX IS 28305.														

Table 12. Nodal Deflections

INPUT LINK LOCK 24.42 SECONDS.
GENERATION LINK LOCK 49.30 SECONDS.

NODAL DEFLECTIONS						
NODE	DISP. ALONG X	DISP. ALONG Y	DISP. ALONG Z	ROTA. ABOUT X	ROTA. ABOUT Y	ROTA. ABOUT Z
1	0.	0.2092358E-06	0.	0.	0.	0.
2	0.	0.2512710E-06	0.	0.	0.	0.
3	0.	0.2758441E-06	0.	0.	0.	0.
4	0.	0.2916618E-06	0.	0.	0.	0.
5	0.	0.3041579E-06	0.	0.	0.	0.
6	0.	0.3165377E-06	0.	0.	0.	0.
7	0.1557000E-06	0.1954083E-06	0.	0.	0.	0.
8	0.1580575E-06	0.2419760E-06	0.	0.	0.	0.
9	0.1738536E-06	0.2667053E-06	0.	0.	0.	0.
10	0.1770327E-06	0.2817398E-06	0.	0.	0.	0.
11	0.1794670E-06	0.2955950E-06	0.	0.	0.	0.
12	0.1917078E-06	0.3083203E-06	0.	0.	0.	0.
13	0.1996930E-06	0.1857440E-06	0.	0.	0.	0.
14	0.2136573E-06	0.2318363E-06	0.	0.	0.	0.
15	0.2275638E-06	0.2574755E-06	0.	0.	0.	0.
16	0.2322954E-06	0.2727010E-06	0.	0.	0.	0.
17	0.2463394E-06	0.2874685E-06	0.	0.	0.	0.
18	0.2399902E-06	0.3011412E-06	0.	0.	0.	0.
19	0.	-0.8514567E-07	0.	0.	0.	0.
20	0.	0.3213378E-08	0.	0.	0.	0.
21	0.1910199E-06	0.1015450E-06	0.	0.	0.	0.
22	0.2215747E-06	0.1791909E-06	0.	0.	0.	0.
23	0.2447372E-06	0.2245536E-06	0.	0.	0.	0.
24	0.2548320E-06	0.2495485E-06	0.	0.	0.	0.
25	0.2606476E-06	0.2659079E-06	0.	0.	0.	0.
26	0.2658883E-06	0.2818343E-06	0.	0.	0.	0.
27	0.2705914E-06	0.2969502E-06	0.	0.	0.	0.
28	0.	0.1175455E-06	0.	0.	0.	0.
29	0.1460822E-06	-0.8722380E-07	0.	0.	0.	0.
30	0.2188217E-06	0.8370516E-07	0.	0.	0.	0.
31	0.2643129E-06	0.1593259E-06	0.	0.	0.	0.
32	0.2576348E-06	0.2037573E-06	0.	0.	0.	0.
33	0.3111048E-06	0.2287063E-06	0.	0.	0.	0.
34	0.3181617E-06	0.2455212E-06	0.	0.	0.	0.
35	0.3248757E-06	0.2636970E-06	0.	0.	0.	0.
36	0.3312854E-06	0.2819004E-06	0.	0.	0.	0.
37	0.1440521E-06	-0.6870270E-09	0.	0.	0.	0.
38	0.1369067E-06	0.1086891E-06	0.	0.	0.	0.
39	0.2483460E-06	0.5940916E-07	0.	0.	0.	0.
40	0.3064001E-06	0.1292546E-06	0.	0.	0.	0.
41	0.3524555E-06	0.1717182E-06	0.	0.	0.	0.
42	0.3703931E-06	0.1957322E-06	0.	0.	0.	0.
43	0.3843449E-06	0.2130493E-06	0.	0.	0.	0.
44	0.3966041E-06	0.2329268E-06	0.	0.	0.	0.
45	0.4026334E-06	0.2456664E-06	0.	0.	0.	0.
46	0.1989412E-06	-0.8576892E-07	0.	0.	0.	0.
47	0.1856189E-06	0.	0.	0.	0.	0.
48	0.2657689E-06	0.4690609E-07	0.	0.	0.	0.
49	0.3267250E-06	0.1087944E-06	0.	0.	0.	0.
50	0.3807807E-06	0.1501832E-06	0.	0.	0.	0.
51	0.4053378E-06	0.1724243E-06	0.	0.	0.	0.

Table 12. Nodal Deflections (Contd)

52	0.4183890E-06	0.1896238E-06	0.	0.	0.	0.
53	0.4322049E-06	0.2101817E-06	0.	0.	0.	0.
54	0.4451132E-06	0.2320101E-06	0.	0.	0.	0.
55	0.1733885E-06	0.1042629E-06	0.	0.	0.	0.
56	0.2100957E-06	-0.8493999E-07	0.	0.	0.	0.
57	0.2073114E-06	-0.1253410E-07	0.	0.	0.	0.
58	0.2047353E-06	-0.1369038E-07	0.	0.	0.	0.
59	0.2971044E-06	-0.1265142E-07	0.	0.	0.	0.
60	0.3773342E-06	0.4559007E-07	0.	0.	0.	0.
61	0.4491129E-06	0.8716688E-07	0.	0.	0.	0.
62	0.4790178E-06	0.1086367E-06	0.	0.	0.	0.
63	0.4993550E-06	0.1258652E-06	0.	0.	0.	0.
64	0.5176002E-06	0.1465449E-06	0.	0.	0.	0.
65	0.5337278E-06	0.1694868E-06	0.	0.	0.	0.
66	0.3125197E-06	-0.4082120E-07	0.	0.	0.	0.
67	0.3960985E-06	0.1383356E-07	0.	0.	0.	0.
68	0.4781111E-06	0.5597007E-07	0.	0.	0.	0.
69	0.5132973E-06	0.7727135E-07	0.	0.	0.	0.
70	0.5336811E-06	0.9528229E-07	0.	0.	0.	0.
71	0.5537065E-06	0.1161750E-06	0.	0.	0.	0.
72	0.5718245E-06	0.1383949E-06	0.	0.	0.	0.
73	0.3520991E-06	-0.1247756E-06	0.	0.	0.	0.
74	0.4469971E-06	-0.7548841E-07	0.	0.	0.	0.
75	0.5467765E-06	-0.3262283E-07	0.	0.	0.	0.
76	0.5889390E-06	-0.1010614E-07	0.	0.	0.	0.
77	0.6164743E-06	0.8217581E-08	0.	0.	0.	0.
78	0.6406931E-06	0.2938182E-07	0.	0.	0.	0.
79	0.6614112E-06	0.5172321E-07	0.	0.	0.	0.
80	0.3685973E-06	-0.1650921E-06	0.	0.	0.	0.
81	0.4707111E-06	-0.1164035E-06	0.	0.	0.	0.
82	0.5764749E-06	-0.7385077E-07	0.	0.	0.	0.
83	0.6234357E-06	-0.5156680E-07	0.	0.	0.	0.
84	0.6494927E-06	-0.3386655E-07	0.	0.	0.	0.
85	0.6756229E-06	-0.1265898E-07	0.	0.	0.	0.
86	0.7001381E-06	0.1078337E-07	0.	0.	0.	0.
87	0.4140131E-06	-0.2759576E-06	0.	0.	0.	0.
88	0.5285834E-06	-0.2293967E-06	0.	0.	0.	0.
89	0.6471398E-06	-0.1874536E-06	0.	0.	0.	0.
90	0.7000404E-06	-0.1648469E-06	0.	0.	0.	0.
91	0.7343913E-06	-0.1460870E-06	0.	0.	0.	0.
92	0.7643968E-06	-0.1245785E-06	0.	0.	0.	0.
93	0.7922324E-06	-0.1009650E-06	0.	0.	0.	0.
94	0.4322718E-06	-0.3282391E-06	0.	0.	0.	0.
95	0.5538024E-06	-0.2811842E-06	0.	0.	0.	0.
96	0.6771820E-06	-0.2396592E-06	0.	0.	0.	0.
97	0.7379197E-06	-0.2155837E-06	0.	0.	0.	0.
98	0.7680170E-06	-0.1987767E-06	0.	0.	0.	0.
99	0.8029088E-06	-0.1754511E-06	0.	0.	0.	0.
100	0.8332407E-06	-0.1515519E-06	0.	0.	0.	0.
101	0.4851547E-06	-0.4657766E-06	0.	0.	0.	0.
102	0.6168448E-06	-0.4200715E-06	0.	0.	0.	0.
103	0.7507177E-06	-0.3791780E-06	0.	0.	0.	0.
104	0.8182851E-06	-0.3541585E-06	0.	0.	0.	0.
105	0.8551991E-06	-0.3368883E-06	0.	0.	0.	0.

Table 12. Nodal Deflections (Contd)

106	0.8935033E-06	-0.3140405E-06	0.	0.	0.	0.
107	0.9253481E-06	-0.2909484E-06	0.	0.	0.	0.
108	0.5052627E-06	-0.5289561E-06	0.	0.	0.	0.
109	0.6426343E-06	-0.4832571E-06	0.	0.	0.	0.
110	0.7812479E-06	-0.4424030E-06	0.	0.	0.	0.
111	0.8550439E-06	-0.4167988E-06	0.	0.	0.	0.
112	0.8912258E-06	-0.3994977E-06	0.	0.	0.	0.
113	0.9314468E-06	-0.3765017E-06	0.	0.	0.	0.
114	0.9670270E-06	-0.3521224E-06	0.	0.	0.	0.
115	0.5644164E-06	-0.6929720E-06	0.	0.	0.	0.
116	0.7115687E-06	-0.6480381E-06	0.	0.	0.	0.
117	0.8591119E-06	-0.6078183E-06	0.	0.	0.	0.
118	0.9367003E-06	-0.5822536E-06	0.	0.	0.	0.
119	0.9797672E-06	-0.5644615E-06	0.	0.	0.	0.
120	0.1026423E-05	-0.5401983E-06	0.	0.	0.	0.
121	0.1064248E-05	-0.5164069E-06	0.	0.	0.	0.
122	0.5868036E-06	-0.7675775E-06	0.	0.	0.	0.
123	0.7404362E-06	-0.7218533E-06	0.	0.	0.	0.
124	0.8922578E-06	-0.6915724E-06	0.	0.	0.	0.
125	0.9762046E-06	-0.6553533E-06	0.	0.	0.	0.
126	0.1018639E-05	-0.6373686E-06	0.	0.	0.	0.
127	0.1065540E-05	-0.6135972E-06	0.	0.	0.	0.
128	0.1105927E-05	-0.5897101E-06	0.	0.	0.	0.
129	0.6531709E-06	-0.9583719E-06	0.	0.	0.	0.
130	0.8133644E-06	-0.9137710E-06	0.	0.	0.	0.
131	0.9732946E-06	-0.8736083E-06	0.	0.	0.	0.
132	0.1060905E-05	-0.8473707E-06	0.	0.	0.	0.
133	0.1108225E-05	-0.8296343E-06	0.	0.	0.	0.
134	0.1161882E-05	-0.8045506E-06	0.	0.	0.	0.
135	0.1206980E-05	-0.7793608E-06	0.	0.	0.	0.
136	0.6780665E-06	-0.1044149E-05	0.	0.	0.	0.
137	0.8425852E-06	-0.9992827E-06	0.	0.	0.	0.
138	0.1007901E-05	-0.9585282E-06	0.	0.	0.	0.
139	0.1098628E-05	-0.9324688E-06	0.	0.	0.	0.
140	0.1148666E-05	-0.9133715E-06	0.	0.	0.	0.
141	0.1202403E-05	-0.8888557E-06	0.	0.	0.	0.
142	0.1250607E-05	-0.8632009E-06	0.	0.	0.	0.
143	0.7515433E-06	-0.1261924E-05	0.	0.	0.	0.
144	0.9199619E-06	-0.1218440E-05	0.	0.	0.	0.
145	0.1090684E-05	-0.1178260E-05	0.	0.	0.	0.
146	0.1188229E-05	-0.1151159E-05	0.	0.	0.	0.
147	0.1243916E-05	-0.1131915E-05	0.	0.	0.	0.
148	0.1302581E-05	-0.1106923E-05	0.	0.	0.	0.
149	0.1353884E-05	-0.1080957E-05	0.	0.	0.	0.
150	0.7789360E-06	-0.1359161E-05	0.	0.	0.	0.
151	0.9514855E-06	-0.1315334E-05	0.	0.	0.	0.
152	0.1124539E-05	-0.1275136E-05	0.	0.	0.	0.
153	0.1228302E-05	-0.1247278E-05	0.	0.	0.	0.
154	0.1285983E-05	-0.1227021E-05	0.	0.	0.	0.
155	0.1344574E-05	-0.1202649E-05	0.	0.	0.	0.
156	0.1401320E-05	-0.1175152E-05	0.	0.	0.	0.
157	0.8597473E-06	-0.1604599E-05	0.	0.	0.	0.
158	0.1034008E-05	-0.1562337E-05	0.	0.	0.	0.
159	0.1210800E-05	-0.1522928E-05	0.	0.	0.	0.

Table 12. Nodal Deflections (Contd)

160	0.1320313E-05	-0.1494414E-05	0.	0.	0.	0.
161	0.1382673E-05	-0.1474336E-05	0.	0.	0.	0.
162	0.1448603E-05	-0.1448518E-05	0.	0.	0.	0.
163	0.1508705E-05	-0.1420721E-05	0.	0.	0.	0.
164	0.3921552E-06	-0.1712778E-05	0.	0.	0.	0.
165	0.1067605E-05	-0.1671035E-05	0.	0.	0.	0.
166	0.1245884E-05	-0.1631591E-05	0.	0.	0.	0.
167	0.1364436E-05	-0.1601522E-05	0.	0.	0.	0.
168	0.1426670E-05	-0.1581189E-05	0.	0.	0.	0.
169	0.1494731E-05	-0.1554890E-05	0.	0.	0.	0.
170	0.1558194E-05	-0.1526551E-05	0.	0.	0.	0.
171	0.9778813E-06	-0.1987784E-05	0.	0.	0.	0.
172	0.1158313E-05	-0.1946322E-05	0.	0.	0.	0.
173	0.1335903E-05	-0.1908358E-05	0.	0.	0.	0.
174	0.1457824E-05	-0.1878269E-05	0.	0.	0.	0.
175	0.1529852E-05	-0.1856469E-05	0.	0.	0.	0.
176	0.1600474E-05	-0.1830654E-05	0.	0.	0.	0.
177	0.1670155E-05	-0.1800840E-05	0.	0.	0.	0.
178	0.1010617E-05	-0.2108982E-05	0.	0.	0.	0.
179	0.1191343E-05	-0.2067802E-05	0.	0.	0.	0.
180	0.1372227E-05	-0.2029396E-05	0.	0.	0.	0.
181	0.1503601E-05	-0.1997543E-05	0.	0.	0.	0.
182	0.1575680E-05	-0.1975448E-05	0.	0.	0.	0.
183	0.1648537E-05	-0.1949213E-05	0.	0.	0.	0.
184	0.1721803E-05	-0.1918841E-05	0.	0.	0.	0.
185	0.1107161E-05	-0.2412400E-05	0.	0.	0.	0.
186	0.1288067E-05	-0.2372629E-05	0.	0.	0.	0.
187	0.1465989E-05	-0.2335989E-05	0.	0.	0.	0.
188	0.1600720E-05	-0.2304151E-05	0.	0.	0.	0.
189	0.1683123E-05	-0.2280502E-05	0.	0.	0.	0.
190	0.1761213E-05	-0.2253718E-05	0.	0.	0.	0.
191	0.1838308E-05	-0.2222988E-05	0.	0.	0.	0.
192	0.1142507E-05	-0.2545969E-05	0.	0.	0.	0.
193	0.1326007E-05	-0.2506015E-05	0.	0.	0.	0.
194	0.1503525E-05	-0.2469572E-05	0.	0.	0.	0.
195	0.1648204E-05	-0.2436093E-05	0.	0.	0.	0.
196	0.1727311E-05	-0.2413013E-05	0.	0.	0.	0.
197	0.1811351E-05	-0.2384785E-05	0.	0.	0.	0.
198	0.1889098E-05	-0.2354698E-05	0.	0.	0.	0.
199	0.1247304E-05	-0.2879299E-05	0.	0.	0.	0.
200	0.1425563E-05	-0.2841799E-05	0.	0.	0.	0.
201	0.1604259E-05	-0.2806210E-05	0.	0.	0.	0.
202	0.1752188E-05	-0.2772699E-05	0.	0.	0.	0.
203	0.1839141E-05	-0.2748947E-05	0.	0.	0.	0.
204	0.1928187E-05	-0.2720194E-05	0.	0.	0.	0.
205	0.2006463E-05	-0.2690979E-05	0.	0.	0.	0.
206	0.1288501E-05	-0.3024614E-05	0.	0.	0.	0.
207	0.1462048E-05	-0.2988617E-05	0.	0.	0.	0.
208	0.1642626E-05	-0.2952893E-05	0.	0.	0.	0.
209	0.1797714E-05	-0.2918570E-05	0.	0.	0.	0.
210	0.1885212E-05	-0.2894639E-05	0.	0.	0.	0.
211	0.1976973E-05	-0.2865612E-05	0.	0.	0.	0.
212	0.2062429E-05	-0.2834846E-05	0.	0.	0.	0.
213	0.1397671E-05	-0.3389375E-05	0.	0.	0.	0.

Table 12. Nodal Deflections (Contd)

214	0.1570046E-05	-0.3354995E-05	0.	0.	0.	0.
215	0.1742990E-05	-0.3322083E-05	0.	0.	0.	0.
216	0.1908462E-05	-0.3286580E-05	0.	0.	0.	0.
217	0.1997492E-05	-0.3263168E-05	0.	0.	0.	0.
218	0.2097645E-05	-0.3233912E-05	0.	0.	0.	0.
219	0.2190903E-05	-0.3201858E-05	0.	0.	0.	0.
220	0.1441525E-05	-0.3546789E-05	0.	0.	0.	0.
221	0.1611320E-05	-0.3513830E-05	0.	0.	0.	0.
222	0.1781476E-05	-0.3481763E-05	0.	0.	0.	0.
223	0.1958149E-05	-0.3445095E-05	0.	0.	0.	0.
224	0.2045667E-05	-0.3422888E-05	0.	0.	0.	0.
225	0.2150989E-05	-0.3392941E-05	0.	0.	0.	0.
226	0.2244865E-05	-0.3362530E-05	0.	0.	0.	0.
227	0.1556832E-05	-0.3941642E-05	0.	0.	0.	0.
228	0.1721900E-05	-0.3911138E-05	0.	0.	0.	0.
229	0.1880876E-05	-0.3882873E-05	0.	0.	0.	0.
230	0.2064939E-05	-0.3846803E-05	0.	0.	0.	0.
231	0.2164493E-05	-0.3824152E-05	0.	0.	0.	0.
232	0.2267554E-05	-0.3797714E-05	0.	0.	0.	0.
233	0.2370003E-05	-0.3766527E-05	0.	0.	0.	0.
234	0.1603391E-05	-0.4108932E-05	0.	0.	0.	0.
235	0.1762872E-05	-0.4080397E-05	0.	0.	0.	0.
236	0.1924269E-05	-0.4052473E-05	0.	0.	0.	0.
237	0.2107561E-05	-0.4019453E-05	0.	0.	0.	0.
238	0.2206003E-05	-0.3998767E-05	0.	0.	0.	0.
239	0.2314645E-05	-0.3973349E-05	0.	0.	0.	0.
240	0.2423139E-05	-0.3944529E-05	0.	0.	0.	0.
241	0.1632607E-05	-0.4210237E-05	0.	0.	0.	0.
242	0.1803542E-05	-0.4294454E-05	0.	0.	0.	0.
243	0.1967786E-05	-0.4268875E-05	0.	0.	0.	0.
244	0.2153402E-05	-0.4233778E-05	0.	0.	0.	0.
245	0.2258839E-05	-0.4218368E-05	0.	0.	0.	0.
246	0.2368056E-05	-0.4194566E-05	0.	0.	0.	0.
247	0.2454263E-05	-0.4051554E-05	0.	0.	0.	0.

APPENDIX B
EXPLANATION OF ONE-HALF OPTICAL PATH
DIFFERENCE CALCULATION

To calculate the $1/2$ O.P.D. the following analysis was used. First, a mathematical parabola of 250 cm focal length was derived. The equation for this is

$$y = X^2/4f = 0.00254000002X^2 \text{ in.}; f = 98.425196 \text{ in.}$$

Then the computer distortion data Δy was listed for selected X radii. Then the error in distortion (Δy_0) at $X = 0$ was forced to zero by making $y = 0$ at $X = 0$. Then each corrected error $\Delta y - \Delta y_0$ was computed. The new surface of revolution was described mathematically by letting $y'' = y + (\Delta y - \Delta y_0)$. To determine how closely the new curve, y'' , approximated a new parabola (thus a new optical surface of satisfactory imaging characteristics), a new mathematical parabola (y') was generated, choosing a focal length (f') based on the $y + (\Delta y - \Delta y_0)$ value found at radius X of 12.79 inches (32.5 cm) from the center of the mirror. (See sample calculation in Table 4.) It was found through experience that this focal length gave the least error (difference along the y axis) between the new parabola (y') and the y'' curve. The sum of the maximum positive and negative deviation between the two curves ($y' - y''$) will give the $1/2$ O.P.D. In the sample calculation in Table 4 this amounted to 1.05 micro-inches or a $1/2$ O.P.D. of $\lambda/19$.

APPENDIX C

THERMAL ANALYSIS OF THE PHOTOHELIOGRAPH PRIMARY MIRROR

The initial primary mirror configuration (a uniform thick disk) was established for the thermal investigation. The diameter of the disk was established by the current dimension of the mirror at that time which was 80 cm (31.5 in.), with a thickness of one inch (see Figures 17 and 18).

The boundary conditions for the model were:

1. The front surface was sun illuminated with the exception of a shaded circle in the center which had a diameter of 10 cm (3.94 in.).
2. The back surface had a uniform temperature of 70°F.
3. The edges were adiabatic.

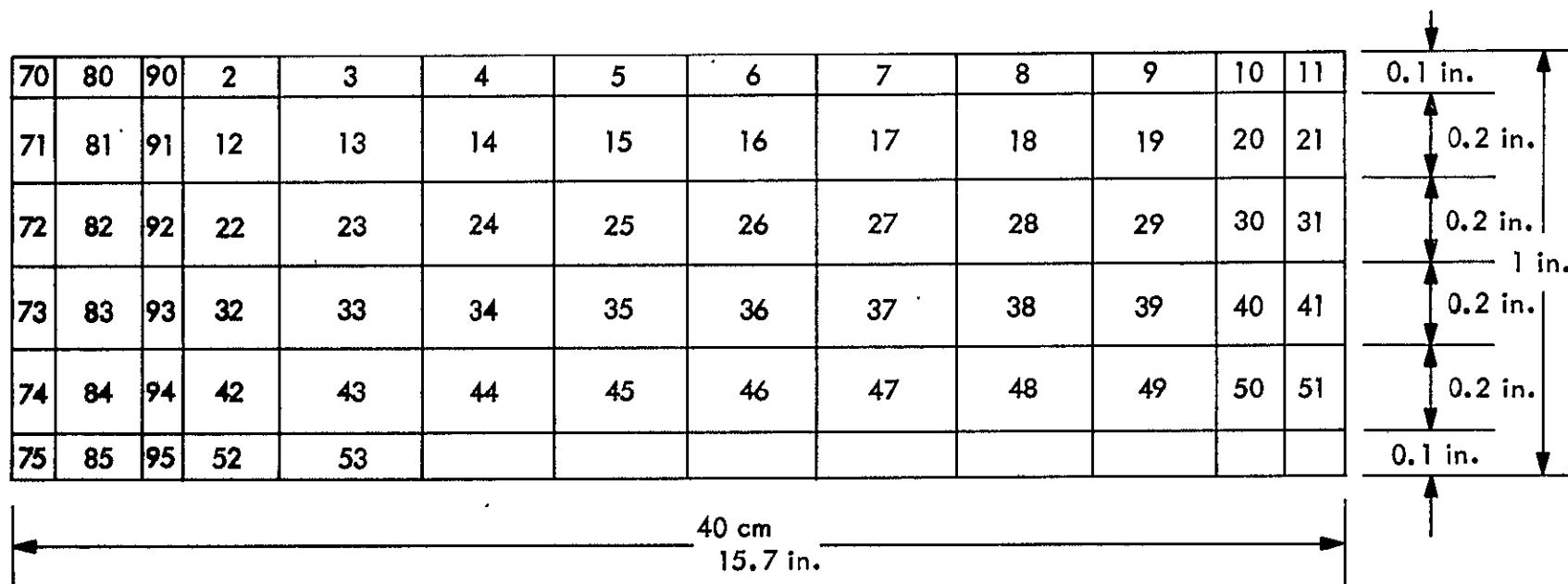
As usual, the model was discretized into convenient elements, for the purpose of the computer analysis. Figure 17 shows the model which was programmed.

Once the mathematical model was completely described, a program could be written to do the required analysis. The analysis was accomplished by use of finite difference techniques. These techniques were implemented by means of a general heat transfer computer program named Chrysler Improved Numerical Differencing Analyzer, commonly known by its acronym, CINDA.

This program has the capability to do the thermal analysis as well as the menial calculations necessary to set up the thermal network. By listing material properties, and geometrical characteristics a subroutine can be called on to multiply the volume of a node by the density and specific heat and arrive at the thermal capacity of the node. In a similar manner, constant values can be loaded and called up in a subroutine to calculate the thermal conductance between a pair of nodes.

To illustrate the program, a sample problem is presented and explained. In Table 13, the first card titled BCD 3THERMAL SPCS prepares the computer system for a thermal problem. The following three cards are title cards describing the boundary conditions.

The network is set up by the card "BCD 3NODE DATA" and the cards that follow down to the card "END". Note that this data is listed in triplets. The first data in the triplet lists the node numbers, the second data value is the initial temperature of the node, and the third data value is the capacity of the node. In the particular example shown, the capacitance is zero. Later in the



NOTE DISTORTION TO SCALES:
RADI TO CENTERS OF TOP ROW OF NODES

$$\begin{aligned}
 r_{70} &= 0 & r_{80} &= 1.0 \text{ in.} & r_{90} &= 1.93 \text{ in.} & r_2 &= 2.75 \text{ in.} \\
 r_3 &= 3.93 \text{ in.} & r_4 &= 5.50 \text{ in.} & r_5 &= 7.07 \text{ in.} & r_6 &= 8.64 \text{ in.} \\
 r_7 &= 10.2 \text{ in.} & r_8 &= 11.80 \text{ in.} & r_9 &= 13.35 \text{ in.} & r_{10} &= 14.50 \text{ in.} \\
 r_{11} &= 15.30 \text{ in.}
 \end{aligned}$$

DEPTHS TO CENTERS OF FIRST COLUMN OF NODES

$$\begin{aligned}
 X_{70} &= 0.05 \text{ in.} & X_{71} &= 0.20 \text{ in.} & X_{72} &= 0.40 \text{ in.} & X_{73} &= 0.60 \text{ in.} \\
 X_{74} &= 0.08 \text{ in.} & X_{75} &= 0.95 \text{ in.}
 \end{aligned}$$

Figure 17. Subdivision of Plane Gregorian Mirror for Heat Transfer Calculations

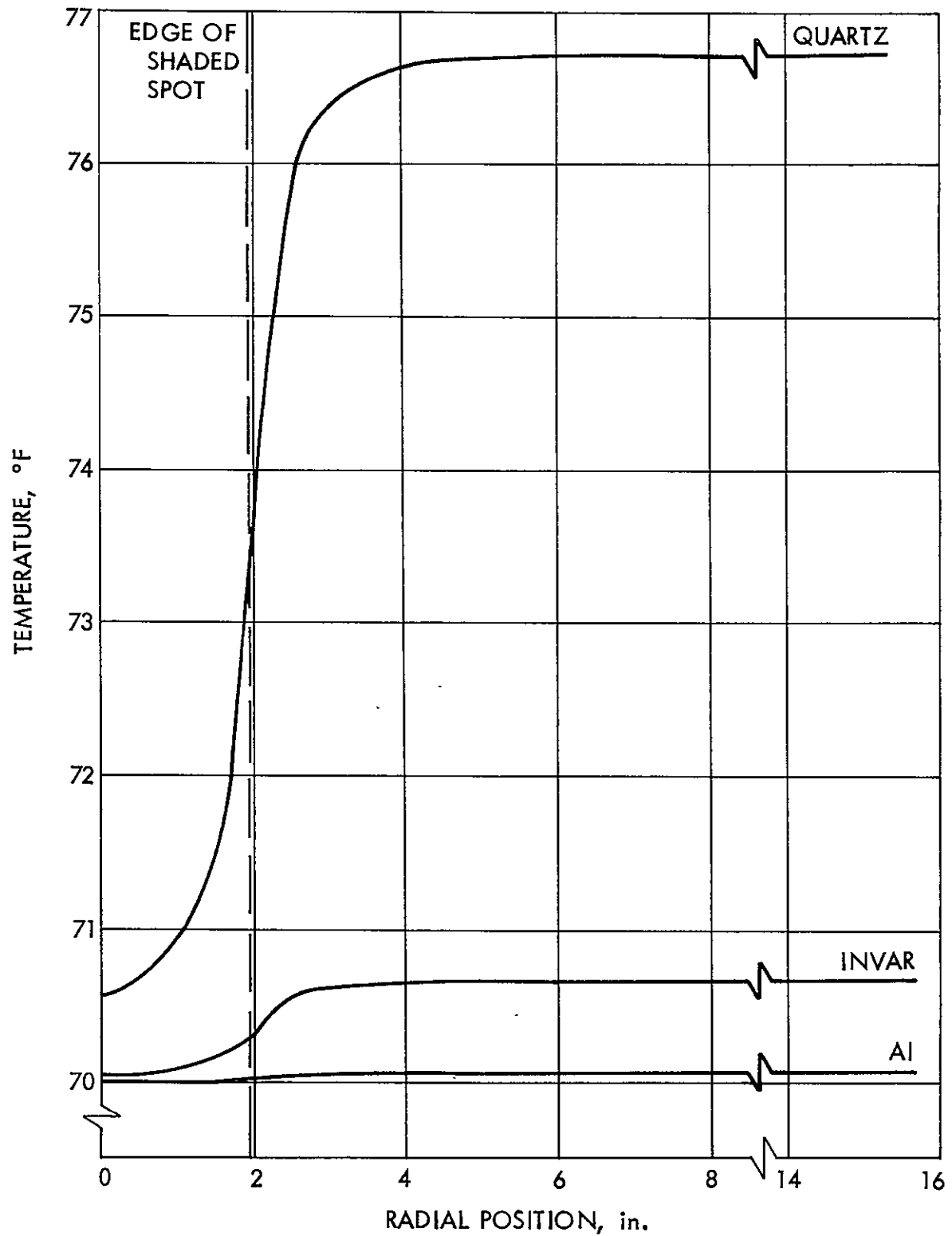


Figure 18. Steady State Temperature Distribution in Gregorian Mirror with 10cm. dia. Shaded Spot and Uniform 70°F Back Surface Temperature

Table 13. Chrysler Improved Numerical Differencing Analyzer

```

BCD 3THERMAL SPCS
BCD 9OVERALL ANALYSIS OF TAPERED GREGORIAN MIRROR WITH INTE
BCD 6RNAL CODJLING CHANNEL,MATL-ULE QUARTZ
BCD 5FLOW-TURB.,UNIFORM IN TO OUT
END
BCD 3NODE DATA
1,70.,0,2,70.,0,3,70.,0,4,70.,0,5,70.,0,6,70.,0
7,70.,0,8,70.,0,9,70.,0,10,70.,0,11,70.,0,12,70.,0
13,70.,0,14,70.,0,15,70.,0,16,70.,0,17,70.,0,18,70.,0
19,70.,0,20,70.,0,21,70.,0,22,70.,0,23,70.,0,24,70.,0
25,70.,0,26,70.,0,27,70.,0,28,70.,0,29,70.,0,30,70.,0
31,70.,0,32,70.,0,33,70.,0,34,70.,0,35,70.,0,36,70.,0
37,70.,0,38,70.,0,39,70.,0,40,70.,0,41,70.,0,42,70.,0
43,70.,0,44,70.,0,45,70.,0,46,70.,0,47,70.,0,48,70.,0
49,70.,0,50,70.,0,51,70.,0,52,70.,0,53,70.,0,54,70.,0
55,70.,0,56,70.,0,57,70.,0,58,70.,0,59,70.,0,60,70.,0
61,70.,0,62,70.,0,63,70.,0,64,70.,0,65,70.,0,66,70.,0
67,70.,0,68,70.,0,69,70.,0,70,70.,0,71,70.,0,72,70.,0
73,70.,0,74,70.,0,75,70.,0,76,70.,0,77,70.,0,78,70.,0
79,70.,0,80,70.,0,81,70.,0,82,70.,0,83,70.,0,84,70.,0
85,70.,0,86,70.,0,87,70.,0,88,70.,0,89,70.,0,90,70.,0
91,70.,0,92,70.,0,93,70.,0,94,70.,0,95,70.,0,96,70.,0
97,70.,0,98,70.,0,99,70.,0,100,70.,0,101,70.,0,102,70.,0
103,70.,0,104,70.,0,105,70.,0,106,70.,0,107,70.,0,108,70.,0
109,70.,0,110,70.,0,111,70.,0,112,70.,0,113,70.,0,114,70.,0
115,70.,0,116,70.,0,117,70.,0,118,70.,0,119,70.,0,120,70.,0
121,70.,0,122,70.,0,123,70.,0,124,70.,0,125,70.,0,126,70.,0
127,70.,0,128,70.,0,129,70.,0,130,70.,0,131,70.,0,132,70.,0
133,70.,0,134,70.,0,135,70.,0,136,70.,0,137,70.,0,138,70.,0
139,70.,0,140,70.,0,141,70.,0,142,70.,0,143,70.,0,144,70.,0
145,70.,0,146,70.,0,147,70.,0,148,70.,0,149,70.,0,150,70.,0
151,70.,0,152,70.,0,153,70.,0,154,70.,0,155,70.,0,156,70.,0
157,70.,0,158,70.,0,159,70.,0,160,70.,0,161,70.,0,162,70.,0
163,70.,0,164,70.,0,165,70.,0,166,70.,0,167,70.,0,168,70.,0
169,70.,0,170,70.,0,171,70.,0,172,70.,0,173,70.,0,174,70.,0
175,70.,0,176,70.,0,177,70.,0,178,70.,0,179,70.,0,180,70.,0
181,70.,0,182,70.,0,183,70.,0,184,70.,0,185,70.,0,186,70.,0
187,70.,0,188,70.,0,189,70.,0,190,70.,0
191,70.,-1,192,70.,-1,193,70.,-1,194,70.,-1
195,70.,-1,196,70.,-1,197,70.,-1,198,70.,-1
199,70.,-1,200,70.,-1,201,70.,-1,202,70.,-1
203,70.,-1,204,70.,-1,205,70.,-1,206,70.,-1
207,70.,-1,208,70.,-1,209,70.,-1,210,70.,-1
211,70.,-1,212,70.,-1,213,70.,-1,214,70.,-1
215,70.,-1,216,70.,-1,217,70.,-1,218,70.,-1
219,70.,-1,220,70.,-1,221,70.,-1,222,70.,-1
223,70.,-1,224,70.,-1,225,70.,-1,226,70.,-1
227,70.,-1,228,70.,-1,229,70.,-1,230,70.,-1
231,70.,-1,232,70.,-1,233,70.,-1,234,70.,-1
235,70.,-1,236,70.,-1,237,70.,-1,238,70.,-1
239,70.,-1,240,70.,-1,241,70.,-1,242,70.,-1
243,70.,-1,244,70.,-1,245,70.,-1,246,70.,-1
247,70.,0,-248,70.,0,-249,70.,0,-250,70.,0,-251,70.,0
-252,70.,0,-253,70.,0,-254,70.,0,-255,70.,0,-256,70.,0
-257,70.,0,-258,70.,0,-259,70.,0,-260,70.,0
END

```

Table 13. Chrysler Improved Numerical Differencing Analyzer (Contd)

RELATIVE NODE NUMBERS			ACTUAL NODE NUMBERS									
1	THRU	10	1	2	3	4	5	6	7	8	9	10
11	THRU	20	11	12	13	14	15	16	17	18	19	20
21	THRU	30	21	22	23	24	25	26	27	28	29	30
31	THRU	40	31	32	33	34	35	36	37	38	39	40
41	THRU	50	41	42	43	44	45	46	47	48	49	50
51	THRU	60	51	52	53	54	55	56	57	58	59	60
61	THRU	70	61	62	63	64	65	66	67	68	69	70
71	THRU	80	71	72	73	74	75	76	77	78	79	80
81	THRU	90	81	82	83	84	85	86	87	88	89	90
91	THRU	100	91	92	93	94	95	96	97	98	99	100
101	THRU	110	101	102	103	104	105	106	107	108	109	110
111	THRU	120	111	112	113	114	115	116	117	118	119	120
121	THRU	130	121	122	123	124	125	126	127	128	129	130
131	THRU	140	131	132	133	134	135	136	137	138	139	140
141	THRU	150	141	142	143	144	145	146	147	148	149	150
151	THRU	160	151	152	153	154	155	156	157	158	159	160
161	THRU	170	161	162	163	164	165	166	167	168	169	170
171	THRU	180	171	172	173	174	175	176	177	178	179	180
181	THRU	190	181	182	183	184	185	186	187	188	189	190
191	THRU	200	191	192	193	194	195	196	197	198	199	200
201	THRU	210	201	202	203	204	205	206	207	208	209	210
211	THRU	220	211	212	213	214	215	216	217	218	219	220
221	THRU	230	221	222	223	224	225	226	227	228	229	230
231	THRU	240	231	232	233	234	235	236	237	238	239	240
241	THRU	250	241	242	243	244	245	246	247	248	249	250
251	THRU	260	251	252	253	254	255	256	257	258	259	260
BCD 3CONDUCTOR DATA												
111,1,2,34,35,67,68,0												
112,2,3,35,36,68,69,0												
113,3,4,36,37,69,70,0												
114,4,5,37,38,70,71,0												
115,5,6,38,39,71,72,0												
116,6,7,39,40,72,73,0												
117,7,8,40,41,73,74,0												
118,8,9,41,42,74,75,0												
119,9,10,42,43,75,76,0												
1110,10,11,43,44,76,77,0												
1111,11,12,44,45,77,78,0												
1112,12,13,45,46,78,79,0												
1113,13,14,46,47,79,80,0												
1114,14,15,47,48,80,81,0												
1115,15,16,48,49,81,82,0												
1116,16,17,49,50,82,83,0												
1117,17,18,50,51,83,84,0												
1118,18,19,51,52,84,85,0												
1119,19,20,52,53,85,86,0												
1120,20,21,53,54,86,87,0												
1121,21,22,54,55,87,88,0												
1122,22,23,55,56,88,89,0												
1123,23,24,56,57,89,90,0												
1124,24,25,57,58,90,91,0												
1125,25,26,58,59,91,92,0												
1126,26,27,59,60,92,93,0												
1127,27,28,60,61,93,94,0												

Table 13. Chrysler Improved Numerical Differencing Analyzer (Contd)

1128,28,29,61,62,94,95,0
1129,29,30,62,63,95,96,0
1130,30,31,63,64,96,97,0
1131,31,32,64,65,97,98,0
1132,32,33,65,66,98,99,0
121,1,34,34,67,0
122,2,35,35,68,0
123,3,36,36,69,0
124,4,37,37,70,0
125,5,38,38,71,0
126,6,39,39,72,0
127,7,40,40,73,0
128,8,41,41,74,0
129,9,42,42,75,0
1210,10,43,43,76,0
1211,11,44,44,77,0
1212,12,45,45,78,0
1213,13,46,46,79,0
1214,14,47,47,80,0
1215,15,48,48,81,0
1216,16,49,49,82,0
1217,17,50,50,83,0
1218,18,51,51,84,0
1219,19,52,52,85,0
1220,20,53,53,86,0
1221,21,54,54,87,0
1222,22,55,55,88,0
1223,23,56,56,89,0
1224,24,57,57,90,0
1225,25,58,58,91,0
1226,26,59,59,92,0
1227,27,60,60,93,0
1228,28,61,61,94,0
1229,29,62,62,95,0
1230,30,63,63,96,0
1231,31,64,64,97,0
1232,32,65,65,98,0
1233,33,66,0
2233,66,99,0
321,67,100,0
322,68,101,0
323,69,102,0
324,70,103,0
325,71,104,0
326,72,105,0
327,73,106,0
328,74,107,0
329,75,108,0
3210,76,109,0
3211,77,110,0
3212,78,111,0
3213,79,112,0
3214,80,113,0
3215,81,114,0
3216,82,115,0
3217,83,116,0

Table 13. Chrysler Improved Numerical Differencing Analyzer (Contd)

3218,84,215,0
3219,85,111,0
3220,86,219,0
3221,87,112,0
3222,88,223,0
3223,89,113,0
3224,90,227,0
3225,91,114,0
3226,92,231,0
3227,93,115,0
3228,94,235,0
3229,95,116,0
3230,96,239,0
3231,97,117,0
3232,98,243,0
3233,99,118,0
411,100,101,0
412,101,102,0
413,102,103,0
414,103,104,0
415,104,194,0
416,192,105,0
417,105,198,0
418,196,106,0
419,106,202,0
4110,200,107,0
4111,107,206,0
4112,204,108,0
4113,108,210,0
4114,208,109,0
4115,109,214,0
4116,212,110,0
4117,110,218,0
4118,216,111,0
4119,111,222,0
4120,220,112,0
4121,112,226,0
4122,224,113,0
4123,113,230,0
4124,228,114,0
4125,114,234,0
4126,232,115,0
4127,115,238,0
4128,236,116,0
4129,116,242,0
4130,240,117,0
4131,117,246,0
4132,244,118,0
421,100,119,0
422,101,120,0
423,102,121,0
424,103,122,0
425,104,123,0
426,193,124,0
427,105,125,0
428,197,126,0

Table 13. Chrysler Improved Numerical Differencing Analyzer (Contd)

429,106,127,0
4210,201,128,0
4211,107,129,0
4212,205,130,0
4213,108,131,0
4214,209,132,0
4215,109,133,0
4216,213,134,0
4217,110,135,0
4218,217,136,0
4219,111,137,0
4220,221,138,0
4221,112,139,0
4222,225,140,0
4223,113,141,0
4224,229,142,0
4225,114,143,0
4226,233,144,0
4227,115,145,0
4228,237,146,0
4229,116,147,0
4230,241,148,0
4231,117,149,0
4232,245,150,0
4233,118,151,0
511,119,120,0
512,120,121,0
513,121,122,0
514,122,123,0
515,123,124,0
516,124,125,0
517,125,126,0
518,126,127,0
519,127,128,0
5110,128,129,0
5111,129,130,0
5112,130,131,0
5113,131,132,0
5114,132,133,0
5115,133,134,0
5116,134,135,0
5117,135,136,0
5118,136,137,0
5119,137,138,0
5120,138,139,0
5121,139,140,0
5122,140,141,0
5123,141,142,0
5124,142,143,0
5125,143,144,0
5126,144,145,0
5127,145,146,0
5128,146,147,0
5129,147,148,0
5130,148,149,0
5131,149,150,0

Table 13. Chrysler Improved Numerical Differencing Analyzer (Contd)

5132,150,151,0
521,119,183,0
522,120,184,0
523,121,185,0
524,122,152,0
525,123,153,0
526,124,154,0
527,125,156,0
528,126,157,0
529,127,158,0
5210,128,159,0
5211,129,160,0
5212,130,161,0
5213,131,162,0
5214,132,163,0
5215,133,164,0
5216,134,165,0
5217,135,166,0
5218,136,167,0
5219,137,168,0
5220,138,169,0
5221,139,170,0
5222,140,171,0
5223,141,172,0
5224,142,173,0
5225,143,174,0
5226,144,175,0
5227,145,176,0
5228,146,177,0
5229,147,178,0
5230,148,179,0
5231,149,180,0
5232,150,181,0
5233,151,182,0
611,183,184,0
612,184,185,0
613,185,152,0
614,152,153,0
615,153,154,0
616,154,156,0
617,156,157,0
618,157,158,0
6110,158,159,0
6111,159,160,0
6112,160,161,0
6113,161,162,0
6114,162,163,0
6115,163,164,0
6116,164,165,0
6117,165,166,0
6118,166,167,0
6119,167,168,0
6120,168,169,0
6121,169,170,0
6122,170,171,0
6123,171,172,0

Table 13. Chrysler Improved Numerical Differencing Analyzer (Contd)

```

6124,172,173,0
6125,173,174,0
6126,174,175,0
6127,175,176,0
6128,176,177,0
6129,177,178,0
6130,178,179,0
6131,179,180,0
6132,180,181,0
6133,181,182,0
621,183,186,0
622,184,187,0
623,185,188,0
711,186,187,0
712,187,188,0
721,186,189,0
722,187,190,0
723,188,155,0
811,189,190,0
812,190,155,0
901,191,247,192,247,193,247,194,247,0
902,195,248,196,248,197,248,198,248,0
903,199,249,200,249,201,249,202,249,0
904,203,250,204,250,205,250,206,250,0
905,207,251,208,251,209,251,210,251,0
906,211,252,212,252,213,252,214,252,0
907,215,253,216,253,217,253,218,253,0
908,219,254,220,254,221,254,222,254,0
909,223,255,224,255,225,255,226,255,0
910,227,256,228,256,229,256,230,256,0
911,231,257,232,257,233,257,234,257,0
912,235,258,236,258,237,258,238,258,0
913,239,259,240,259,241,259,242,259,0
914,243,260,244,260,245,260,246,260,0
LND
BCD 3CONSTANTS DATA
NLUOP,1500,1,0630,2,0797,3,183 $K1=K,K2=RHO,K3=C SUB P
4,70,5,0.43 $K4=INITIAL TEMP.,K5=ABSORBED SOLAR FLUX
6,370,7,144. $K6=CONVECTIVE COEFFICIENT
10,0,12,91,13,32,14,0,15,31,16,14,17,246,18,29
11,-33
DRLXCA,0.001,ARLXCA,0.001 $TEMP. CHANGES FOR STEADY SOLUTION
197,30,198,005,199,1.1 $K197=TIMEEND,K198=OUTPUT,K199=CSGFAC
1301,800,1302,523,1303,310,1304,719,1305,895
1306,527,1307,1.43,1308,661,1309,1.76,1310,796
1311,2.08,1312,.931,1313,2.41,1314,1.07,1315,2.73
1316,1.20,1317,3.05,1318,1.34,1319,3.38,1320,1.47
1321,3.70,1322,1.61,1323,4.03,1324,1.74,1325,4.35
1326,1.87,1327,4.58,1328,2.01,1329,5.00,1330,2.14
1331,5.33,1332,2.28,1333,2.85,1400,1.36,1401,884
1402,526,1403,1.22,1404,1.52,1405,2.42,1406,2.97
1407,3.52,1408,4.07,1409,4.62,1410,5.16,1411,5.72
1412,6.27,1413,6.82,1414,7.37,1415,7.90,1416,8.47
1417,9.02,1418,4.82,1419,2.35,1420,1.75,1421,1.07
1422,2.52,1423,3.25,1424,1.95,1425,5.46,1426,2.58
1427,7.03,1428,3.22,1429,8.19,1430,3.57,1431,8.75

```

Table 13. Chrysler Improved Numerical Differencing Analyzer (Contd)

1432,3.85,1433,9.56,1434,4.07,1435,10.0,1436,4.25
 1437,10.5,1438,4.34,1439,10.5,1440,4.38,1441,10.6
 1442,4.38,1443,10.5,1444,4.31,1445,10.3,1446,4.20
 1447,9.89,1448,4.01,1449,9.35,1450,3.80,1451,4.49
 1452,4.40,1453,5.13,1454,2.85,1455,2.03,1456,1.66
 1457,3.10,1458,7.61,1459,3.22,1460,8.18,1461,3.56
 1462,8.92,1463,3.83,1464,9.49,1465,4.04,1466,9.94
 1467,4.21,1468,10.3,1469,4.29,1470,10.4,1471,4.32
 1472,10.4,1473,4.30,1474,10.3,1475,4.20,1476,10.0
 1477,4.08,1478,9.55,1479,3.86,1480,3.83,1481,4.49
 1482,2.84,1483,5.05,1484,3.30,1485,1.96,1486,5.24
 1487,3.42,1488,2.03,1489,5.25,1490,3.42
 111,7.15,112,4.90,113,5.45,114,4.78,115,4.20
 116,6.06,117,8.58,118,8.37,119,9.29,1110,9.76
 1111,11.2,1112,11.4,1113,12.5,1114,13.3,1115,14.1
 1116,15.0,1117,16.2,1118,16.2,1119,17.6,1120,17.8
 1121,19.5,1122,19.4,1123,21.2,1124,21.0,1125,22.8
 1126,22.7,1127,24.4,1128,24.3,1129,26.1,1130,26.6
 1131,27.8,1132,43.5
 121,47.4,122,30.9,123,18.4,124,42.5,125,53.0
 126,31.1,127,84.7,128,39.1,129,104.1,1210,47.1
 1211,123.1,1212,55.1,1213,142.1,1214,63.1,1215,162.1
 1216,71.0,1217,181.1,1218,79.0,1219,200.1,1220,87.0
 1221,219.1,1222,95.0,1223,238.1,1224,103.1,1225,258.1
 1226,111.1,1227,277.1,1228,119.1,1229,296.1,1230,127.1
 1231,315.1,1232,135.1,1233,137.1
 2233,169.1
 321,35.2,322,23.0,323,13.7,324,31.6,325,39.4
 326,62.3,327,62.9,328,78.3,329,77.1,3210,94.2
 3211,91.4,3212,110.1,3213,106.1,3214,126.1,3215,120.1
 3216,142.1,3217,134.1,3218,158.1,3219,149.1,3220,174.1
 3221,163.1,3222,190.1,3223,177.1,3224,206.1,3225,191.1
 3226,222.1,3227,206.1,3228,238.1,3229,220.1,3230,254.1
 3231,234.1,3232,270.1,3233,125.1
 411,1.21,412,8.29,413,9.21,414,8.09,415,18.6
 416,21.4,417,21.4,418,22.0,419,22.0,4110,26.9
 4111,26.9,4112,31.0,4113,31.0,4114,34.0,4115,34.0
 4116,38.9,4117,38.9,4118,42.0,4119,42.0,4120,46.9
 4121,46.9,4122,51.0,4123,51.0,4124,55.0,4125,55.0
 4126,58.8,4127,58.8,4128,62.9,4129,62.9,4130,66.9
 4131,66.9,4132,136.1
 421,20.5,422,12.3,423,7.18,424,16.4,425,20.0
 426,16.8,427,30.8,428,20.0,429,36.5,4210,23.2
 4211,43.7,4212,28.8,4213,52.7,4214,34.9,4215,62.3
 4216,42.0,4217,72.6,4218,49.9,4219,83.6,4220,59.0
 4221,96.6,4222,69.4,4223,110.1,4224,81.6,4225,126.1
 4226,96.0,4227,143.1,4228,115.1,4229,162.1,4230,136.1
 4231,183.1,4232,162.1,4233,103.1
 511,3.73,512,16.4,513,18.7,514,16.8,515,26.1
 516,22.5,517,32.7,518,32.7,519,37.2,5110,39.5
 5111,44.1,5112,43.6,5113,46.5,5114,48.1,5115,49.4
 5116,50.9,5117,53.1,5118,51.5,5119,53.7,5120,52.6
 5121,55.4,5122,53.2,5123,55.6,5124,52.9,5125,54.8
 5126,52.1,5127,53.6,5128,50.6,5129,51.6,5130,49.7
 5131,48.7,5132,72.7
 521,10.2,522,6.40,523,3.78

Table 13. Chrysler Improved Numerical Differencing Analyzer (Contd)

```

524,8.83,525,11.4,526,6.83,527,19.2,528,9.11,529,24.9
5210,11.6,5211,31.2,5212,14.4,5213,38.3,5214,17.5
5215,46.4,5216,21.0,5217,55.3,5218,25.1,5219,65.1
5220,29.6,5221,77.4,5222,34.7,5223,91.4,5224,41.2
5225,108.,5226,48.6,5227,128.,5228,58.0,5229,153.
5230,69.3,5231,183.,5232,82.9,5233,108.
611,4.51,612,30.9,613,34.4
614,29.2,615,41.2,616,32.8,617,43.0,618,39.2
6110,40.3,6111,39.5,6112,44.0,6113,43.5,6114,46.4
6115,47.9,6116,49.1,6117,50.5,6118,52.6,6119,51.0
6120,53.5,6121,52.1,6122,54.7,6123,52.5,6124,54.6
6125,52.0,6126,53.8,6127,50.9,6128,52.3,6129,49.1
6130,49.8,6131,47.8,6132,46.7,6133,68.6
621,7.38,622,4.82,623,2.86
711,4.67,712,32.0
721,7.25,722,4.73,723,2.81
811,4.67,812,32.0
1334,1.63
901,3.62,902,4.54,903,5.46,904,6.39,905,7.31 $AREAS FOR
906,8.24,907,9.16,908,10.1,909,11.0,910,11.9 $CONVECTIVE
911,12.9,912,13.8,913,14.7,914,15.6 $CONDUCTORS
921,6.16,922,4.02,923,2.39,924,5.53,925,5.89,926,4.05 $A S
927,11.0,928,5.09,929,13.5,930,5.12,931,16.0,932,7.16 $R J
933,18.5,934,8.20,935,21.0,936,9.23,937,23.5,938,10.3 $E F U
939,26.0,940,11.3,941,28.5,942,12.3,943,31.0,944,13.4 $A D R
945,33.5,946,14.4,947,36.0,948,15.5,949,38.5,950,16.5 $S R C
951,41.0,952,17.5,953,7.26 $ E
19,-1,20,0,21,14.,22,68.,23,80.,24,22,25,19,26,18,27,-61
28,3.2,29,55,30,-8,31,56,32,-6,33,57,34,-7
35,-50,36,17
37,-44 $NO. OF POINTS FOR TRANSIENT PLOTS
38,18,39,19,40,20,41,21,42,24
43,2,44,1,45,2 $FOR SKPTST CALLS
46,0,47,1 $FOR STUARY CALLS
50,0.,51,CUND,52,901
END
BCD 3ARRAY DATA
-1,SPACE,100,END
-2,0.0,1.60,1.90,2.20,2.61,2.93,3.34,3.68,4.05,4.43,4.81,5.18,5.56,5.93,6.31,6.68,7.06,7.43,7.80,8.18,8.56,8.93 $AND
9.31,9.68,10.06,10.43,10.81,11.18,11.56,11.93,12.31 $BOT-
12.68,12.92,END $TOM ROWS OF NODES
-3,SPACE,33,END
-4,SPACE,33,END
-5,0.0,1.60,1.90,2.20,2.61,2.82,2.93,3.04,3.34,3.57 $ROW OF
3.68,3.79,4.05,4.32,4.43,4.54,4.81,5.07,5.18,5.29,5.56 $NODES
5.82,5.93,6.04,6.31,6.57,6.68,6.79,7.06,7.32,7.43,7.54 $CON-
7.80,8.07,8.18,8.29,8.56,8.82,8.93,9.04,9.31,9.57,9.68 $TAIN-
9.79,10.06,10.32,10.43,10.54,10.81,11.07,11.18,11.29 $ING
11.56,11.82,11.93,12.04,12.31,12.57,12.68,12.79,12.92 $COOL-
END $ING COIL
-6,SPACE,61,END
-7,SPACE,100,END
-8,SPACE,100,END
-9,SPACE,100,END
-10,SPACE,100,END

```

Table 13. Chrysler Improved Numerical Differencing Analyzer (Contd)

```

-11,SPACE,100,END
-12,SPACE,100,END
-13
BCD 8RADIAL POSITION,INCHES F-FRONT ROW, C-DEPTH OF
BCD 4COOLANT TUBE, B-BACK ROW
END
-14
BCD 8TEMPERATURE DEGR FES F
BCD 4
END
-15
BCD 8STEADY TEMPERATURE, INTERNALLY-COOLED GREGORIAN
BCD 4ULE QUARTZ, TURB. FLOW
END
-16
BCD 8AXIAL DISTANCE FROM FRONT SURFACE, INCHES X-COL.
BCD 43,Y-COL. 5,Z-COL. 20
END
-17
BCD 8TIME, HOURS A-NODE 3, B-NODE 5, C-NODE 20, D-NODE 1
BCD 455,E-NODE 153,H-NODE 169
END
-18,.065,.195,.325,.500,.833,1.466,2.30,3.15,END
-19,.065,.195,.325,.500,.845,1.452,END
-20,.065,.195,.325,.390,.640,.832,1.212,END
-21
BCD 8TRANSIENT TEMPERATURE, INTERNALLY-COOLED GREGORIA
BCD 4N,ULE QUARTZ, TURB. FLOW
END
END
BCD 3EXECUTION
MLTPLY(K2,K3,K10) $COMPUTE RHO-C PRODUCT
BCDARY(A1,K1301,K1302,K1303,K1304,K1305,K1306,K1307,K1308
K1309,K1310,K1311,K1312,K1313,K1314,K1315,K1316
K1317,K1318,K1319,K1320,K1321,K1322,K1323,K1324
K1325,K1326,K1327,K1328,K1329,K1330,K1331,K1332
K1333)
ARYMPY(K11,A1,K10,A1)
BRKARY(A1,C1,C2,C3,C4,C5,C6,C7,C8,C9,C10,C11,C12,C13,C14,C15
C16,C17,C18,C19,C20,C21,C22,C23,C24,C25,C26,C27,C28
C29,C30,C31,C32,C33)
BRKARY(A1,C34,C35,C36,C37,C38,C39,C40,C41,C42,C43,C44,C45
C46,C47,C48,C49,C50,C51,C52,C53,C54,C55,C56,C57
C58,C59,C60,C61,C62,C63,C64,C65,C66)
BRKARY(A1,C67,C68,C69,C70,C71,C72,C73,C74,C75,C76,C77,C78
C79,C80,C81,C82,C83,C84,C85,C86,C87,C88,C89,C90
C91,C92,C93,C94,C95,C96,C97,C98,C99)
MLTPLY(K1334,K10,C33)
BCDARY(A1,K1400,K1401,K1402,K1403,K1404,K1405,K1406,K1407
K1408,K1409,K1410,K1411,K1412,K1413,K1414,K1415
K1416,K1417,K1418,K1419,K1420,K1421,K1422,K1423
K1424,K1425,K1426,K1427,K1428,K1429,K1430,K1431
K1432,K1433,K1434,K1435,K1436,K1437,K1438,K1439
K1440,K1441,K1442,K1443,K1444,K1445,K1446,K1447
K1448,K1449,K1450,K1451,K1452,K1453,K1454,K1455
K1456,K1457,K1458,K1459,K1460,K1461,K1462,K1463

```

Table 13. Chrysler Improved Numerical Differencing Analyzer (Contd)

	K1464,K1465,K1466,K1467,K1468,K1469,K1470,K1471 K1472,K1473,K1474,K1475,K1476,K1477,K1478,K1479 K1480,K1481,K1482,K1483,K1484,K1485,K1486,K1487 K1488,K1489,K1490)
ARYMPY(K12,A1,K10,A1)	
BRKARY(A1,C100,C101,C102,C103,C104,C105,C106,C107,C108 C109,C110,C111,C112,C113,C114,C115,C116,C117 C118,C119,C120,C121,C122,C123,C124,C125,C126 C127,C128,C129,C130,C131,C132,C133,C134,C135 C136,C137,C138,C139,C140,C141,C142,C143,C144 C145,C146,C147,C148,C149,C150,C151,C152,C153 C154,C155,C156,C157,C158,C159,C160,C161,C162 C163,C164,C165,C166,C167,C168,C169,C170,C171 C172,C173,C174,C175,C176,C177,C178,C179,C180 C181,C182,C183,C184,C185,C186,C187,C188,C189 C190)	
BLDARY(A1,K111,K112,K113,K114,K115,K116,K117,K118,K119 K1110,K1111,K1112,K1113,K1114,K1115,K1116 K1117,K1118,K1119,K1120,K1121,K1122,K1123 K1124,K1125,K1126,K1127,K1128,K1129,K1130 K1131,K1132)	
ARYMPY(K13,A1,K1,A1)	
BRKARY(A1,G111,G112,G113,G114,G115,G116,G117,G118,G119 G1110,G1111,G1112,G1113,G1114,G1115,G1116 G1117,G1118,G1119,G1120,G1121,G1122,G1123 G1124,G1125,G1126,G1127,G1128,G1129,G1130 G1131,G1132)	
BLDARY(A1,K121,K122,K123,K124,K125,K126,K127,K128,K129 K1210,K1211,K1212,K1213,K1214,K1215,K1216 K1217,K1218,K1219,K1220,K1221,K1222,K1223 K1224,K1225,K1226,K1227,K1228,K1229,K1230 K1231,K1232,K1233)	
ARYMPY(K11,A1,K1,A1)	
BRKARY(A1,G121,G122,G123,G124,G125,G126,G127,G128,G129 G1210,G1211,G1212,G1213,G1214,G1215,G1216 G1217,G1218,G1219,G1220,G1221,G1222,G1223 G1224,G1225,G1226,G1227,G1228,G1229,G1230 G1231,G1232,G1233)	
MLTPLY(K2233,K1,G2233)	
BLDARY(A1,K321,K322,K323,K324,K325,K326,K327,K328,K329 K3210,K3211,K3212,K3213,K3214,K3215,K3216 K3217,K3218,K3219,K3220,K3221,K3222,K3223 K3224,K3225,K3226,K3227,K3228,K3229,K3230 K3231,K3232,K3233)	
ARYMPY(K11,A1,K1,A1)	
BRKARY(A1,G321,G322,G323,G324,G325,G326,G327,G328,G329 G3210,G3211,G3212,G3213,G3214,G3215,G3216 G3217,G3218,G3219,G3220,G3221,G3222,G3223 G3224,G3225,G3226,G3227,G3228,G3229,G3230 G3231,G3232,G3233)	
MLTPLY(K621,K1,G621)	
MLTPLY(K622,K1,G622)	
MLTPLY(K623,K1,G623)	
MLTPLY(K711,K1,G711)	
MLTPLY(K712,K1,G712)	
MLTPLY(K721,K1,G721)	

Table 13. Chrysler Improved Numerical Differencing Analyzer (Contd)

MLTPLY(K722,K1,G722)
MLTPLY(K723,K1,G723)
MLTPLY(K811,K1,G811)
MLTPLY(K812,K1,G812)
BLDARY(A1,K411,K412,K413,K414,K415,K416,K417,K418,K419
K4110,K4111,K4112,K4113,K4114,K4115,K4116
K4117,K4118,K4119,K4120,K4121,K4122,K4123
K4124,K4125,K4126,K4127,K4128,K4129,K4130
K4131,K4132)
ARYMPY(K13,A1,K1,A1)
BRKARY(A1,G411,G412,G413,G414,G415,G416,G417,G418,G419
G4110,G4111,G4112,G4113,G4114,G4115,G4116
G4117,G4118,G4119,G4120,G4121,G4122,G4123
G4124,G4125,G4126,G4127,G4128,G4129,G4130
G4131,G4132)
BLDARY(A1,K421,K422,K423,K424,K425,K426,K427,K428,K429
K4210,K4211,K4212,K4213,K4214,K4215,K4216
K4217,K4218,K4219,K4220,K4221,K4222,K4223
K4224,K4225,K4226,K4227,K4228,K4229,K4230
K4231,K4232,K4233)
ARYMPY(K11,A1,K1,A1)
BRKARY(A1,G421,G422,G423,G424,G425,G426,G427,G428,G429
G4210,G4211,G4212,G4213,G4214,G4215,G4216
G4217,G4218,G4219,G4220,G4221,G4222,G4223
G4224,G4225,G4226,G4227,G4228,G4229,G4230
G4231,G4232,G4233)
BLDARY(A1,K511,K512,K513,K514,K515,K516,K517,K518,K519
K5110,K5111,K5112,K5113,K5114,K5115,K5116
K5117,K5118,K5119,K5120,K5121,K5122,K5123
K5124,K5125,K5126,K5127,K5128,K5129,K5130
K5131,K5132)
ARYMPY(K13,A1,K1,A1)
BRKARY(A1,G511,G512,G513,G514,G515,G516,G517,G518,G519
G5110,G5111,G5112,G5113,G5114,G5115,G5116
G5117,G5118,G5119,G5120,G5121,G5122,G5123
G5124,G5125,G5126,G5127,G5128,G5129,G5130
G5131,G5132)
BLDARY(A1,K521,K522,K523,K524,K525,K526,K527,K528,K529
K5210,K5211,K5212,K5213,K5214,K5215,K5216
K5217,K5218,K5219,K5220,K5221,K5222,K5223
K5224,K5225,K5226,K5227,K5228,K5229,K5230
K5231,K5232,K5233)
ARYMPY(K11,A1,K1,A1)
BRKARY(A1,G521,G522,G523,G524,G525,G526,G527,G528,G529
G5210,G5211,G5212,G5213,G5214,G5215,G5216
G5217,G5218,G5219,G5220,G5221,G5222,G5223
G5224,G5225,G5226,G5227,G5228,G5229,G5230
G5231,G5232,G5233)
BLDARY(A1,K611,K612,K613,K614,K615,K616,K617,K618
K6110,K6111,K6112,K6113,K6114,K6115,K6116
K6117,K6118,K6119,K6120,K6121,K6122,K6123
K6124,K6125,K6126,K6127,K6128,K6129,K6130
K6131,K6132)
ARYMPY(K15,A1,K1,A1)
BRKARY(A1,G611,G612,G613,G614,G615,G616,G617,G618
G6110,G6111,G6112,G6113,G6114,G6115,G6116

Table 13. Chrysler Improved Numerical Differencing Analyzer (Contd)

	G6117,G6118,G6119,G6120,G6121,G6122,G6123
	G6124,G6125,G6126,G6127,G6128,G6129,G6130
	G6131,G6132)
	BLDARY(A1,K901,K902,K903,K904,K905,K906,K907,K908
	K909,K910,K911,K912,K913,K914)
	ARYMPY(K16,A1,K6,A1)
	ARYDIV(K16,A1,K7,A1)
	BRKARY(A1,G901,G902,G903,G904,G905,G906,G907,G908
	G909,G910,G911,G912,G913,G914)
	CSGDMP
	SKPTST(K20,K43,K44,K44)
	OPNPLT
	CTNDSS
	BLDARY(A3,T1,T2,T3,T4,T5,T6,T7,T8,T9,T10,T11,T12,T13
	T14,T15,T16,T17,T18,T19,T20,T21,T22,T23,T24
	T25,T26,T27,T28,T29,T30,T31,T32,T33)
	BLDARY(A4,T183,T184,T185,T152,T153,T154,T156,T157,T158
	T159,T160,T161,T162,T163,T164,T165,T166,T167
	T168,T169,T170,T171,T172,T173,T174,T175,T176
	T177,T178,T179,T180,T181,T182)
	BLDARY(A6,T100,T101,T102,T103,T104,T194,T247,T192,T105
	T198,T248,T196,T106,T202,T249,T200,T107,T206
	T250,T204,T108,T210,T251,T208,T109,T214,T252
	T212,T110,T218,T253,T216,T111,T222,T254,T220
	T112,T226,T255,T224,T113,T230,T256,T228,T114
	T234,T257,T232,T115,T238,T258,T236,T116,T242
	T259,T240,T117,T246,T260,T244,T118)
	PLOTX2(K19,K20,K21,K22,K23,K24,A13,A14,A15,K11,A2,A3)
	PLOTX2(K20,K20,K21,K22,K23,K26,A13,A14,A15,K11,A2,A4)
	PLOTX2(K20,K20,K21,K22,K23,K25,A13,A14,A15,K27,A5,A6)
	BLDARY(A3,T3,T36,T69,T102,T121,T185,T188,T155)
	BLDARY(A4,T5,T38,T71,T104,T123,T153)
	BLDARY(A6,T20,T53,T86,T219,T221,T138,T169)
	PLOTX2(K19,K20,K28,K22,K23,K29,A16,A14,A15,K30,A18,A3)
	PLOTX2(K20,K20,K28,K22,K23,K31,A16,A14,A15,K32,A19,A4)
	PLOTX2(K20,K20,K28,K22,K23,K33,A16,A14,A15,K34,A20,A6)
	STFSQS(K4,K17,T1)
	STFSEP(K197,TIMEND)
	STFSEP(K198,OUTPUT)
	STFSEP(K199,CSGFAC)
	CNFRWD
	PLOTX2(K19,K20,K35,K22,K23,K36,A17,A14,A21,K37,A1,A7)
	PLOTX2(K20,K20,K35,K22,K23,K38,A17,A14,A21,K37,A1,A8)
	PLOTX2(K20,K20,K35,K22,K23,K39,A17,A14,A21,K37,A1,A9)
	PLOTX2(K20,K20,K35,K22,K23,K40,A17,A14,A21,K37,A1,A10)
	PLOTX2(K20,K20,K35,K22,K23,K41,A17,A14,A21,K37,A1,A11)
	PLOTX2(K20,K20,K35,K22,K23,K42,A17,A14,A21,K37,A1,A12)
	PLTND
	SKPTST(K20,K45,K44,K44)
	ENDFIL
	END
	BCD 3VARIABLES 1
	BLDARY(A1,K925,K926,K927,K928,K929
	K930,K931,K932,K933,K934,K935,K936,K937,K938
	K939,K940,K941,K942,K943,K944,K945,K946,K947
	K948,K949,K950,K951,K952,K953)

Table 13. Chrysler Improved Numerical Differencing Analyzer (Contd)

```

ARYMPY(K18,A1,K5,A1)
BRKARY(A1,Q5,Q6,Q7,Q8,Q9,Q10,Q11,Q12,Q13,Q14,Q15,Q16,Q17
      Q18,Q19,Q20,Q21,Q22,Q23,Q24,Q25,Q26,Q27,Q28,Q29
      Q30,Q31,Q32,Q33)
ADD(Q5,Q6,Q7,Q8,Q9,Q10,Q11,Q12,Q13,Q14,Q15,Q16,Q17,Q18
    Q19,Q20,Q21,Q22,Q23,Q24,Q25,Q26,Q27,Q28,Q29,Q30,Q31
    Q32,Q33,K50)
END
BCD 3VARIABLES 2
END
BCD 3OUTPUT CALLS
INDEX(K46,K47)
STDARY(K46,T3,A7)
STDARY(K46,T5,A8)
STDARY(K46,T20,A9)
STDARY(K46,T155,A10)
STDARY(K46,T153,A11)
STDARY(K46,T169,A12)
STDARY(K46,TIMEN,A1)
PRNTMP
END PRINT(K5,K46)

```

program the correct value will be calculated and loaded into these locations, except for those nodes that are either a boundary node, which is noted by a minus sign in front of the node number, or an arithmetic node which is noted by a negative capacitance value.

The next block of data is computer generated and assigns numbers to each node listing first the diffusion nodes (those nodes with capacitance) then the arithmetic nodes and last the boundary nodes.

Following this block of data is the "BCD 3CONDUCTOR DATA". In this block the first value is the conductor number, followed by paired numbers which are node numbers which have this conductor value between them. The final number lists the value of the conductor. Again the conductor value input is zero. The correct value will be calculated at a later time and will replace the zero.

The next block of data is the "BCD 3CONSTANTS DATA". This block of data lists the constants which are necessary to run the program, geometrical factors, and physical characteristics of the materials being considered. It is from this stored constant data that the thermal capacitance and thermal conductivity are calculated.

Following the "BCD 3CONSTANTS DATA" block is the "BCD 3ARRAY DATA". Arrays are established which allow operations on groups of data, allow storage area for data to be plotted and store labels for tables and plots.

The next block of data is the "BCD 3EXECUTION". It is in this block that the many subroutines are called up to do the computations to completely define the network and finally call upon the thermal analysis subroutine which is desired. In the sample case the card CINDSS calls upon a steady state subroutine to get the steady state solution. Following this is a card GNFRWD which calls up a transient subroutine.

Other instructions are given in this block also. The computer is instructed to print out certain data values desired where those values are constant. The computer is also instructed regarding plots for the steady state, and the transient solutions.

Following the "BCD 3EXECUTION" block is the "BCD 3VARIABLES 1" where it is required that the data of impressed source (solar, electrical, etc.) for any node be located. The impressed source is zeroed out after each iteration and reloaded at the beginning of each iteration. The impressed source data can either be constant values, time variant or temperature variant. If a print statement is included in this block, the command is honored after each

iteration and a printout will appear. This can be utilized to good advantage when a problem in the program exists. Since the printout appears after each iteration, much paper will be used so it is not recommended that this be done except for trouble shooting purposes.

In the "BCD 3VARIABLES 2" block post solution operations are performed. Examples of such operations are the rate of heat flow between nodes and the integral of this heat flow rate over a given period of time. Any calculations which are to be done after an iteration has been completed is to be called out in this block.

The final block in the program is the "BCD 3OUTPUT CALLS". Throughout the program much data is stored in many locations, but it is not printed out or plotted unless a specific instruction is given. In this particular program data are stored by the command "STOARY" which the plot subroutine in the "EXECUTION" block utilizes for the transient plots.

It was pointed out in the "VARIABLES 1" block that a print statement there would cause a printout after each iteration. A print statement in the "OUTPUT CALLS" block causes the data to be printed out after each time step. Each block must end with an "END" card.

The output of the program can be either in printed or graphical form. Table 14 shows the temperature listing for each node in the printed form. The first three columns indicate the relative node numbers of the temperatures listed in that line. For instance, the first line reads 1 THRU 5. The five numbers following are the temperatures of nodes 1, 2, 3, 4 and 5.

Figure 18 is a hand plot of the temperature of the front and back surface of the plane mirror. The back surface curve is a constant 70°F. There are three curves for three different materials - Quartz, Invar and Aluminum. This is the thermal data which was given to the stress analysis group for inputs to their program. Figure 19 is an example of a computer-generated plot.

Considerations other than thermal governed the configuration of the mirror. In the early stages, two configurations were considered. The plane mirror, Figure 17, which has been discussed before, and a tapered mirror shown in Figure 20. Figures 17 and 20 show a cross-section of one half of the mirror. The rectangles shown in these figures are revolved about the centerline to generate a quadrilateral torus. Figure 21 is a top view of the mirror showing the surface of revolution and node boundaries.

Table 14. Overall Analysis

TIME _O.	CTIMEU O.	CSGM(IN(.)) _O.	DTMPC(O) O.	ARLXCC(34) 9.92775E-C4 .	
1 THRU 5	7.395459E 01	7.423918E 01	7.442421E 01	7.475536E 01	7.620230E 01
6 THRU 10	7.625100E 01	7.645342E 01	7.639831E 01	7.656263E 01	7.648894E 01
11 THRU 15	7.665577E 01	7.659982E 01	7.671919E 01	7.673662E 01	7.692125E 01
16 THRU 20	7.689173E 01	7.70839CE 01	7.707161E 01	7.727699E 01	7.726568E 01
21 THRU 25	7.748041E 01	7.748084E 01	7.770890E 01	7.771927E 01	7.794160E 01
26 THRU 30	7.795134E 01	7.817066E 01	7.816694E 01	7.833995E 01	7.823281E 01
31 THRU 35	7.822353E 01	7.76551CE 01	7.704234E 01	7.395130E 01	7.421717C 01
36 THRU 40	7.437632E 01	7.463567E 01	7.543930E 01	7.533432E 01	7.558724E 01
41 THRU 45	7.546266E 01	7.569654E 01	7.55304E 01	7.578629E 01	7.566444E 01
46 THRU 50	7.590814E 01	7.580232E 01	7.605422E 01	7.595799E 01	7.621476E 01
51 THRU 55	7.613708E 01	7.640733E 01	7.633295E 01	7.660959E 01	7.655065E 01
56 THRU 60	7.683748E 01	7.678910E 01	7.707254E 01	7.702304E 01	7.730191E 01
61 THRU 65	7.724183E 01	7.747584E 01	7.732597E 01	7.738453E 01	7.685072E 01
66 THRU 70	7.648608E 01	7.394583E 01	7.417755E 01	7.429543E 01	7.445996E 01
71 THRU 75	7.476376E 01	7.434458E 01	7.475209E 01	7.444984E 01	7.486224E 01
76 THRU 80	7.454062E 01	7.494649E 01	7.465393E 01	7.506601E 01	7.479399E 01
81 THRU 85	7.521627E 01	7.49509CE 01	7.537387E 01	7.513123E 01	7.556611E 01
86 THRU 90	7.532857E 01	7.576652E 01	7.554980E 01	7.599376E 01	7.579050E 01
91 THRU 95	7.623093E 01	7.602754E 01	7.646130E 01	7.625662E 01	7.664416E 01
96 THRU 100	7.637608E 01	7.659759E 01	7.605392E 01	7.594129E 01	7.393606E 01
101 THRU 105	7.410804E 01	7.416531E 01	7.420729E 01	7.396938E 01	7.370834E 01
106 THRU 110	7.382057E 01	7.389564E 01	7.401432E 01	7.416304E 01	7.431473E 01
111 THRU 115	7.451231E 01	7.470755E 01	7.493228E 01	7.516681E 01	7.540302E 01
116 THRU 120	7.559977E 01	7.562801E 01	7.516555E 01	7.391152E 01	7.395875E 01
121 THRU 125	7.393217E 01	7.386327E 01	7.356375E 01	7.303650E 01	7.327512E 01

Table 14. Overall Analysis (Contd)

126	THRU	130	7.298229E 01	7.327549F 01	7.301550E 01	7.333521E 01	7.309726E 01
131	THRU	135	7.345766E 01	7.321559E 01	7.360661E 01	7.335342E 01	7.377334E 01
136	THRU	140	7.351491E 01	7.397829E 01	7.369709E 01	7.419440E 01	7.389916E 01
141	THRU	145	7.443246E 01	7.411454E 01	7.468434E 01	7.433200E 01	7.493348E 01
146	THRU	150	7.453405E 01	7.514446E 01	7.467016E 01	7.521225E 01	7.465909E 01
151	THRU	155	7.495599E 01	7.365129E 01	7.350551E 01	7.338677E 01	7.377420E 01
156	THRU	160	7.330086E 01	7.324726E 01	7.325043E 01	7.323831E 01	7.329159E 01
161	THRU	165	7.330865E 01	7.339599E 01	7.342706E 01	7.353446E 01	7.357110E 01
166	THRU	170	7.369729E 01	7.373850E 01	7.389106E 01	7.393036E 01	7.410326E 01
171	THRU	175	7.413900E 01	7.433475E 01	7.435942E 01	7.457935E 01	7.458117E 01
176	THRU	180	7.482101E 01	7.477918E 01	7.502420E 01	7.489630E 01	7.509092E 01
181	THRU	185	7.481469E 01	7.495559E 01	7.384786E 01	7.377103E 01	7.372161E 01
186	THRU	190	7.380906E 01	7.377261F 01	7.376811E 01	7.379518E 01	7.377557E 01
191	THRU	195	7.376275E 01	7.256272E 01	7.197134E 01	7.262079E 01	7.386701E 01
196	THRU	200	7.250520E 01	7.190397E 01	7.241040E 01	7.396071E 01	7.260695E 01
201	THRU	205	7.194317E 01	7.239016E 01	7.407530E 01	7.271717E 01	7.208176E 01
206	THRU	210	7.252443E 01	7.421749E 01	7.283141E 01	7.224820E 01	7.266182E 01
211	THRU	215	7.437634E 01	7.300300E 01	7.243791E 01	7.279705E 01	7.455884E 01
216	THRU	220	7.317444E 01	7.264923E 01	7.298850E 01	7.475756E 01	7.338649E 01
221	THRU	225	7.288076E 01	7.317468E 01	7.498180E 01	7.361333E 01	7.313476E 01
226	THRU	230	7.340516E 01	7.522538E 01	7.385243E 01	7.340488E 01	7.364532E 01
231	THRU	235	7.546455E 01	7.409116E 01	7.367831E 01	7.389106E 01	7.570347E 01
236	THRU	240	7.432407E 01	7.395568E 01	7.414920E 01	7.585039E 01	7.445825E 01
241	THRU	245	7.417687E 01	7.439533E 01	7.561769E 01	7.461128E 01	7.427994E 01
246	THRU	250	7.454375E 01	7.005500E 01	7.014500E 01	7.025600E 01	7.038700E 01
251	THRU	255	7.053800E 01	7.071000E 01	7.090300E 01	7.111500E 01	7.134900E 01
256	THRU	260	7.160300E 01	7.187700E 01	7.217100E 01	7.248700E 01	7.282200E 01

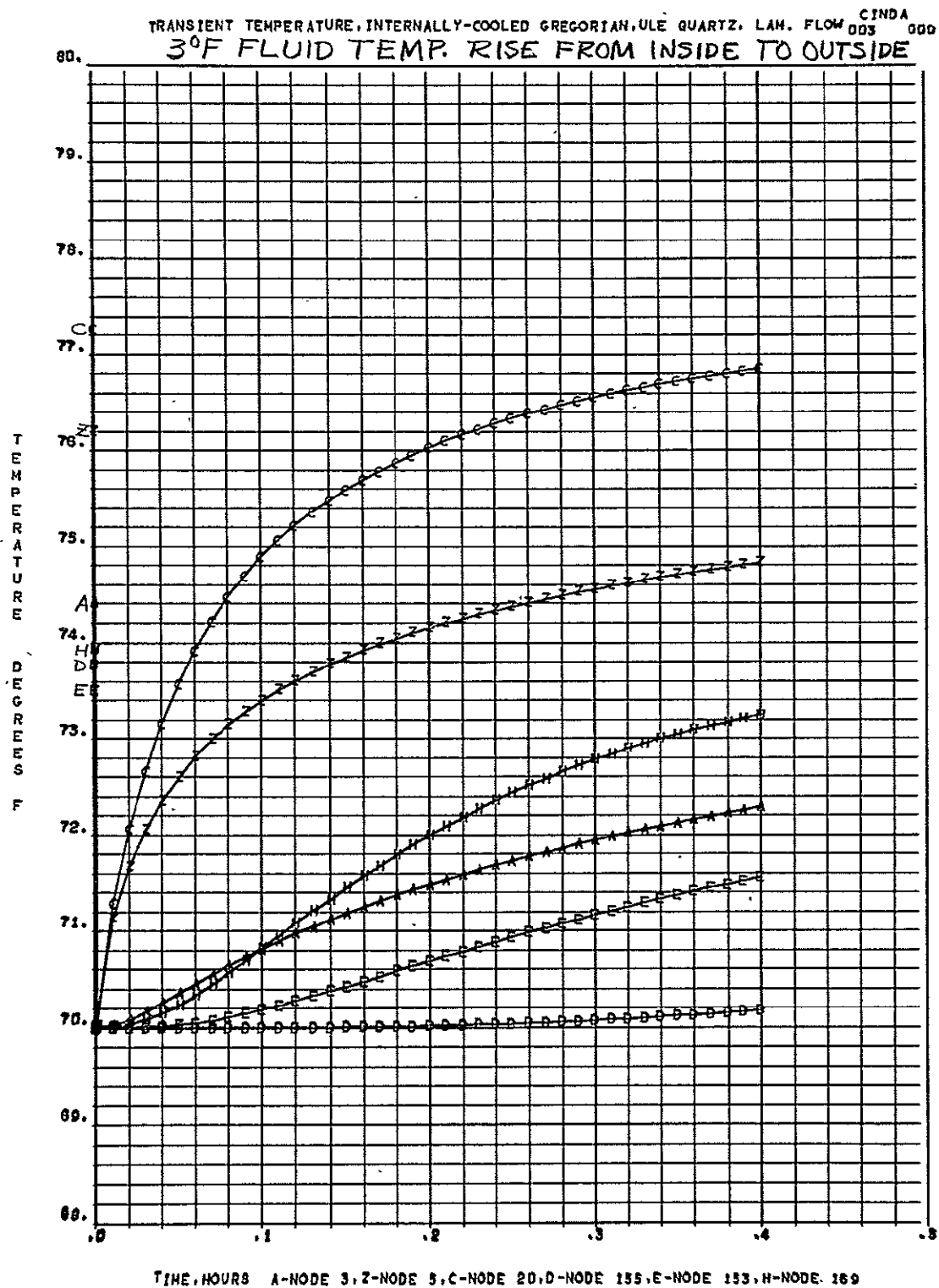


Figure 19. 3°F Fluid Temperature Rise from Inside to Outside

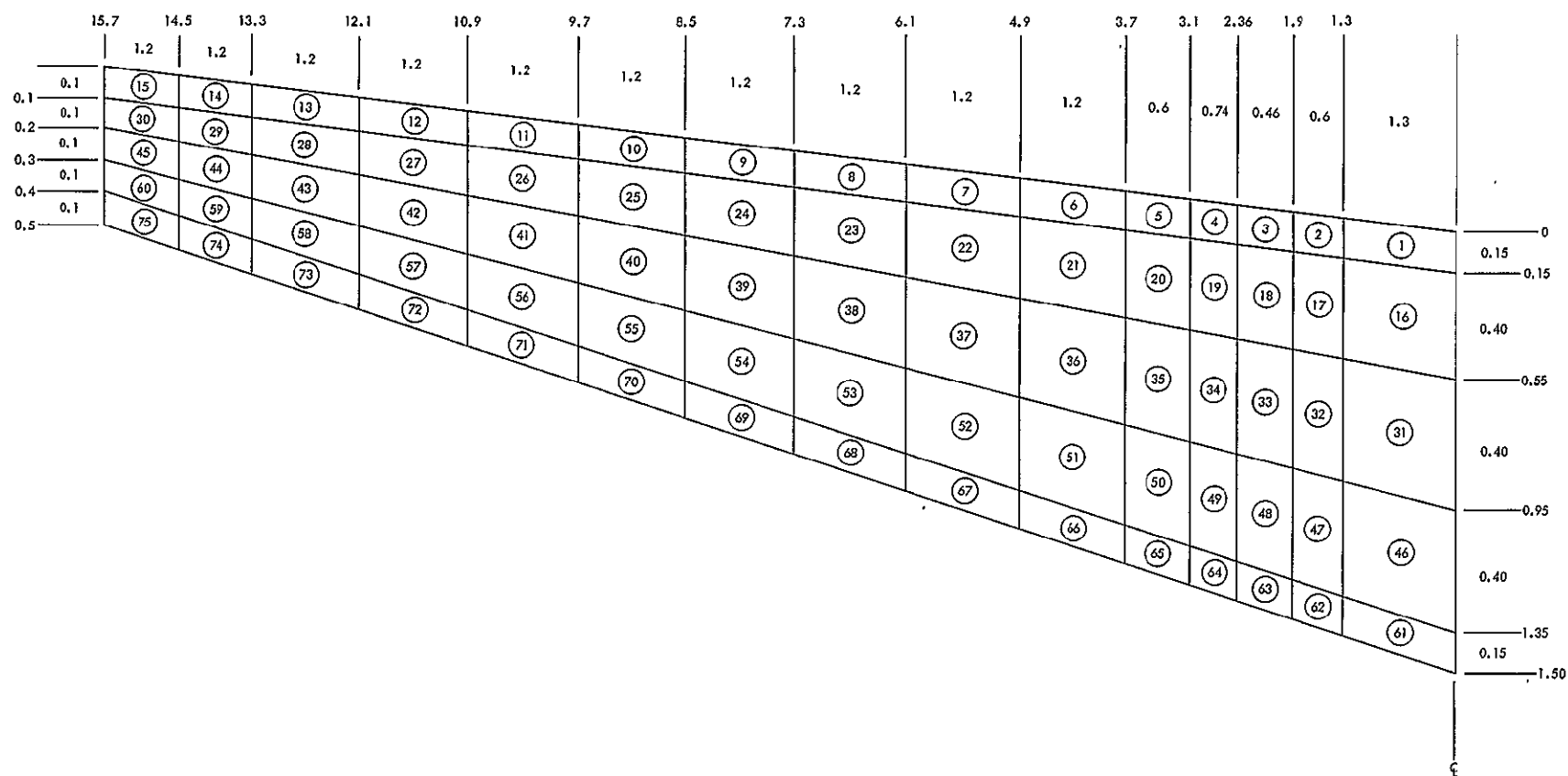
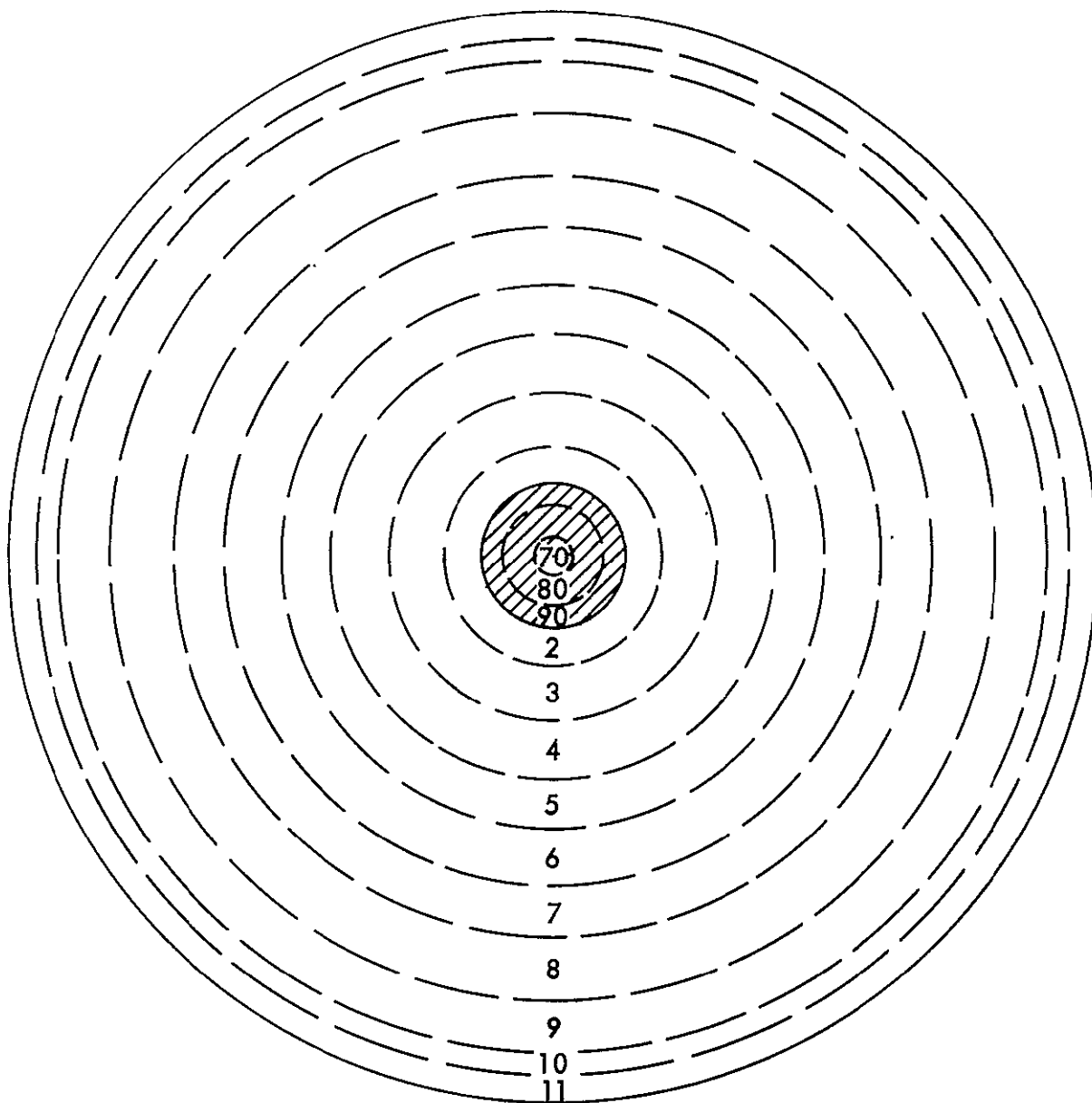


Figure 20. Tapered Gregorian Primary Mirror



DOTTED LINES REPRESENT INTERNAL NODE BOUNDARIES
 CROSS-HATCHED AREA IS SHADED BY SECONDARY
 RADII TO OUTER BOUNDARIES OF NODES:

$r_{70} = 1/2 \text{ in.}$	$r_3 = 4.71 \text{ in.}$	$r_7 = 11.0 \text{ in.}$	$r_{10} = 14.9 \text{ in.}$
$r_{80} = 1.5 \text{ in.}$	$r_4 = 6.28 \text{ in.}$	$r_8 = 12.6 \text{ in.}$	$r_{11} = 15.7 \text{ in.}$
$r_{90} = 2.36 \text{ in.}$	$r_5 = 7.85 \text{ in.}$	$r_9 = 14.1 \text{ in.}$	
$r_2 = 3.14 \text{ in.}$	$r_6 = 9.42 \text{ in.}$		

Figure 21. Radial Subdivision of Plane Gregorian Mirror

The diameter of the tapered mirror was the same as the plane (80 cm) and tapered from 1-1/2 inches thick at the center to 1/2 inch at the periphery.

The boundary conditions for the thermal analysis are as follows:

1. One solar constant was uniformly incident on the front surface with the exception of an on-center spot 12 cm in diameter. This spot represents the effects of shading by the secondary assembly, excepting the web.
2. A solar absorptance of 0.14 was used for all cases.
3. Heat was removed only at the bottom surface of the mirror. (The method of accomplishing this boundary condition is not defined).

Four different temperature distributions were specified for the bottom surface:

1. A uniform temperature along the entire radius, equal in value to the initial (uniform) temperature of the mirror.
2. A uniform temperature along the radius from the edge of the shaded spot to the periphery, equal in value to the initial mirror temperature.
3. Temperature increasing parabolically from the initial mirror temperature at the periphery to 3°F above this temperature at the edge of the shaded spot.
4. Temperature increasing parabolically from the initial mirror temperature at the edge of the shaded spot to 3°F above this temperature at the periphery.

The results of this investigation are shown on plots in Figures 22 to 39. The four temperature distributions listed above are illustrated by the lower curves in Figures 22, 24, 26, and 28 respectively.

It should be noted that a value of 70°F was used as the initial value for the plane mirror, while 50°F was used for the tapered mirror. This difference has no significance; and it does not affect the thermal distortions, since they depend on temperature differences rather than the scale employed.

The results for each combination of geometry and back surface temperature distribution are presented by a pair of figures. The first figure of each pair presents the steady radial temperature distribution in terms of the temperatures of the front and back rows of nodes. The top curve pertains to the front row and the bottom curve to the back row, in every case. No attempt

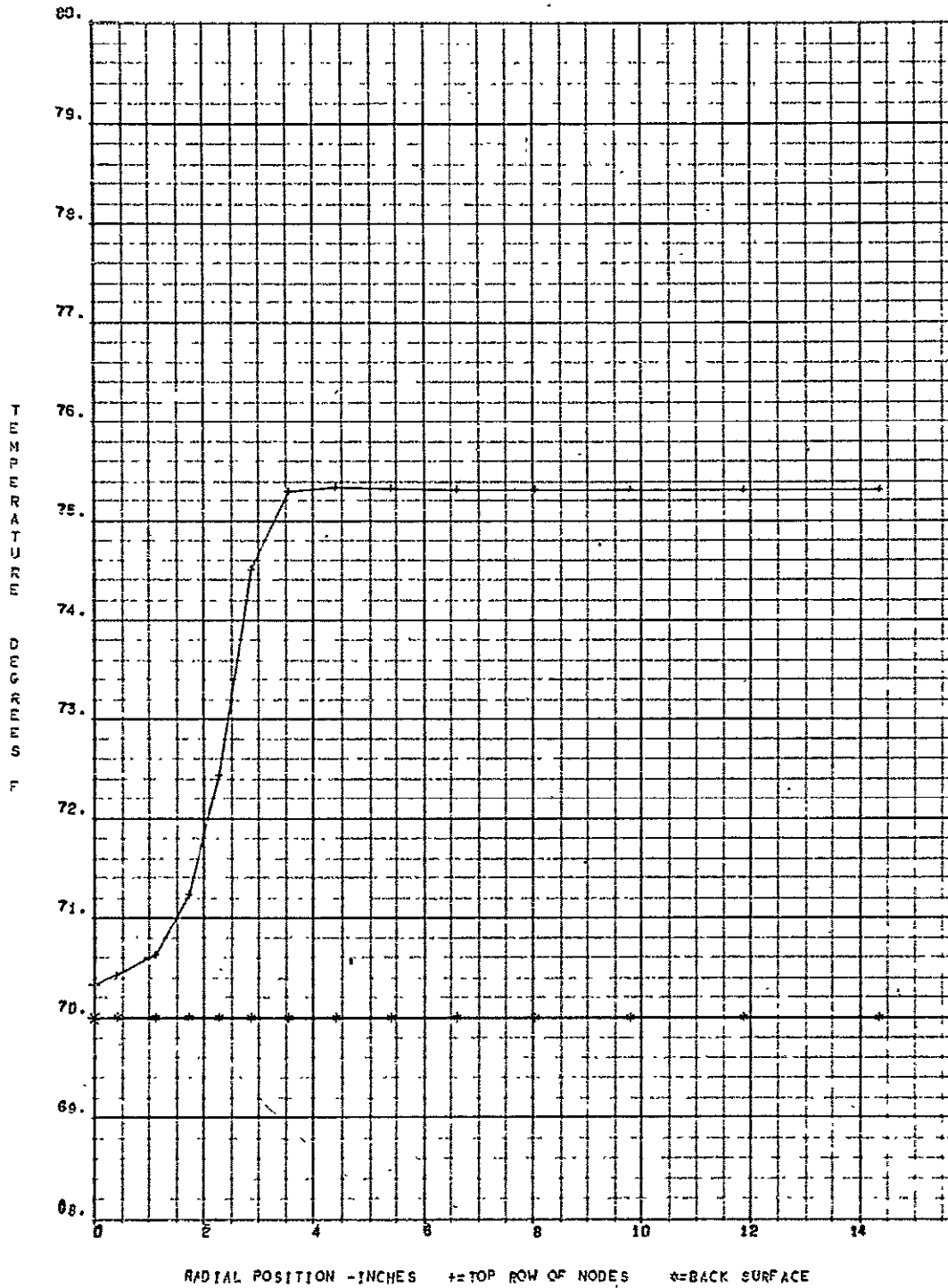


Figure 22.

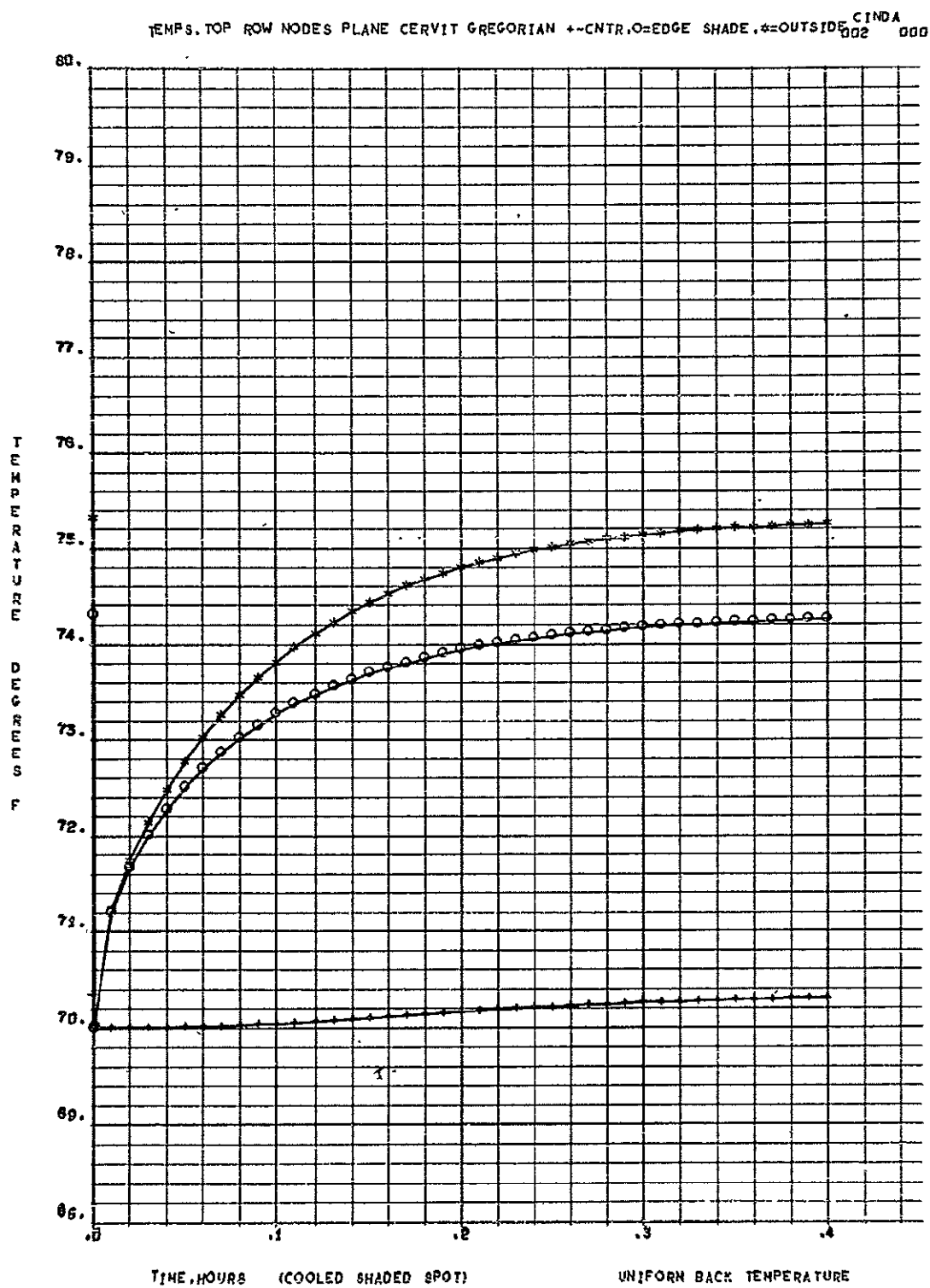


Figure 23.

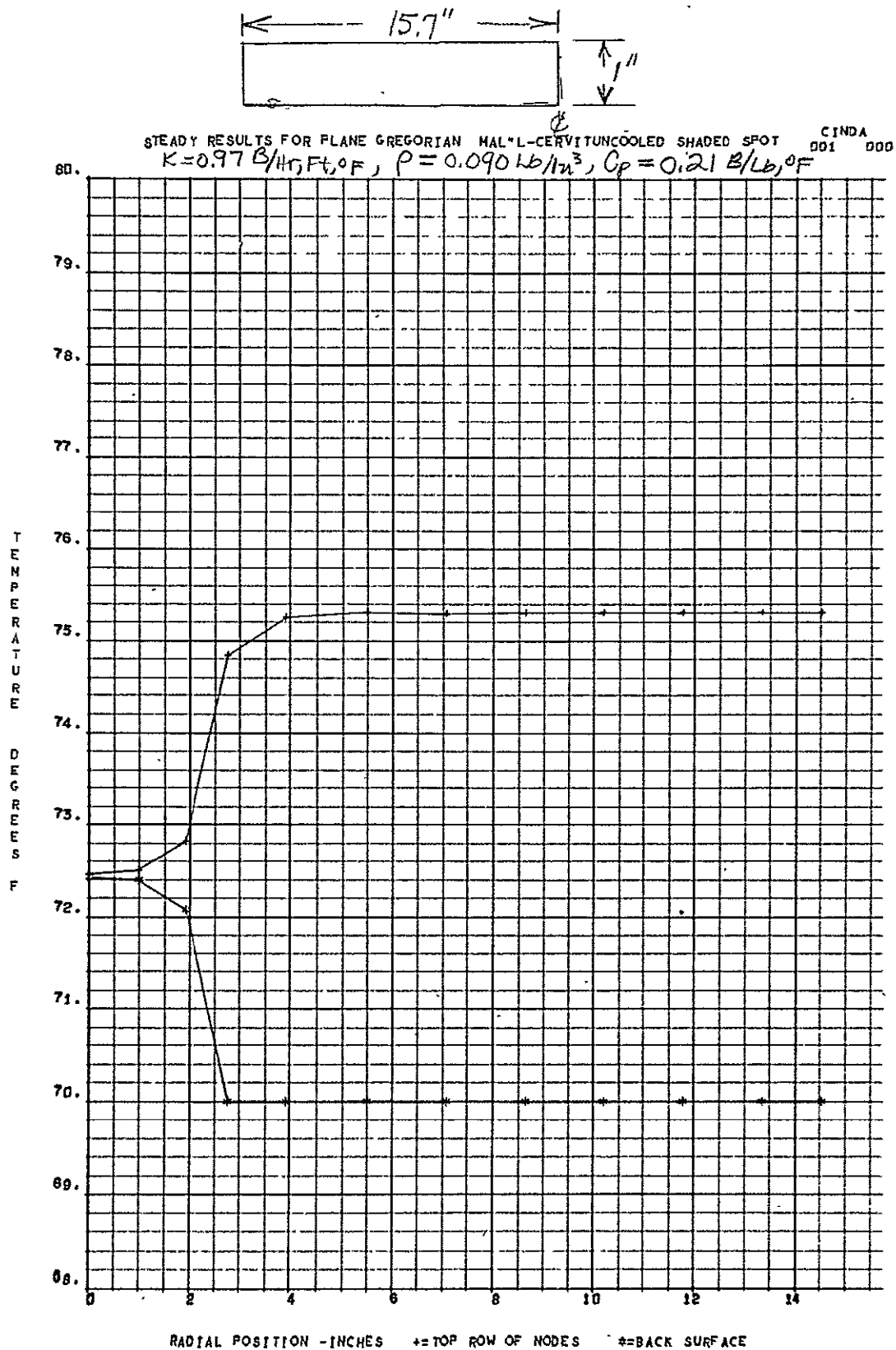


Figure 24.

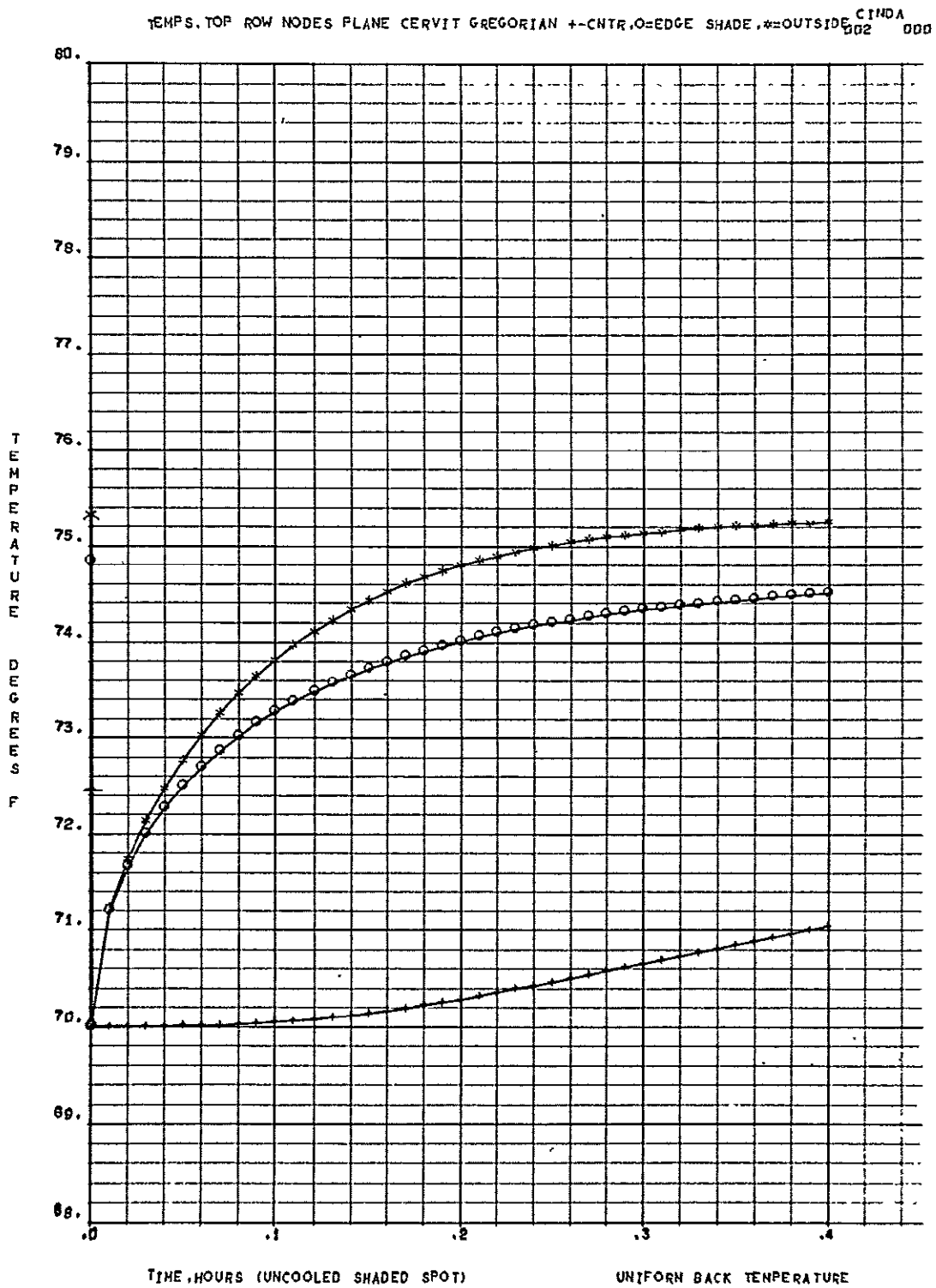
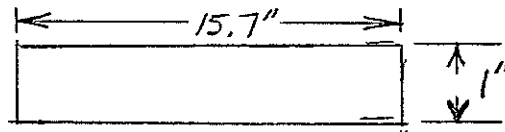


Figure 25.



STEADY RESULTS FOR PLANE GREGORIAN MAL-L-CERVITUNCOOLED SHADED SPOT
 $K = 0.97 \text{ B/HR, FT, OF}$, $P = 0.090 \text{ LB/IN}^3$, $C_p = 0.21 \text{ B/LB, OF}$

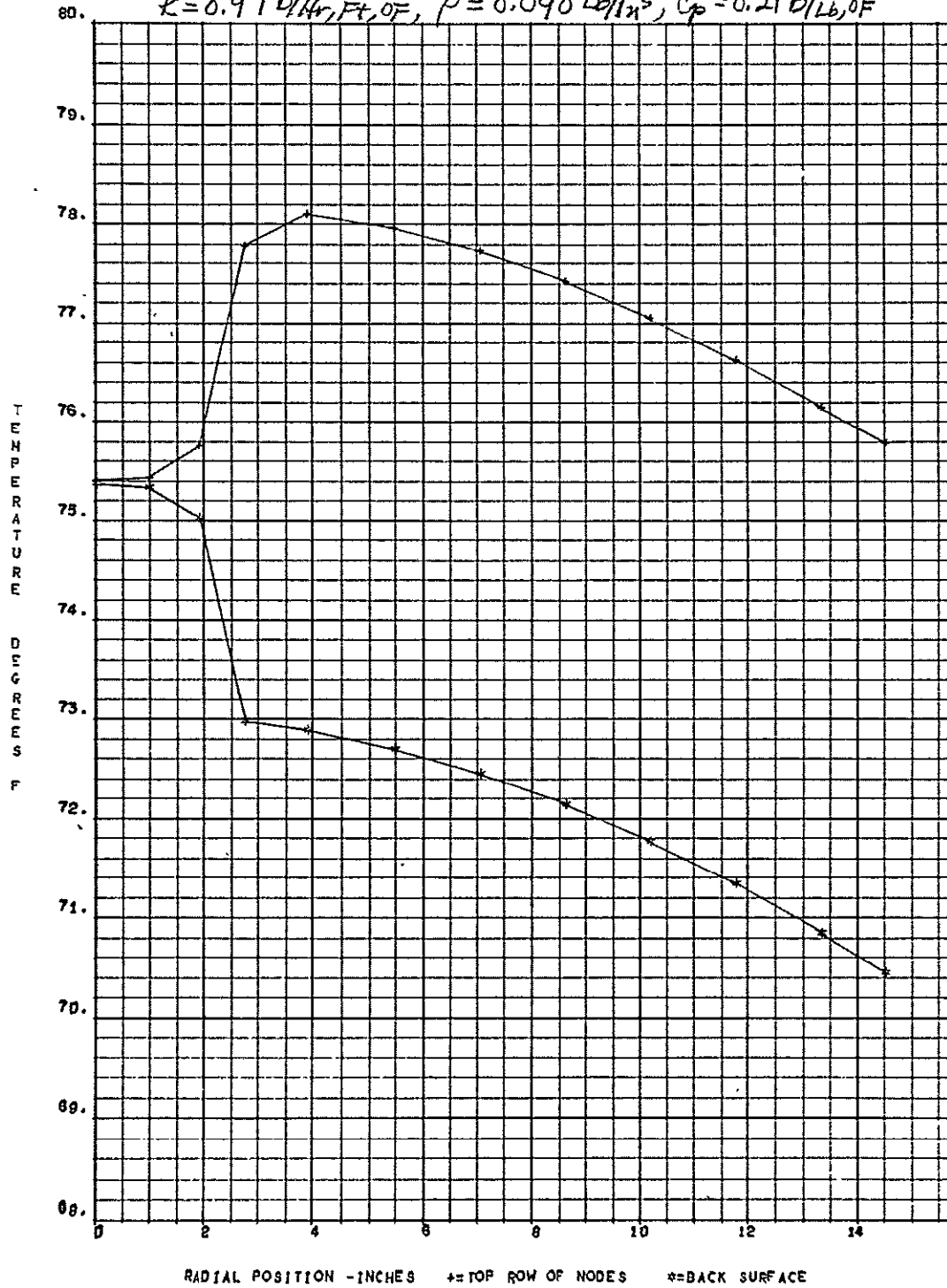


Figure 26.

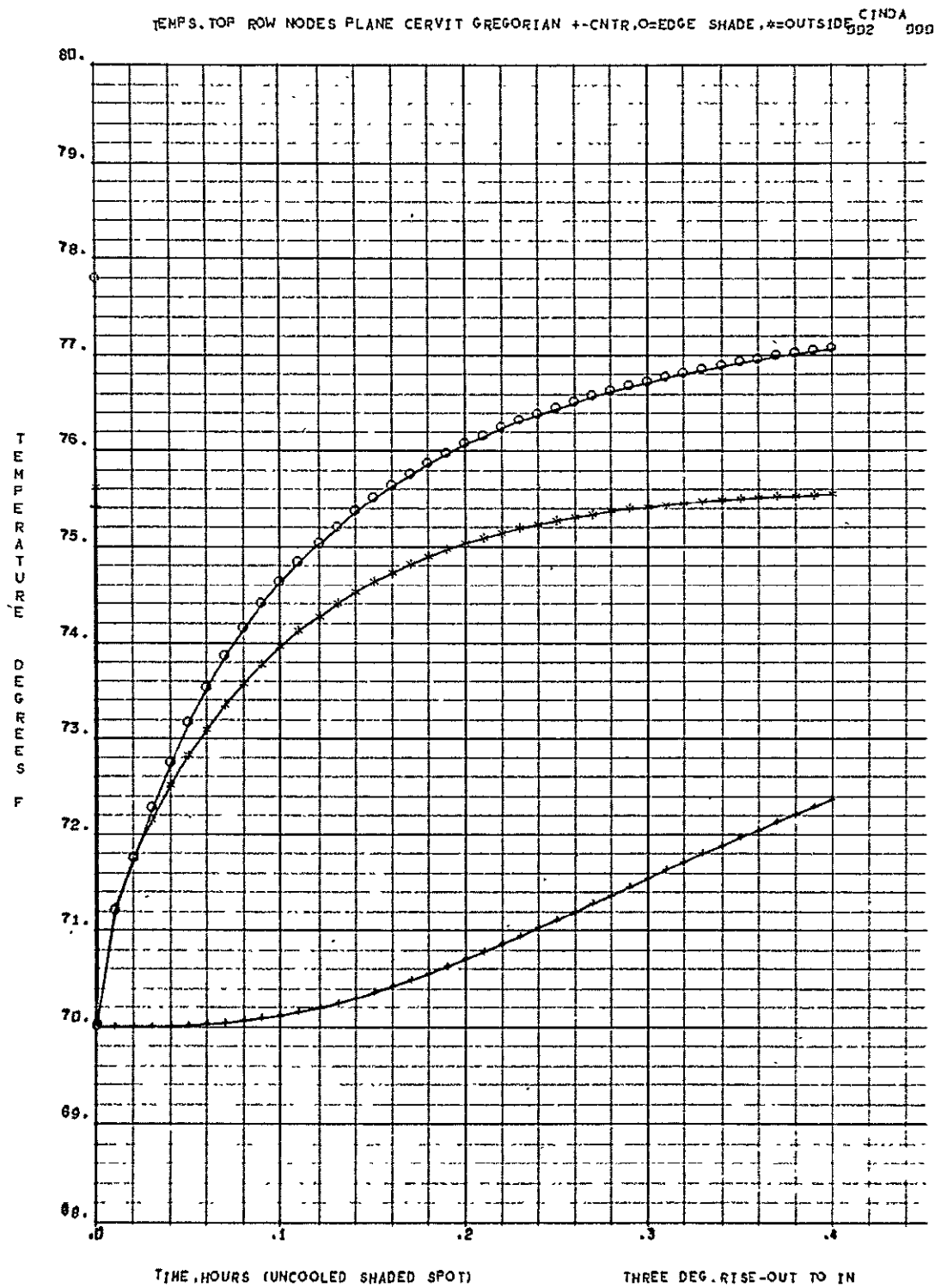


Figure 27.

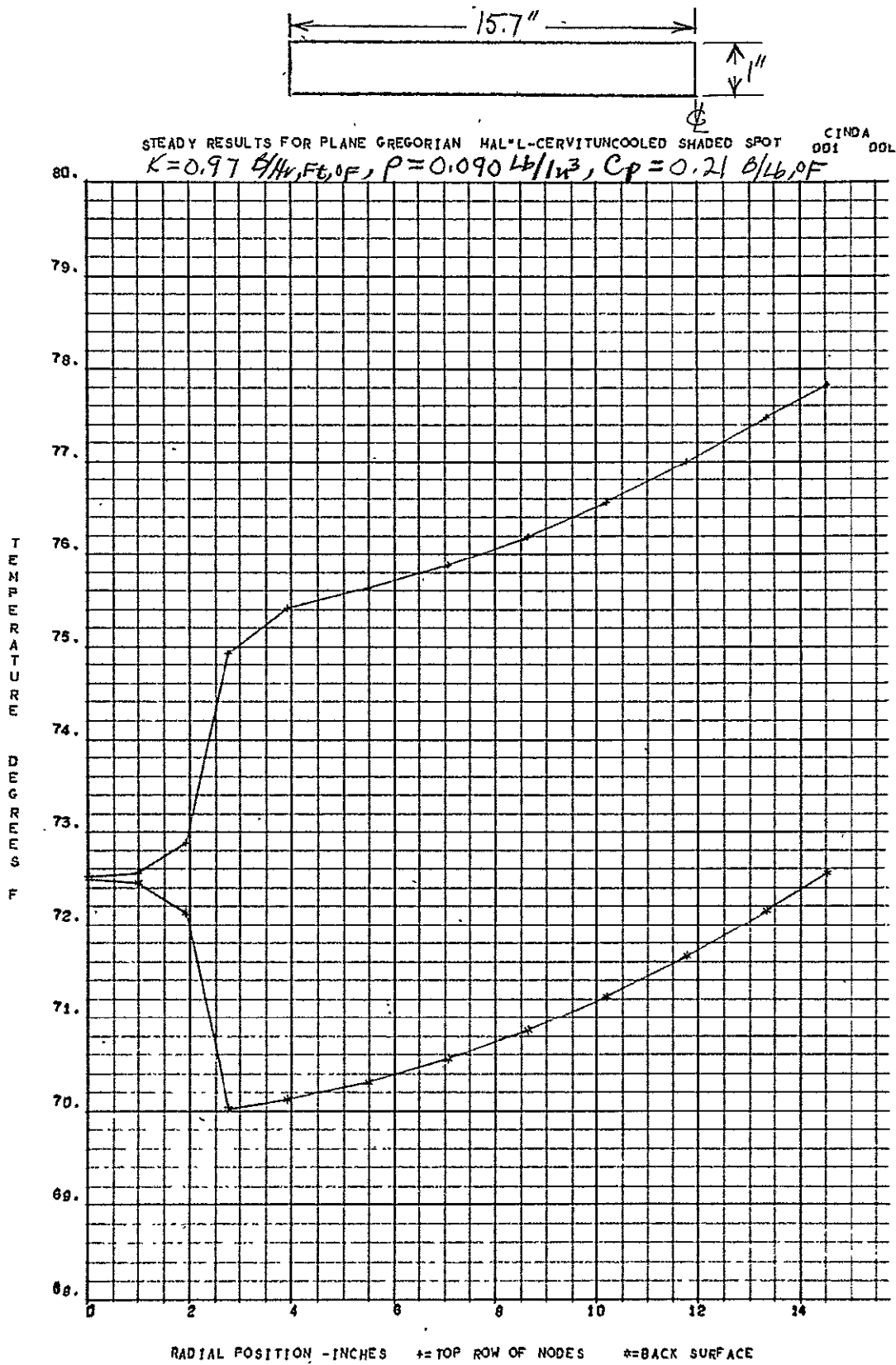


Figure 28.

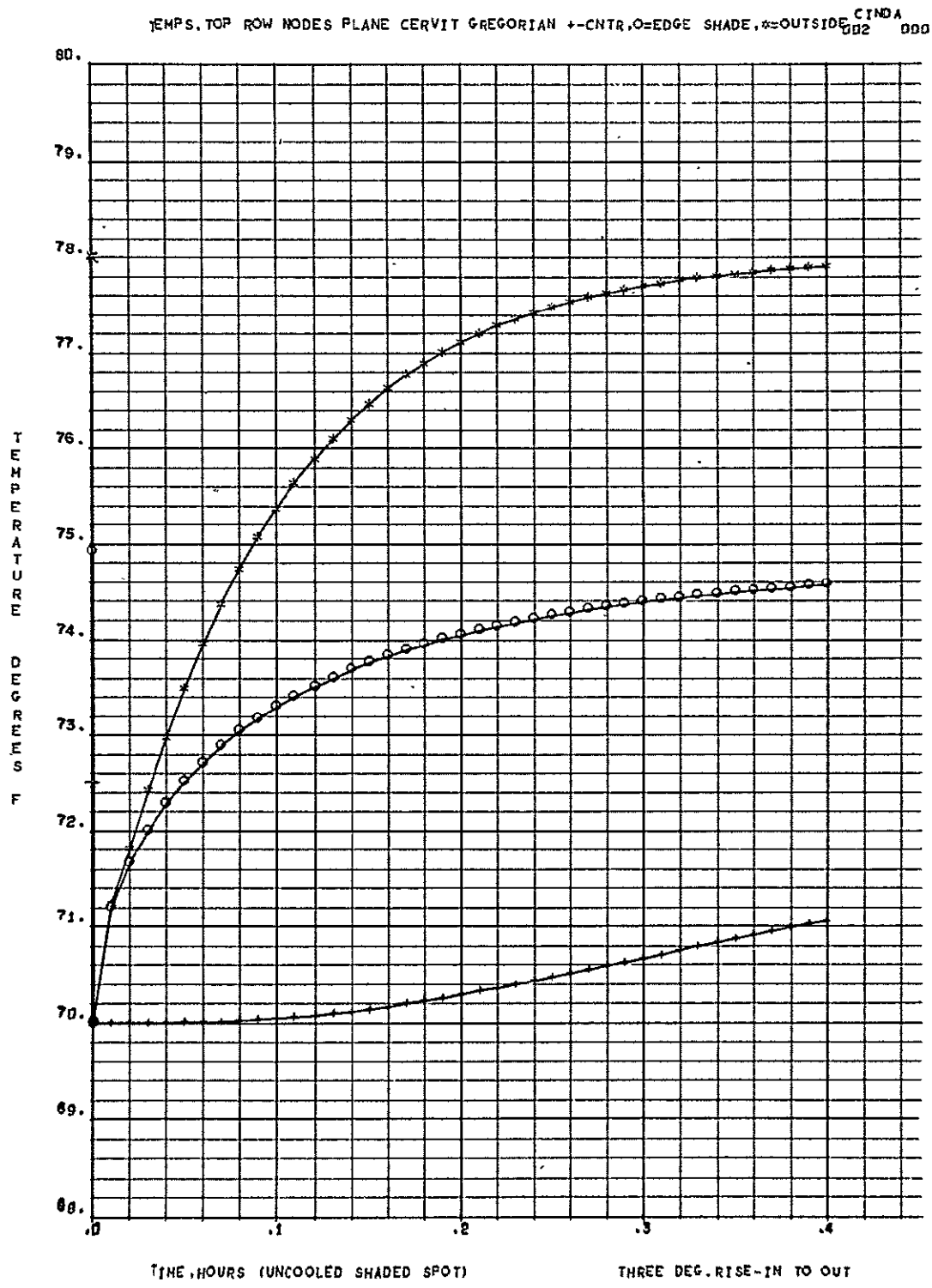


Figure 29.

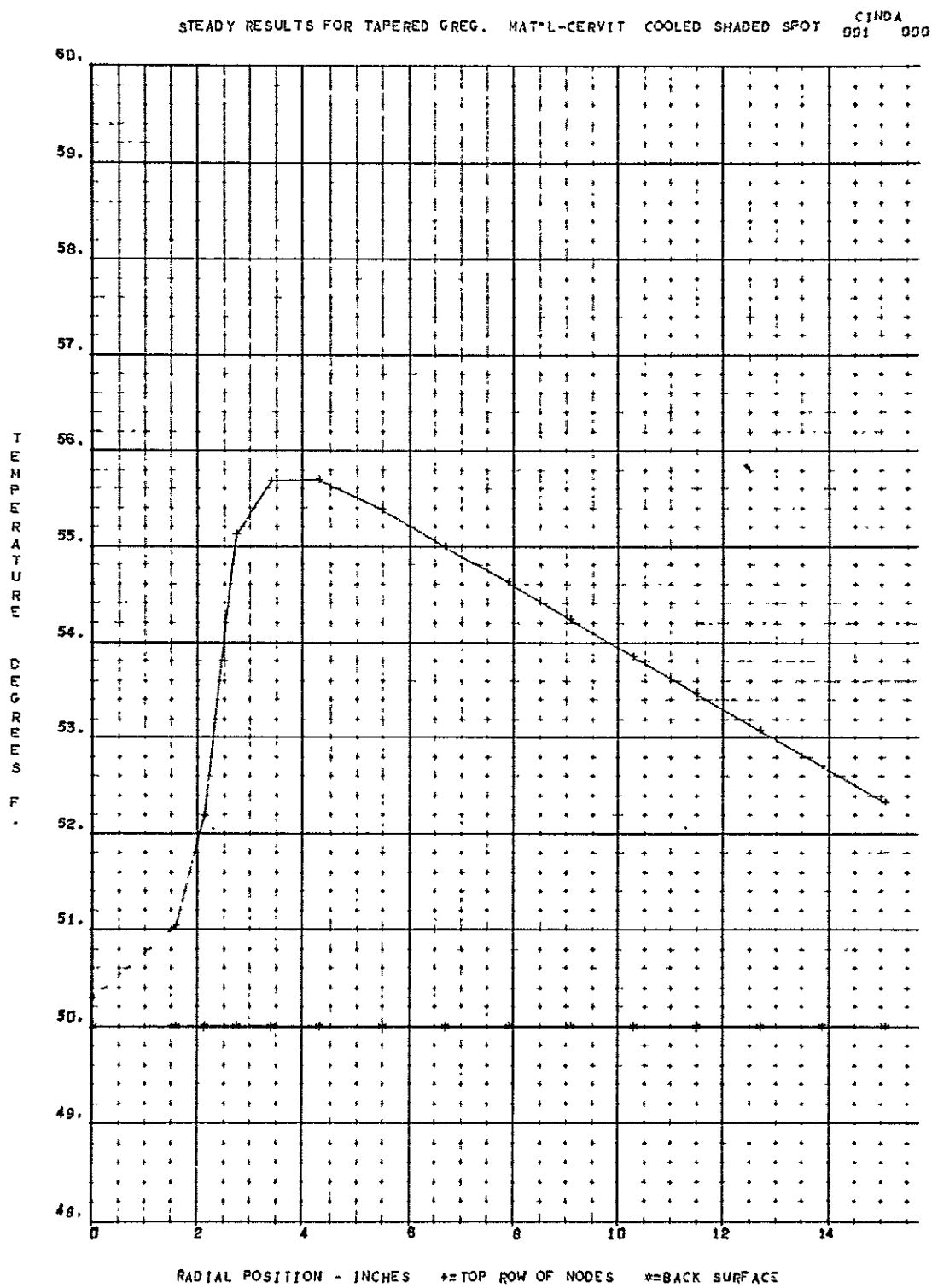


Figure 30.

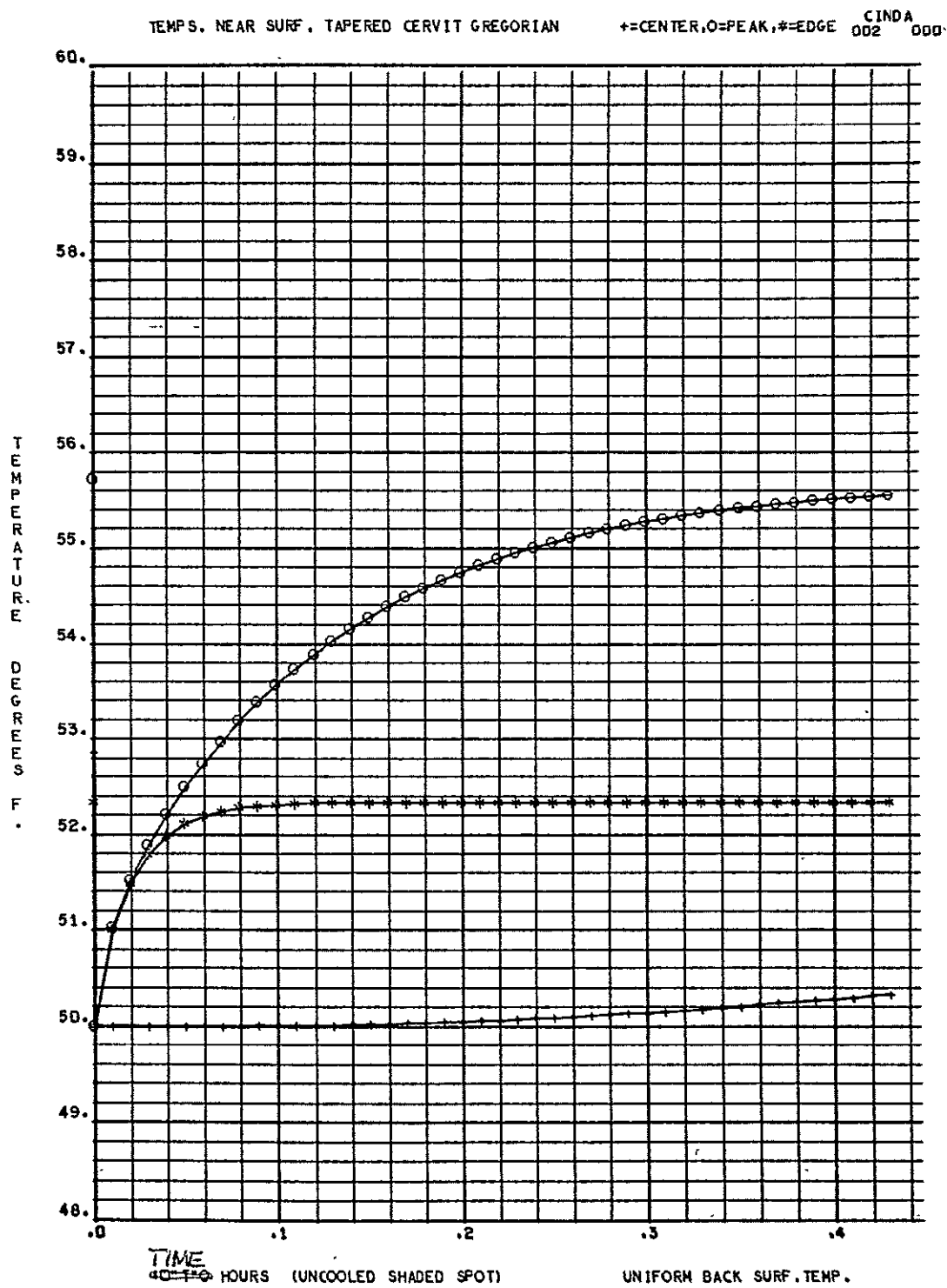


Figure 31.

STEADY RESULTS FOR TAPERED GREG. MAT'L-CERVIT UNCOOLED SHADED SPOT CINDA
001 000

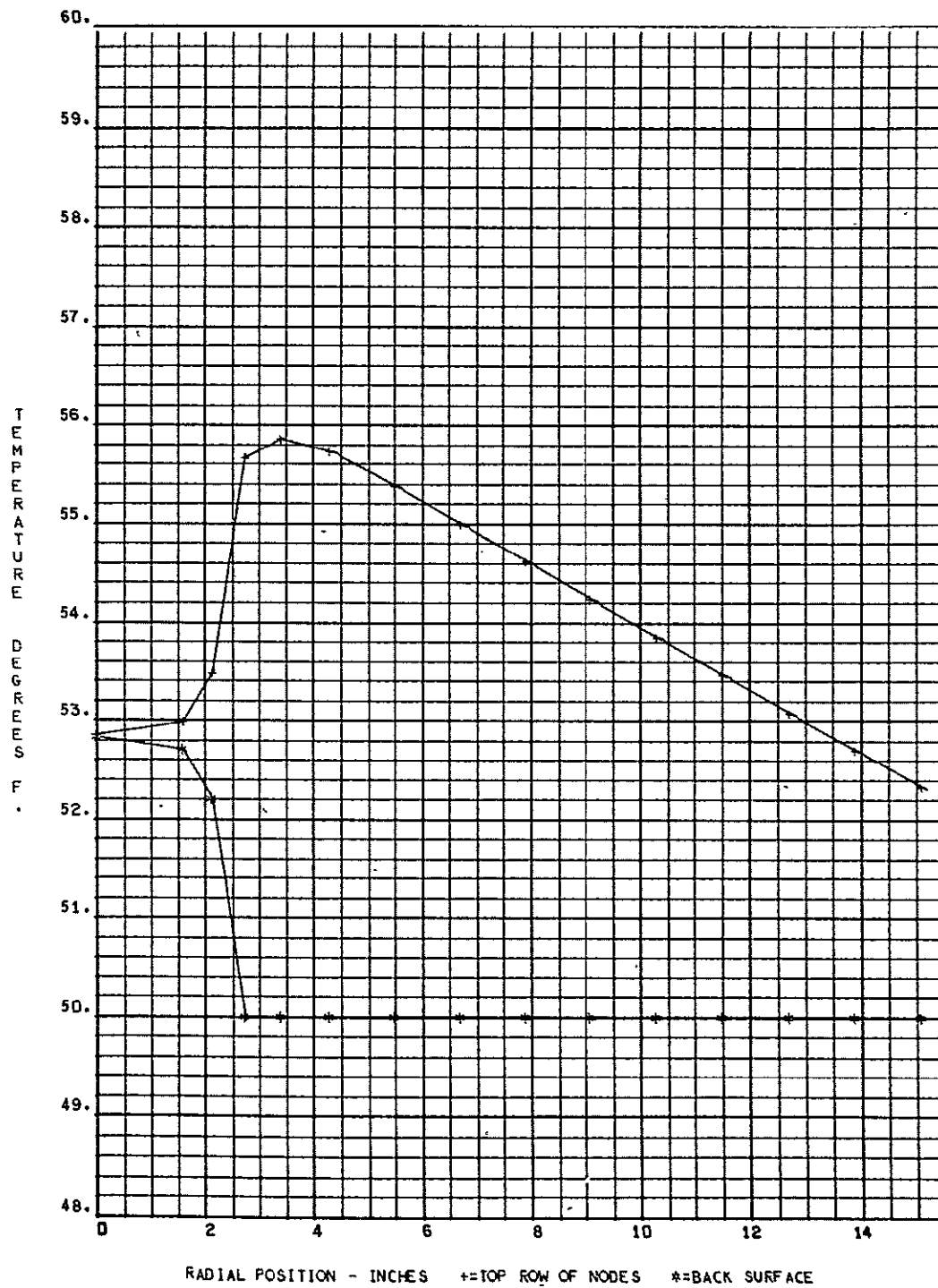


Figure 32.

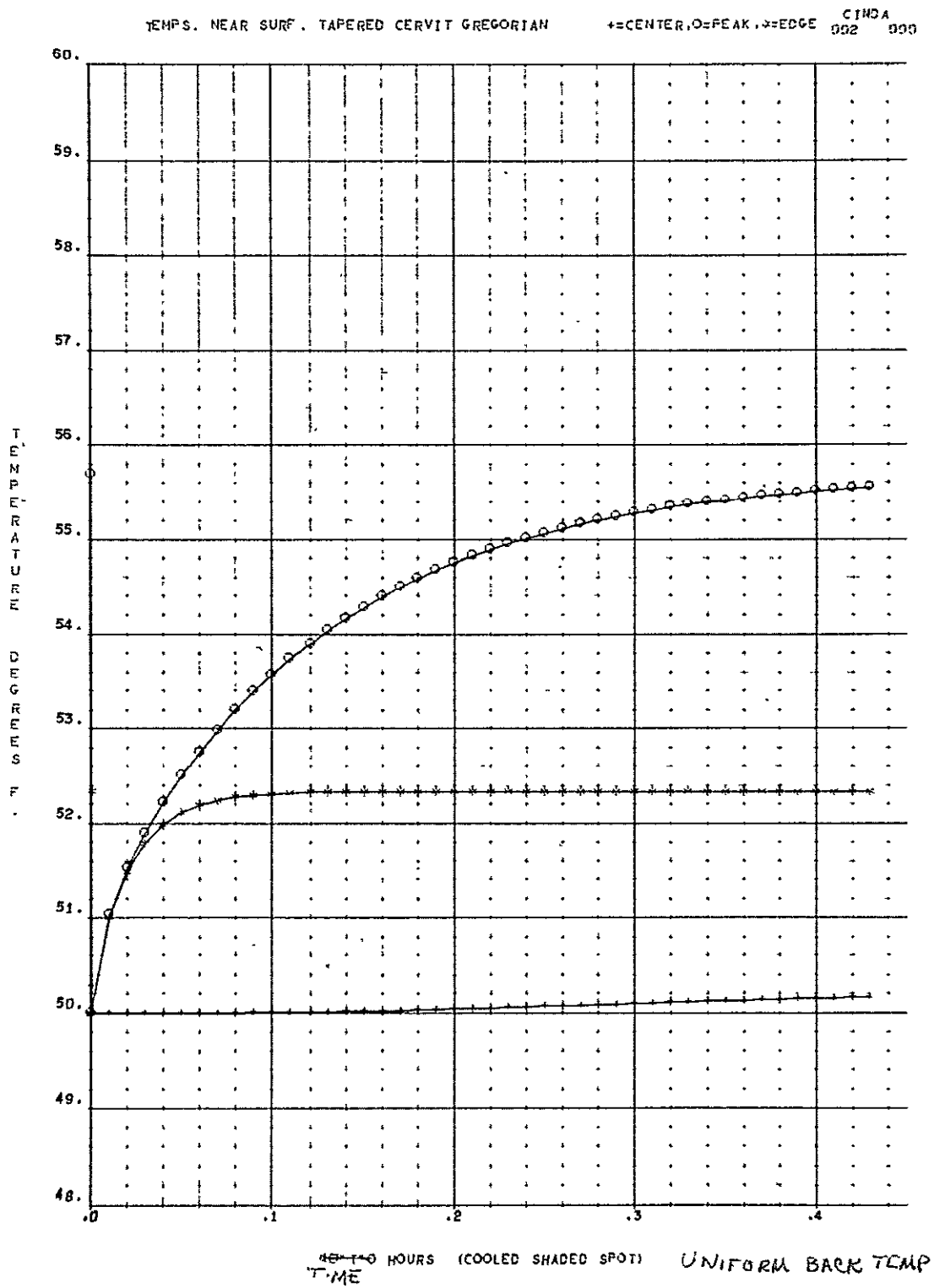


Figure 33.

STEADY RESULTS FOR TAPERED GREG. MAT'L-CERVIT. UNCOOLED SHADED SPOT

CINDA
001 000

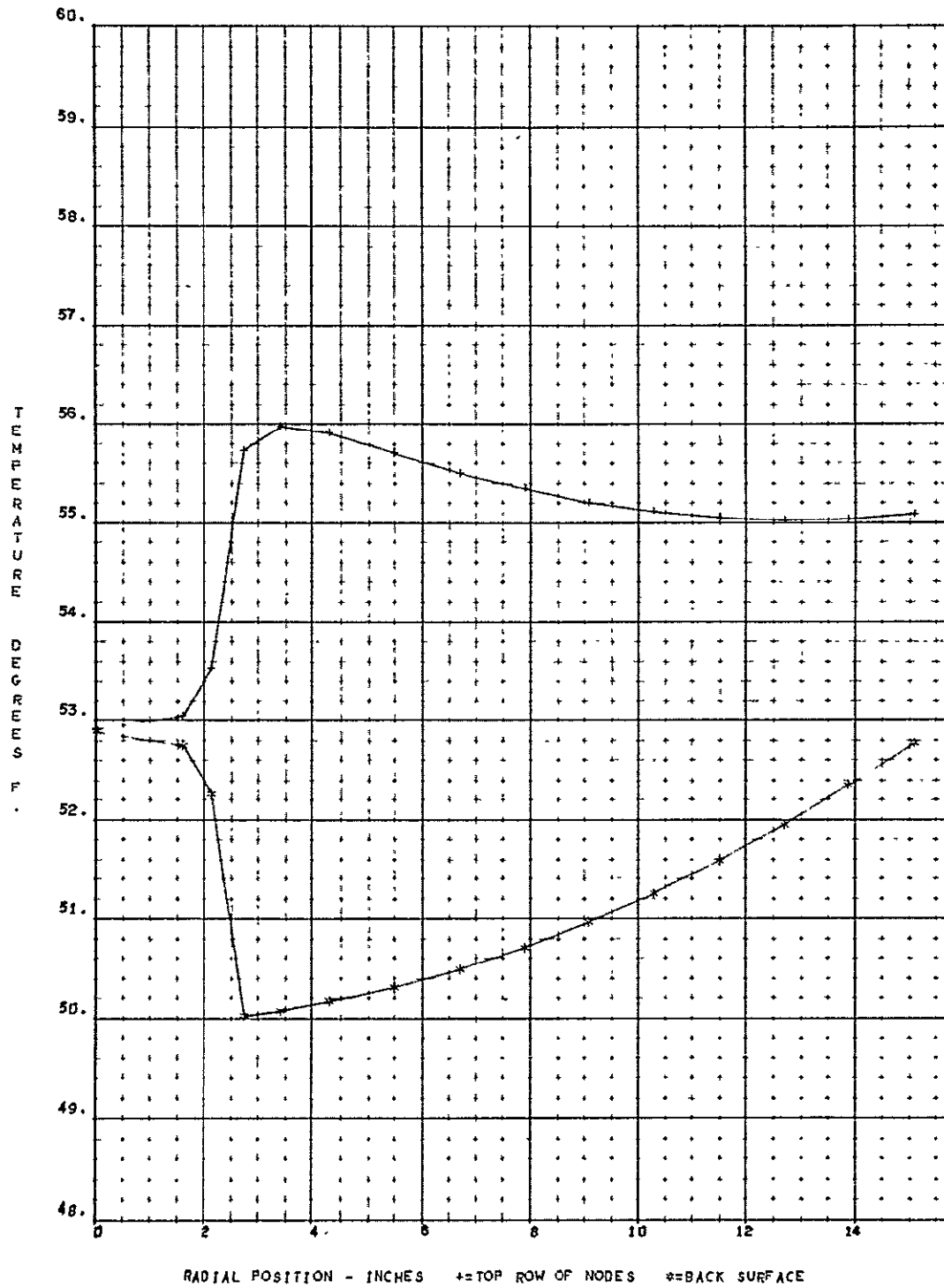


Figure 34.

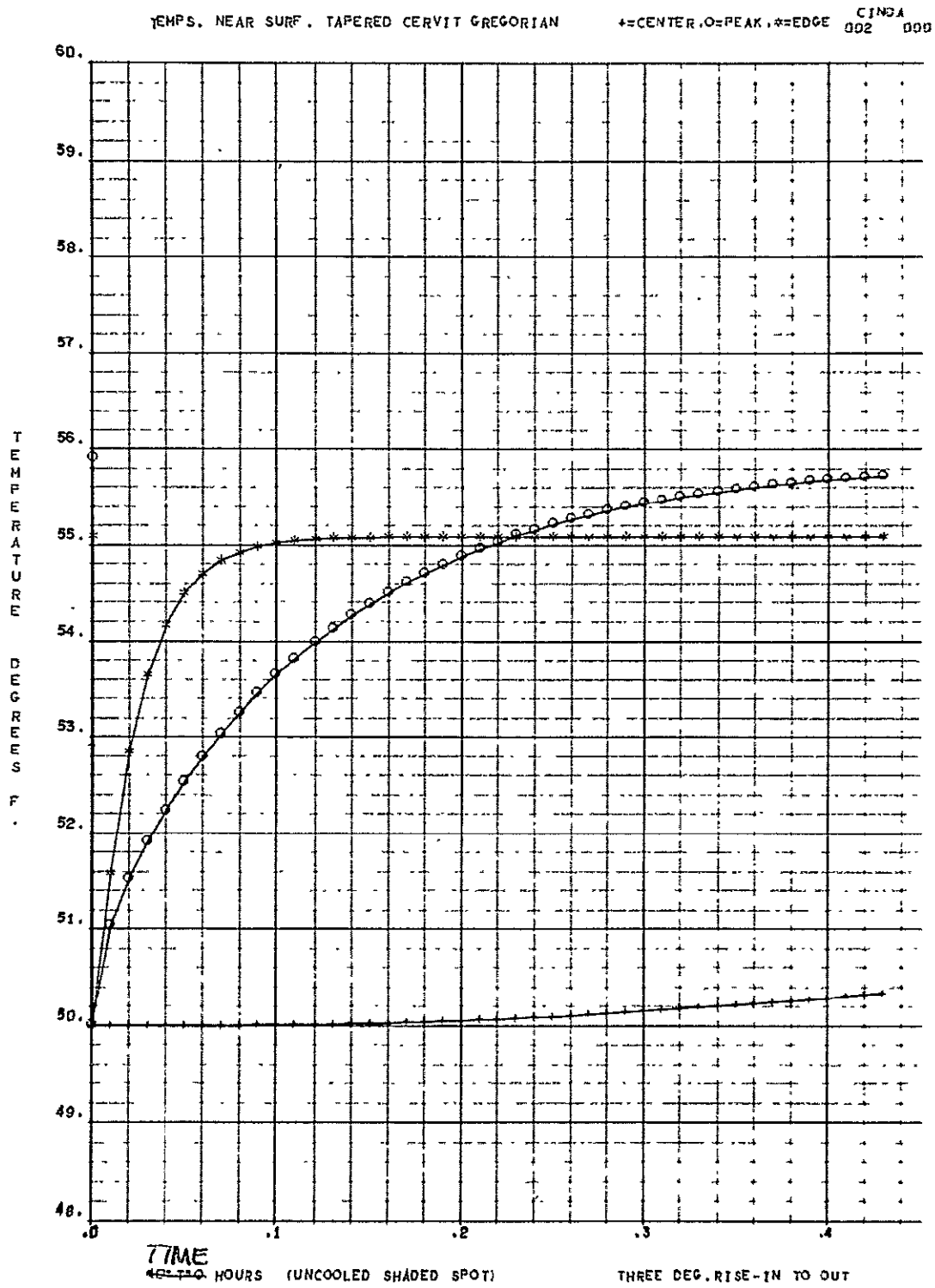


Figure 35.

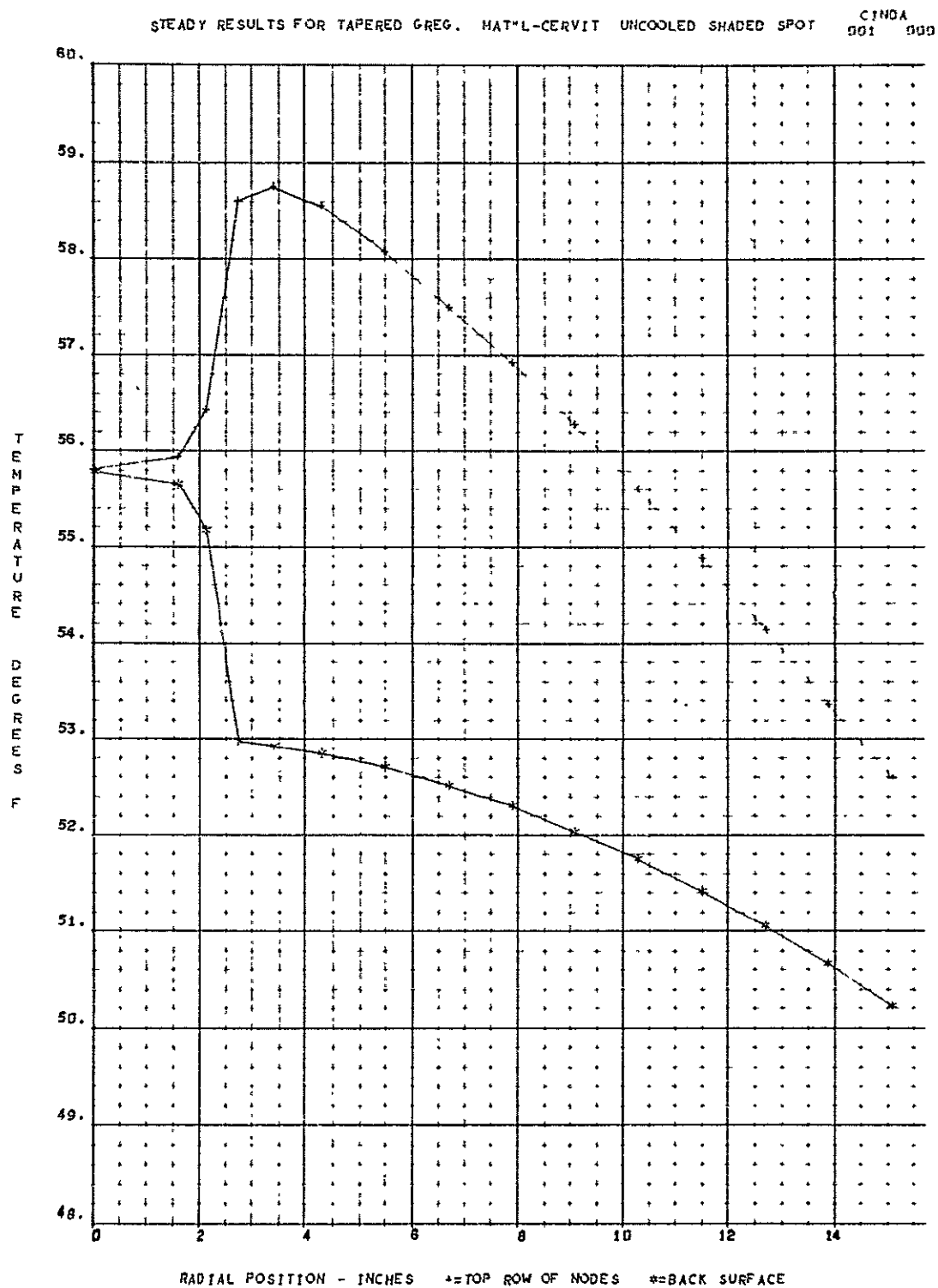


Figure 36.

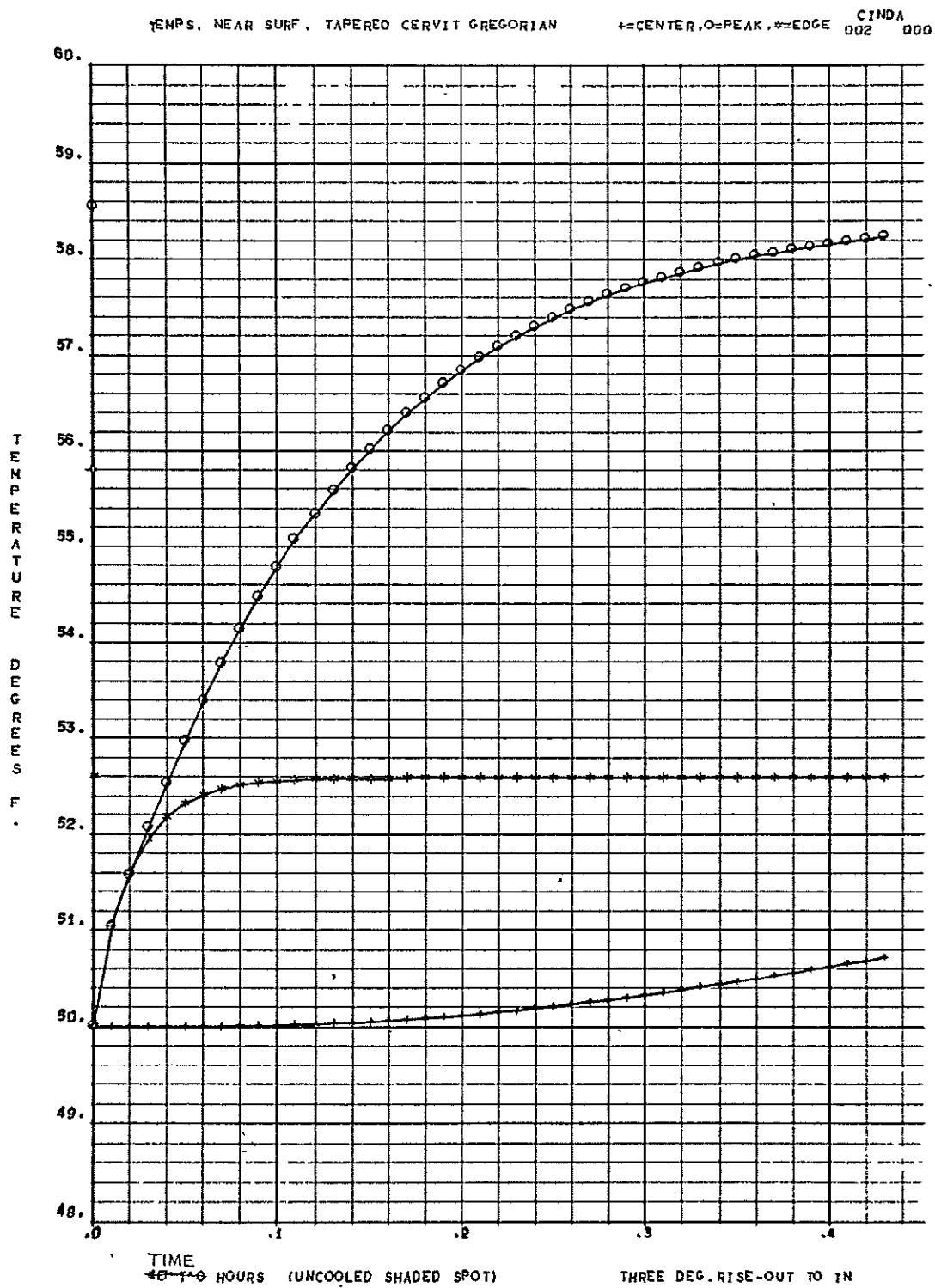


Figure 37.

CHECK CASE TO DETERMINE EFFECT OF CONDUCTOR VALUES FOR RADIAL TRANSFER. (OVER)

STEADY RESULTS FOR TAPERED GREG. MAT'L-CERVIT UNCOOLED SHADED SPOT

CINDA
091 090

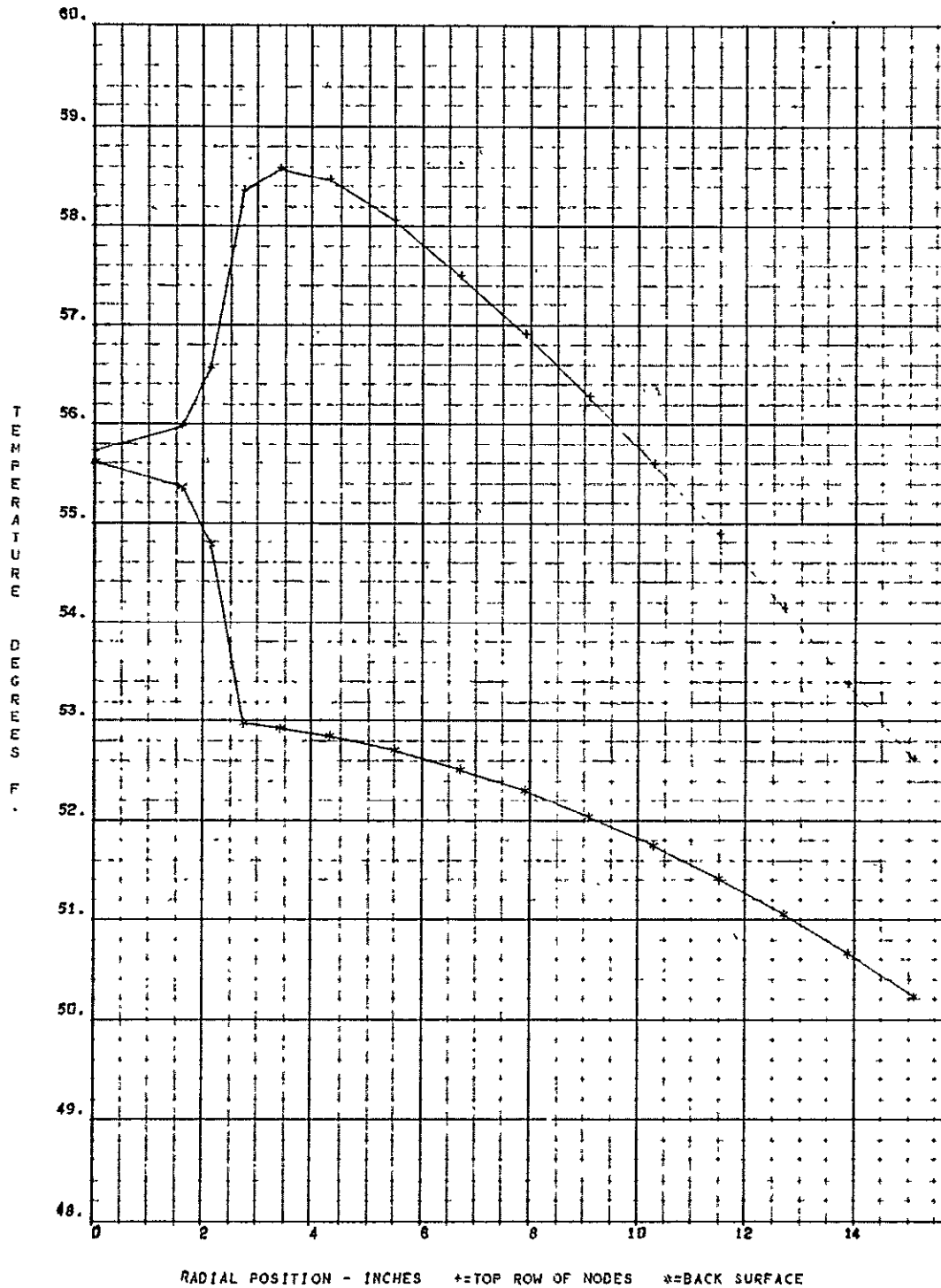


Figure 38.

CHECK CASE

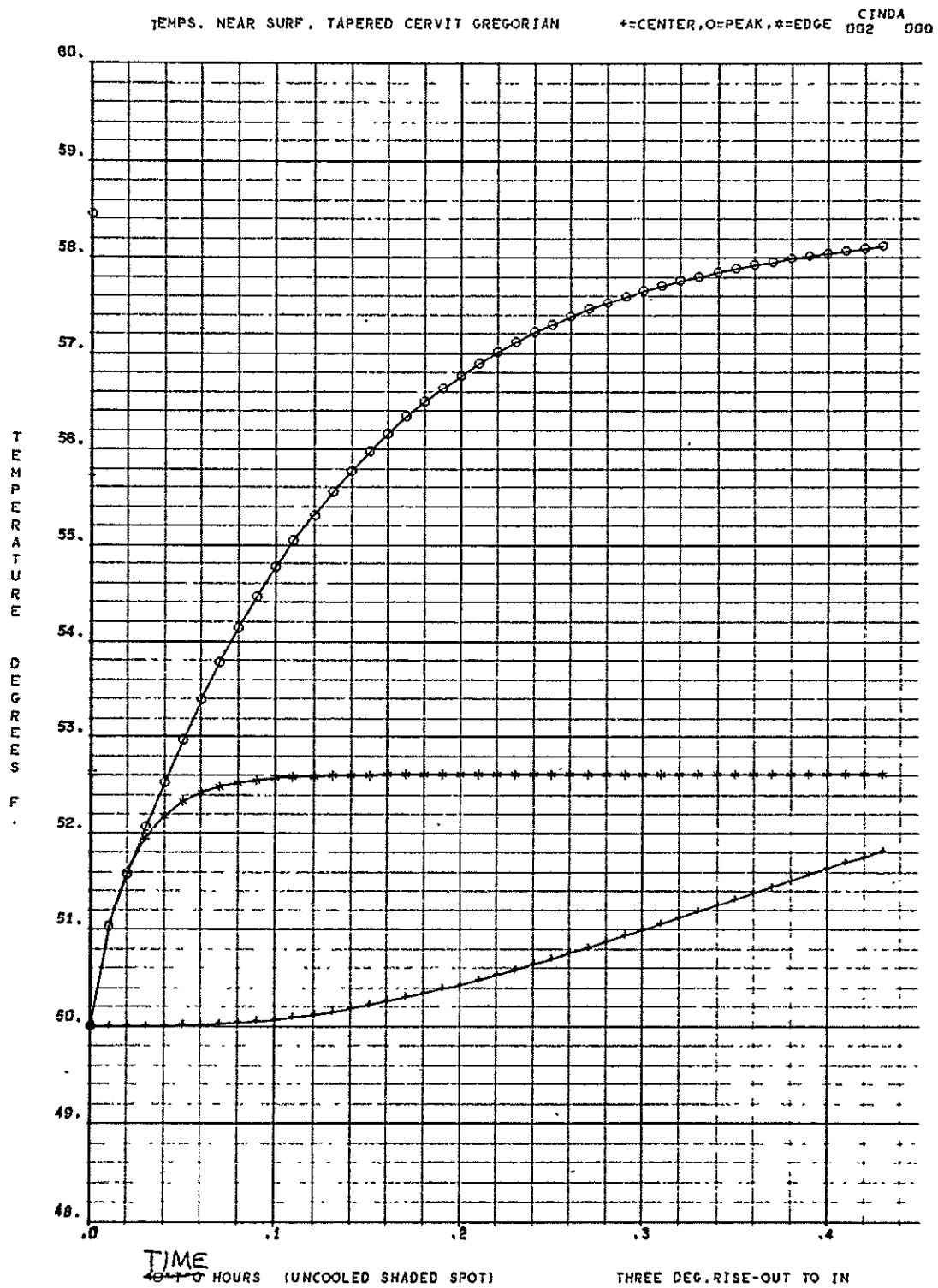


Figure 39.

was made to obtain smooth curves for the steady state results, so unrealistically sharp corners appear in these curves. The second figure in each pair presents the transient results in terms of the temperatures of three nodes in the top row. The curve drawn through the +'s is for the center node; that through the 0's is for the node just inside the edge of the shaded spot in the case of the plane mirror, and for the node centered about 2 inches beyond the edge of the shaded spot in the case of the tapered mirror; that through the *'s is for the node at the periphery of the mirror (see Figure 23 for example).

It is noted that the temperature difference between the front and back rows of nodes of the plane mirror approaches a nearly constant value of about 5.3°F for radii greater than 4 inches, irrespective of the temperature distribution along the back surface. This indicates that radial conduction is not a very important factor in establishing the temperature distribution, and this indication is supported by other features of the results for both the plane and tapered mirrors. One feature which supports it is that the steady temperature of the shaded region is much lower if this region is cooled from the back than if it is not cooled.

The transient plots for the plane mirror indicate that the temperature near the periphery approaches steady state closely at the end of 0.3 hour, irrespective of the temperature distribution on the back surface. The temperature near the edge of the shaded spot approaches equilibrium less rapidly; because it depends on radial conduction; and it is more sensitive to the temperature distribution on the back surface. The temperature at the center of the mirror approaches equilibrium very slowly because of the low thermal diffusivity of the material.

The results for the tapered mirror (Figures 30 to 39) follow the same trends as those for the plane mirror, although the distributions are somewhat more complicated because of the radial variation in mirror thickness. The radial distribution of the temperature difference between the front and back rows of nodes is virtually independent of the radial distribution of back surface temperature. The plots of transient temperatures show that equilibrium at the three radial locations is approached in the same order as for the plane mirror. However, the node near the periphery of the tapered mirror approaches equilibrium more rapidly than the corresponding node of the plane mirror, because of the reduced thickness at that position, while the node near the edge of the

shaded spot approaches equilibrium less rapidly, because of the increased thickness at that position.

After the 80 cm primary mirror investigation was completed, the mirror size was reduced to 65 cm diameter. It was recognized that the ATM constraint of $0.6 \frac{\text{BTU}}{\text{HR}}$ heat transfer to the spar for each attachment point would require that the mirror temperature would have to be held close to the 70°F ATM spar temperature. Also, the problem of getting a system to accomplish the controlled temperature on the back surface seemed insurmountable.

For these reasons an investigation of a 65 cm diameter mirror with internal cooling channels for the purpose of circulating a cooling fluid was begun. The material U. L. E. (ultra low expansion) fused silica made such a design possible due to its fusibility. Figure 40 shows a cross section of one half of the mirror.

A detailed analysis was made of the steady and transient temperature distributions in an annular segment of the 65 cm Gregorian primary with an internal cooling channel. The purpose of this analysis was to obtain a detailed picture of the temperature distribution around the cooling channel, so that the effect of local thermal distortions on the mirror figure might be better assessed.

The configuration of a cross section of one-half the mirror, shown in Figure 41, is the same in all essential thermal respects to the latest version, namely, it is 65 cm in diam. and tapers from a thickness of 2 in. at the center to 1 in. at the periphery. A circular cooling channel of 1/4-in. diam. spirals from the edge of the shaded spot to the outer edge, with successive turns spaced 3/4 in. apart on centers. The tube centers are 1/2 in. from the illuminated surface of the mirror.

The segment of the mirror selected for detailed analysis was the thickest section of the illuminated portion of the mirror, as shown between sections A-A and B-B in Figure 41. The selection of this segment was made to obtain results at a position where local thermal distortions should be greatest. The spiral nature of the cooling channel was ignored so that the segment could be treated as circular in shape for simplicity of analysis. The resulting segment is in the form of a ring with a concentric circular channel, as shown by the sectional view in Figure 42. To further simplify the analysis, large-scale radial temperature gradients were ignored, which yielded symmetry of the temperature about the cylindrical surface passing vertically through the center

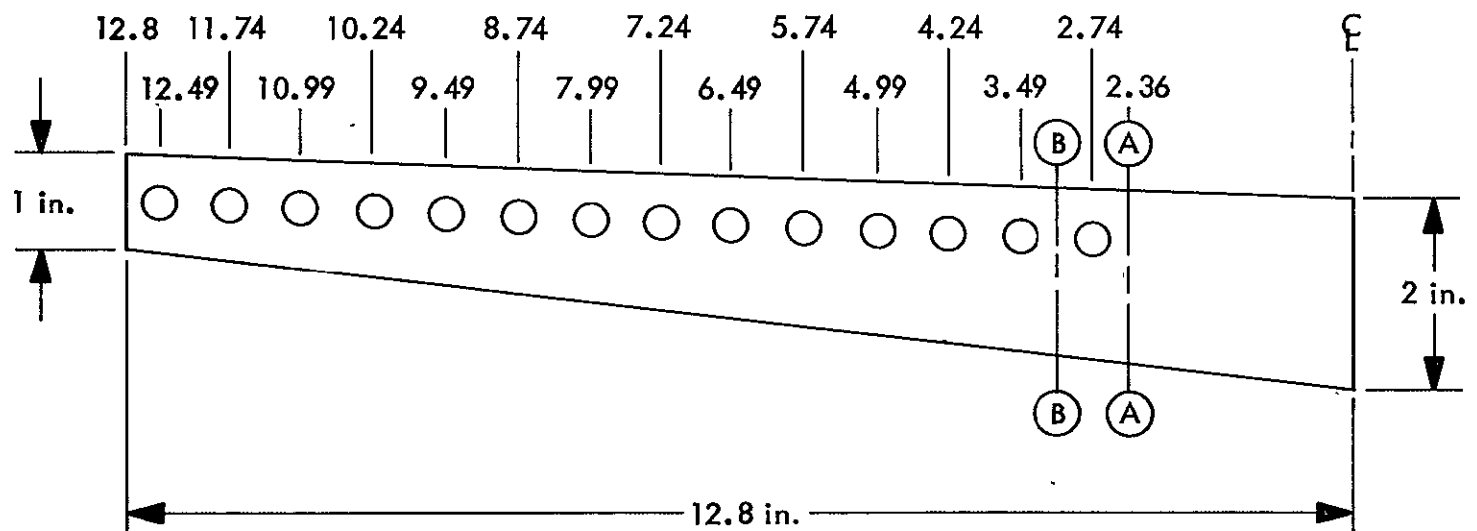


Figure 41. Set-up for Detailed Analysis of Tapered Gregorian Primary

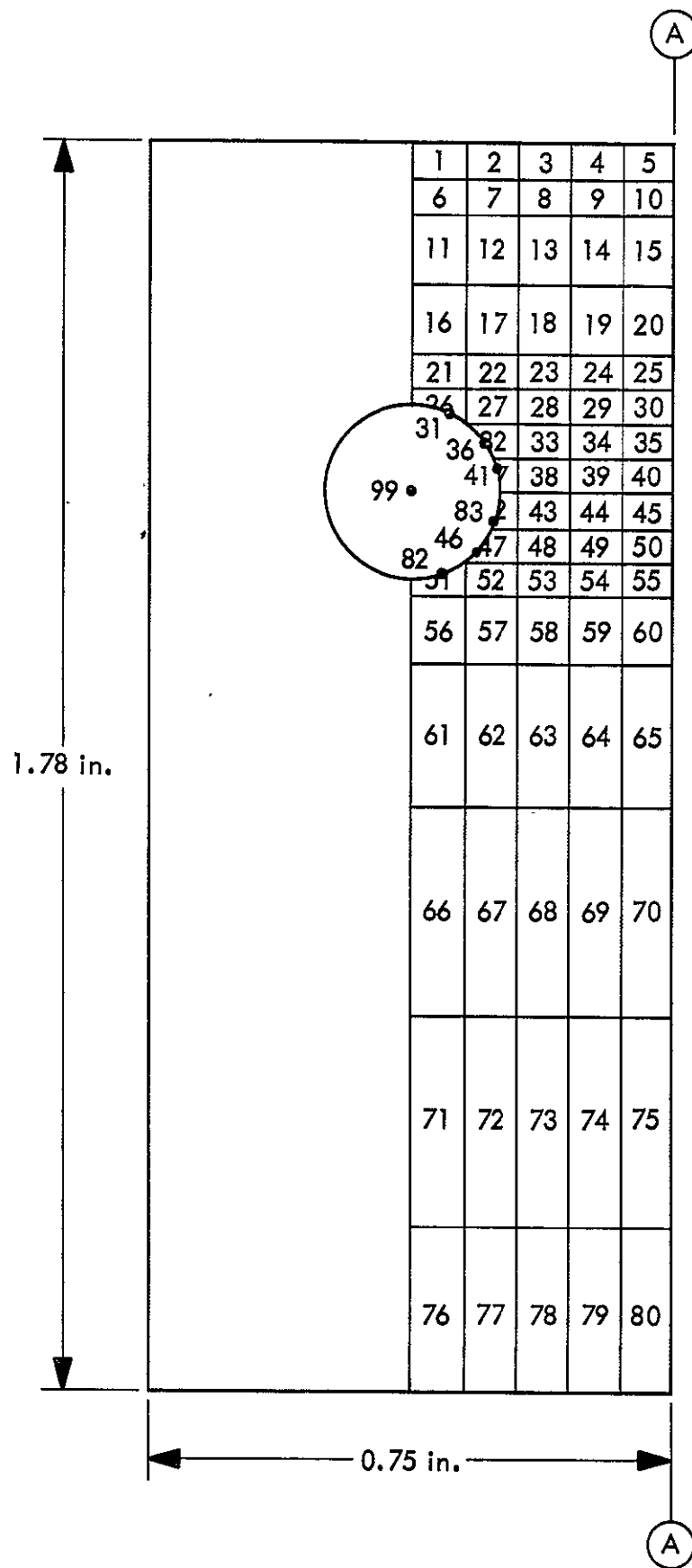


Figure 42. Section of 65cm. Tapered Gregorian Primary

of the tube, so that only half of the segment need be analyzed. The segment was subdivided vertically and horizontally into 76 elements, as shown in Figure 42. Convective resistance between the wall of the channel and the coolant fluid was taken into account, since a rough analysis indicated that this resistance was significant compared to that due to conduction through the mirror. Results were obtained for both laminar and turbulent convective resistances. (Laminar flow corresponds roughly to a 3°F rise in coolant fluid temperature between inlet and outlet to the primary mirror, whereas turbulent flow corresponds to a rise no greater than 1.5°F .)

The coolant fluid is represented by node 99 in Figure 42. Although the temperature of the coolant increases as it flows through the channel, the variation in one turn is small, so it was ignored. To help account for the transient thermal process undergone by the entire primary mirror cooling system at the start of viewing, the temperature of the coolant was varied with time in some cases. The types of variation will be described later in discussing the results.

Results are given in Figures 43 through 45 for the temperature distribution in the mirror segment due to solar irradiation and turbulent flow of a coolant fluid having a steady 70°F temperature, corresponding to an infinite flow rate. Figure 43 shows results for the steady radial temperature distribution between adjacent turns of the cooling channel. The upper curve in Figure 43 gives the temperature variation of the top row of nodes, from node 1 on the left to node 5 on the right. The lower curve in this figure gives the temperature variation of the row of nodes directly opposite the tube, from node 37 on the left to node 40 on the right. It is observed that the radial variation in temperature between adjacent turns of the channel is rather weak, particularly near the illuminated surface. This observation applies for all the steady results presented herein.

The vertical variation in the steady temperature distribution is shown in Figure 44. The upper curve presents the results for the row of nodes located approximately midway between adjacent turns, extending from node 5 at the top to node 80 at the bottom. The lower curve presents the results for the row of nodes extending from node 1 at the top to node 76 at the bottom. The two curves show that the temperature drop from the front surface of the mirror to

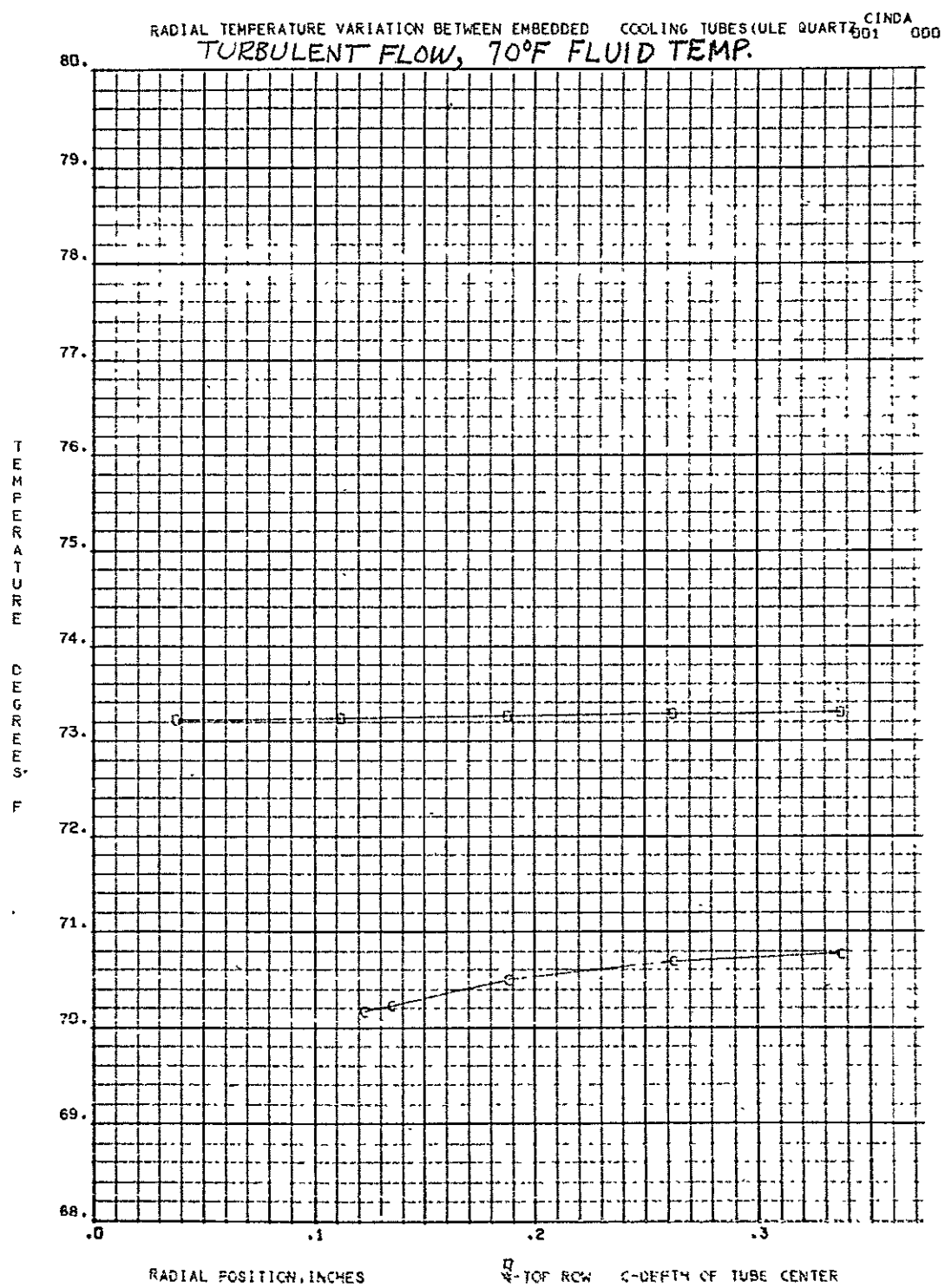


Figure 43.

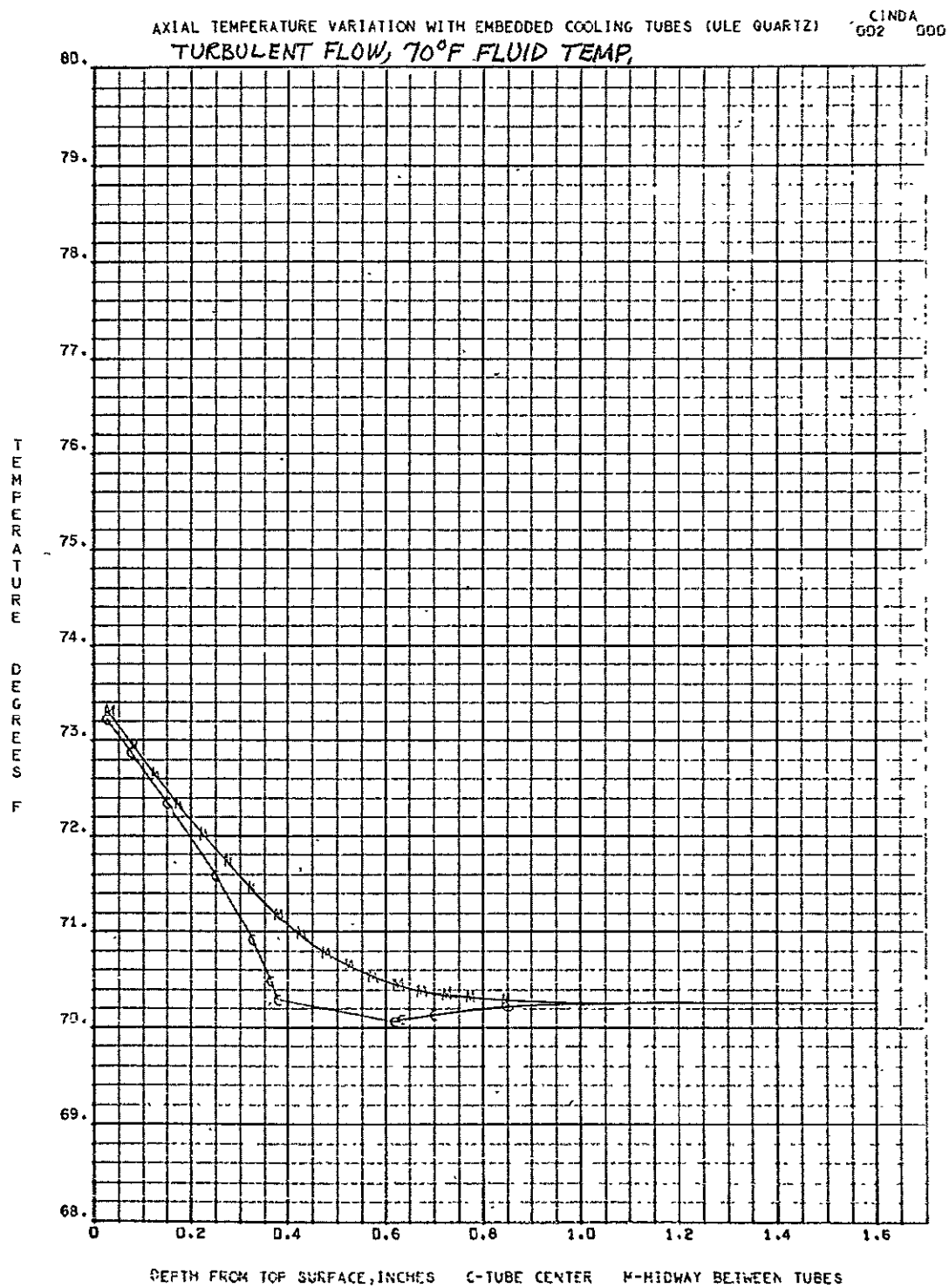


Figure 44.

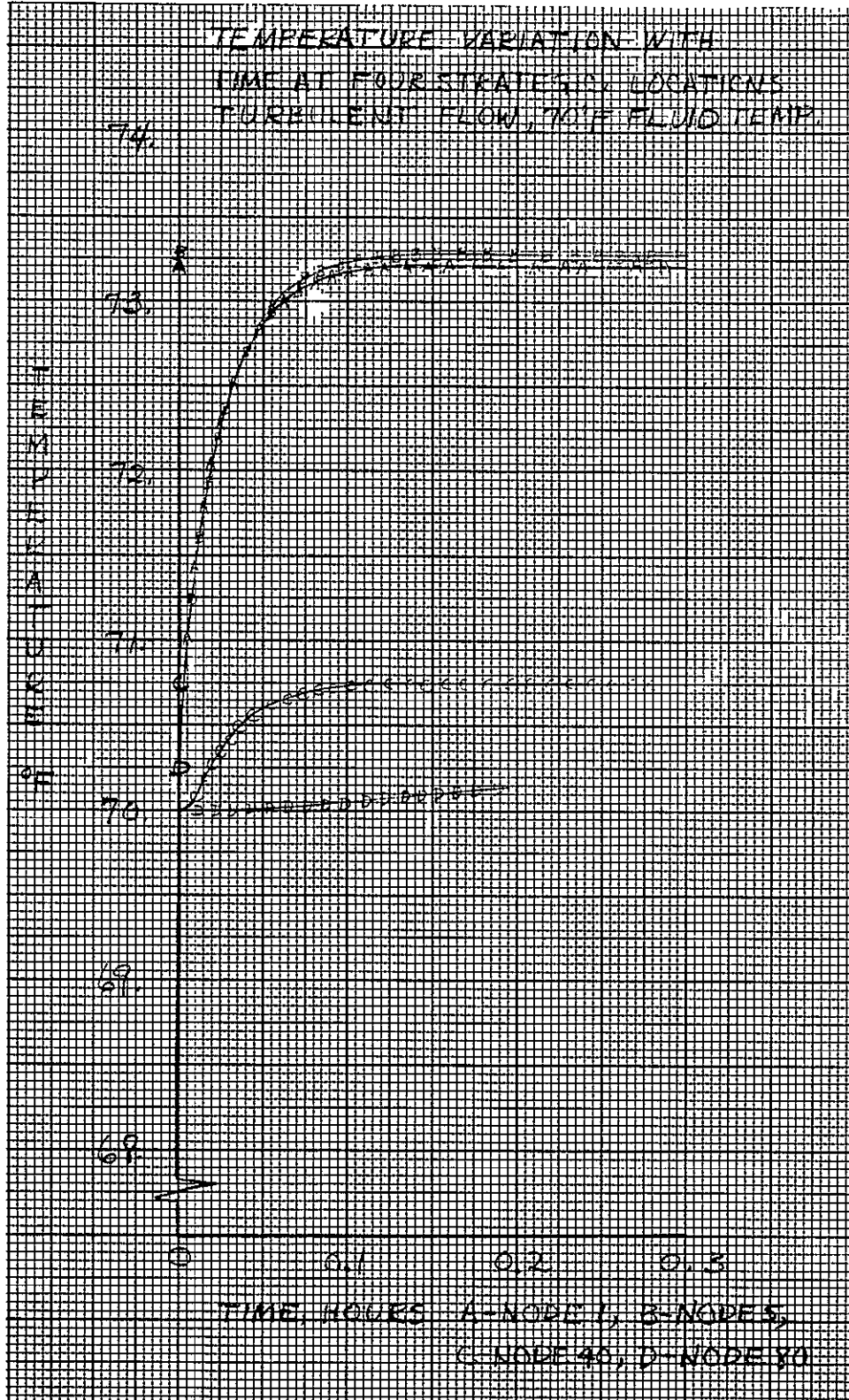


Figure 45.

the back is about 3°F . The variation is smooth except for the portion of the bottom curve which accounts for the presence of the channel. An interesting but unimportant feature of this curve is that the temperature rises slightly from the wall of the channel to the back surface of the mirror. In other words, not all of the solar heat absorbed at the front surface of the mirror is transferred to the coolant fluid before it is conducted to the region below the tube.

Figure 45 presents the transient temperature variation at four locations in the mirror. The temperature is initially 70°F throughout. It is observed that at nodes 1, 5, and 40 the temperatures have very nearly reached steady state (indicated by corresponding symbols on vertical axis) about five minutes after the solar flux has been suddenly applied. The temperature at node 80 approaches steady state less rapidly, but this is relatively unimportant because of the small change in temperature at this node.

Figures 46, 47, and 48 present results of the same type as those just discussed, except that the convective resistances are typical of laminar, rather than turbulent, flow. The higher steady temperatures shown in Figures 46 and 47, compared to those in Figures 43 and 44, are due to the larger temperature differences between the channel wall and the fluid required to transfer the absorbed solar energy to the fluid. In other words, for a given temperature distribution prior to solar irradiation, the temperature at any point in the solid rises to a higher level with laminar flow through the coolant channel than with turbulent flow. The transient results for laminar flow, presented in Figure 48, indicate that steady state is approached much less rapidly than with turbulent flow. This is due to the higher resistance to convective heat transfer which occurs with laminar flow, compared to turbulent flow. Not only does the temperature at any point in the mirror rise higher with laminar flow, but it does so more slowly.

In actual operation, the entire coolant system, including the radiator, pump, accumulator, tubing, etc. will undergo a transient thermal process after a change from nighttime to daytime conditions. Hence the coolant fluid will not remain at a fixed value, as assumed in obtaining the above results, but it will go through a transient also. To obtain a reasonable estimate of the variation of coolant temperature with time would require thermal analysis of the entire system. This is beyond the scope of the present investigation. To gain some feeling for the effects of transients in the coolant temperature, two types of

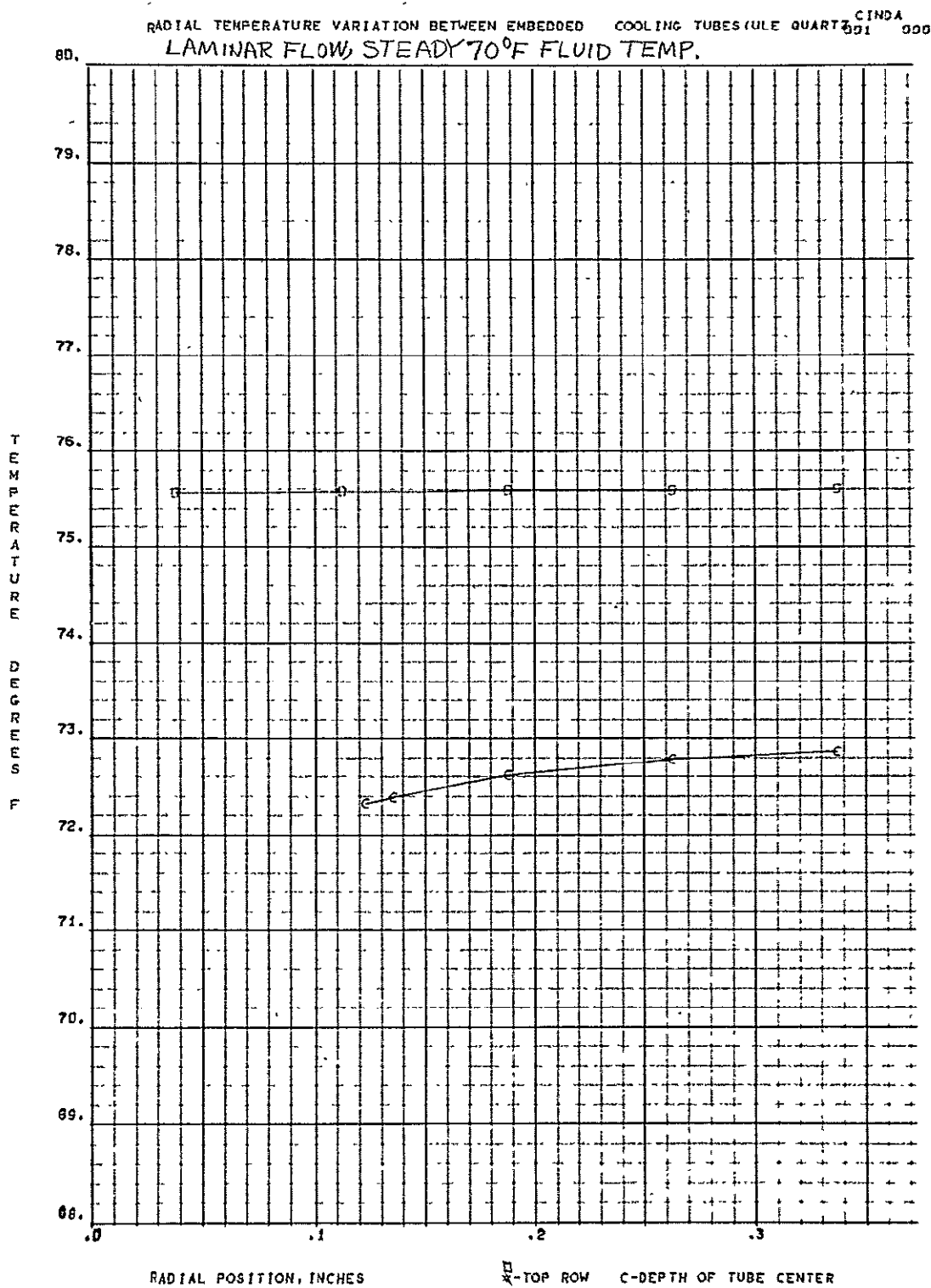


Figure 46.

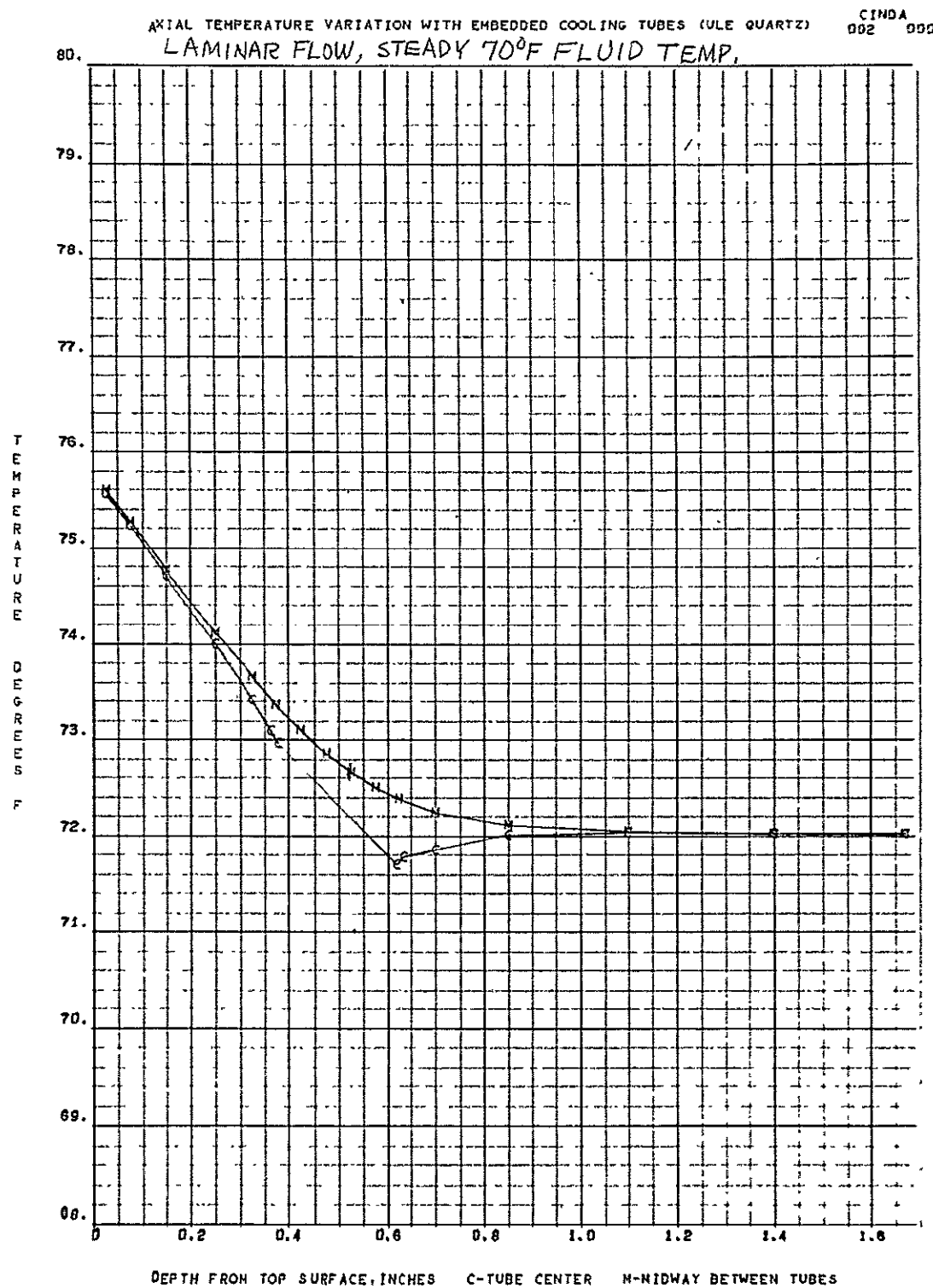


Figure 47.

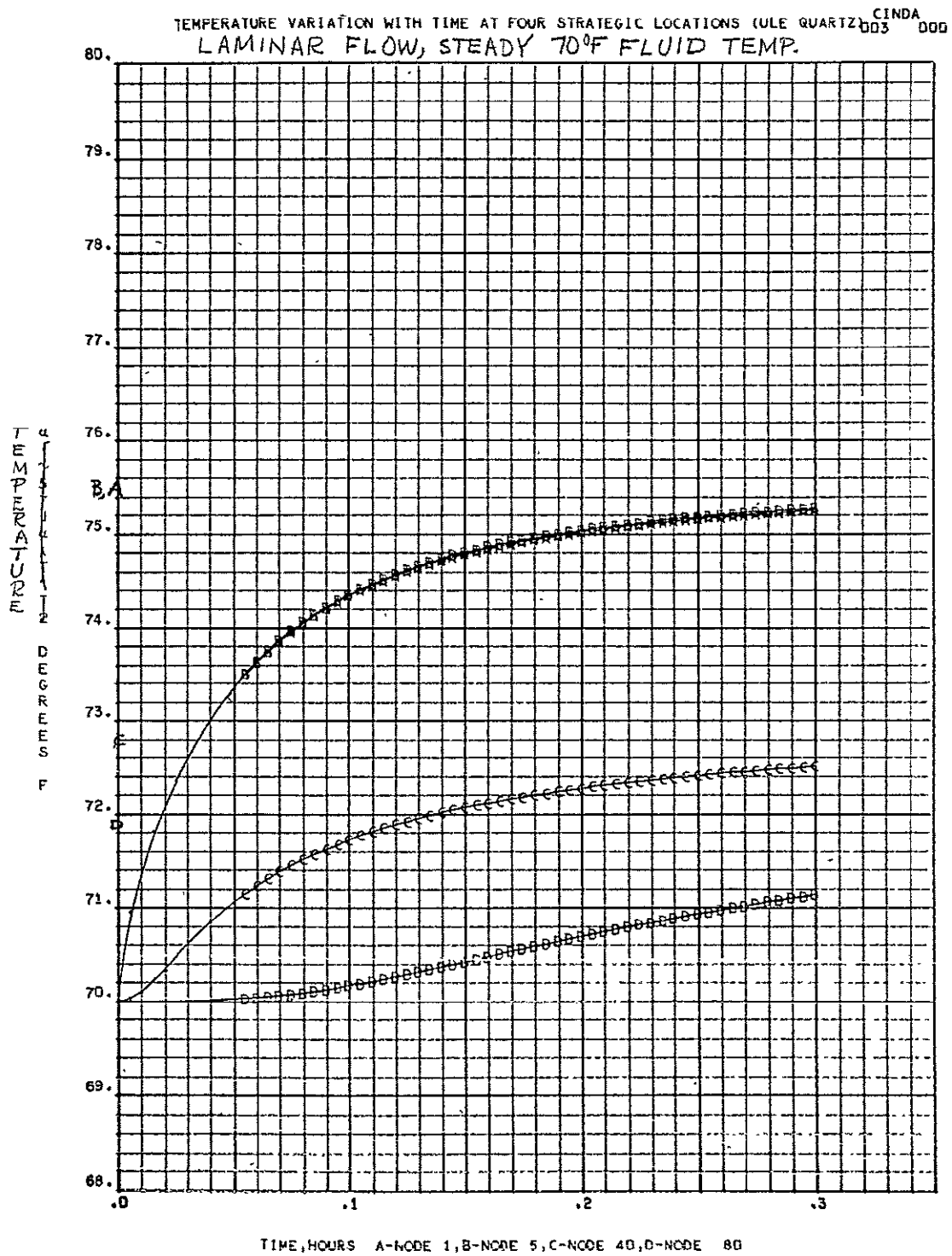


Figure 48.

transient variation were assumed. One was a step increase of 2°F in the coolant temperature at the same instant as the start of solar irradiation. This type of variation gives a lower limit on the time required to reach steady state. The other type of variation was a rising exponential, given by

$$T_{qq} = T_{o,qq} + \Delta T \left[1 - e^{-t/t_c} \right], \quad (1)$$

$$(\text{when } t = t_c; \left[1 - e^{-1} \right] = .632 = 63.2\%)$$

where $T_{o,qq}$ is the initial coolant temperature, ΔT is the maximum rise in temperature above the initial value, t is time, and t_c is the time constant for the transient change, i. e., the time required for 63.2% of the change to occur. The rising exponential is a more realistic type of variation since it predicts an asymptotic approach to steady state. By varying t_c , one may alter the rate at which steady state is approached. In the results presented here a value for ΔT of 2°F was used in equation (1), to permit direct comparison with the results for the step change in coolant temperature. A value of 0.1 hr. was used throughout for t_c .

The steady state results in Figures 49, 50, 51 and 52 are all 2°F higher than the corresponding results presented above for a steady coolant temperature. This follows logically from the fact that the steady fluid temperature is 2°F higher than formerly. The transient results for a 2°F step rise in coolant temperature with turbulent flow, presented in Figure 53, indicate that steady state is nearly achieved at the end of about five minutes, as before. When the coolant temperature rises exponentially, the mirror temperatures approach steady state less rapidly, as shown by the results in Figure 54. This is primarily due to the continual change in coolant temperature during the period shown.

The transient results for laminar flow are more sensitive to transient changes in coolant temperature, as demonstrated by the curves in Figures 55 and 56. Both a step change and an exponential change in coolant temperature cause a significant increase in the departure of the transient from the steady state values at the end of 0.3 of an hour.

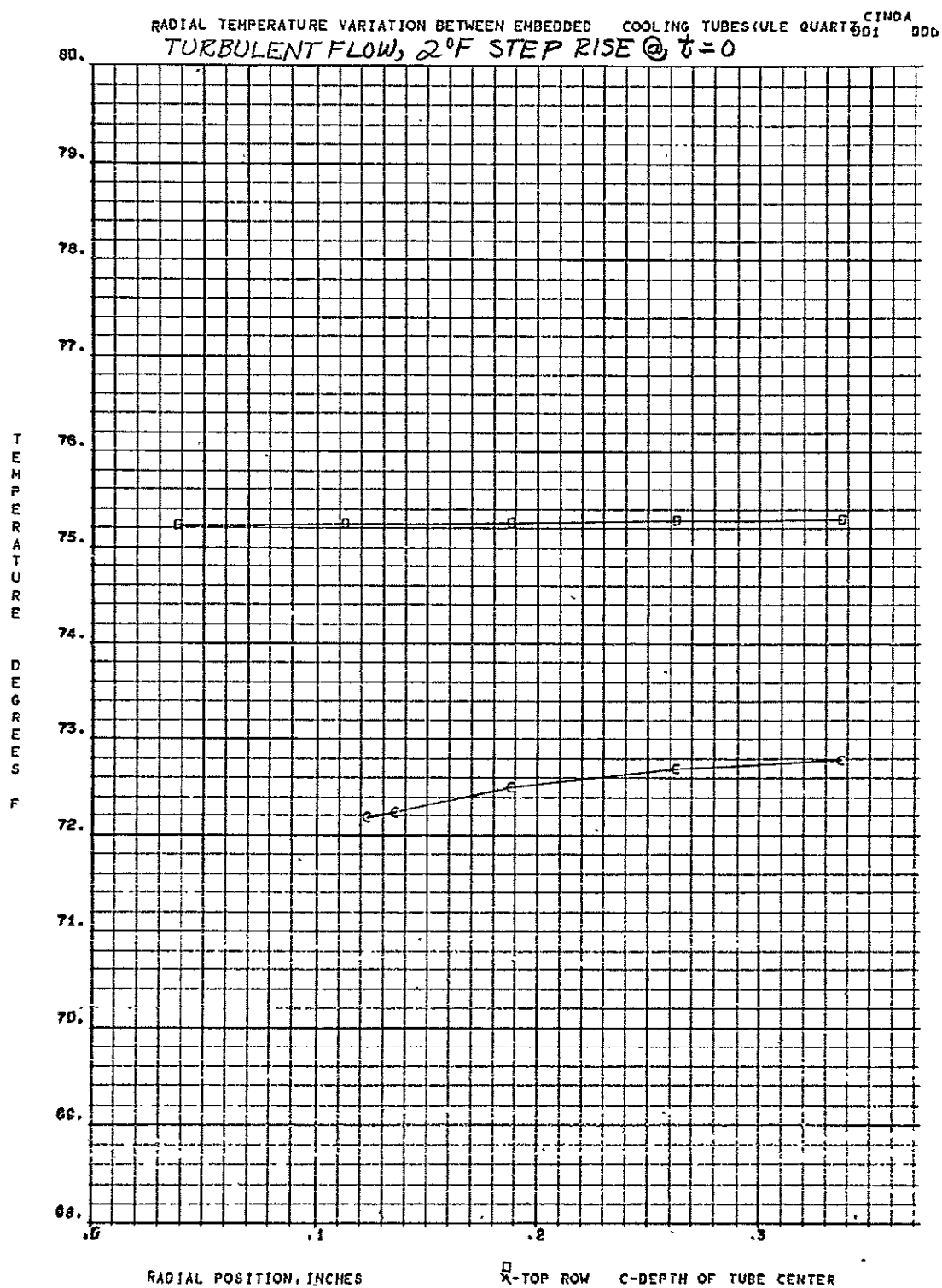


Figure 49.

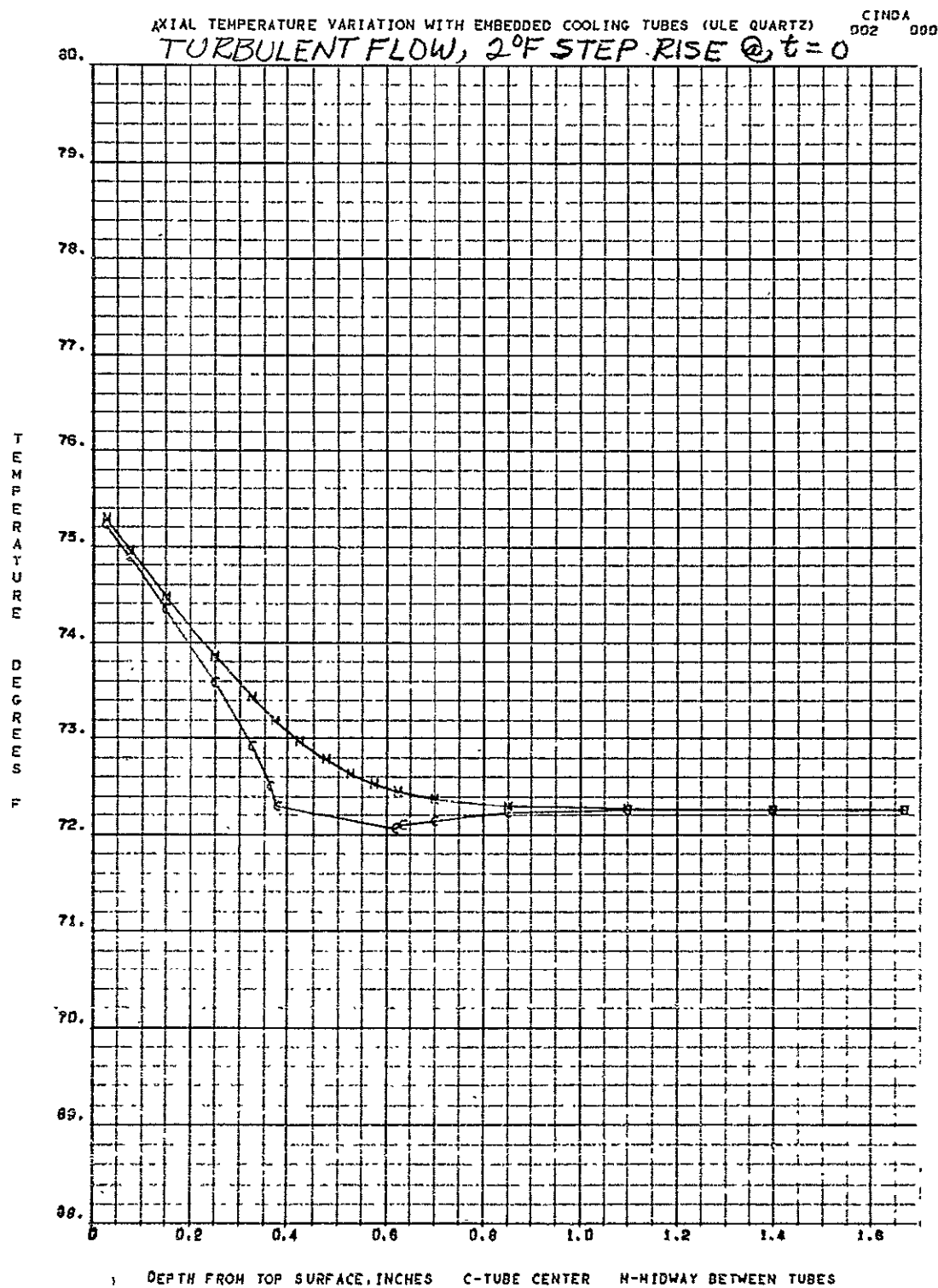


Figure 50.

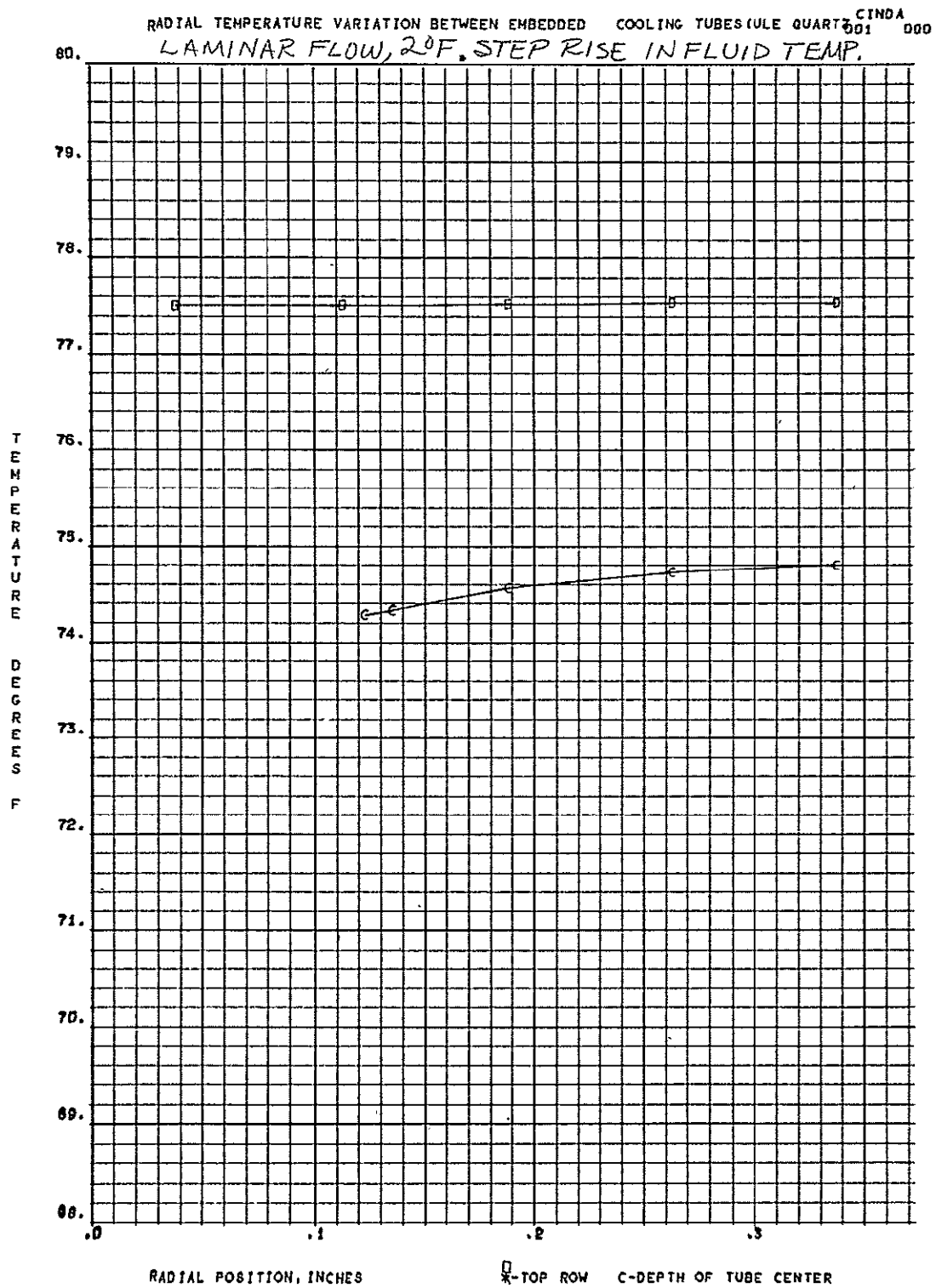


Figure 51.

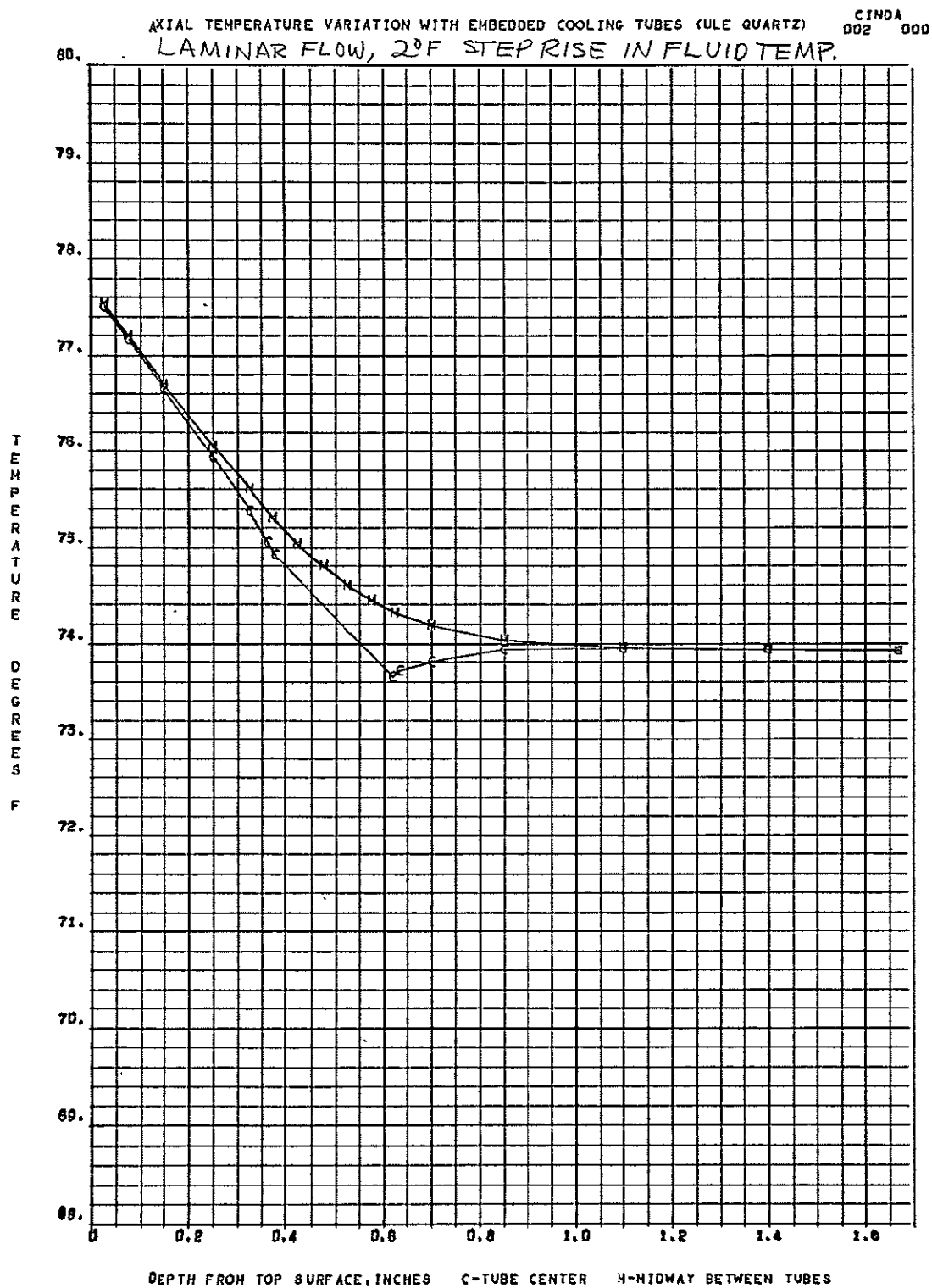


Figure 52.

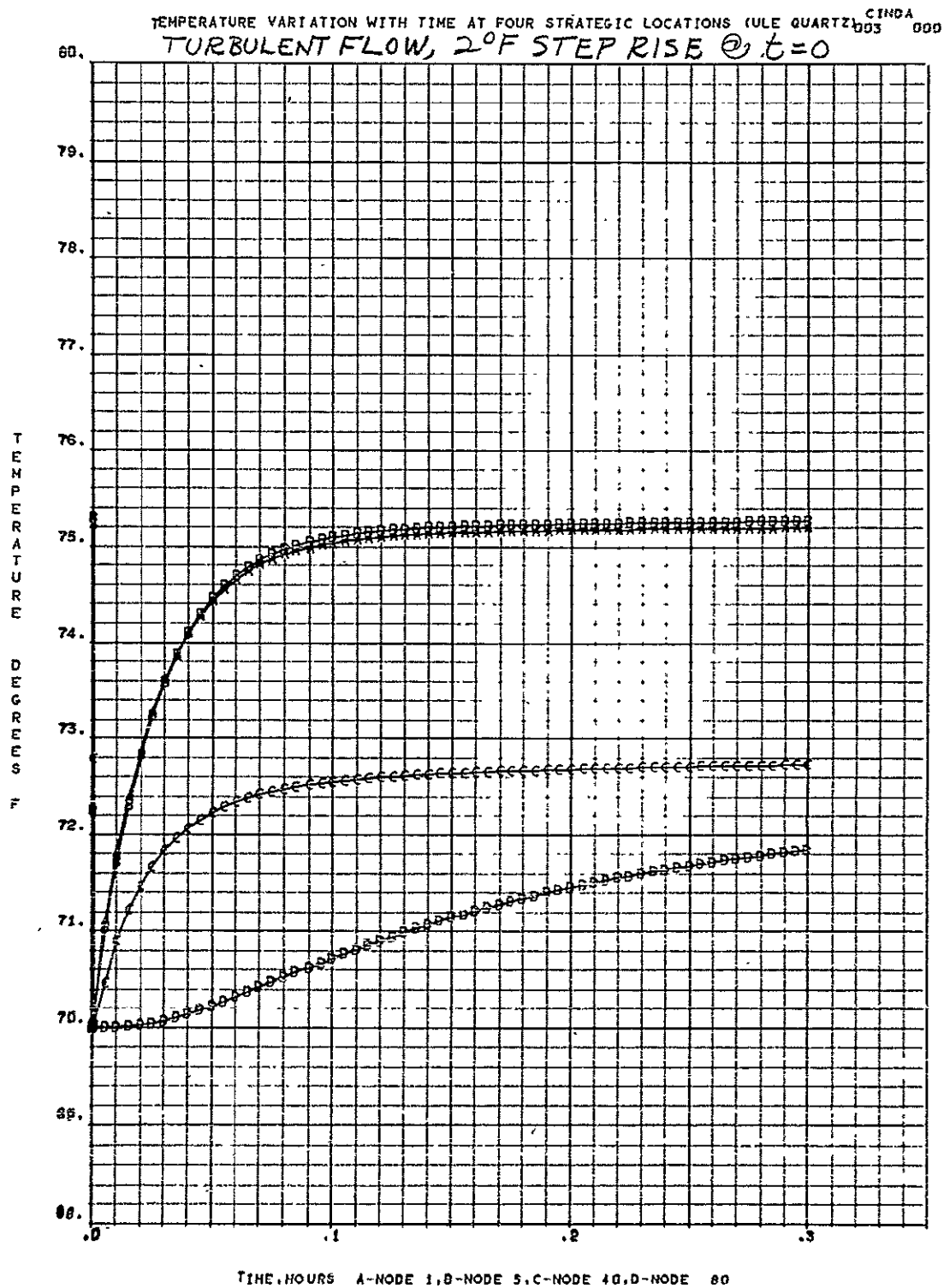


Figure 53.

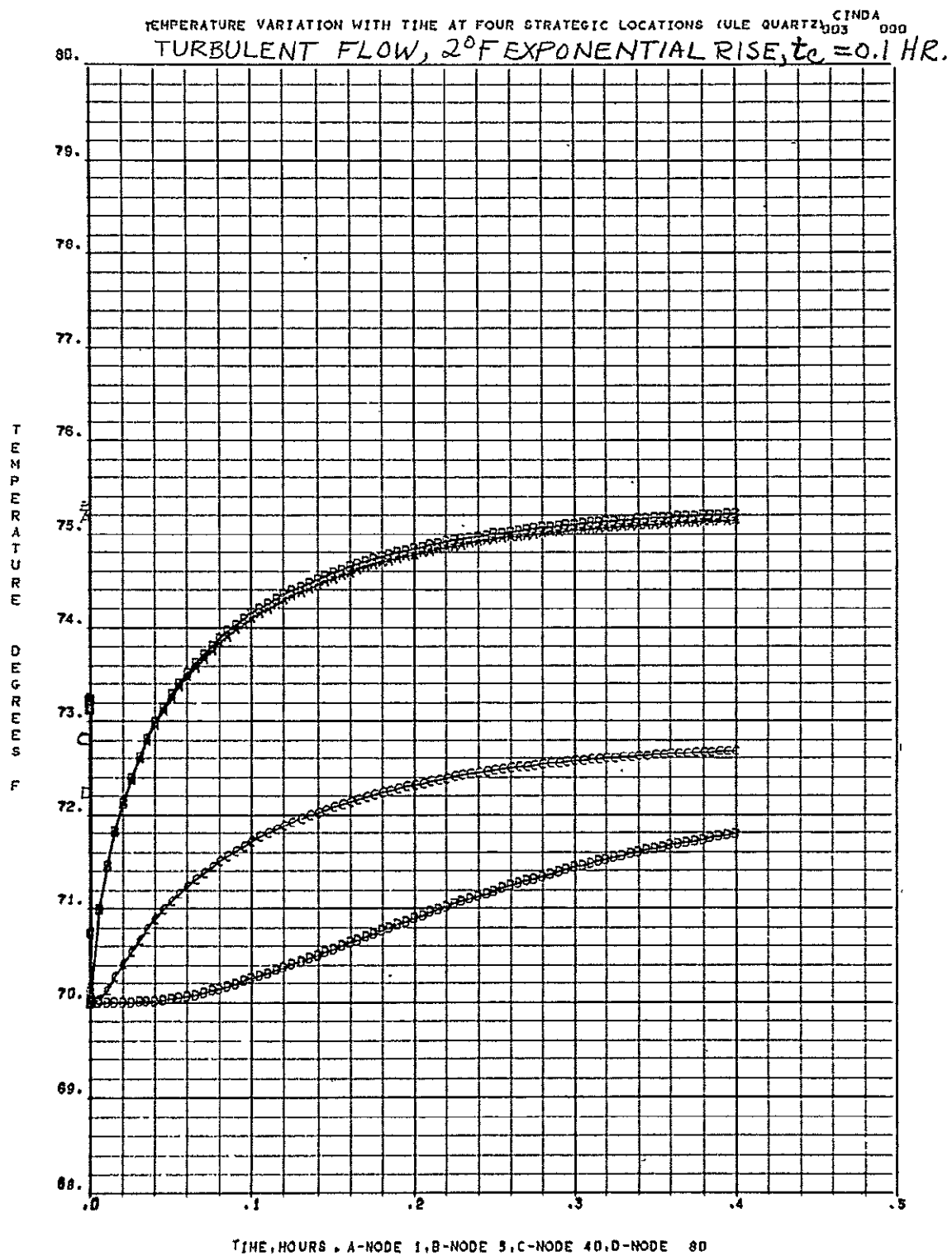


Figure 54.

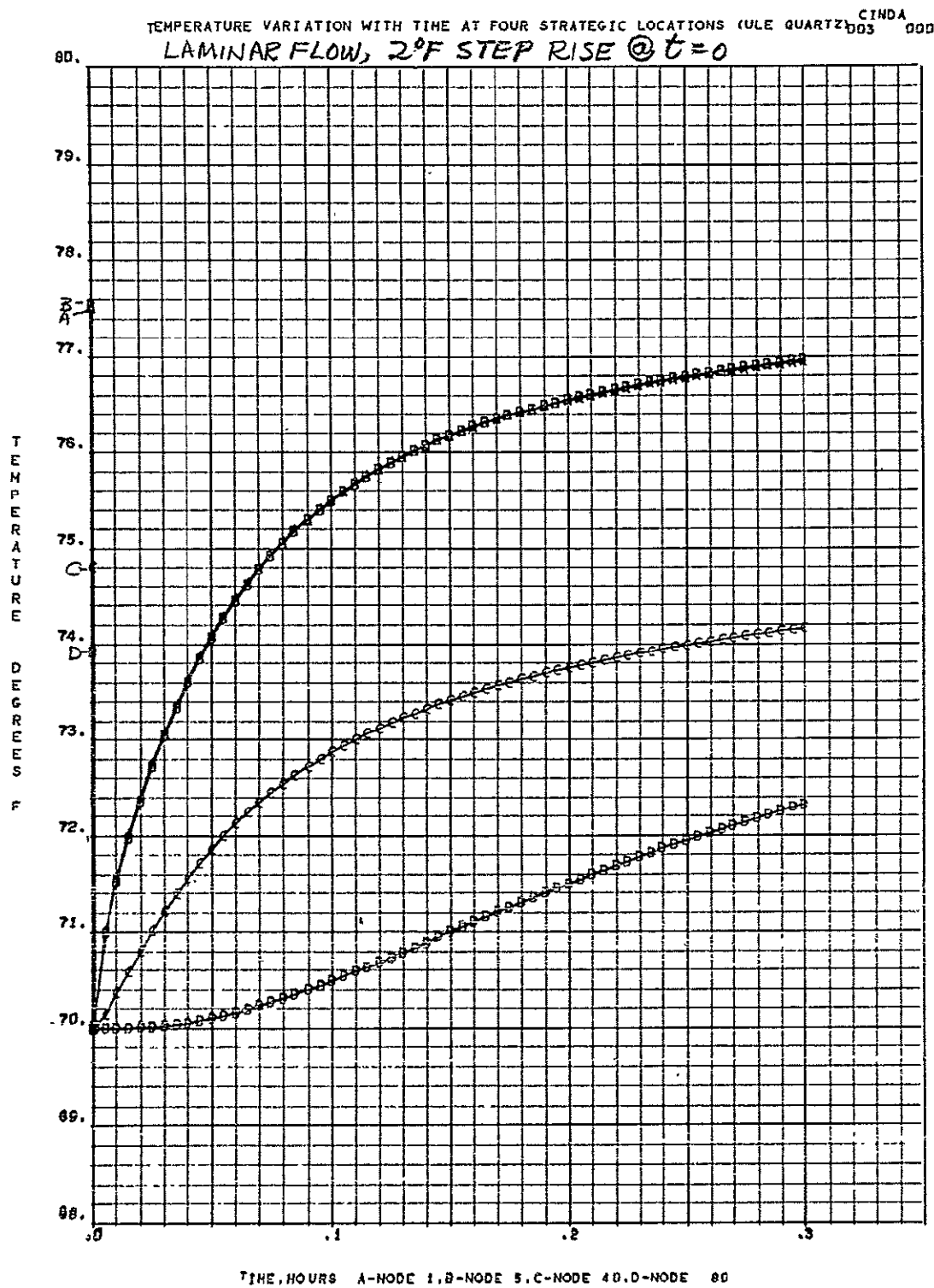


Figure 55.

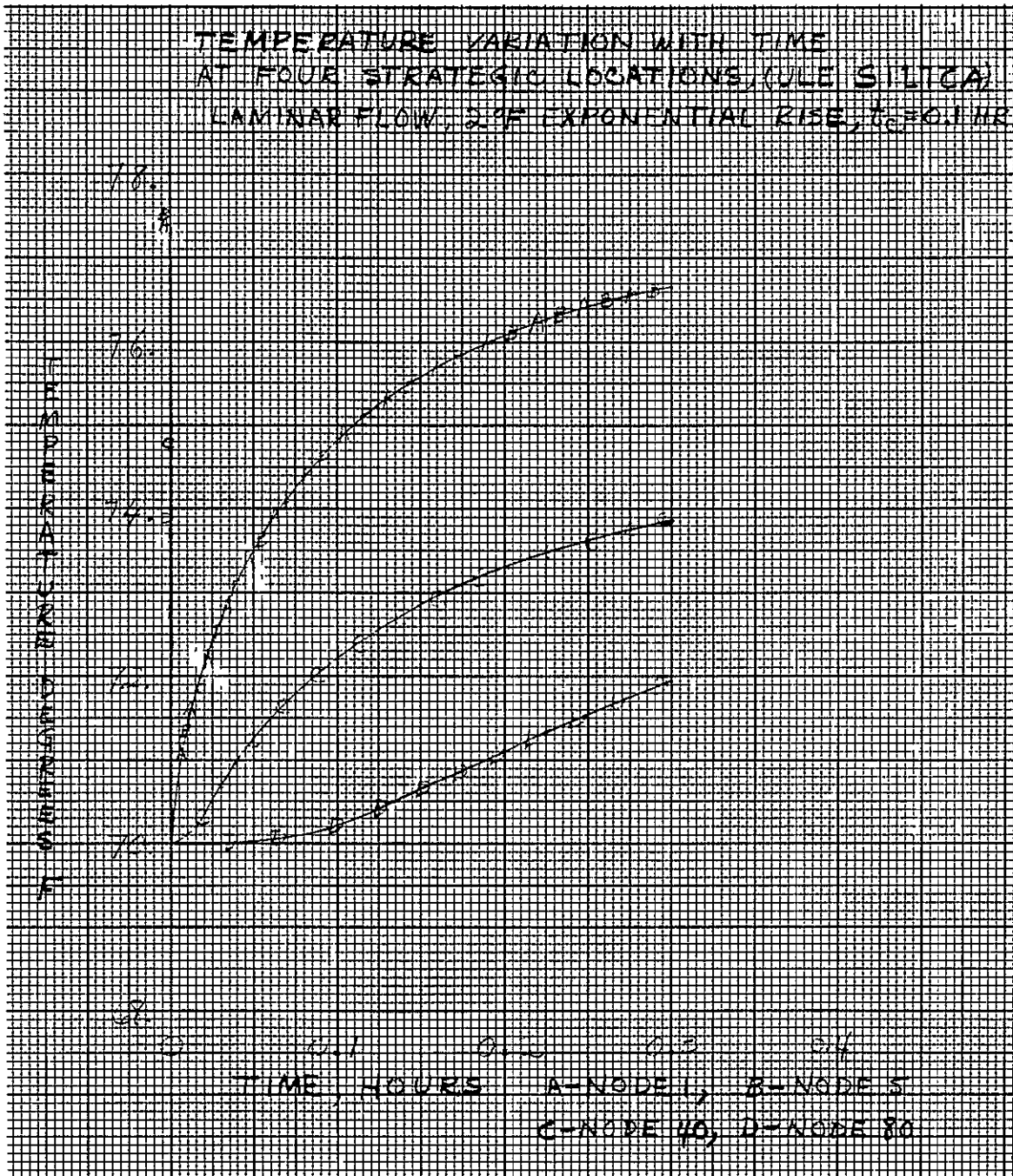
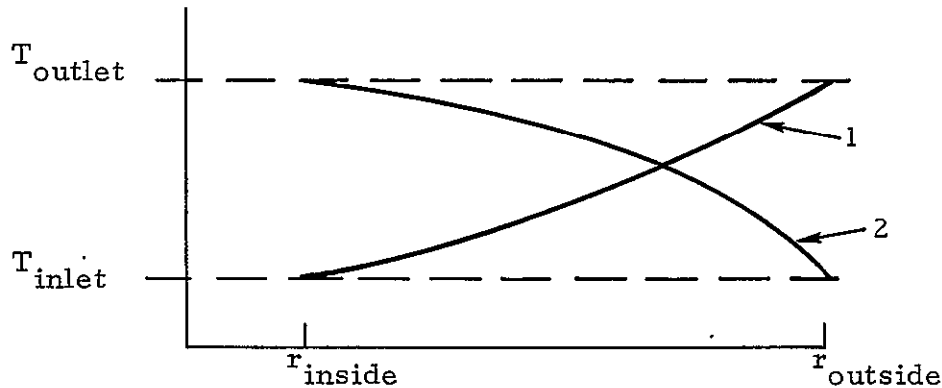


Figure 56.

The transient and steady state temperature distributions for the entire 65 cm primary mirror made of U. L. E. with internal cooling channels are shown in Figures 57 thru 74. The results of this study are complementary to the detailed analysis which describes in detail the temperature distribution in the vicinity of one cooling channel. As in the detailed analysis, the convective resistance between the channel wall and the bulk of the coolant fluid is taken into account in order to gain a more realistic picture of the transient and steady state temperature distributions.

The major assumptions on which this analysis is based are as follows:

1. The cooling channels are concentric, rather than spiral. This corresponds to zero spacing between infinitesimal channels and was used to permit the temperature and thermal distortion distributions to be treated as axially symmetric. Due to the limitation in the number of nodes which can be handled by the thermal distortion program, the analysis would have been impossible without this assumption. It would have been possible to thermally analyze the nonaxially symmetric situation. However, the time required to set up the data and carry out the computations would have been much longer, because several times as many nodes would have been required.
2. The fluid temperature was assumed to be either uniform in the radial direction or to vary in a continuous fashion. Continuous variation is consistent with a spiral cooling channel pattern. It might be impossible to achieve it with concentric channels, but this is thought to be unimportant, since the desire was to simulate the spiral pattern as closely as possible. Two directions of flow were considered. If the inlet is at the inside, the fluid temperature increases parabolically from inside to outside, as shown by curve 1 in the sketch below. If the inlet is at the outside, the temperature again varies parabolically, but as shown by curve 2. Since laminar and turbulent flow correspond to different flow rates, the difference between inlet and outlet temperatures is not the same for the two types of flow. A 1°F difference was used for turbulent flow, which difference corresponds to a Reynolds number of 6380. A 3°F difference was used for laminar flow, corresponding to a Reynolds



number of 1600. These Reynolds numbers pertain to a fluid of 80/20 methanol/water and a circular cross section flow channel, 1/4 inch in diameter.

3. The cooling channel was assumed to extend from the periphery of the central shaded spot to the periphery of the mirror. This is not consistent with the latest version of the primary mirror, which shows the spiral extending into the outer portion of the shaded spot. However, the thermal distortion program will not permit treatment of more turns of the channel than the number considered, namely 14. A note of caution is in order, however, since the mirror is supported at the hub, and this portion comes to equilibrium quite slowly, in a relative sense, as shown by the attached results. In other words, cooling the shaded portion might decrease the time required for the mirror to approach an equilibrium position, although the distorted figure may be insensitive to whether or not this portion is cooled.
4. The effects of an internal radial inlet or return channel in the primary mirror were not considered, since this channel would destroy axial symmetry. The necessity for assuming such symmetry has already been explained.

5. The cooling channels were spaced $3/4$ inch apart on centers. To simplify the thermal distortion analysis, the $1/4$ -in. diam. circular channels were replaced by square channels of equal cross-sectional area. This may have a mild effect on the temperature distribution, but any such effect is thought to be relatively unimportant.
6. Heat is removed from the mirror solely by the coolant fluid. That is, losses through the mounts and by radiation from the surfaces of the mirror were neglected. It is thought that this assumption has negligible effect on the temperature distribution for the present material and configuration. However, this does not necessarily hold if conductive mounts are used to support the mirror at its hub and if the material of the mirror is changed to one which has a higher thermal diffusivity.

The subdivision of the mirror for the thermal analysis was essentially the same as for the thermal distortion analysis. However, a different node numbering scheme was used. Figure 40 shows the discretized mirror and numbering scheme. (It may be noted that the notches in the hub were disregarded in the thermal analysis. The effect of this assumption on the results of the analysis is thought to be negligible.) Nodes with zero thermal capacity were placed at the four surfaces of each square flow channel to permit more accurate and more detailed results to be obtained. The temperature of the fluid in each channel was represented by a separate node to permit specification of the fluid temperature distribution along the radius of the mirror.

Representative results are presented in Figures 57 through 74. Each group of three figures (Figures 57-59, 60-62, 63-65, 66-68, 69-71, 72-74, presents the results for one type of flow and one fluid temperature distribution. The type of flow specifies the magnitude of the convective resistance, whereas the fluid temperature distribution establishes the base for the temperatures in the mirror. The first figure in each triplet presents the radial steady-state temperature distribution. The upper sawtooth curve, denoted by symbol F, gives the distribution through the upper, or front, row of nodes from node 1 through node 33. The curve denoted by symbol B gives the distribution through the back row of nodes from node 183 through node 182. The lower sawtooth curve, denoted by symbol C, gives the temperature distribution through the row of

nodes in line with the cooling tubes extending from node 100 through node 118. The relative maxima in curve F correspond to locations midway between tubes, whereas the relative minima correspond to locations centered (radially) above the tubes. Thus, the temperature difference between the maxima and minima gives approximately the fluctuation in surface temperature due to the presence of the internal cooling channels. However, the magnitudes obtained for these fluctuations from the present analysis are approximately twice as large in all cases as the fluctuations obtained from the detailed analysis. The results of the detailed analysis are probably more accurate due to the finer subdivisions used therein. In any event, the maximum fluctuation given by the present analysis is about 0.25°F and occurs for turbulent flow. The relative maxima in the curve denoted C correspond to locations midway between tubes, whereas the relative minima are fluid temperatures. Thus a curve drawn through the minima would represent the fluid temperature distribution with radial position on the mirror. Such a curve was not drawn, to avoid confusion. The points denoted C which are intermediate to the maxima and minima represent the temperatures of the coolant channel walls. The temperature differences between the channel walls and the fluid are much smaller for turbulent flow than for laminar flow, as can be seen by comparing the "C" curves in Figures 57 and 66. The vertical distances between the minima and those points between the minima and maxima represent these differences. Due to the larger values of these differences for laminar flow, as well as the larger radial variations of fluid temperature, the temperature level in the mirror is generally considerably higher for laminar than for turbulent flow.

The second figure in each triplet presents representative axial steady temperature distributions. The curve denoted X pertains to the column of nodes inside the shaded spot from node 3 at the top through node 155 at the bottom. The curve denoted Y pertains to the column of nodes just outside the shaded spot from node 5 at the top through node 153 at the bottom. The curve denoted Z pertains to the column of nodes centered at a radius of 8.18 in., from node 20 at the top to node 169 at the bottom. At this location, the thickness of the mirror is about 1.4 in.

The third figure in each triplet gives the variation with time of the nodes at the top and bottom of each of the columns for which results are presented in the second figure. The steady state temperatures of each of these nodes are

denoted by the locations of the corresponding symbols on the vertical axis. In general, the transient results are carried out to 0.4 hours, the exception being those shown in Figure 59.

Figures 57 through 59 present the results for the case of turbulent flow and a uniform fluid temperature. A uniform fluid temperature corresponds to an infinite flow rate, so this case is included primarily for its simplicity and for comparison purposes. It is observed from Figure 57 that the temperature difference between the front and back rows of nodes is roughly constant for radii greater than 3 inches. The drooping characteristic of curves F and B for radii approaching the periphery is due to shielding of the bevelled edge of the mirror.

The constancy of the steady-state temperature difference across the present mirror is in contrast with the variable difference reported earlier for the tapered Cervit mirror, which was cooled at the back surface. (See, for example, Figure 32). This feature of the present results is apparently due to the uniform spacing of the cooling coils relative to the front surface of the mirror. It should also be noted that the average temperature difference between the front and back surfaces is considerably smaller with the present design than with the earlier one. The reason for the smaller temperature difference becomes apparent upon consideration of the results in Figure 58. Curves Y and Z indicate that by far the major portion of the temperature difference across the mirror occurs between the front surface and the coolant tubes, which are centered $1/2$ inch below the front surface. This feature of the results is consistent with the geometry and the thermal boundary conditions. The negative temperature difference indicated by curve Z between the bottom of the tube at 0.65 in. and the node in the bottom row at 1.2 in. is considerably larger than that obtained from the detailed analysis. (See, for example, Figure 44.) As a result, the temperature difference between the front and back rows of nodes is smaller in the present analysis than in the earlier one. This difference between the two sets of results is due to the coarser subdivisions used in the present analysis. The results of the detailed analysis are probably more accurate, so the present results may give optimistic estimates of the magnitudes of the thermal distortions.

By comparing the results in Figures 57, 60, and 63, it may be noted that the temperature difference between the front and back rows of nodes at a

particular radial location is essentially independent of the radial variation in fluid temperature. This holds for laminar as well as turbulent flow, and it indicates that radial conduction is relatively unimportant. A similar feature was noted earlier in the results for the Cervit mirror.

The transient results in Figures 59, 62, and 65 indicate that the temperatures at a radius of about 8.2 in. are very near equilibrium 0.15 hours after the start of illumination. Examination of the detailed results reveals that the elements at smaller radii and near the front surface approach equilibrium almost as rapidly. However, the elements in the back row approach equilibrium much less rapidly. A feeling can be gained for the last statement by examining the curves labeled E in Figure 59, 62, and 65. In addition, the curves labeled A and D indicate that elements inside the shaded spot approach equilibrium slowly; and this is particularly the case for those elements at the bottom of the hub. Comparison of the results in Figures 59, 62, and 65 reveals that equilibrium is approached at a rate, at a given node, which is essentially independent of the radial distribution of fluid temperature.

Turning to the results for laminar flow in Figures 66, 67, and 68; 69, 70, and 71; and 72, 73, and 74, it is observed that the steady temperature difference across most of the mirror is about 0.8°F larger than was the case for turbulent flow. This is due to the fact that the convective resistance is larger for laminar flow than for turbulent flow. As stated earlier, this is graphically illustrated by curve C in Figure 66. The curves in Figures 68, 71, and 74 show that equilibrium is approached much less rapidly with laminar flow than with turbulent flow. The reason is the same as above; the convective resistance is higher for the former than for the latter.

A later design change came about in an effort to optimize the configuration with respect to distortion in the 1-g field. This amounted to additional material 1 in. thick at the hub and tapering to meet the original slope at a radius of 9.8 inches (Configuration No. 2, Figure 2). This new mirror configuration with the discretized elements and assigned node numbers is shown in Figure 75. These node numbers which are circled show the addition. The results of adding this material had a very slight effect on the temperature distribution. This can be seen by comparing Figures 80 and 84 which show the temperature profiles of the front and back surfaces for configuration No. 1 and configuration No. 2 respectively.

Figures 76 through 87 show the front and back surface temperature profiles for those conditions which were analyzed for thermal distortion. As indicated in Figure 76 the top curve is for the front surface and the bottom curve is for the back surface.

Calculations have been performed to estimate the pressure drop of methanol water (80/20) through a circular cooling channel of diameter D and length L with constant radial spacing, Δr , between the centers of adjacent turns of a spiral pattern. The flow rates used are those required to maintain a 1°F or 2°F temperature difference between inlet and outlet of a 65-cm-diam. mirror with a 12-cm-diam. shaded spot. The mirror absorbs 0.14 of one solar constant. A standard equation for pressure drop was used, namely

$$\Delta p = f \frac{L}{D} \frac{\rho V^2}{2g_c} \quad (2)$$

where f is the so-called Darcy-Weisbach friction factor. This equation does not account for curvature in the tube, but this is not thought to be important. The friction factor for a smooth tube was used. No allowance was made for pressure drops through fittings.

The following equation was derived for the total length of the cooling channel for a mirror with inner radius r_i and outer radius r_o and for a spacing between adjacent turns of r :

$$L = \frac{2\pi}{\Delta r} \left[r_i(r_o - r_i) + \frac{(r_o - r_i)^2}{2} \right] \quad (3)$$

The results are summarized below.

Tube Diameter (in.)	Radial Spacing (in.)	Total Channel Length (ft.)	Temp. Diff. (°F)	Mass Flow Rate (lb/in. ²)	Pressure Drop (lb/in. ²)
1/8	3/8	110	2	143	171
3/16	3/8	110	2	143	24.4
3/16	9/16	73.4	2	143	16.3
1/4	3/8	110	2	143	6.32
1/4	3/4	55	2	143	3.16
1/4	3/4	55	1	286	10.3

Since turbulent flow would be a greater problem with respect to vibrations due to the fluid flow, it has been decided that laminar flow will be used. An estimated internal pressure of 16 psia was considered to be the maximum pressure internal to the mirror.

This pressure has been based on the design where the pump is placed close to the outlet where the fluid exits the mirror. The minimum pressure of the system would be at this point, i. e., the outlet of the mirror and the pump itself; therefore, the system must be designed so that the pressure at this point is above the boiling point of the coolant.

A study was made to determine if it was feasible to use radiative cooling in order to effect the back surface temperatures which has been studied. Figures 88 and 89 show the required sink temperature (T_2) for the back surface of the mirror to be at 70, 80, 90 and 100°F, with a view factor between the mirror and sink varying from 0.5 to 1.0. The inset of Figure 88 shows a means of obtaining a view factor of 1.0 between the mirror and the cold plate. The difference between the two models is that the solar absorptivity of Figure 88 is 0.14 and that for 89 is 0.11.

For the mirror to have a back surface temperature of 70°F (T_1 of Figure 88) with view factor of 1.0, the sink plate temperature would have to be maintained at -40°F (T_2); therefore, a refrigeration system would be required.

An investigation was made for a refrigeration system which could be used, but none was found available. The major problem with the system is that the compressor for the refrigeration cycle operates on the refrigerant vapor only. In a 1-g field the liquid can be separated from the vapor. In the

space application no practical method has been devised to ensure that only vapor goes into the compressor.

For these reasons this method of controlling the mirror temperature is not feasible.

Figure 16 shows, among other things, a temperature mapping of a steady-state computer analysis. This is the method utilized to transfer the temperature data to the stress analysis group. These temperatures are from the printed listings on Table 14.

Much of this written report has been taken directly from Dr. M.W. Wildin's memos which he wrote while working on the primary mirror.

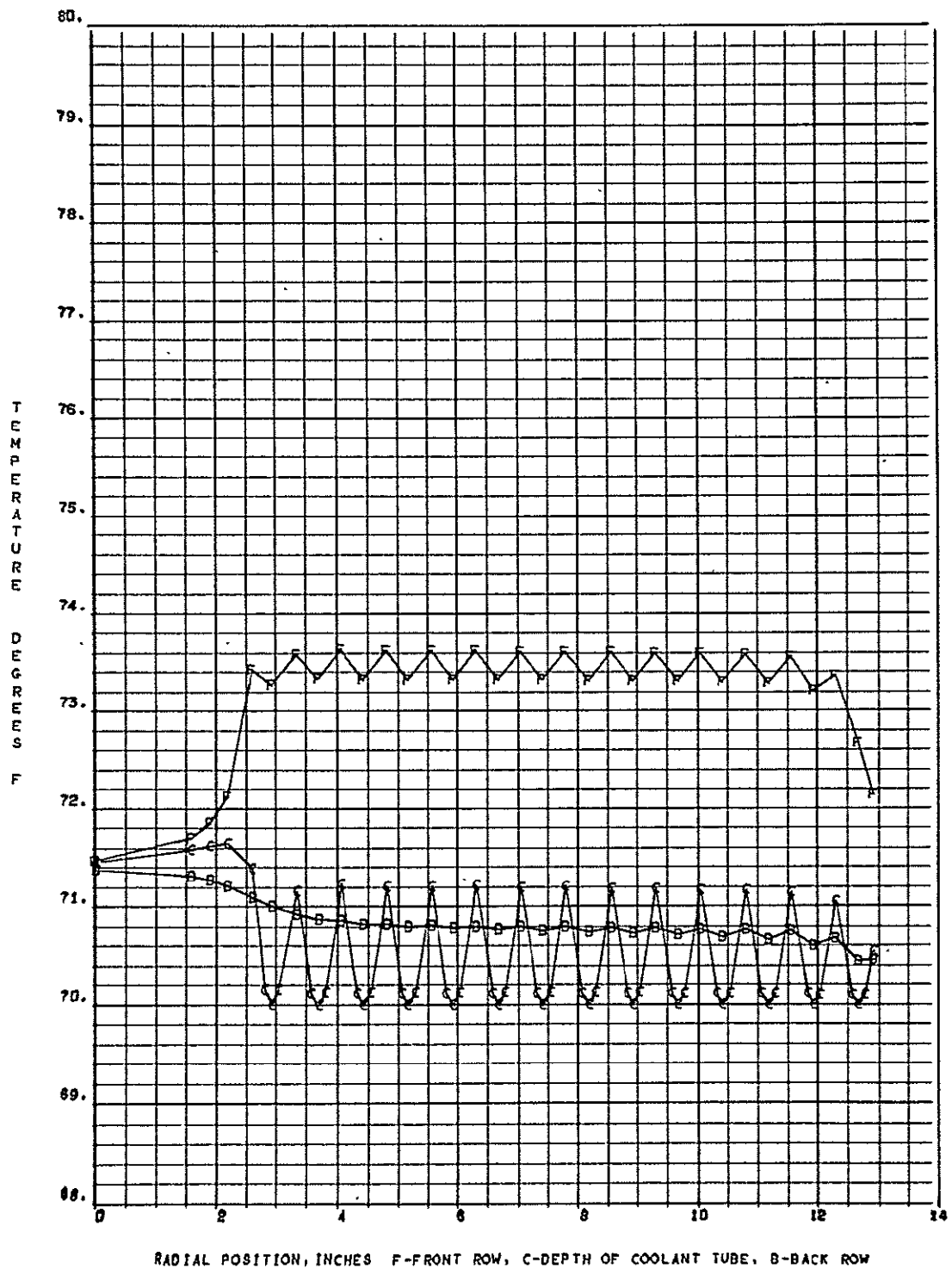


Figure 57.

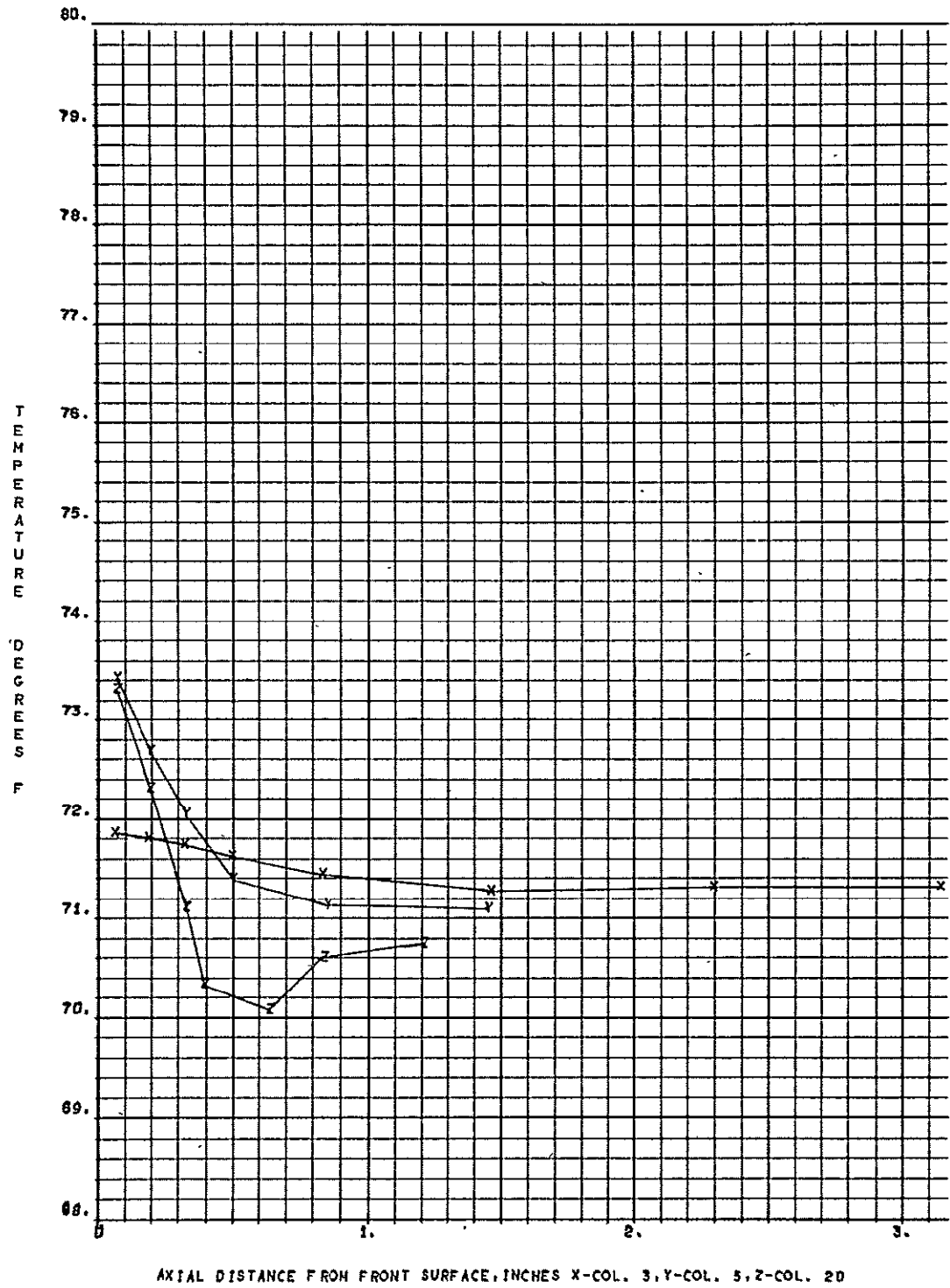


Figure 58.

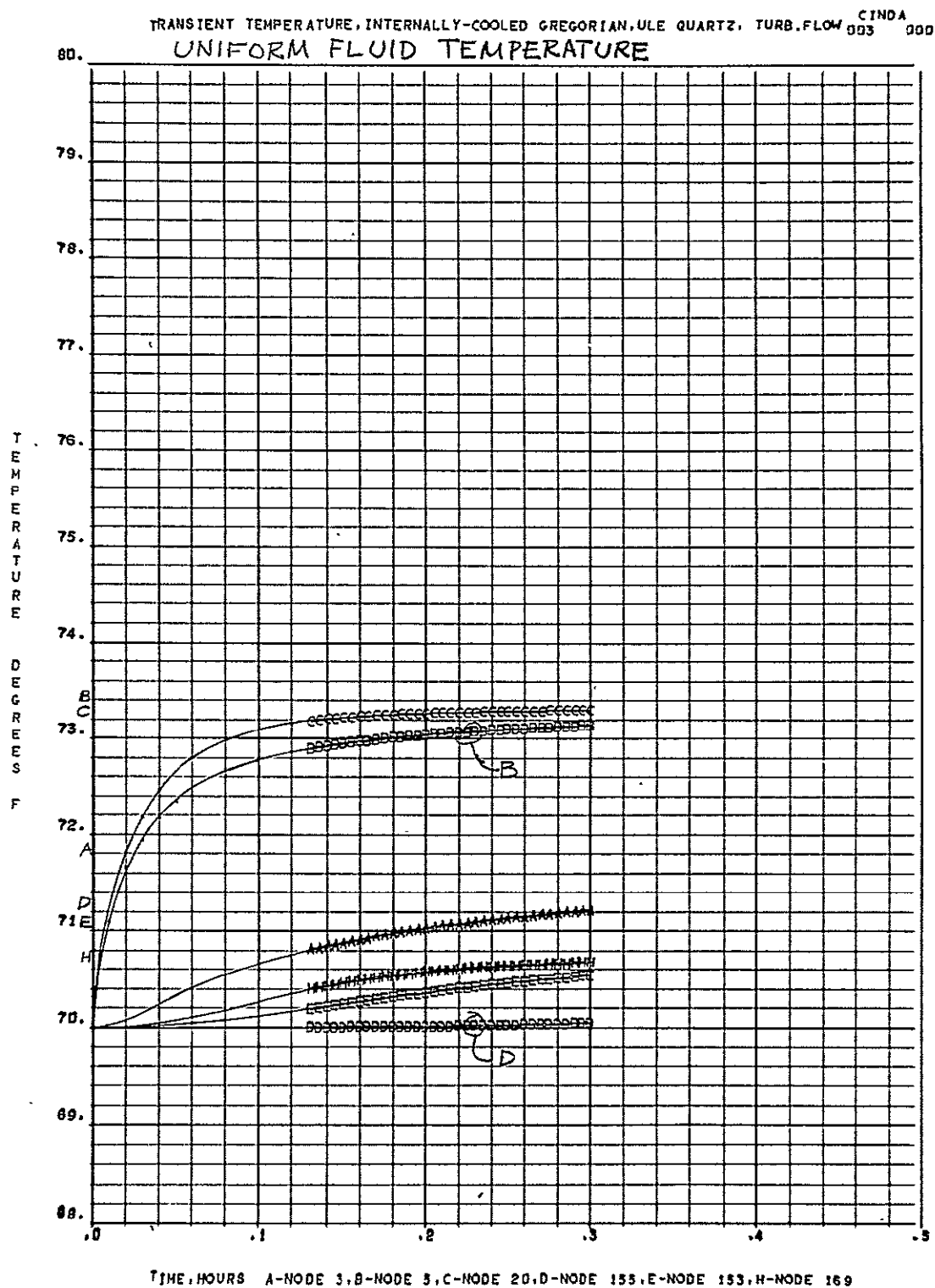


Figure 59.

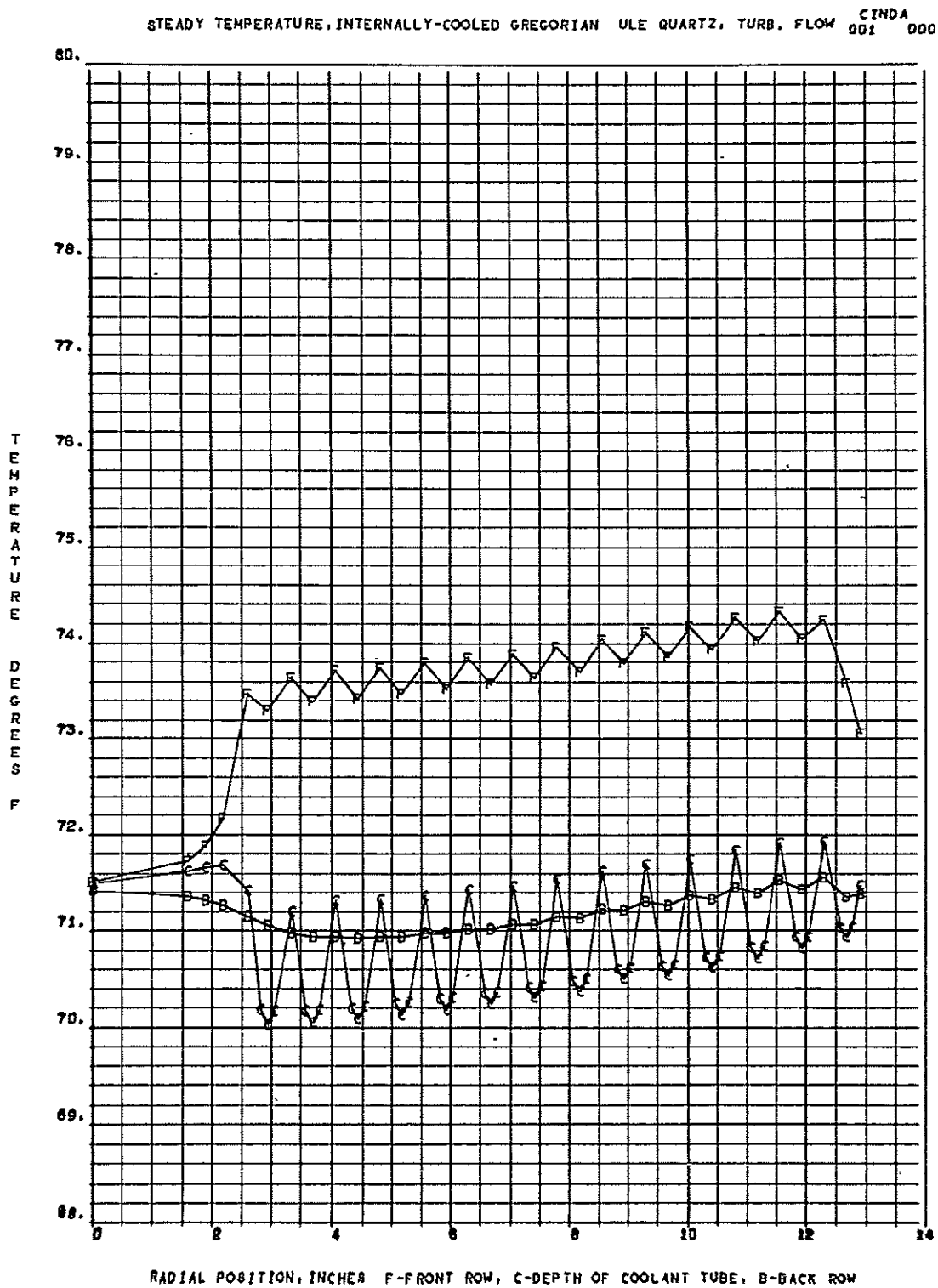


Figure 60.

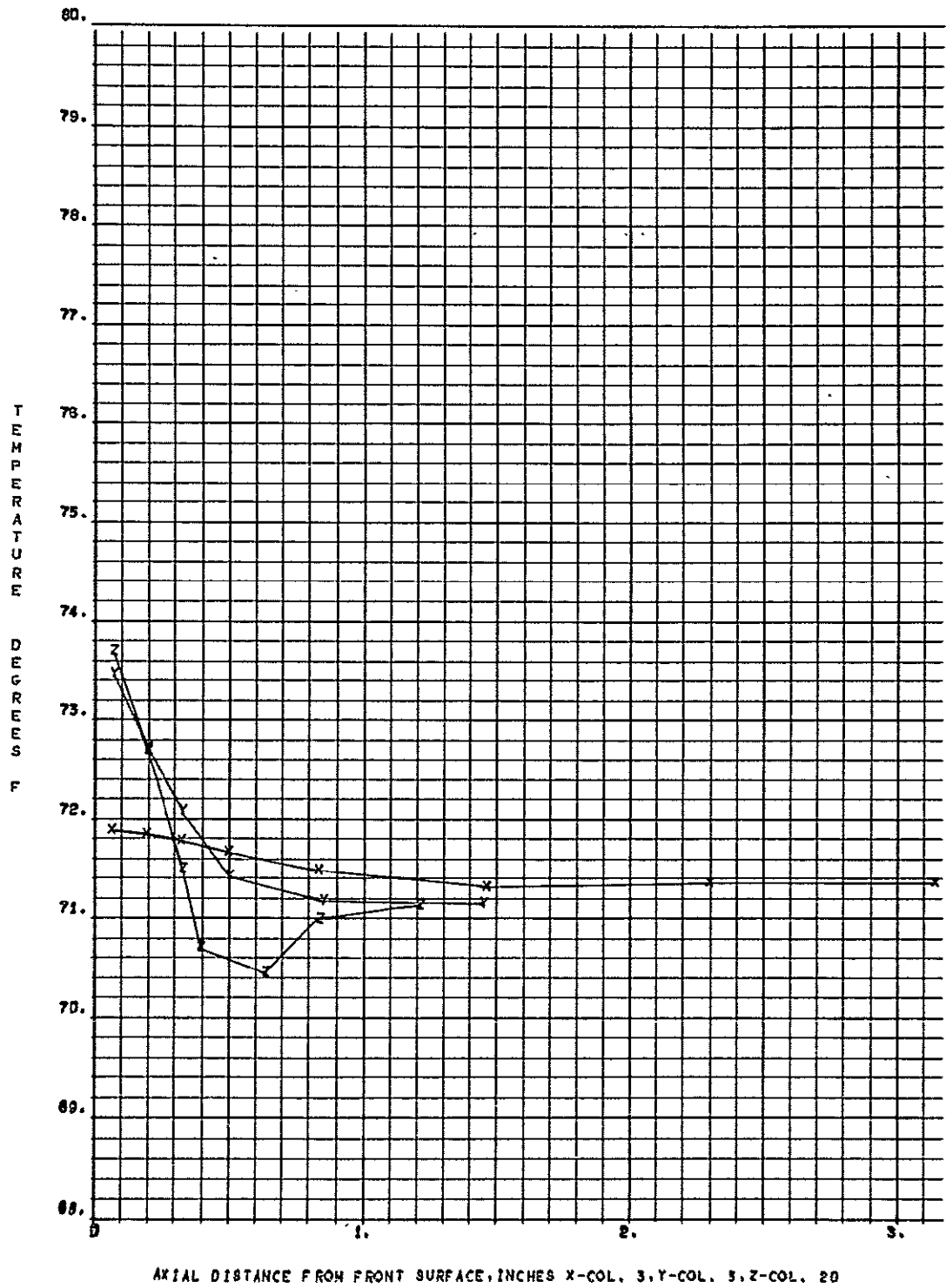


Figure 61.

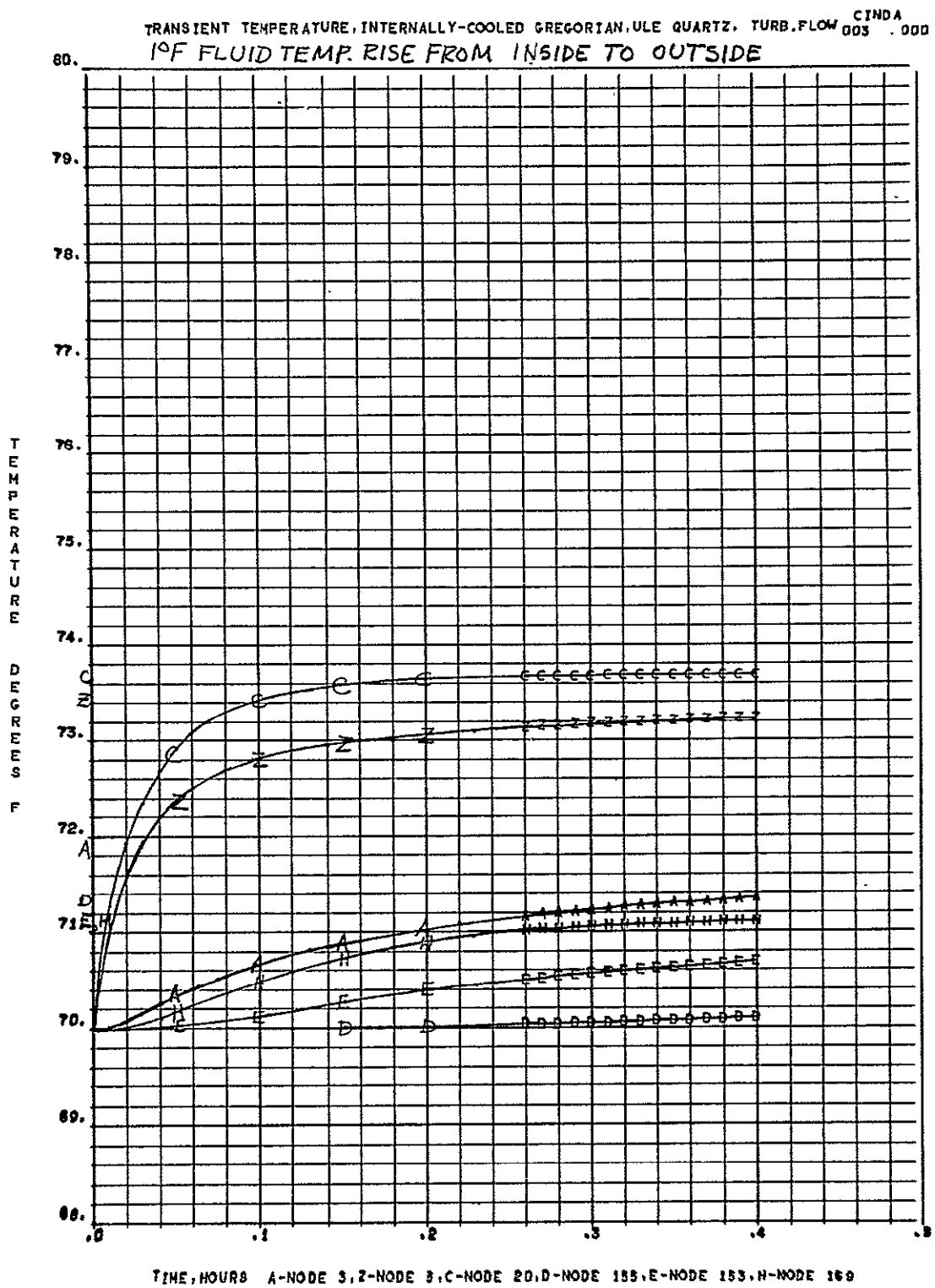


Figure 62.

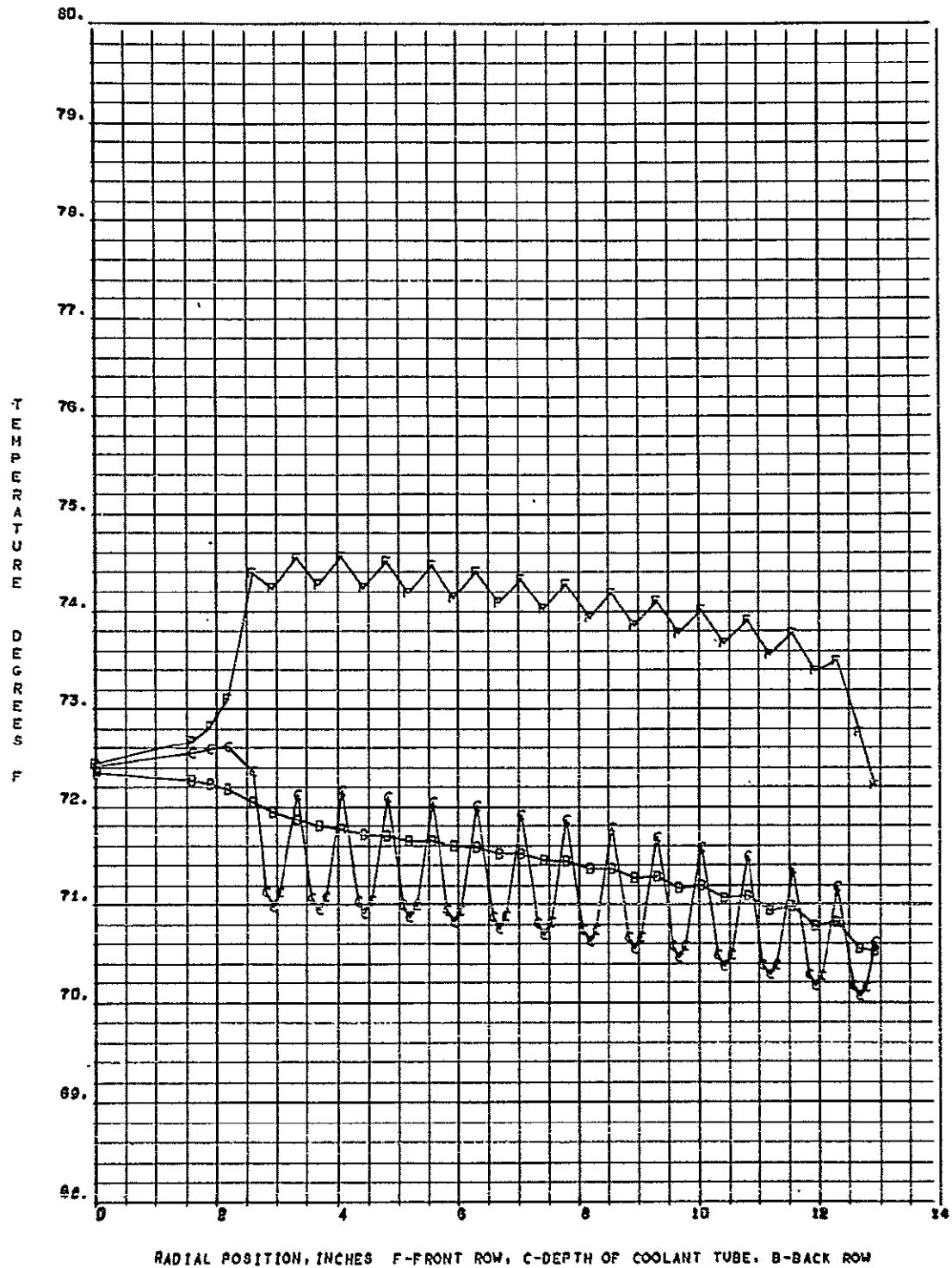


Figure 63.

STEADY TEMPERATURE, INTERNALLY-COOLED GREGORIAN ULE QUARTZ, TURB. FLOW CINDA 002 000

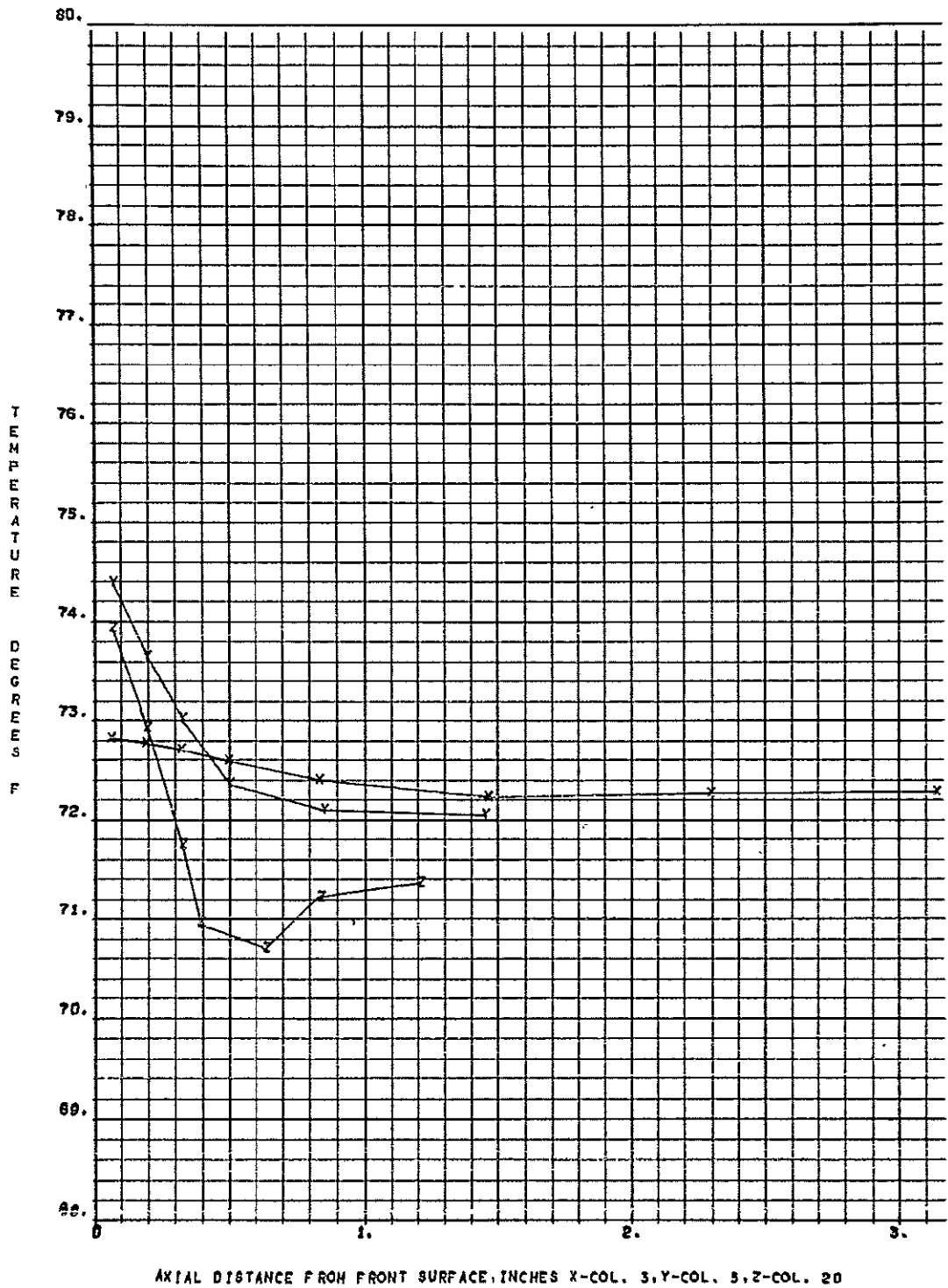


Figure 64.

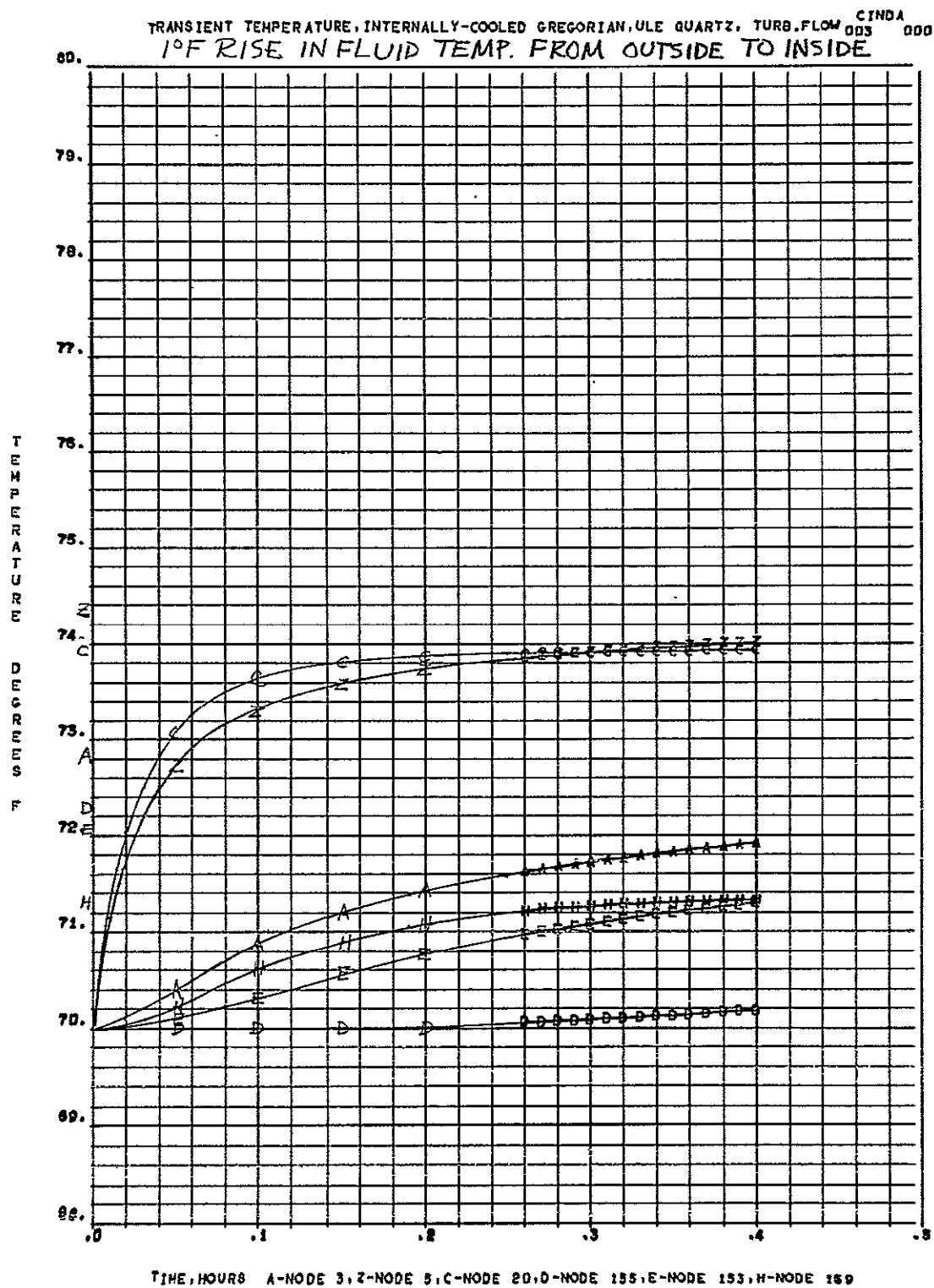


Figure 65.

STEADY TEMPERATURE, INTERNALLY-COOLED GREGORIAN ULE QUARTZ, LAM. FLOW CINDA 001 000

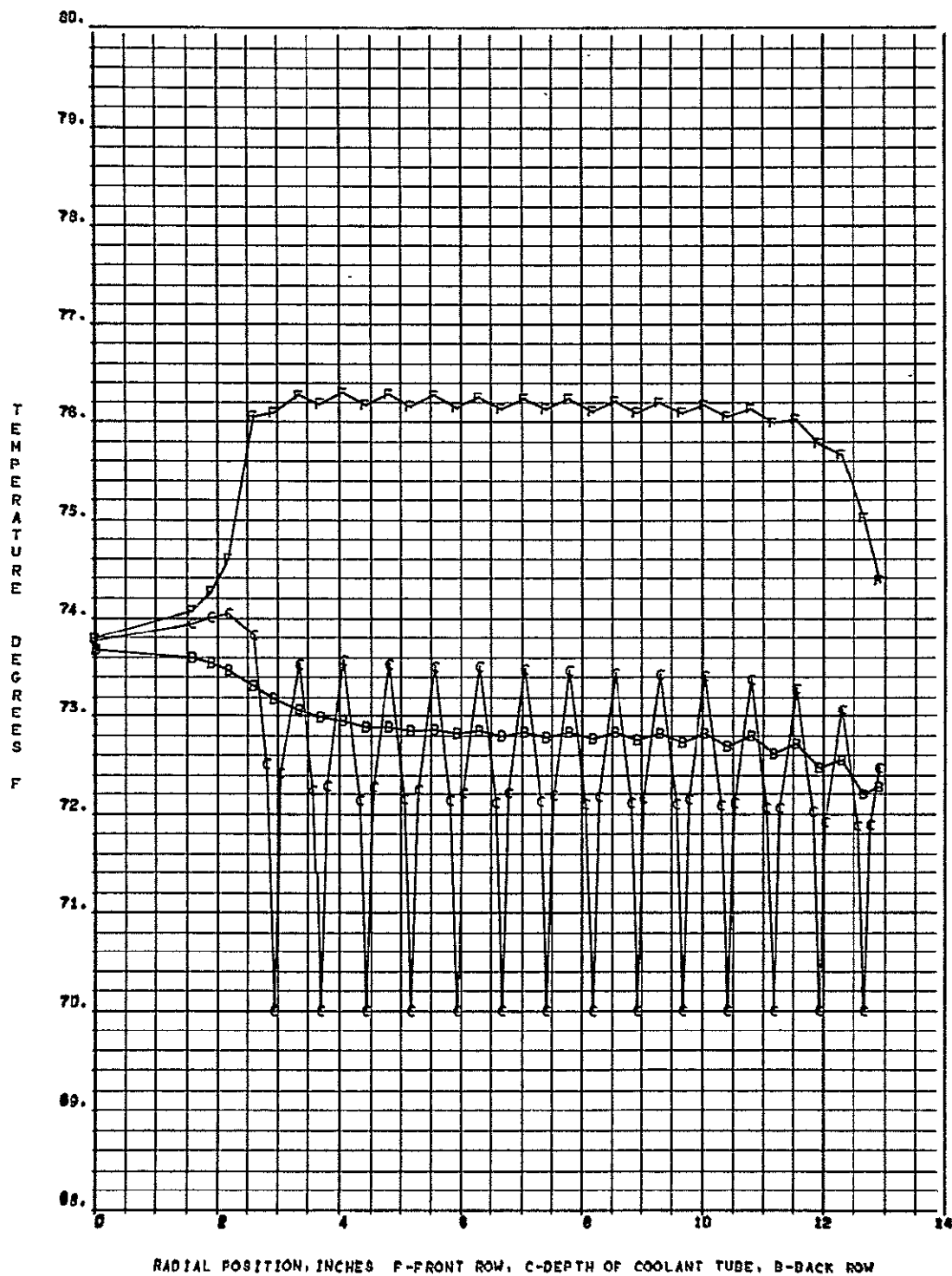


Figure 66.

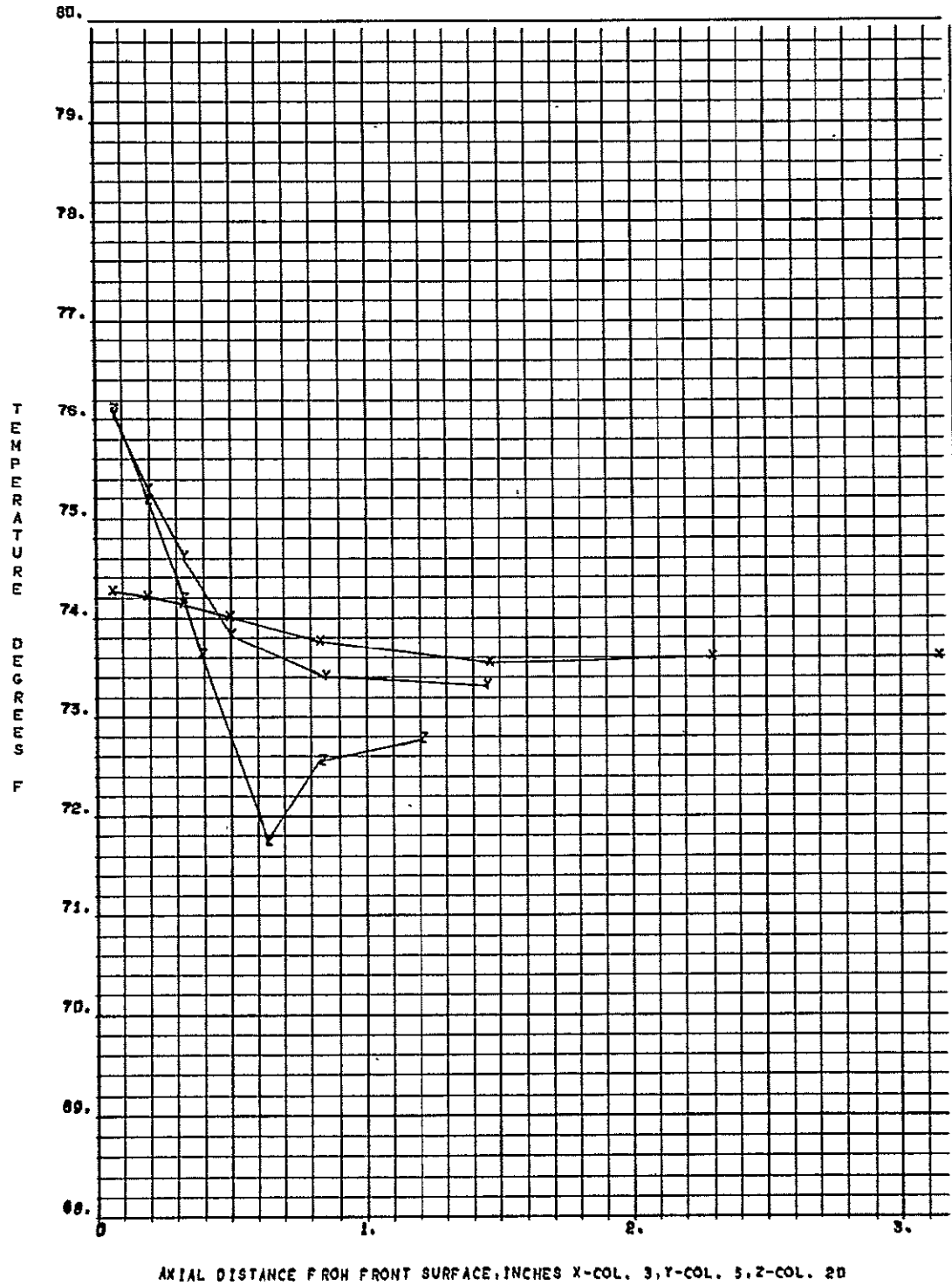


Figure 67.

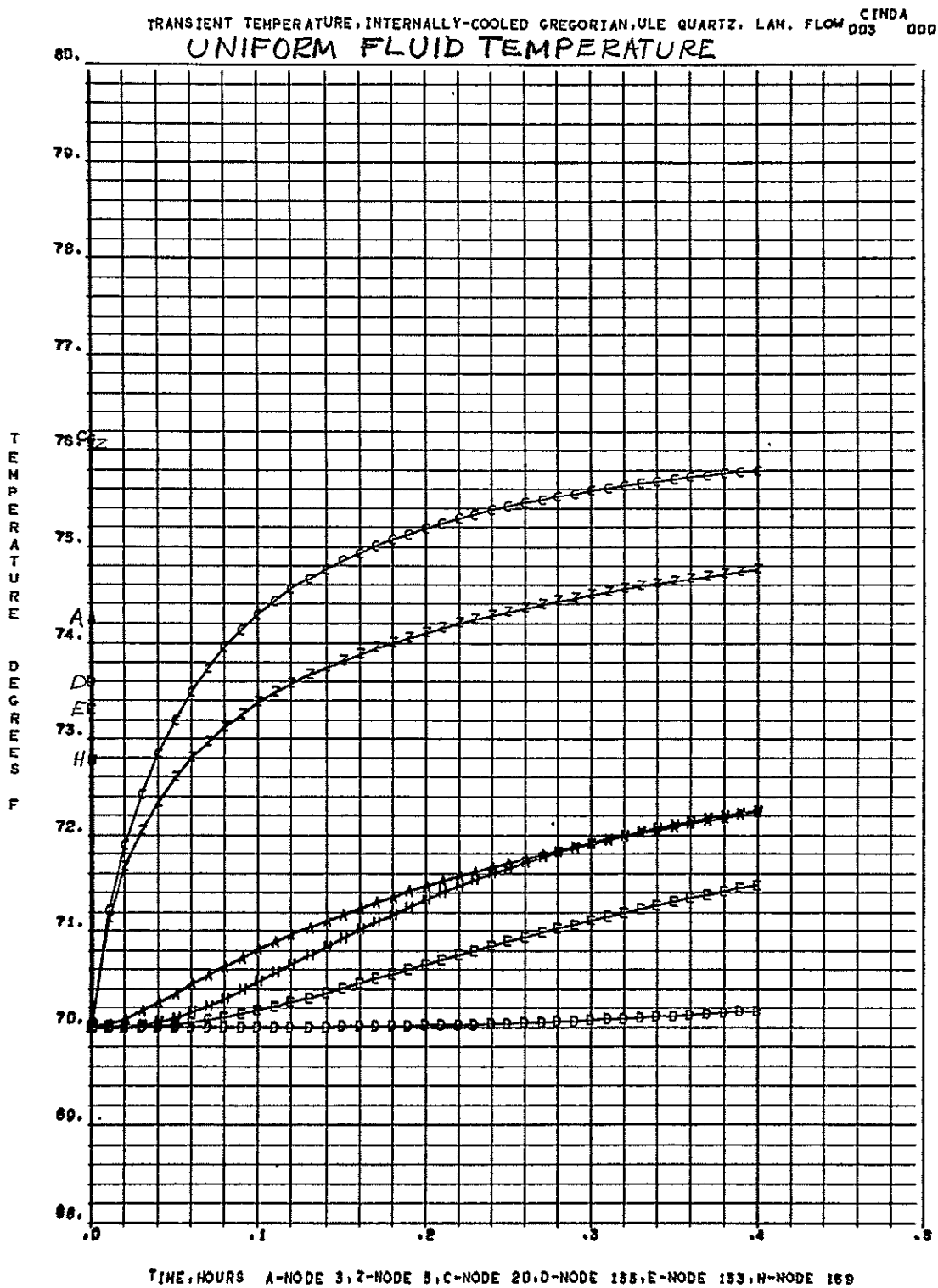


Figure 68.

STEADY TEMPERATURE, INTERNALLY-COOLED GREGORIAN ULE QUARTZ, LAM. FLOW ^{CINDA} 001 000

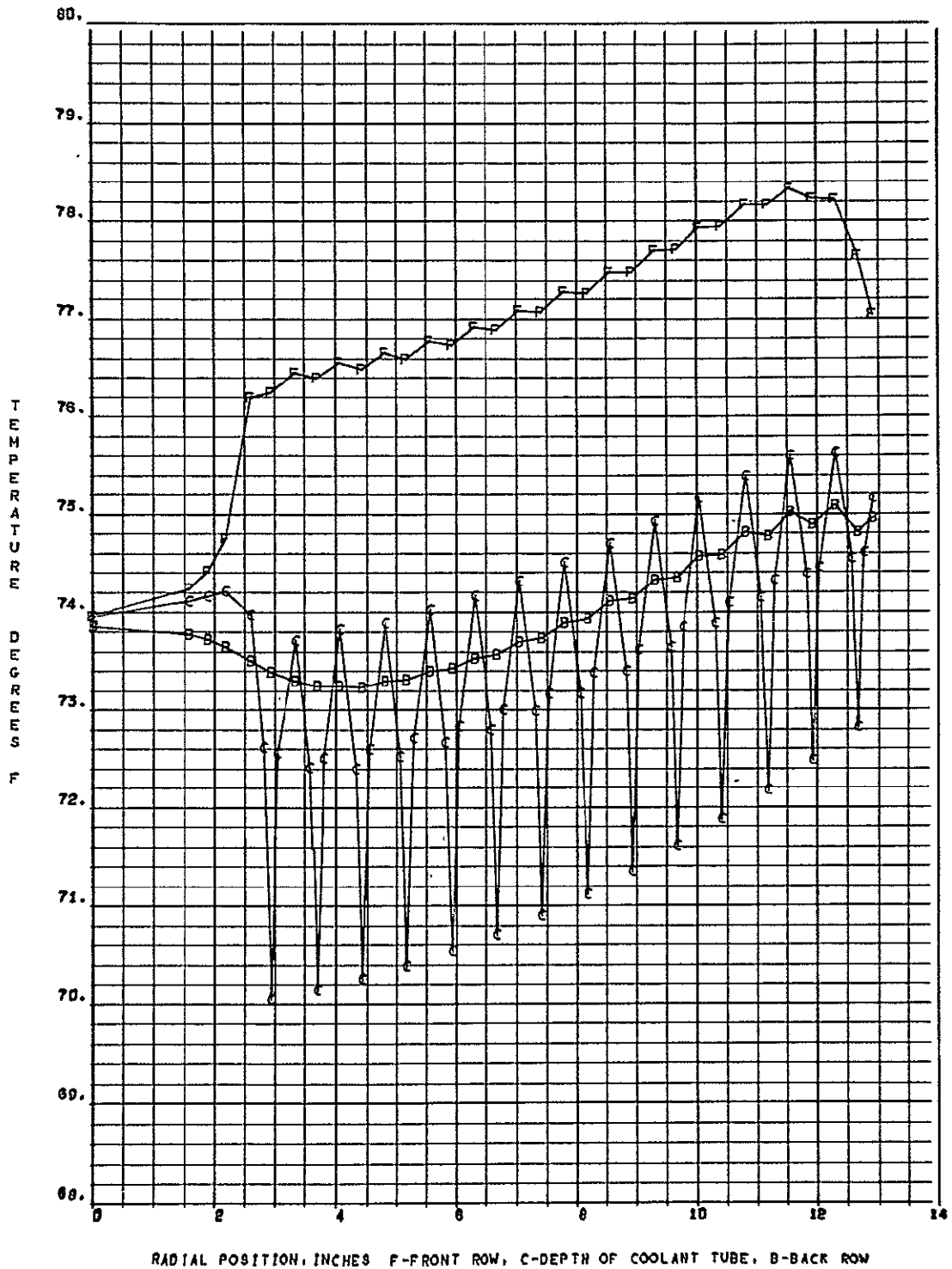


Figure 69.

STEADY TEMPERATURE, INTERNALLY-COOLED GREGORIAN ULE QUARTZ, LAM. FLOW ^{CINDA} 002 000

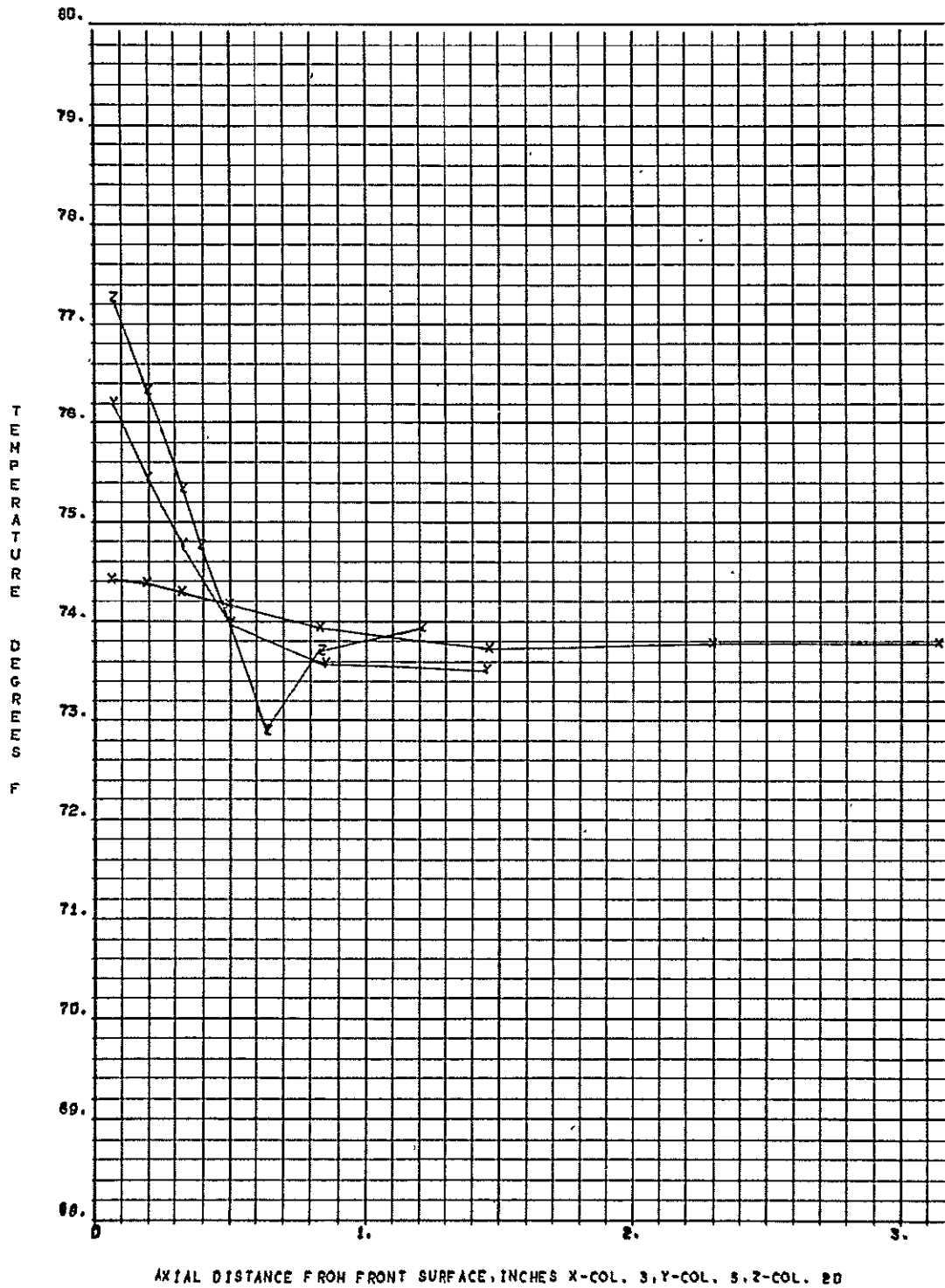


Figure 70.

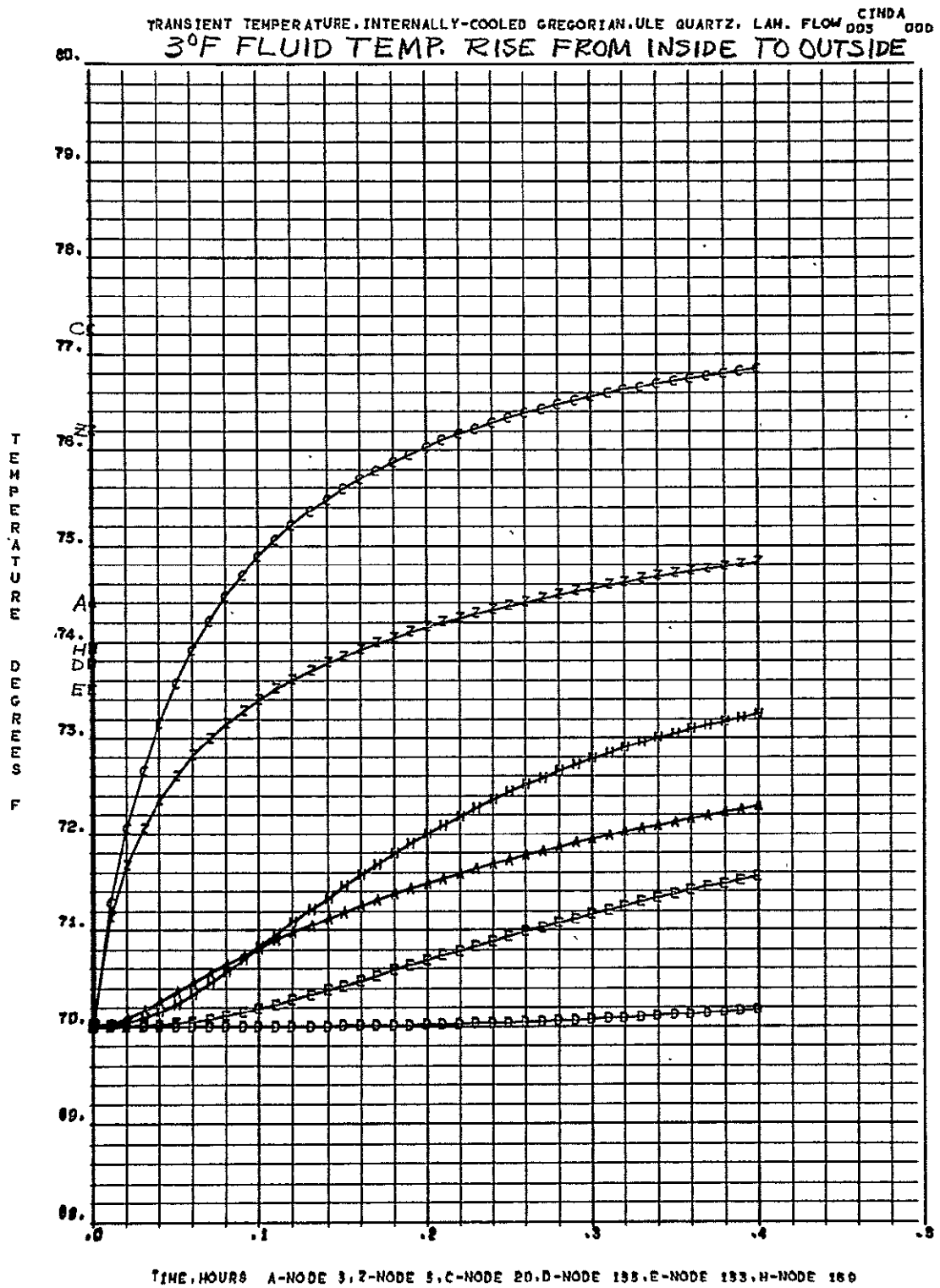


Figure 71.

STEADY TEMPERATURE, INTERNALLY-COOLED GREGORIAN ULE QUARTZ, LAM. FLOW CINDA
001 000

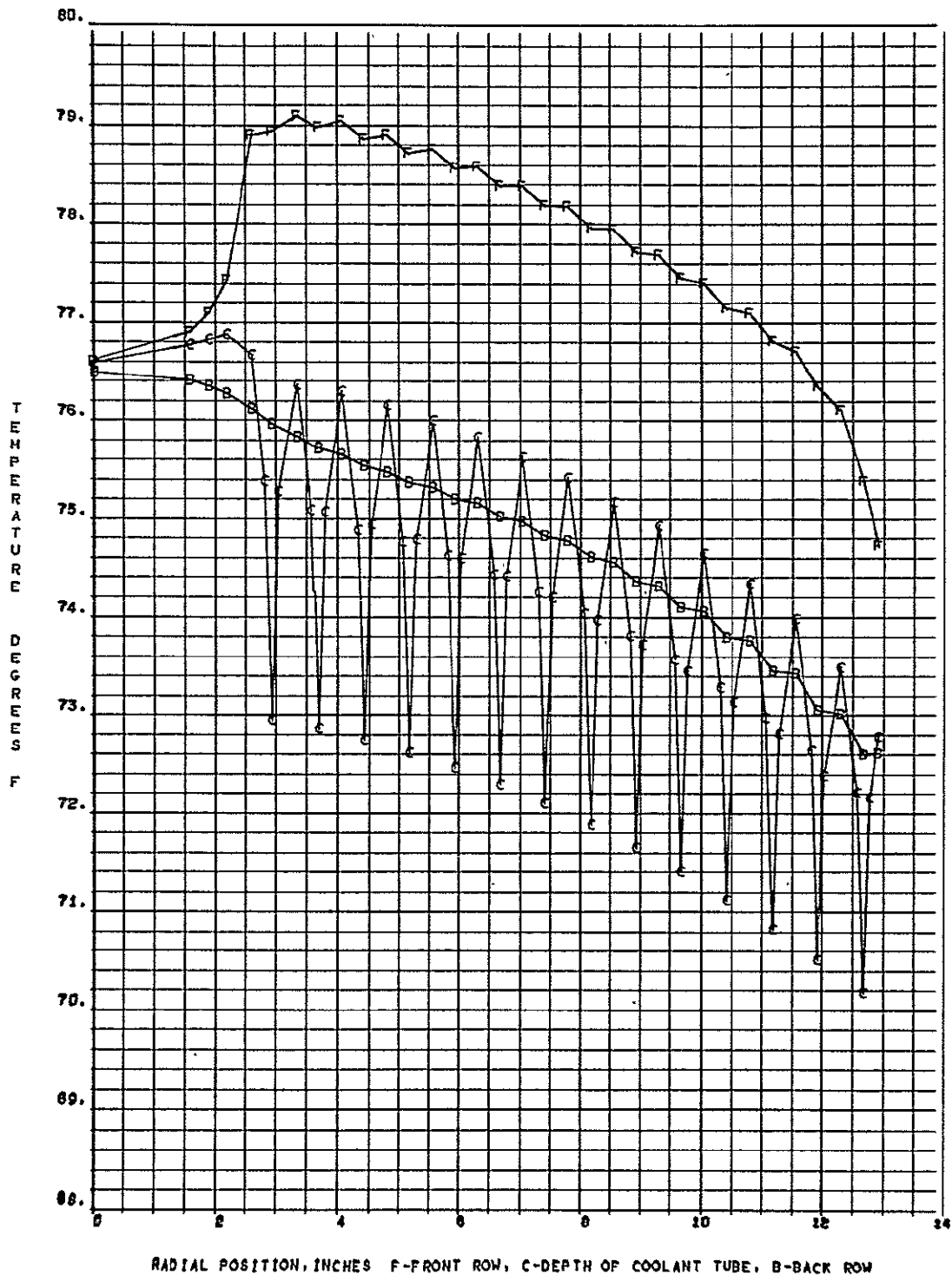


Figure 72.

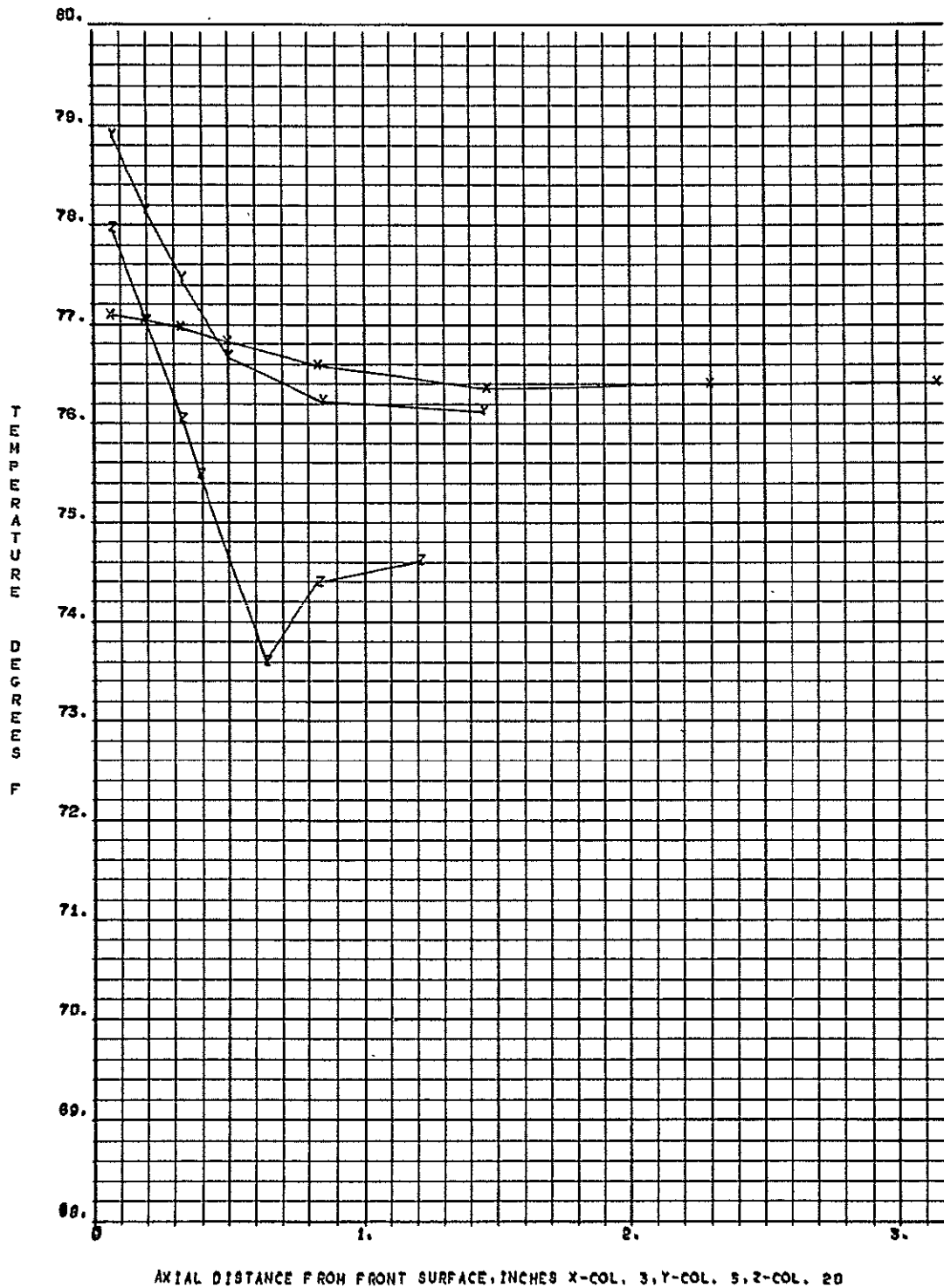


Figure 73.

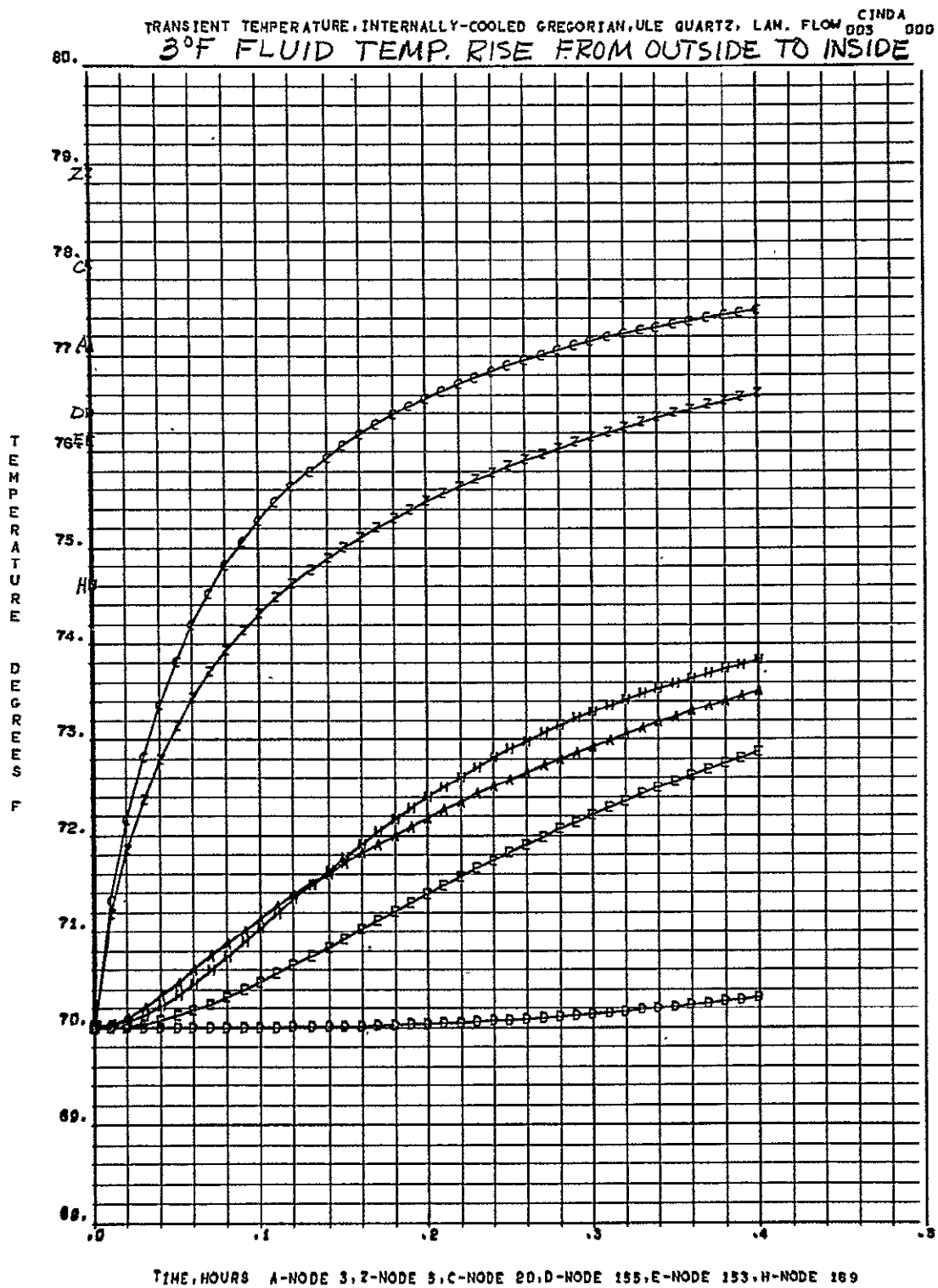


Figure 74.

XEROX PRODUCTION REPORT

DATE-10-30-70	HOURS-8	METER READING	IMPRESSIONS
OPERATOR-10. PULMAN	END-	BILLED -	
MACHINE No.- 7000	BEGIN-1417026	DIV. ADMIN.-	
CIRCLE ONE OF BELOW	TOTAL-	REJECT -	
FILE CFSTI IN		REMAKE -	
		TOTAL -	

No. ORIGINALS/OR DOC. ACCESSION No.	No. PAGES	No. COPY	No. TMP.	No. ORIGINALS/OR DOC. ACCESSION No.	No. PAGES	No. COPY	No. TMP.
1 AD 600 915				21			
2 N 70 29537				22			
3				23			
4				24			
5				25			
6				26			
7				27			
8				28			
9				29			
10				30			
11				31			
12				32			
13				33			
14				34			
15				35			
16				36			
17				37			
18				38			
19				39			
20				40			

TOTALS -

TOTALS -

REMARKS:

XEROX PRODUCTION REPORT

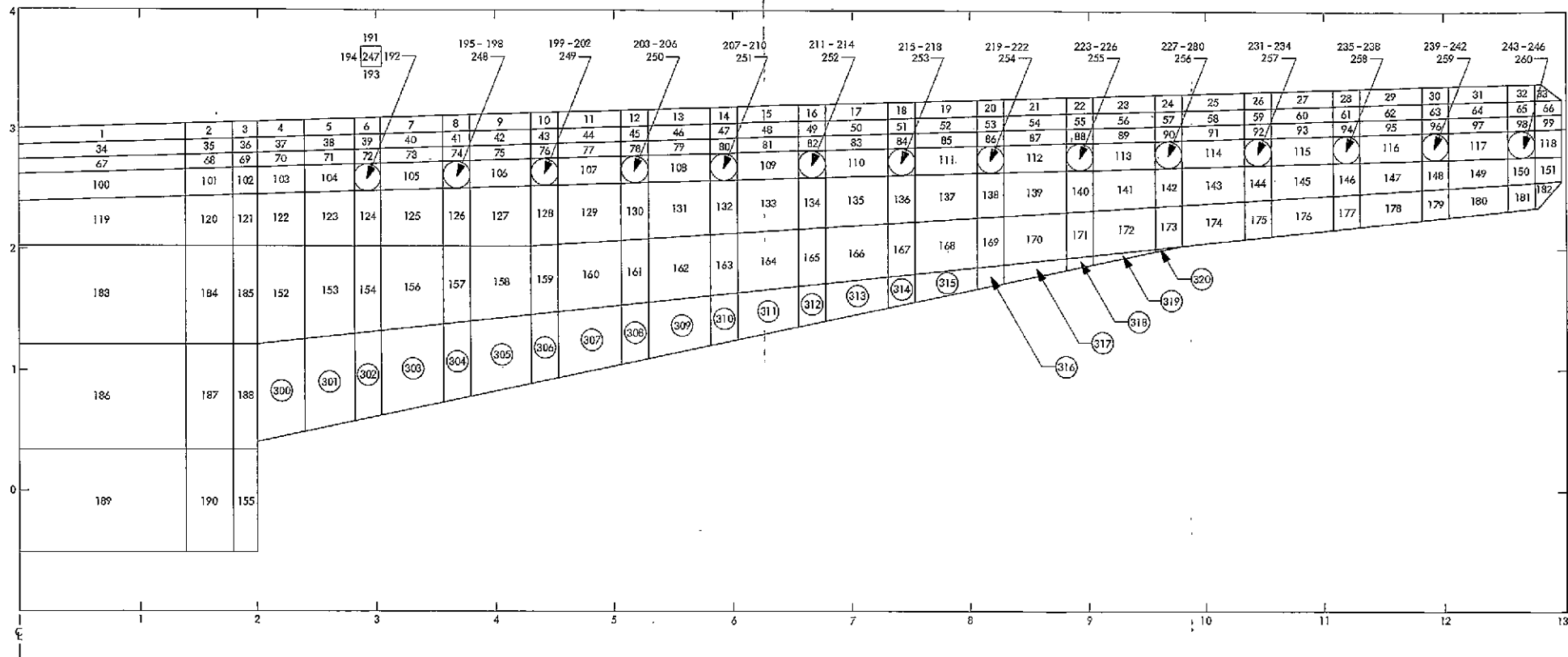
DATE-10-30-70	HOURS-8	METER READING	IMPRESSIONS
OPERATOR-W. PULMAN		END-	BILLED -
MACHINE No.-1000		BEGIN-	DIV. ADMIN.-
CIRCLE ONE OF BELOW		TOTAL-	REJECT -
<input checked="" type="checkbox"/> STANDARD	<input checked="" type="checkbox"/> ADMIN		REMAKE -
			TOTAL -

No.	ORIGINALS / OR DOC. ACCESSION No.	No. PAGES	No. COPY	No. IMP.	No.	ORIGINALS / OR DOC. ACCESSION No.	No. PAGES	No. COPY	No. IMP.
1				21					
2				22					
3				23					
4				24					
5				25					
6				26					
7				27					
8				28					
9				29					
10				30					
11				31					
12				32					
13				33					
14				34					
15				35					
16				36					
17				37					
18				38					
19				39					
20				40					

TOTALS -

TOTALS -

REMARKS:



FOLDOUT FRAME 1

FOLDOUT FRAME 2

Figure 75.

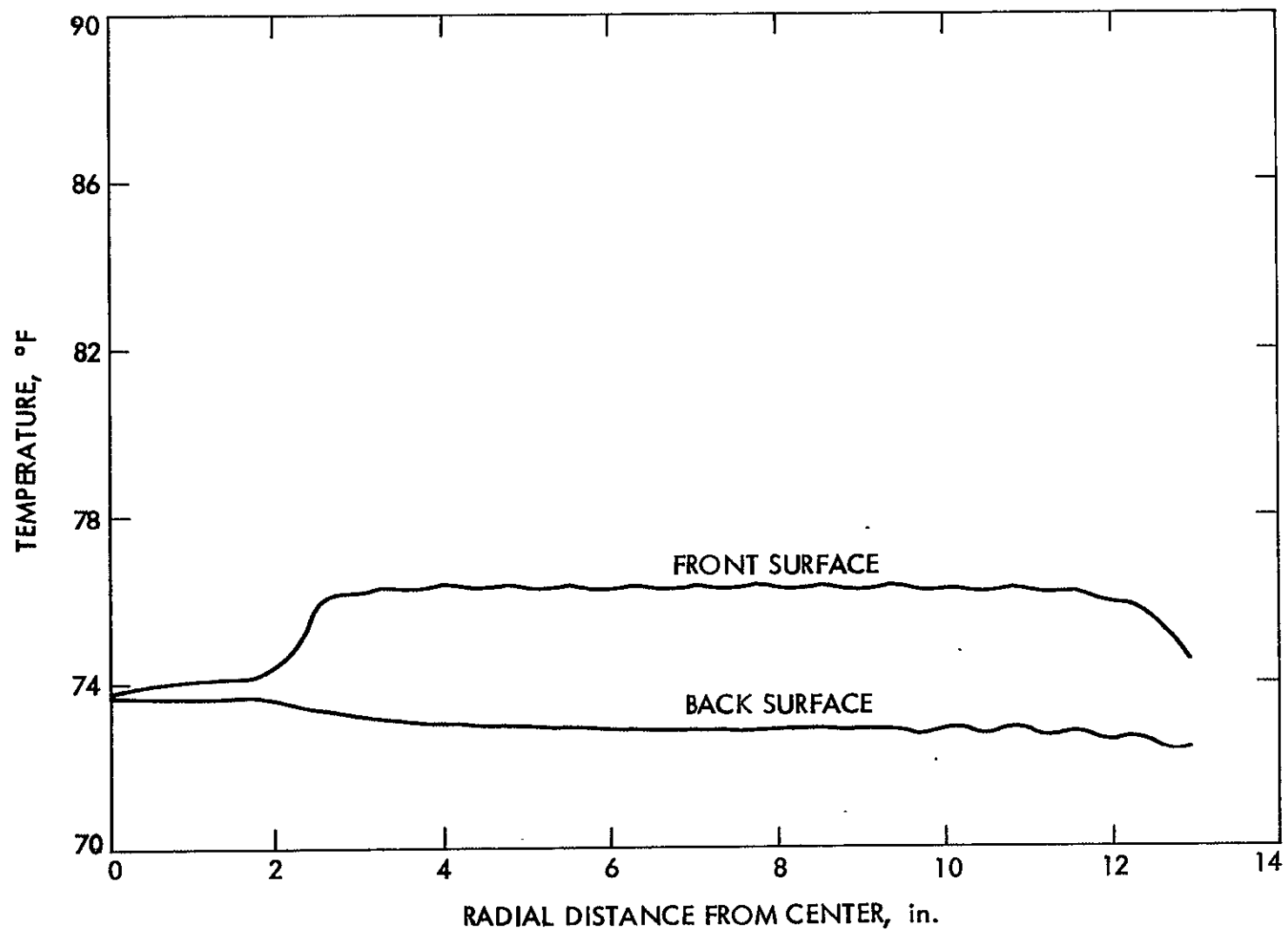


Figure 76. Laminar Flow, Uniform 70°F Coolant Temperature, ULE Fused SiO₂ Configuration Number 1

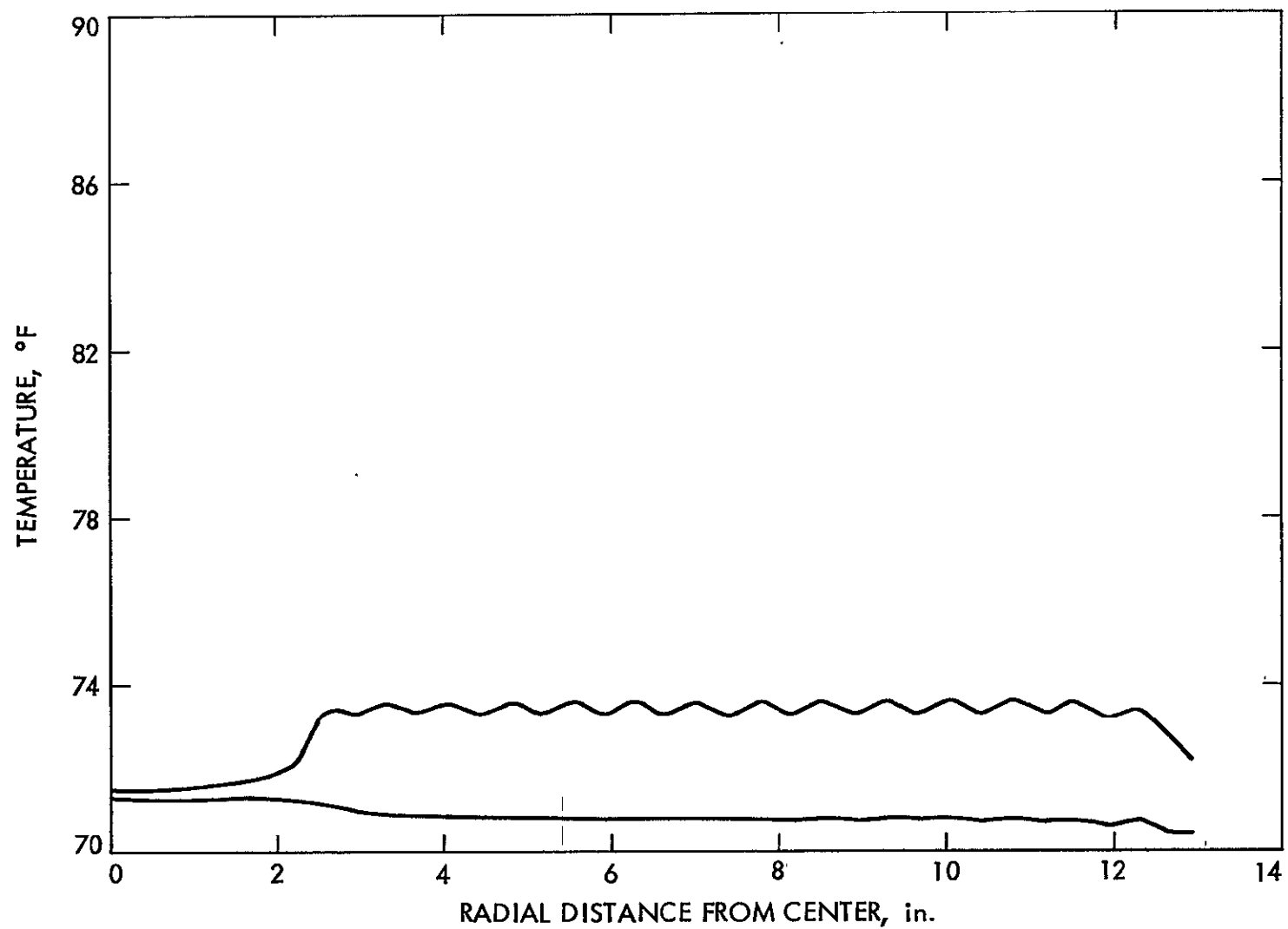


Figure 77. Turbulent Flow, Uniform 70° F Coolant Temperature, SiO₂ Configuration Number 1

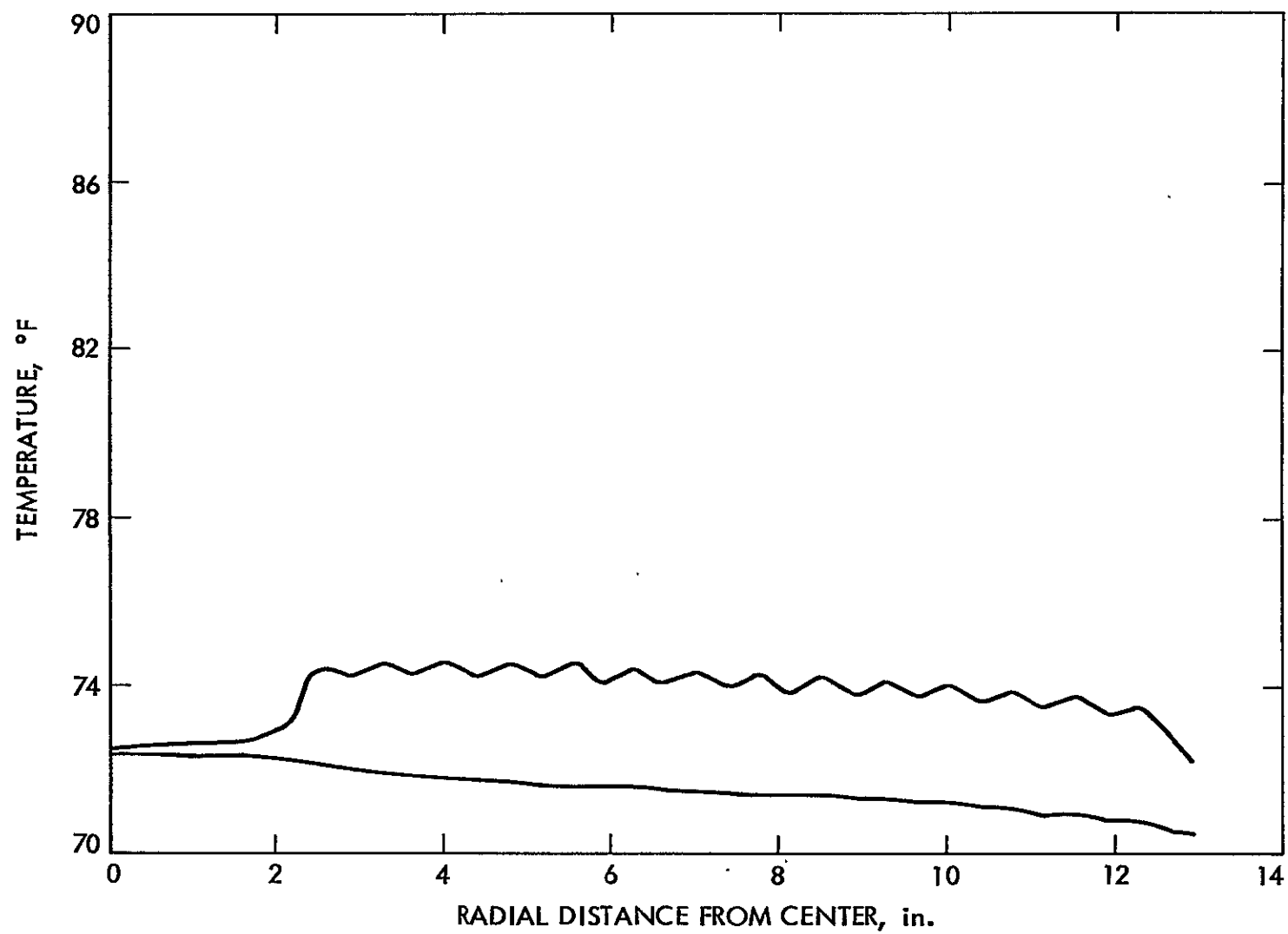


Figure 78. Turbulent Flow from Outside to Inside, ULE Fused SiO₂, Configuration Number 1

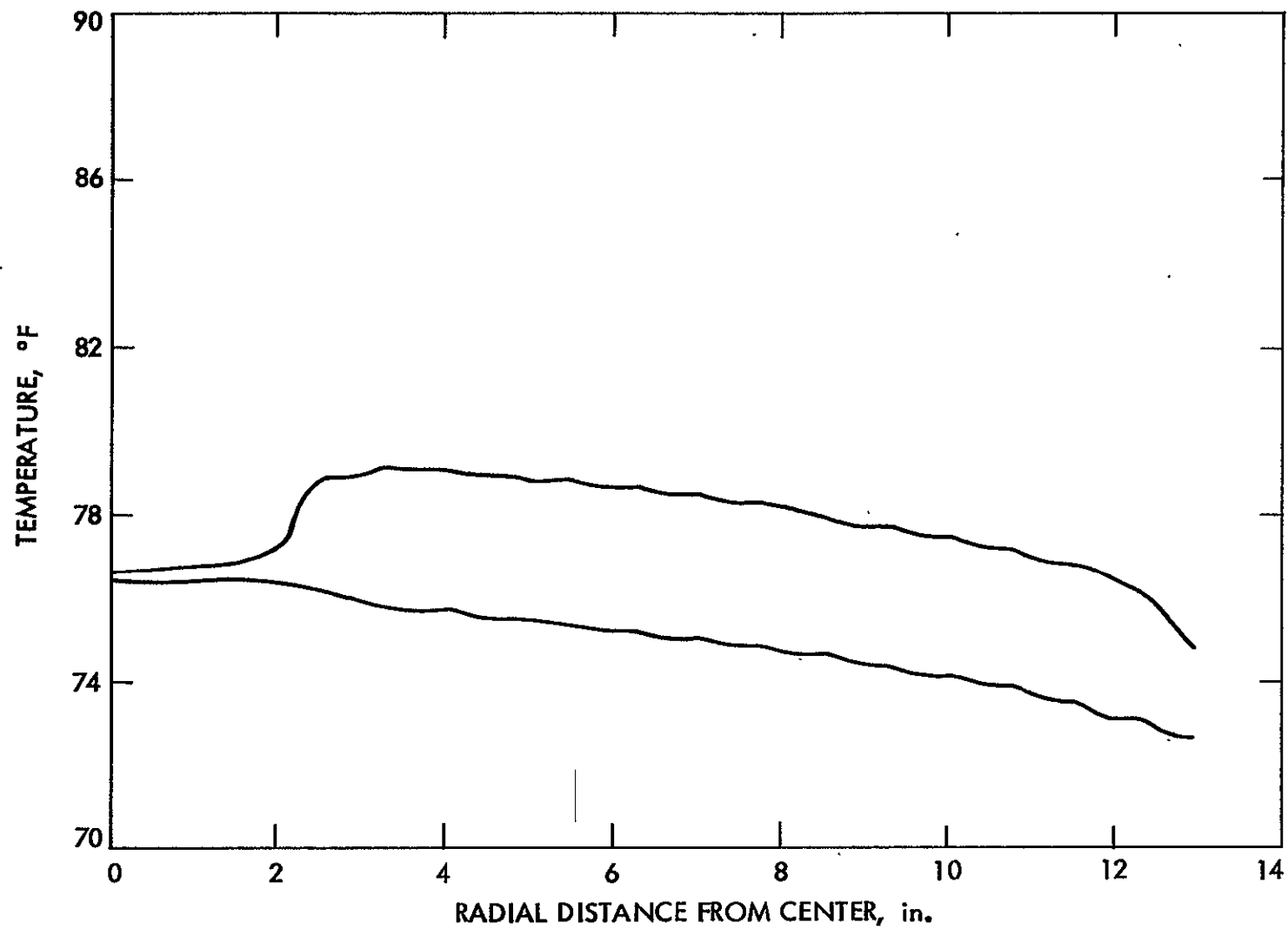


Figure 79. Laminar Flow from Outside to Inside, ULE Fused SiO₂, Configuration Number 1

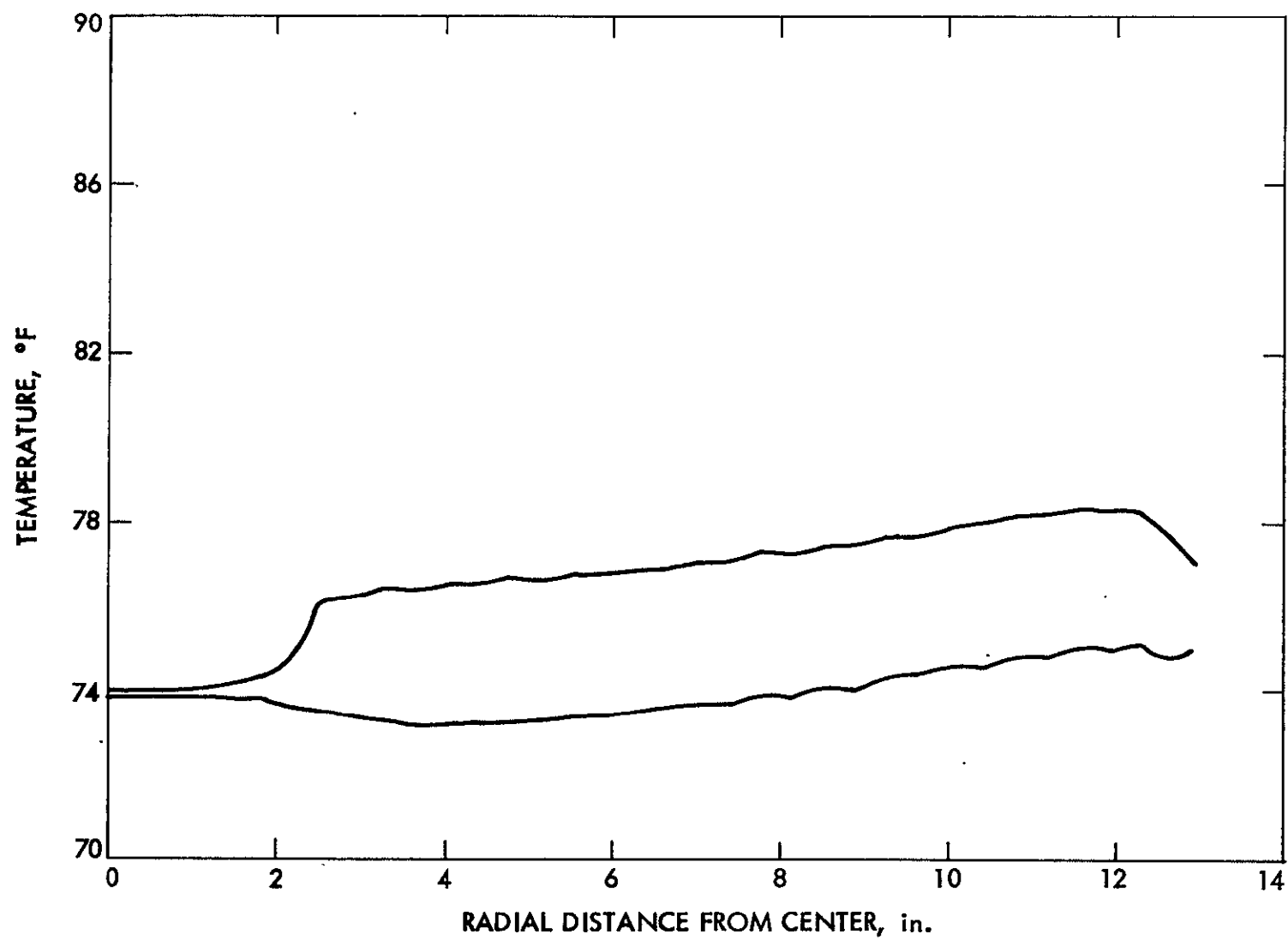


Figure 80. Laminar Flow form Inside to Outside, ULE Fused SiO_2 , Configuration Number 1

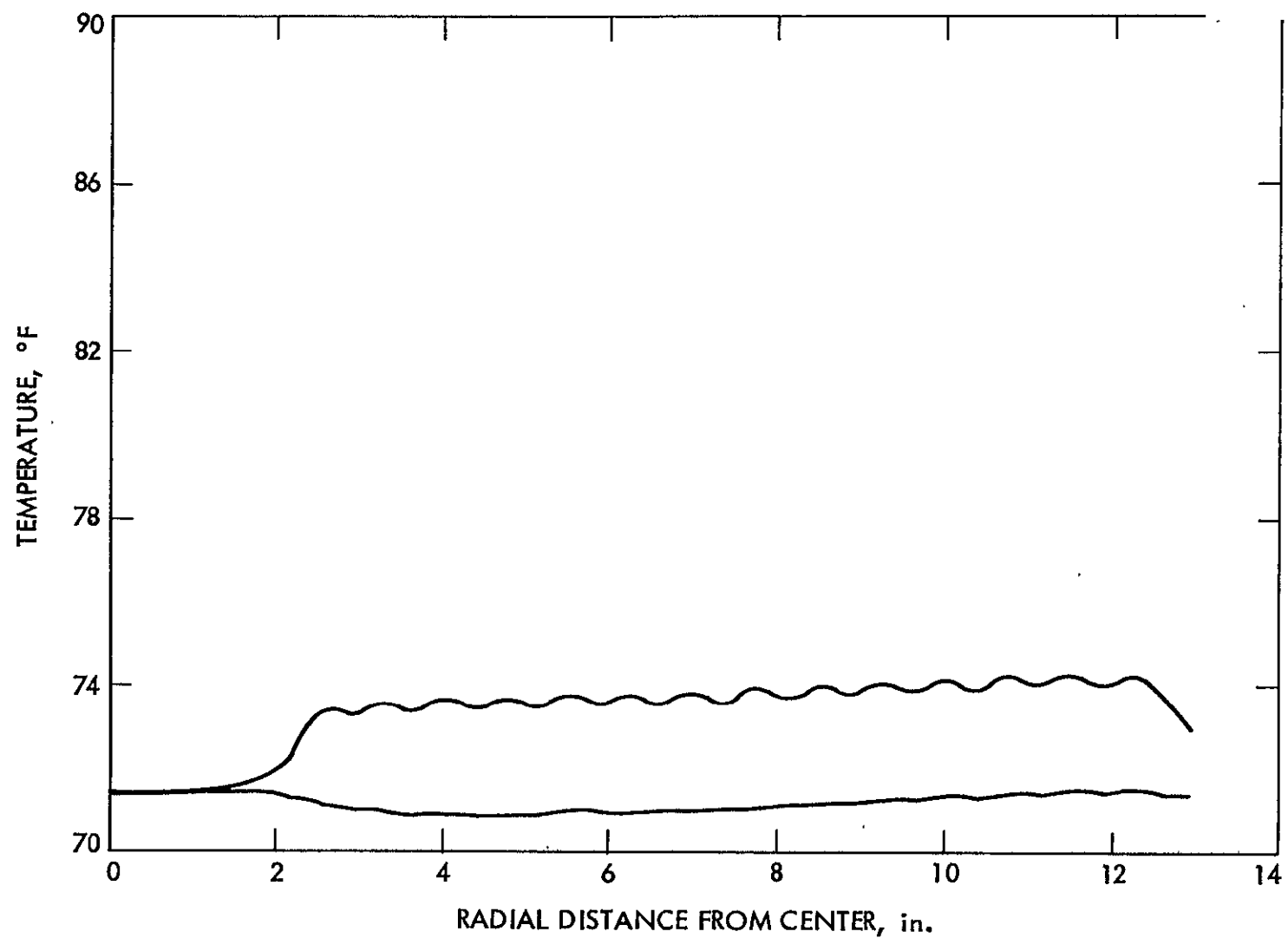


Figure 81. Turbulent Flow from Inside to Outside, ULE Fused SiO₂, Configuration Number 1

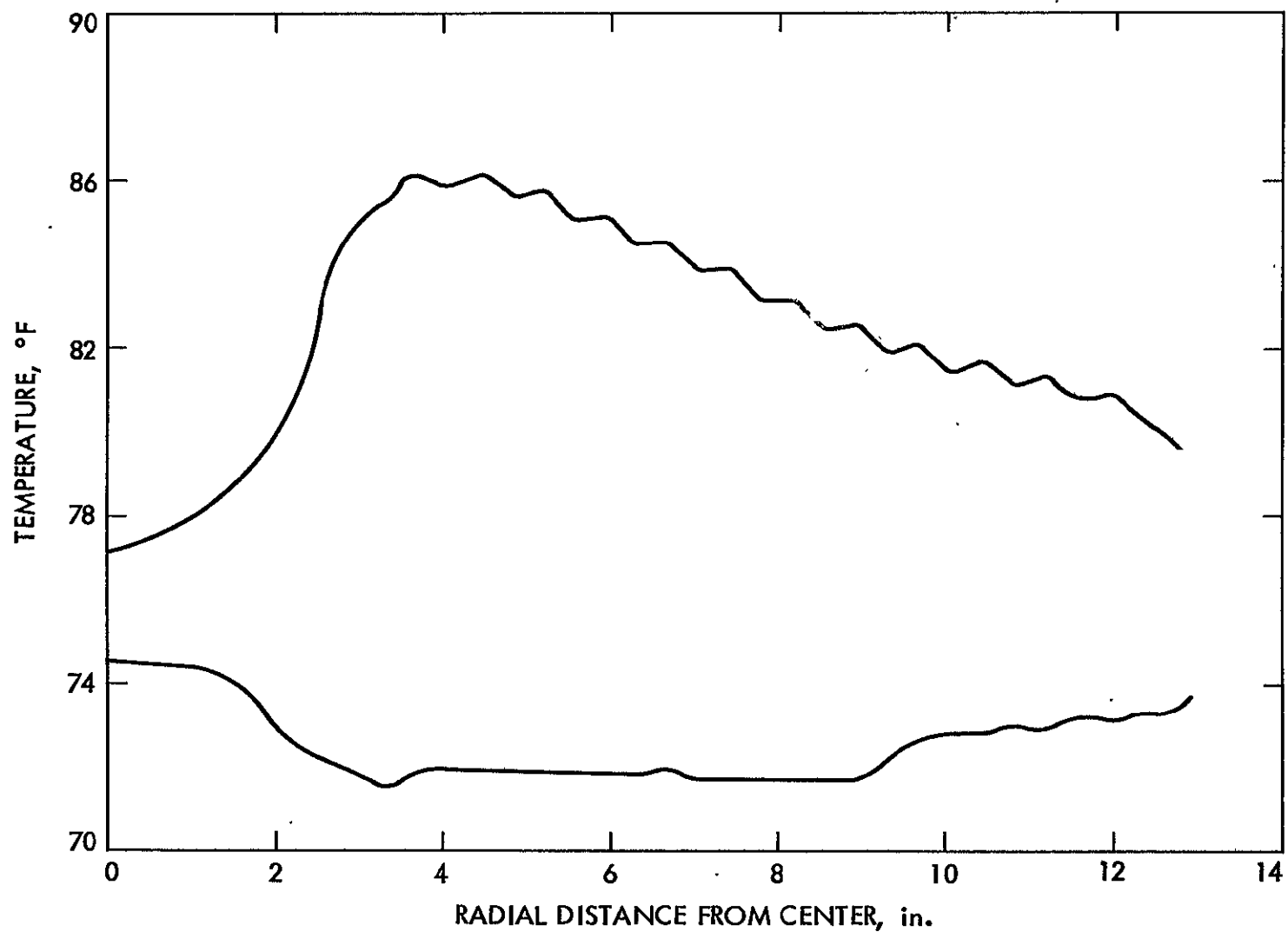


Figure 82. Temperature Gradient on Mirror Back, 3°F Rise from Inside to Outside, ULE Fused SiO₂, Configuration Number 2

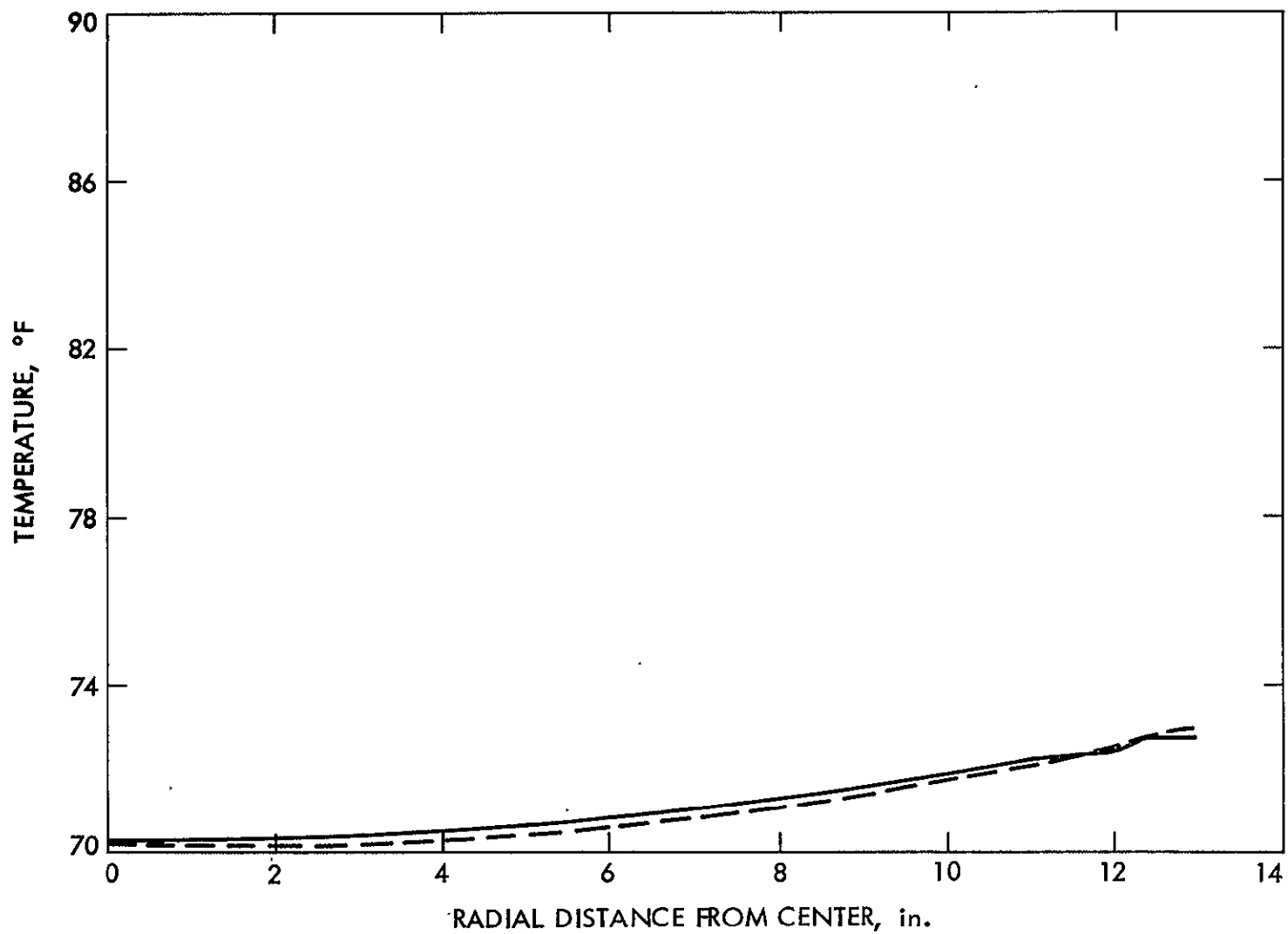


Figure 83. Temperature Gradient on Mirror Back 3°F Rise from Inside to Outside Beryllium Configuration Number 2

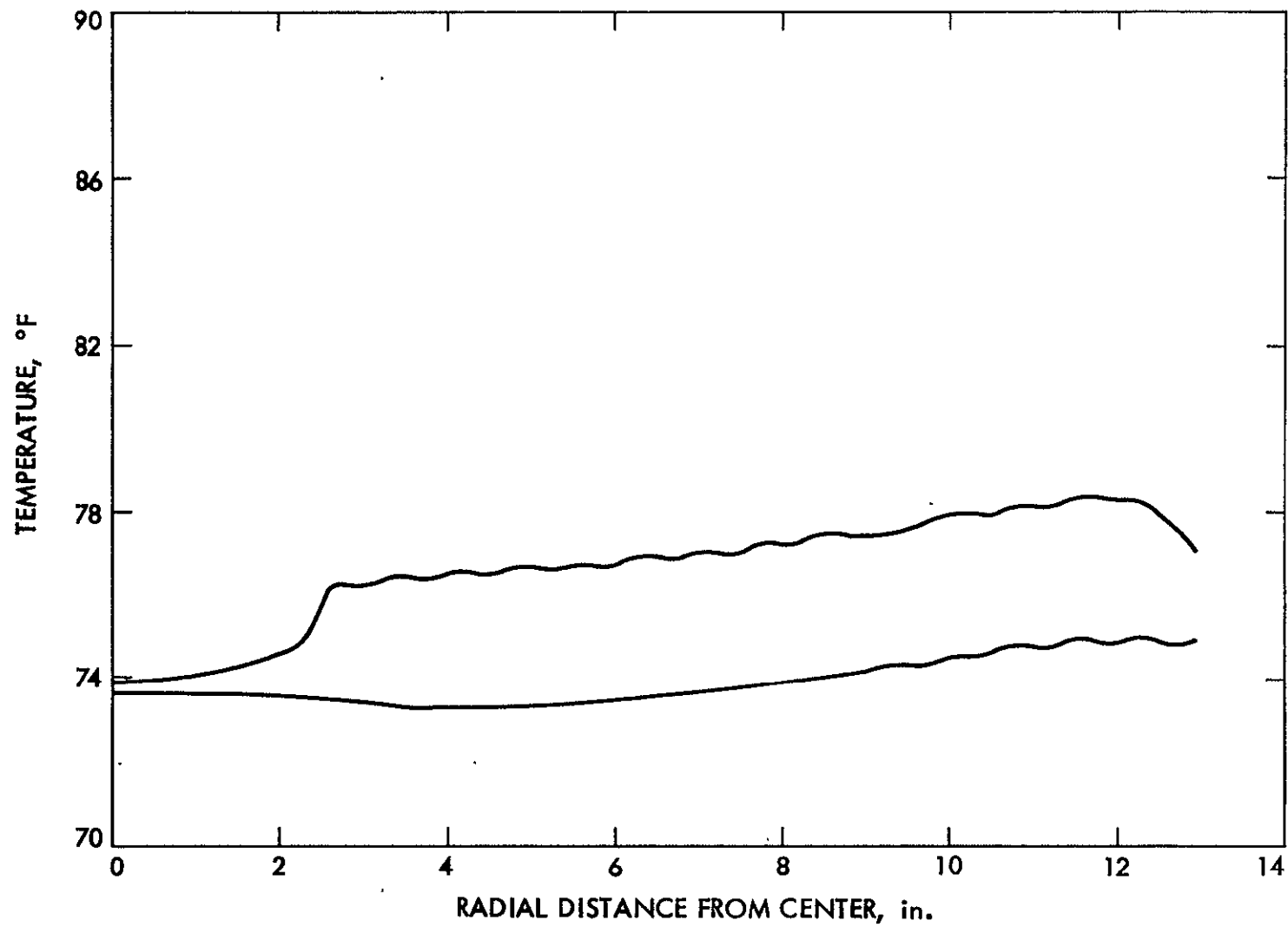


Figure 84. Laminar Flow from Inside to Outside, ULE Fused SiO₂, Configuration Number 2

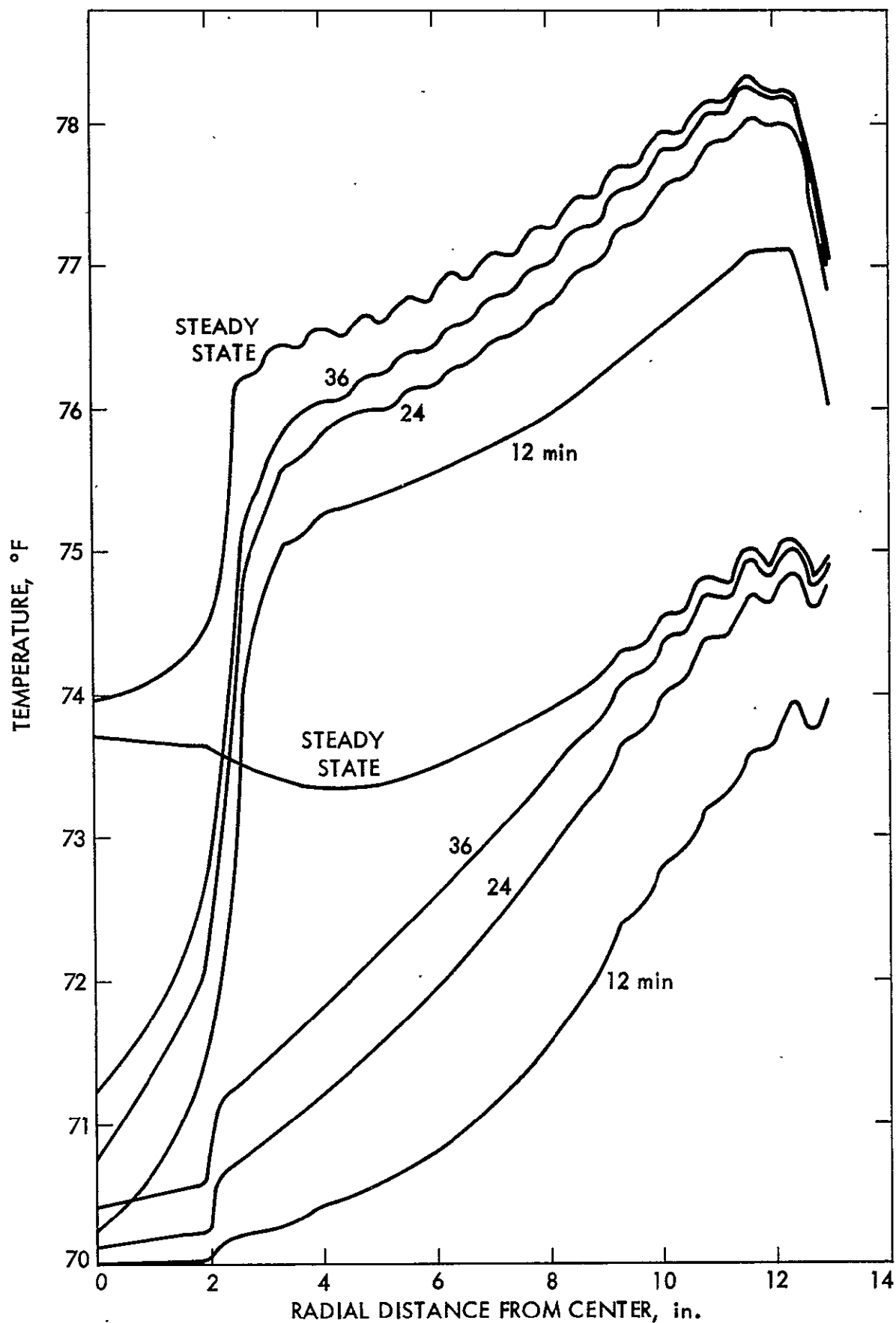


Figure 85. Laminar Flow from Inside to Outside, ULE Fused SiO₂, Configuration Number 2

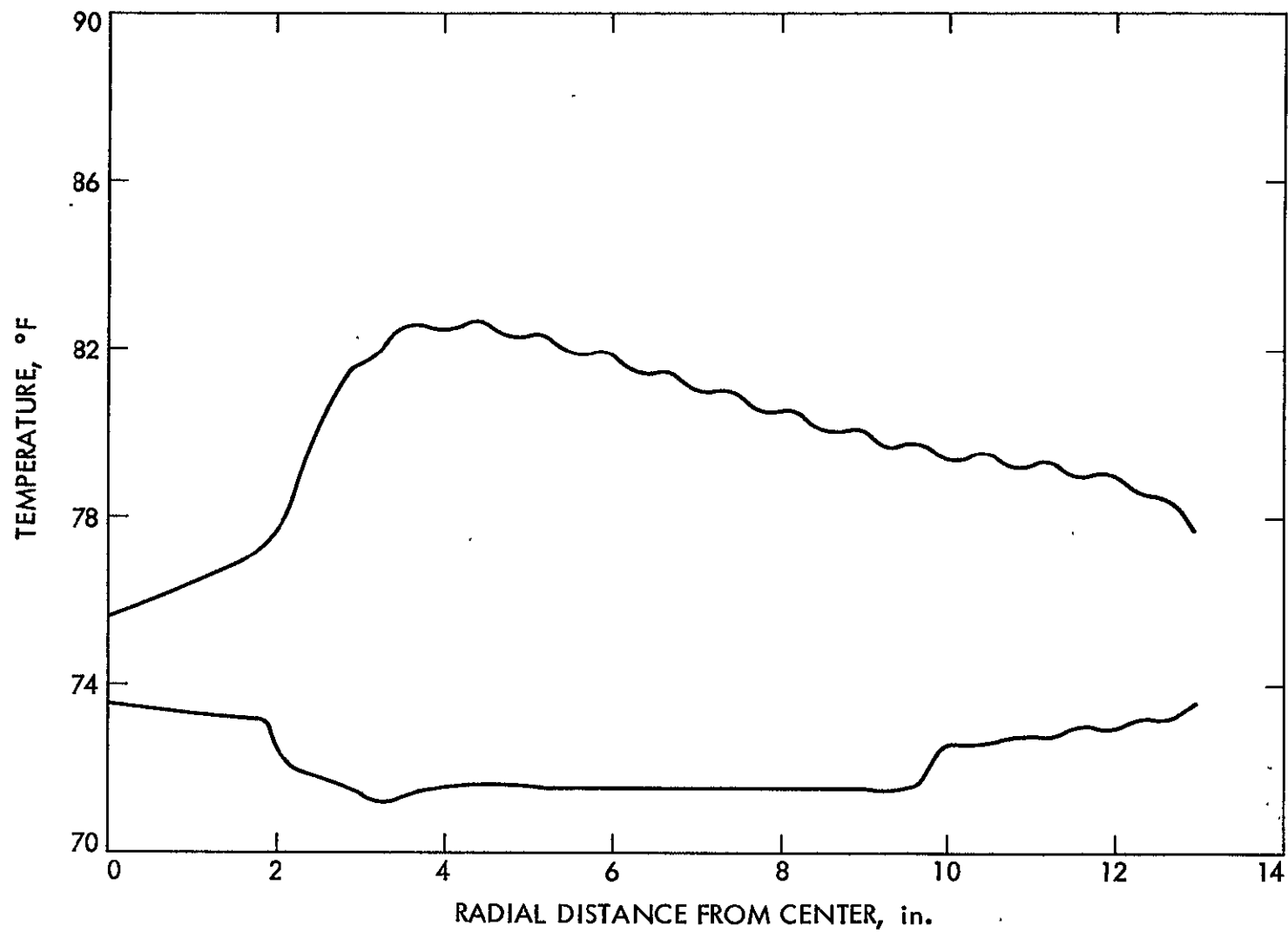


Figure 86. Temperature Gradient on Mirror Back 3°F Rise from Inside to Outside
CER-VIT Configuration Number 2

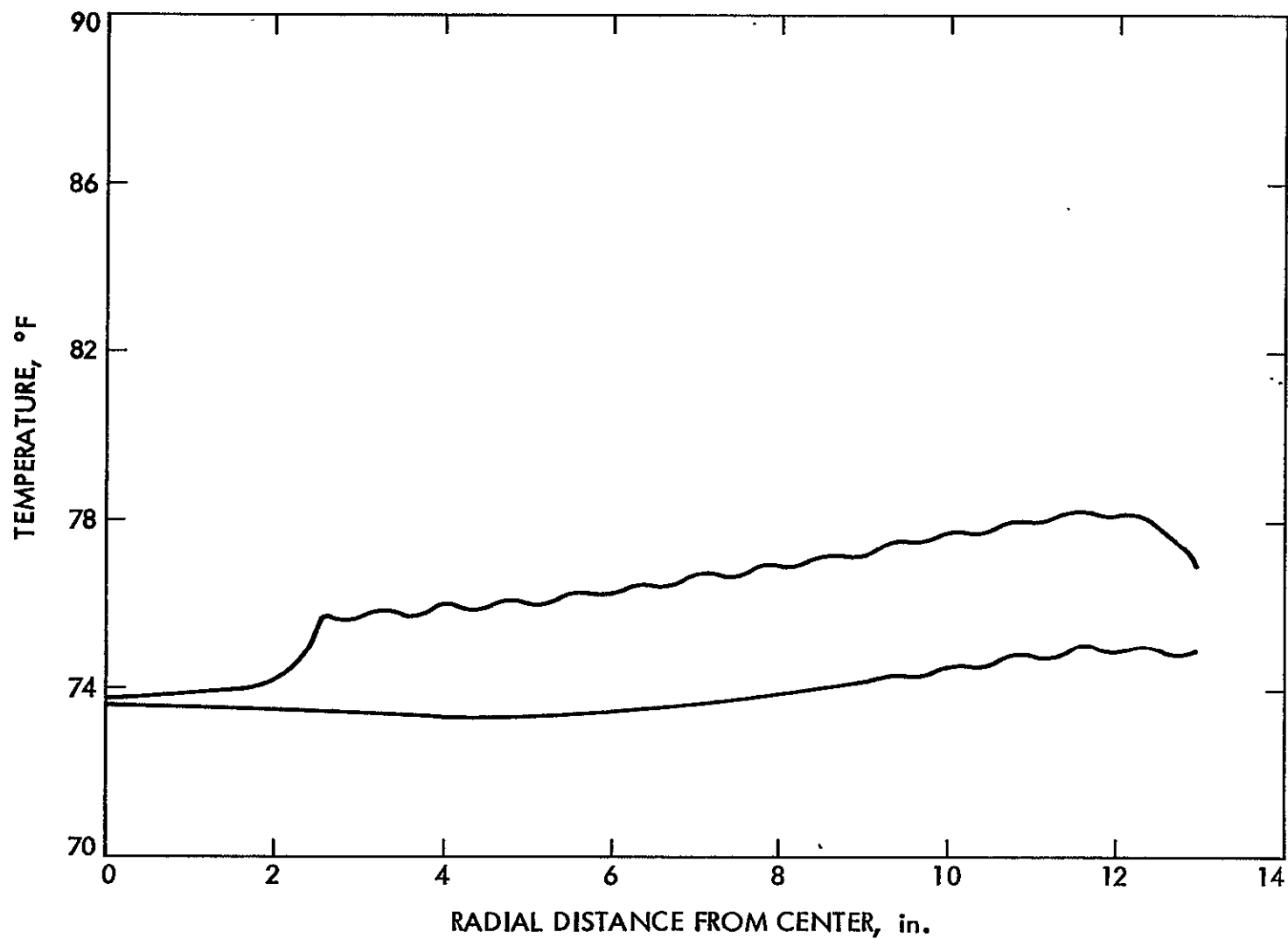


Figure 87. Laminar Flow from Inside to Outside Mirror Front Face 0.35 in. Thick at Mirror Center, Increasing Linearly to 0.50 in. Thick at the Mirror O.D. ULE Fused SiO₂ Configuration Number 2

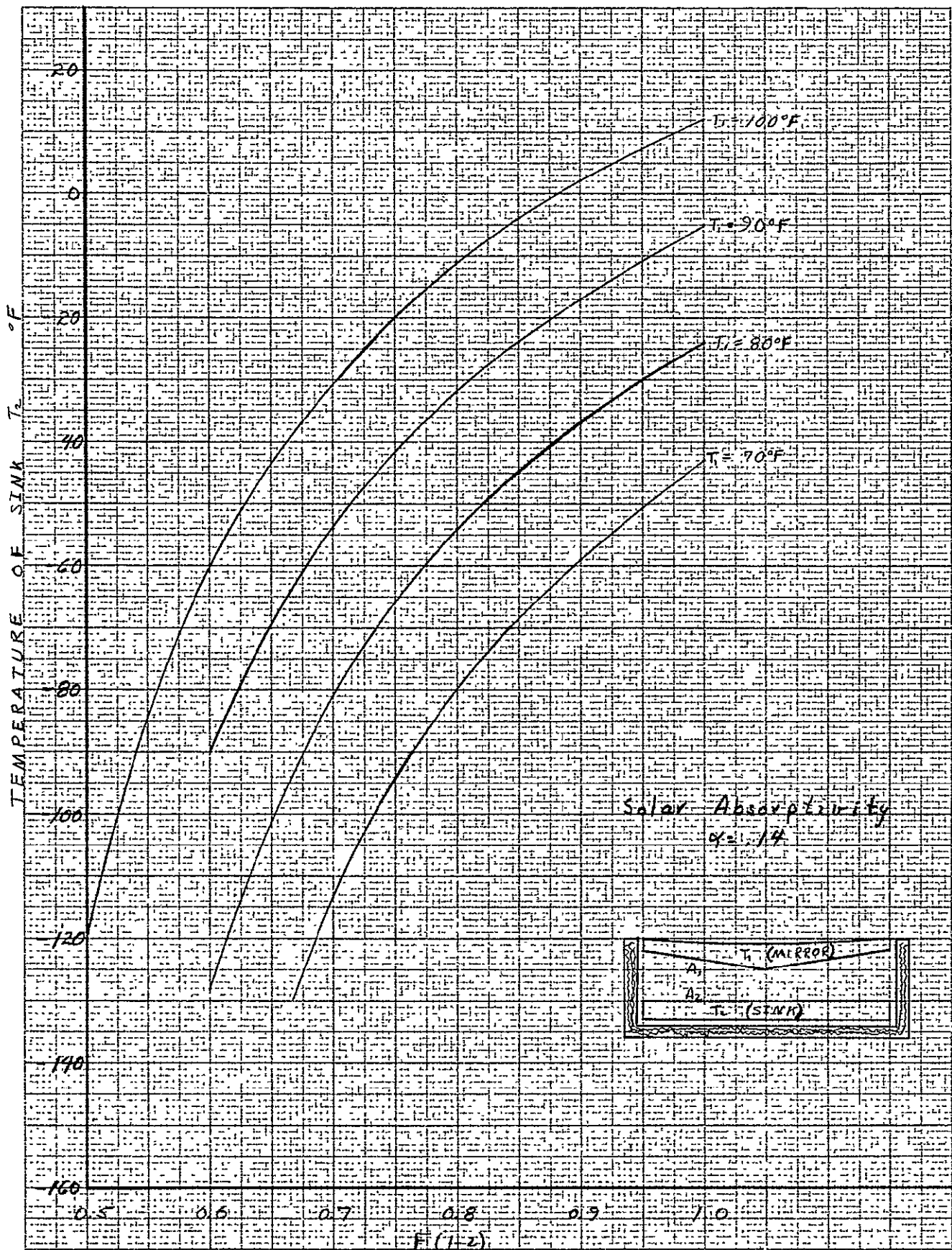


Figure 88.

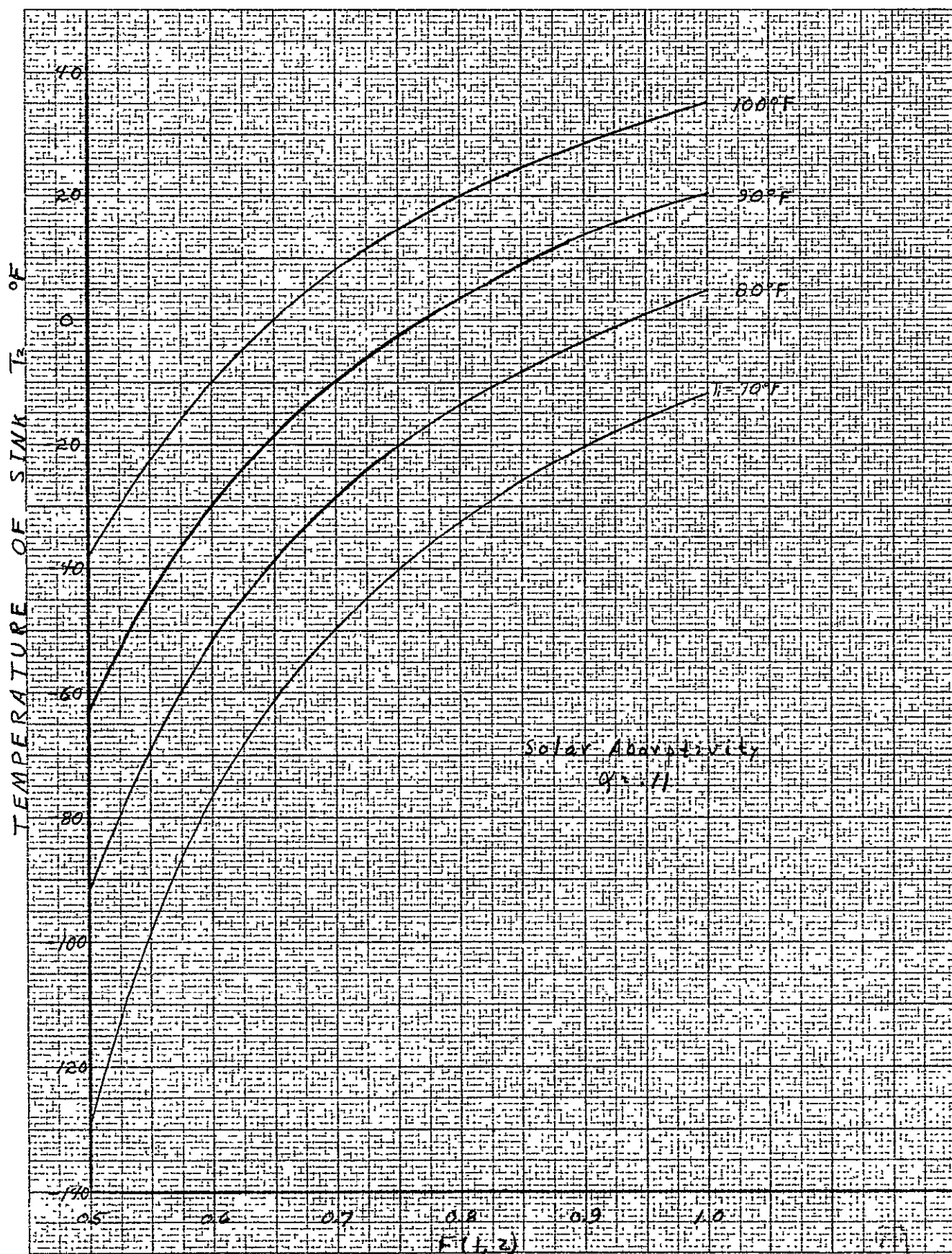


Figure 89.